Metabolic flexibility in early diabetes development

Inaugural-Dissertation

zur Erlangung des Doktorgrades

der Mathematisch-Naturwissenschaftlichen Fakultät

der Heinrich-Heine-Universität Düsseldorf

vorgelegt von

Anna Katharina Scheel

aus Münster (Westfalen)

Düsseldorf, März 2024

aus dem Institut für Klinische Biochemie und Pathobiochemie
des Deutschen Diabetes-Zentrums
Leibniz-Zentrum für Diabetes-Forschung
an der Heinrich-Heine-Universität Düsseldorf

Gedruckt mit der Genehmigung der
Mathematisch-Naturwissenschaftlichen Fakultät der
Heinrich-Heine-Universität Düsseldorf

Berichterstatter:
1. Prof. Dr. Hadi Al-Hasani
2. Prof. Dr. Eckhard Lammert

Tag der mündlichen Prüfung: 29.08.2024

Summary

The closely related RabGTPase-activating proteins (RabGAPs) TBC1D1 and TBC1D4 (AS160) are key regulators of energy flux and GLUT4-mediated glucose uptake in skeletal muscle and adipose tissue. In humans and rodents, genetic variants of the two RabGAPs have been associated with insulin resistance and obesity. In Arctic populations, a common TBC1D4 *p.Arg684Ter* loss-of-function variant in skeletal muscle defines a specific subtype of type 2 diabetes mellitus (T2DM). The Arctic *TBC1D4* variant is hypothesized as an evolutionary adaptation to a traditional low-carbohydrate high-protein (LCHP) diet, whereas a Western high-carbohydrate low-protein (HCLP) diet presumably promotes the development of T2DM in homozygous carriers of the *p.Arg684Ter* variant. The present study aimed to elucidate how Arctic and Western diets affect metabolic flexibility, the mechanisms of insulin resistance and the individual contributions of skeletal muscle and adipose tissue in the regulation of whole-body glycemia. Therefore, whole-body and tissue-specific RabGAP-deficient mice were metabolically characterized during LCHP and HCLP dietary interventions.

The present study demonstrates that an Arctic diet protects *Tbc1d4*-deficient (D4KO) mice from postprandial hyperglycemia by improving insulin-stimulated glucose uptake in oxidative and glycolytic skeletal muscle. Proteome analysis of skeletal muscle revealed changes primarily in intracellular trafficking in D4KO mice fed an Arctic diet. In particular, deubiquitinating enzymes and proteins associated with endosomal recycling were found to be increased in skeletal muscle, indicating a potential mechanism for controlling TBC1D4-regulated sorting and degradation of GLUT4. These findings suggest that the Arctic diet may prevent the onset of T2DM in individuals with homozygous TBC1D4 *p.Arg684Ter* gene variants by overcoming genetically induced skeletal muscle insulin resistance. This highlights the Arctic diet as a potential approach for precision medicine. Furthermore, Arctic diet feeding resulted in enhanced insulin-stimulated glucose uptake in adipose tissue of *Tbc1d1*-deficient and *Tbc1d1/Tb1cd4* double-deficient mice, which was associated with reduced adipose tissue mass. Therefore, the current study highlights the pivotal role of TBC1D1 in the regulation of lipid and glucose metabolism, indicating its potential protective function against diet-induced obesity and insulin resistance.

Zusammenfassung

Die RabGTPase-aktivierenden Proteine (RabGAPs) TBC1D1 und TBC1D4 (AS160) sind wichtige Regulatoren des Energieflusses und der GLUT4-vermittelten Glukoseaufnahme im Skelettmuskel und Fettgewebe. Bei Menschen und Nagern wurden genetische Varianten der beiden RabGAPs mit Insulinresistenz und Fettleibigkeit in Verbindung gebracht. In arktischen Populationen definiert eine häufige TBC1D4 *p.Arg684Ter*-Variante in der Skelettmuskulatur einen spezifischen Subtyp von Typ-2-Diabetes mellitus (T2DM). Es wird angenommen, dass die arktische TBC1D4-Variante eine evolutionäre Adaptation an eine traditionelle Diät darstellt, während eine westliche Diät die Entwicklung von T2DM bei homozygoten Trägern der *p.Arg684Ter*-Variante vermutlich fördert. In der vorliegenden Studie sollte geklärt werden, wie sich arktische und westliche Diäten auf die metabolische Flexibilität, die Mechanismen der Insulinresistenz und die individuellen Beiträge der Skelettmuskulatur und des Fettgewebes auf die Regulierung der Ganzkörperglykämie auswirken. Daher wurden Ganzkörper- und gewebespezifische RabGAP-defiziente Mäuse während verschiedener Diätinterventionen metabolisch charakterisiert.

Die vorliegende Studie zeigt, dass eine arktische Ernährung *Tbc1d4*-defiziente (D4KO) Mäuse vor postprandialer Hyperglykämie schützt, indem sie die insulinstimulierte Glukoseaufnahme in der oxidative und glykolytische Skelettmuskulatur verbessert. Eine Proteomanalyse der Skelettmuskulatur zeigte, dass eine arktische Diät zu Veränderungen im intrazellulären Transport bei D4KO-Mäusen führt. Insbesondere wurde festgestellt, dass deubiquitinierende Enzyme und Proteine, die mit endosomalem Recycling in Verbindung stehen, in der Skelettmuskulatur erhöht sind, was auf einen möglichen Mechanismus der TBC1D4-regulierten Sortierung und des Abbaus von GLUT4 hinweist. Diese Ergebnisse deuten darauf hin, dass die arktische Diät das Entstehung von T2DM bei Personen mit homozygoten TBC1D4 p.Arg684Ter-Genvarianten verhindern kann, indem sie die genetisch bedingte Insulinresistenz der Skelettmuskulatur überwindet. Dies hebt die arktische Diät als einen potenziellen Ansatz für die Präzisionsmedizin hervor. Darüber hinaus führte die Fütterung mit der arktischen Diät zu einer erhöhten insulinstimulierten Glukoseaufnahme im Fettgewebe von Mäusen mit *Tbc1d1*-Defizienz und *Tbc1d1/Tb1cd4*-Defizienz, was mit einer geringeren Fettgewebsmasse einherging. So unterstreicht die aktuelle Studie die zentrale Rolle von TBC1D1 bei der Regulierung des Lipid- und Glukosestoffwechsels und weist auf eine potenzielle Schutzfunktion gegen ernährungsbedingte Fettleibigkeit und Insulinresistenz hin.

Table of contents

1. Introduction

1.1 Diabetes mellitus, obesity and insulin resistance

Diabetes mellitus is an endocrine disorder that manifests primarily as chronic hyperglycemia as a result from inadequate insulin secretion by pancreatic β-cells, insulin action in target tissues or a combination of both [1]. Long-term complications include cardiovascular disorders, including hypertension, which is associated with macro- and microvascular complications, and diabetic kidney disease. Other complications include diabetic retinopathy, leading to reduced or lost vision; peripheral neuropathy, leading to potential foot ulcers and amputation; as well as autonomic neuropathy resulting in gastrointestinal, genitourinary and sexual dysfunction [1, 2]. According to the International Diabetes Federation, 537 million adults worldwide were living with diabetes in 2021, but the incidence is steadily increasing, with the number of diagnosed cases projected to reach 783 million by 2045 [3]. Apart from gestational diabetes and specific monogenic forms, diabetes is classified into two main subtypes [4].

Type 1 diabetes mellitus (T1DM) is an autoimmune disease with progressive destruction of pancreatic β-cells. With a prevalence of 5-10%, T1DM usually begins in childhood [5] and often remains asymptomatic until a sudden onset characterized by weight loss, fatigue, blurred vision, polydipsia, -uria and -phagia and nocturnal enuresis [6]. When firstly diagnosed, 30-46% of children present with diabetic ketoacidosis due to delayed treatment as a result of lack of knowledge and awareness of diabetic symptoms [7–9]. Compared to type 2 diabetes mellitus (T2DM), T1DM is characterized by a lifelong dependence on insulin injections [10].

T2DM represents the predominant subtype of this metabolic disorder, affecting 90–95% of cases with a usual onset in adulthood [11]. Recent approaches have identified T2DM clusters according to clinical and genetic biomarkers that determine distinct diabetic complications and the clinical outcome [12, 13]. Genome-wide association studies (GWAS) have linked more than 83 genes to T2DM and another 53 genes to glucose and insulin concentrations [14, 15]. In addition to genetic predisposition, environmental factors such as nutrition and physical activity are crucial in the development of T2DM [16]. Additionally, increased body fat mass displays a major risk factor for the development of metabolic disorders such as T2DM [17].

Obesity is characterized by excessive visceral adiposity due to either hyperplasia with an increased number of adipocytes or hypertrophy with increased adipocyte size [18]. Furthermore, obesity is

defined by a body mass index (BMI) >30 kg/m² [19]. While 1.9 billion adults worldwide were overweight (BMI >25 kg/m²) in 2016, at least 650 million were obese [20]. The accumulation of visceral adipose tissue leads to chronic low-grade inflammation through the recruitment of macrophages, which release pro-inflammatory cytokines. Additionally, the secretion of specific adipokines from the visceral fat depot links obesity to insulin resistance in peripheral tissues. Despite the high expandability of adipocytes, their lipid storage capacity is limited. Thus, obesity is associated with ectopic fat accumulation and consequent lipotoxicity that promotes insulin resistance in the periphery [21].

Both T2DM and obesity are characterized by insulin resistance, an impaired response to insulin in target tissues: skeletal muscle, adipose tissue and liver. While glucose uptake by skeletal muscle and adipose tissue is decreased, glucose production by the liver is increased [22]. As a result, insulin secretion by β-cells is increased to maintain normoglycemia. Hyperinsulinemia further promotes insulin resistance by promoting hepatic *de novo* lipogenesis (DNL), hyperlipidemia, and expansion of white adipose tissue (WAT) [23]. Consequently, persistent insulin resistance leads to impaired β-cell function and eventual exhaustion [16]. Additionally, individuals with T2DM or obesity present with elevated plasma free fatty acid (FFA) concentrations [24, 25] and increased FFA uptake into skeletal muscle where lipid oxidation is impaired. This further promotes insulin resistance by increased hepatic and intramuscular lipid (IMCL) accumulation [26].

1.2 Impact of lifestyle on metabolic flexibility

The progression of T2DM is associated with impaired metabolic flexibility [27]. Metabolic flexibility defines the ability to adapt the selection and utilization of energy substrates according to the metabolic state, such as fasting or postprandial periods [28], and resting or high energy demand. Most commonly, the term metabolic flexibility is used to explain increased fatty acid (FA) and simultaneously decreased glucose oxidation during insulin resistance [29, 30]. Early studies confirmed metabolic inflexibility in individuals with T2DM and obesity, which exhibit increased glucose and decreased lipid oxidation during post-absorptive conditions [31-33].

1.2.1 Impact of nutritional state on metabolic flexibility

1.2.1.1 Metabolic flexibility in the post-absorptive phase

In the fasting state, energy is mobilized from glycogen and triglyceride stores in skeletal muscle, adipose tissue and liver. A shift from carbohydrate to lipid utilization preserves glucose for vital organs such as the brain, red blood cells and renal medulla that depend on glucose and essential amino acid utilization [34]. While metabolic flexibility maintains normoglycemia by reducing fasting insulin-stimulated glucose uptake into skeletal muscle and adipose tissue, it increases the utilization of non-esterified fatty acids (NEFAs) from white adipose tissue as well as abundant amino acids from hepatic amino acid metabolism [35]. Simultaneously, hepatic glycogenolysis and gluconeogenesis are elevated [36]. Within the first 24 hours of fasting, hepatic glycogen stores are depleted to maintain normoglycemia. After prolonged fasting, energy from adipose tissue and protein stores are utilized [37]. Prolonged fasting or starvation, which rarely occurs in healthy individuals [38], induces ketogenesis, the process of generating ketone bodies (KBs) from fatty acids. Controlled induction of ketogenesis can be enhanced by ketogenic diets, which are characterized by low-carbohydrate and high-fat content, and may offer a potential therapeutic approach for metabolic diseases such as obesity and T2DM [39, 40].

1.2.1.2 Metabolic flexibility in the postprandial phase

Metabolic flexibility in the postprandial state is highly dynamic and complex, regulated by large amounts of macronutrients and plasma concentrations of hormones, each with distinct peak concentrations and specific timeframes [41]. Besides insulin, hormones released from the gut, including bile acids, glucagon-like peptide-1 (GLP-1), fibroblast growth factor 19 (FGF19), and ghrelin, exert anti-inflammatory properties [42-45]. Leptin is secreted by adipose tissue in response to food ingestion and is known to regulate appetite and body weight [46]. However, leptin has also been shown to link nutritional status and inflammation by exerting pro-inflammatory effects [47]. Plasma leptin concentrations are proportional to adipose tissue mass in mice and humans [48, 49]. Obese individuals show elevated plasma leptin levels and resistance to leptin-induced satiety [50]. In the postprandial state, the skeletal muscle accounts for approximately 80% of insulin-stimulated glucose disposal [51, 52], suggesting a critical role of the skeletal muscle in the development of insulin resistance and progression of T2DM [23, 53]. Compared to lean subjects, overweight individuals show hyperinsulinemia after a mixed meal challenge [54] and elevated oxylipin concentrations after a high-fat meal [55]. Postprandial hyperglycemia and -lipidemia are associated

with low-grade inflammation, obesity, T2DM and non-alcoholic fatty liver disease (NAFLD). In modern society, the fed state is frequently maintained for more than 16 hours per day [41, 56], making management of the postprandial state is critical to maintaining metabolic health and flexibility.

1.2.2 Impact of nutrition on metabolic flexibility

The recommended macronutrient intake consists of 45–65% of calories from carbohydrates, 25–35% from fat, and 10–30% of calories from protein [57]. Studies have demonstrated the beneficial effects of specific dietary interventions on metabolic health and lifespan [58, 59]. For instance, caloric restriction has been shown to improve insulin sensitivity, oxidative capacity and reduce inflammation [60]. Other studies propose that dietary composition and balance, rather than total energy intake, determine aging processes [61, 62]. Changes in dietary habits have been linked to the prevalence of lifestyle-related diseases such as obesity, metabolic syndrome, cardiovascular diseases and T2DM [63, 64].

1.2.2.1 Westernization and T2DM

In modern times, low physical activity is regularly combined with a dietary pattern characterized by high caloric density with high amounts of saturated and trans fats as well as processed sugars [65, 66]. Western diets result in daily oscillations between glucose and FA oxidation (FAO) and high variability in plasma insulin concentrations [67]. Studies have shown that high-fat, high-carbohydrate, or combined high-fat high-carbohydrate diets promote the generation of reactive oxygen species (ROS) due to overnutrition, which induces excessive adenosine triphosphate (ATP) production and thus increases mitochondrial membrane potential [68]. Furthermore, plasma concentrations of lipopolysaccharides (LPS), interleukin (IL)-6, TNF-α levels, and expression of Toll-like receptors (TLRs) have been shown to be elevated with a Westernized diet, indicating postprandial inflammatory responses that contribute to the development of insulin resistance [69–73]. Therefore, a Western lifestyle is associated with the development of metabolic complications and diseases such as obesity, T2DM, NAFLD and atherosclerosis [74–76].

The human genome is highly conserved and lacks adaptation to significant dietary changes, particularly over the last centuries [77]. In non-westernized and hunter-gatherer populations, obesity and other metabolic diseases are rare when adhering to traditional lifestyles characterized by “Paleolithic” diets [78–81], consisting solely of unprocessed animal- and plant products [82]. The Western diet has been implicated as a major contributor to diet-induced metabolic

complications, mainly affecting the post-reproductive years [83], thus reducing selective pressure. Consequently, Western dietary patterns have been suggested to increase the risk for T2DM in individuals with a genetic predisposition [84].

1.2.2.2 Dietary carbohydrate restriction as potential treatment for metabolic diseases

Nutrition is crucial in the prevention of metabolic complications and essential in the management of metabolic diseases. Low-carbohydrate (LC) and ketogenic (KD) diets have been advocated for weight loss but are controversial for long-term maintenance [85, 86]. Although LC diets are recommended, their composition is highly heterogeneous and is generally defined as less than 45% or 100 g carbohydrate of daily macronutrients [87–89]. LC diets discussed include the Atkins, the Zone, the South Beach and the Paleo diets. Glucose control and lipid profiles have been shown to improve in individuals with T2DM on a Paleo diet [90, 91].

A KD is considered to be less than 50 g of carbohydrate pre day [88]. Such drastically reduced amounts of dietary carbohydrates result in enhanced mobilization of fat stores with enhanced KB production [92]. Traditional diets of hunter-gatherer populations are typically ketogenic, consisting of high amounts of protein (19–35% of energy), low amounts of carbohydrate (22–40% of energy), and similar or higher amounts of fat (28–58% of energy) compared to a Western diet [93]. Thus, initially elevated postprandial blood glucose and plasma insulin concentrations due to a Western diet were reduced in response to a traditional, low-glycemic and low-insulinemic diet [81, 94, 95]. Additionally, individuals subjected to KD have reduced blood pressure and hunger [87]. Studies have demonstrated anti-inflammatory properties of dietary amino acids, such as inhibition of pro-inflammatory NF-κB and oxidative stress, and reduction of LPS-stimulated TNF-α production [96-98].

Animal studies have yielded controversial results regarding the effects of LC diets and KD on metabolism and diabetes. On the one hand, a very low-carbohydrate diet resulted in elevated serum concentrations of fibroblast growth factor 21 (FGF21), KB, markers of white adipose tissue browning, brown adipose tissue (BAT) activation and hepatic lipogenesis in mice compared to a low-fat diet. Additionally, healthy and diabetic mice subjected to a high glycemic diet exhibited hyperinsulinemia, adiposity associated with decreased energy expenditure and increased hunger [99-102]. A KD was shown to increase the lifespan of mice [103]. On the other hand, a study in mice showed that long-term exposure to a KD resulted in impaired glucose tolerance, reduced insulin secretion associated with decreased β-cell mass, and evidence of hepatic steatosis [104].

Furthermore, diets high in essential BCAA have been associated with obesity, insulin resistance, and T2DM. Elevated plasma branched-chain amino acid (BCAA) concentrations have been linked to insulin resistance when associated with fat intake [105, 106].

Nevertheless, KD and low-glycemic diets may represent a promising approach to preventing metabolic complications in individuals with a genetic predisposition to T2DM or diet-related metabolic diseases.

1.3 Energy substrate metabolism in skeletal muscle, adipose tissue and the liver

The management of whole-body metabolism requires optimal storage, mobilization and utilization of energy substrates during resting or energy-demanding states and during fasting or postprandial periods [28]. Fats, proteins, and carbohydrates are macronutrients that provide energy to fuel the body in all physiological states [107]. ATP is ultimately catabolized from energy substrates that are preferentially utilized depending on the metabolic state. ATP can either be mobilized from endogenous stores or catabolized directly from macronutrient disposal [108, 109]. Fat at 9 kcal/g spares carbohydrate stores and represents a feasible fuel to meet increased energy demands such as during prolonged exercise or fasting [110]. Crosstalk between skeletal muscle, adipose tissue, and the liver is facilitated by neural, hormonal, and circulatory events to allow FA delivery from adipose tissue to muscle during endurance training [111]. During high-intensity exercise, FAO alone cannot meet the high energy demands. Therefore, protein, at 4 kcal/g, can provide approximately 10% of total ATP turnover during prolonged or high-intensity exercise [110, 111]. Carbohydrates, at 4 kcal/g, provide the optimal energy substrate during short-term exercise by optimizing glycogen storage, muscle fueling, and delaying muscle fatigue [110].

1.3.1 Glucose metabolism in skeletal muscle, adipose tissue and the liver

To generate ATP from glucose, insulin-stimulated glucose uptake by skeletal muscle and adipose tissue is followed by its phosphorylation by hexokinase to glucose 6-phosphate (G6P), the initial step of glycolysis, a process in which glucose is metabolized to pyruvate [112]. Pyruvate then enters the mitochondria to undergo the tricarboxylic acid (TCA) cycle in the mitochondrial matrix [113]. Oxidative decarboxylation generates NADH and CO_2 by converting pyruvate to acetyl coenzyme A (CoA), which enters the TCA cycle to generate ATP, NADH and flavin adenine dinucleotide ($FADH_2$) molecules. The rate of the TCA cycle is limited by the availability of NAD

and FAD and is inhibited by NADH. Under aerobic conditions, NADH and $FADH_2$ are further oxidized in the electron transport chain, the final process of ATP synthesis [114]. In the inner mitochondrial membrane, ATP is synthesized from NADH and $FADH_2$ [115]. During periods of oxygen deprivation, such as during high-intensity exercise, pyruvate is converted to lactate by lactate dehydrogenase [116, 117]. Lactate can be converted back to pyruvate by pyruvate dehydrogenase (PDH) and enter the TCA cycle as acetyl-CoA [118]. Moreover, lactate accumulation induces gluconeogenesis in liver and skeletal muscle [119].

In addition to glycolysis, insulin also induces glycogen synthesis by converting G6P to glucose-1-phosphate (G1P), which in turn is converted to uridine diphosphate (UDP)-glucose, which serves as a donor for glycogen synthesis [120]. In the postprandial state, insulin induces phosphorylation and subsequent inactivation of glycogen synthase kinase 3 (GSK-3) via Akt. Inhibition of GSK-3 results in increased glycogen synthase activity with concomitant dephosphorylation and inactivation of glycogen phosphorylase, which suppresses glycogenolysis and promotes glycogen accumulation in the liver and in skeletal muscle. To maintain normoglycemia and adequate energy supply during fasting, skeletal muscle and hepatic glycogen stores are targeted [121]. Compared to the liver, the skeletal muscle has approximately 4 times the glycogen storage capacity and accounts for nearly 79% of endogenous glycogen storage [122], thus playing a critical role in metabolic homeostasis.

1.3.1.1 Insulin-stimulated glucose uptake into skeletal muscle and adipose tissue

Glucose uptake into skeletal muscle and adipose tissue is regulated by the insulin-sensitive glucose transporter type 4 (GLUT4) [123, 124]. In response to elevated postprandial plasma glucose concentrations, pancreatic β-cells secrete insulin, which binds to the extracellular α-subunits of the heterotetrameric insulin receptor (IR) in the membrane of adipocytes and myocytes. Subsequently, the intracellular β-subunits of the IR are transautophosphorylated, resulting in phosphorylation of the insulin receptor substrate (IRS) on multiple tyrosine residues through interaction with the activated IR via a phosphotyrosine binding (PTB) module [125]. Phosphorylated IRS interacts with the regulatory subunit of phosphatidylinositol-3'-kinase (PI3K), p85, which recruits the catalytic p110α subunit. This initiates the phosphorylation of phosphoinositide (PI) lipids and the generation of PI(3,4,5)-trisphosphate from PI(4,5)-bisphosphate and PI(3,4)-bisphosphate from PI(4)-phosphate [126]. Subsequently, 3'-phosphoinositide-dependent kinase-1 (PDK-1) is activates Akt (protein kinase B) by phosphorylation of threonine 308 (T308) [127, 128]. Full activation of Akt

is additionally requires mTORC2-mediated phosphorylation of serine 473 (S473) [129]. Downstream targets of Akt include Rab GTPase-activating proteins (RabGAPs) TBC1D1 and TBC1D4, also known as Akt substrate of 160 kDa (AS160) [130, 131], which can be phosphorylated at multiple phosphorylation sites [132, 133]. TBC1D1 and TBC1D4 target Rab GTPases, which are crucial regulatory proteins of vesicular trafficking [134]. Several Ras-related in brain (Rab) proteins have been implicated in the trafficking of GLUT4, which facilitates glucose uptake into skeletal muscle and adipose tissue [135, 136]. GLUT4 cycles dynamically between intracellular compartments. In the unstimulated state, GLUT4 is located in intracellular storage vesicles (GSVs) [137]. Following insulin stimulation and glucose uptake, membrane-bound GLUT4 is incorporated into the endosomal recycling compartment (ERC) by endocytosis and transported by endosomes to the trans-Golgi network (TGN) for recycling or *de novo* synthesis [138].

Dysregulation of insulin signaling including insulin-stimulated glucose uptake in skeletal muscle and adipose tissue, is a prominent feature of T2DM [139]. Studies demonstrate reduced insulin action in obese individuals due to impaired insulin receptor signaling [140, 141] and blunted activation of several downstream targets such as insulin receptor substrate 1 (IRS1) and Akt [142]. Skeletal muscle insulin resistance is considered to be a driving force in the development of T2DM [53], occurring decades before the onset of β-cell failure and manifest T2DM [143]. While β-cell loss is irreversible, skeletal muscle insulin resistance can be improved [52] and therefore represents a target for therapeutic approaches.

1.3.1.2 Insulin-mediated inhibition of glucose production in the liver

The liver plays a critical role in the regulation and maintenance of systemic glucose homeostasis. In the postprandial state, the liver contributes to the regulation of glucose tolerance [144], while in the fasted state, the liver maintains normoglycemia by mobilizing stored glycogen to provide an adequate glucose supply [145].

Endogenous glucose production includes the process of *de novo* glucose production (gluconeogenesis), which accounts for 90% of hepatic glucose production, and glycogen hydrolysis (glycogenolysis) [146]. Insulin has been implicated in the regulation of hepatic glucose metabolism [147]. While gluconeogenesis is suppressed by approximately 20% in response to insulin, glycogenolysis is entirely diminished [148]. In the postprandial state, gluconeogenic substrates from adipose tissue and skeletal muscle, such as NEFAs, glycerol, and amino acids, are reduced

[149, 150]. While glucose is generally the primary inhibitor of hepatic glycogenolysis, insulin is a crucial activator of glycogen synthesis via multiple signaling pathways. Physiological hyperinsulinemia inhibits hepatic gluconeogenesis via Akt-mediated phosphorylation and inactivation of forkhead-box-O (FOXO)-1 [151, 152]. While in response to insulin Akt/FOXO1 gluconeogenic genes are down-regulated and hepatic gluconeogenesis is suppressed, lipogenesis is promoted [153, 154]. Furthermore, insulin-stimulated activation of Akt mediates phosphorylation and inhibition of GSK-3, which suppresses glycogen synthase [155]. Interestingly, studies have shown that insulin is crucial for glycogen synthesis but not for suppressing glycogenolysis *in vivo* [156].

In individuals with T2DM, gluconeogenesis is primarily responsible for elevated fasting blood glucose concentrations [157]. Hepatic glucose production is elevated in the fasted and postprandial states, the latter is generally associated with insulin resistance [145, 158]. Insulin resistance contributes to elevated hepatic glucose production, which subsequently promotes hyperglycemia in individuals with T2DM. Elevated blood glucose concentrations enhance carbohydrate response element-binding protein (ChREBP) signaling resulting in further activation of glycolytic genes [159]. Impaired inhibition of postprandial glucose production provides substrates for *de novo* lipogenesis and promotes hepatic lipid accumulation [160], which is characteristic of non-alcoholic fatty liver disease (NAFLD) [161]. Further progression of NAFLD to hepatic fibrosis and non-alcoholic steatohepatitis (NASH) increases morbidity and mortality [162]. In contrast, insulin counterregulatory hormones such as glucagon and catecholamines induce mobilization of stored glycogen via glycogen phosphorylase-regulated glycogen hydrolysis [163, 164].

1.3.2 The role of adipose tissue as in whole-body metabolism

Classically, there are two major depots of adipose tissues: white WAT and BAT, which have distinct metabolic roles [165].

WAT serves primarily as an energy reservoir. During periods of overnutrition the white adipose tissue stores excess energy, in the form of TAG in adipocytes, to fuel peripheral tissues during periods of increased energy demand or energy deficit. In lean individuals, the subcutaneous fat is the most prominent WAT depot, accounting for 80% of total adipose tissue mass, and functions primarily as a mechanical and thermal insulator [166, 167]. While subcutaneous WAT is associated with reduced metabolic risk, studies have shown that visceral adipose tissue activity determines metabolic risk [168, 169]. The visceral or abdominal adipose tissue is highly metabolically active

and critical in the development of metabolic syndrome and T2DM [170]. Located in the mesentery and omentum, it is and directly connected to the liver via the portal circulation and provides mechanical protection to the internal organs [171]. In contrast to BAT, WAT adipocytes usually consist of a single, large lipid droplet and few mitochondria [172]. BAT is characterized by multilocular lipid droplets, a high density of mitochondria and the expression of uncoupling protein 1 (UCP1) [173, 174]. UCP1 in mitochondria of brown adipocytes enables non-shivering thermogenesis by uncoupling ATP synthesis from oxidative phosphorylation to generate heat. It was believed to be abundant only in human infants, but studies have demonstrated metabolically active BAT in adults [175, 176]. BAT activation increases FAO and energy expenditure and thus has therapeutic potential in the treatment of metabolic disorders such as obesity and T2DM [177].

Dysregulated adipose tissue function due to weight gain has a crucial impact on the pathogenesis of insulin resistance and T2DM. Several studies demonstrate that metabolic dysfunction due to metabolically unhealthy adipose tissue, is reversible by lifestyle changes and therapeutic interventions that reduce inflammation and restore adipose tissue functionality [178, 179].

1.3.3 Fatty acid metabolism in skeletal muscle, adipose tissue and the liver

The availability of FA varies according to the nutritional state. In the postprandial state, FAs are provided by chylomicron from the circulation. In the fasted state, FAs are released from adipocyte energy stores. Insulin is a key regulator of FA metabolism enhancing lipogenesis, the storage of triacylglycerides (TAG), and suppressing lipolysis, the mobilization of stored TAG [180].

1.3.3.1 Insulin-stimulated storage of lipids

Insulin is a key regulator of lipogenesis by increasing intracellular glucose concentration, activating glycolytic and lipogenic enzymes and further increasing lipogenic gene expression [181, 182]. Under postprandial conditions, chylomicrons in the circulation are hydrolyzed by lipoprotein lipase (LPL), which is activated in adipocytes in response to insulin [180]. Subsequent disposal of FAs from the circulation to target tissues is facilitated by protein-mediated transport. In target tissues, fatty acid translocase/cluster of differentiation 36 (FAT/CD36), plasma membrane-associated fatty acid binding protein (FABPpm), and fatty acid transport proteins (FATP1 and 4) regulate FA uptake [183]. Additionally, FA are provided by glycolysis via *de novo* lipogenesis (DNL). However, DNL contributes significantly to TAG storage in adipocytes only when the energy demand for carbohydrates is exceeded, and therefore accounts for only about 10% of adipose tissue TAG in healthy individuals [184]. DNL is highly regulated by nutrition and in responsive to

hormonal changes. For storage in adipocytes, FA are re-esterified and insulin-stimulated glycolysis provides glycerol-3-phosphate for TAG synthesis [185].

Studies have shown that polyunsaturated FAs reduce the expression of lipogenic genes in the liver [186], whereas a high-carbohydrate diet enhances lipogenesis in the liver and adipose tissue [187]. Under conditions of energy surplus or when the energy storage capacity of adipocytes is exceeded, TAG can also accumulate in skeletal muscle and liver [181].

1.3.3.2 Insulin-mediated inhibition of lipid mobilization

Endogenous TAG stores are mobilized by lipolysis in response to fasting or high energy demands when glycogen stores are depleted. Hydrolysis of TAG in adipocytes produces NEFAs, which are released into the circulation via fatty acid transporters to undergo β-oxidation and serve as fuel for peripheral tissues [188]. Stored TAG and diacylglycerides are hydrolyzed by adipose triglyceride lipase (ATGL) and hormone-sensitive lipase (HSL) to release FA [189]. Monoacylglycerol lipase catalyzes the final step of TAG lipolysis, releasing FA and glycerol, which can be converted to KB and glucose, respectively, by the liver [190, 191] . Similar to lipids, KBs serve as an alternative fuel during fasting to conserve glucose. In target tissues, FA are oxidized by coupling with coenzyme A. Fatty acyl-CoA is converted to fatty acyl-carnitine for transport to mitochondria. In the mitochondria, acyl-carnitine undergoes β-oxidation to form acetyl-CoA, which serves as a substrate for the TCA cycle and NADH and $FADH_2$ for the electron transport chain [192].

Insulin is a key regulator of lipolysis by suppressing ATGL and HSL activity in Akt-dependent and independent manners [193-195]. Additionally, lipolysis has been shown to be suppressed via mTORC1-mediated decrease in ATGL transcription [196]. Elevated basal lipolysis and impaired insulin-induced inhibition of lipolysis have been associated with insulin resistance [197]. In individuals with obesity or T2DM, lipolysis has been shown to be impaired at multiple levels [198], which promotes lipid accumulation and reduces insulin action [199]. Moreover, individuals with obesity or T2DM have a reduced capacity for lipid oxidation in skeletal muscle [200], which has been attributed to reduced mitochondrial density due to reduced mitochondrial biogenesis [201]. However, other studies suggest that respiration, not mitochondrial biogenesis, is impaired in individuals with T2DM [202]. While FAO has been shown to be impaired in skeletal muscle of obese individuals [203], transport, uptake and storage of FAs are enhanced [204].

1.3.4 Amino acid metabolism in skeletal muscle, adipose tissue and the liver

Amino acids (AA) serve for protein biosynthesis and as a source of energy. They are categorized as non-essential and essential AA, which the latter of which cannot be synthesized by the body and must be supplied by nutrition. Non-essential AA are generated as intermediates in glycolysis and the TCA cycle. Essential AA from the diet or degradation from cellular proteins are deaminated to NH_4^+ and a carbon skeleton [205]. Cytotoxic NH_4^+ is excreted via the urea cycle or removed by synthesis of nucleotides or amino acids, while carbon skeletons generate ATP, glucose, and FA. During adequate energy supply, free amino acids can be transaminated to glutamate and pyruvate, enter the TCA cycle, and generate glucose and FA, contributing approximately 10–15% to ATP synthesis [205]. However, during periods of energy deprivation or ingestion of high-protein diets, ATP is largely synthesized from AA. The liver plays a key role in the metabolism of AA. The glucogenic amino acids, glutamine and alanine, comprise 30–40% of all circulating amino acids and are carbon and nitrogen carriers in the glucose-alanine and glucose-glutamine cycles [206]. In the post-absorptive state, glutamine and alanine serve for gluconeogenesis [207], while the hepatic contribution is about 30–40% and the renal contribution to gluconeogenesis is about 20–25%. While alanine-associated gluconeogenesis occurs exclusively in the liver, glutamine-associated gluconeogenesis occurs predominantly in the kidney [208]. Glutamine is mainly produced by skeletal muscle, which accounts for approximately 120 g of glutamine per day, depending on dietary intake and muscle activity [209]. Glutamine and alanine account for approximately 80% of the total AA released by skeletal muscle [210]. In addition to providing energy, AA are important regulators of cell growth, metabolism, and immune pathways [211]. Alterations in AA metabolism have been implicated in the development of obesity and T2DM [212].

1.3.4.1 The role of branched-chain amino acids in insulin resistance

Recently, BCAA catabolism has been associated with insulin resistance in obesity and T2DM. Studies have associated increased plasma BCAA concentrations with obesity and T2DM, highlighting circulating BCAA as potential biomarkers for T2DM [213-215]. However, the underlying mechanism of the association between increased plasma BCAA concentrations and insulin resistance remains unknown.

Protein turnover, namely the balance between protein synthesis and protein breakdown [216], in skeletal muscle, adipose tissue and liver is significantly influenced by plasma insulin and BCAA concentrations [217-219]. The BCAAs leucine, isoleucine, and valine contribute between 15% and

35% of total AA in skeletal muscle and have been shown to be involved in several metabolic processes and signaling pathways [220]. BCAAs are activators of the mTOR signaling pathway, thereby enhancing protein synthesis [221]. In healthy individuals, insulin-mediated suppression of protein breakdown results in decreased plasma BCAA concentrations [222]. Studies have shown that withdrawal of insulin results in a significant increase in plasma BCAA concentrations [223, 224], indicating the strong correlation between insulin and BCAAs. In individuals with insulin resistance, insulin-mediated suppression of protein catabolism is impaired, resulting in muscle wasting [225], which interestingly occurred independently of plasma BCAA concentrations [226]. In contrast, other studies indicate that insulin resistance promotes increases in plasma BCAA concentrations through impaired insulin-mediated inhibition of protein breakdown [227].

It is suggested that BCAAs act as signaling factors promoting insulin resistance via regulation of glucose and lipid metabolism as well as interorgan crosstalk [228-231].

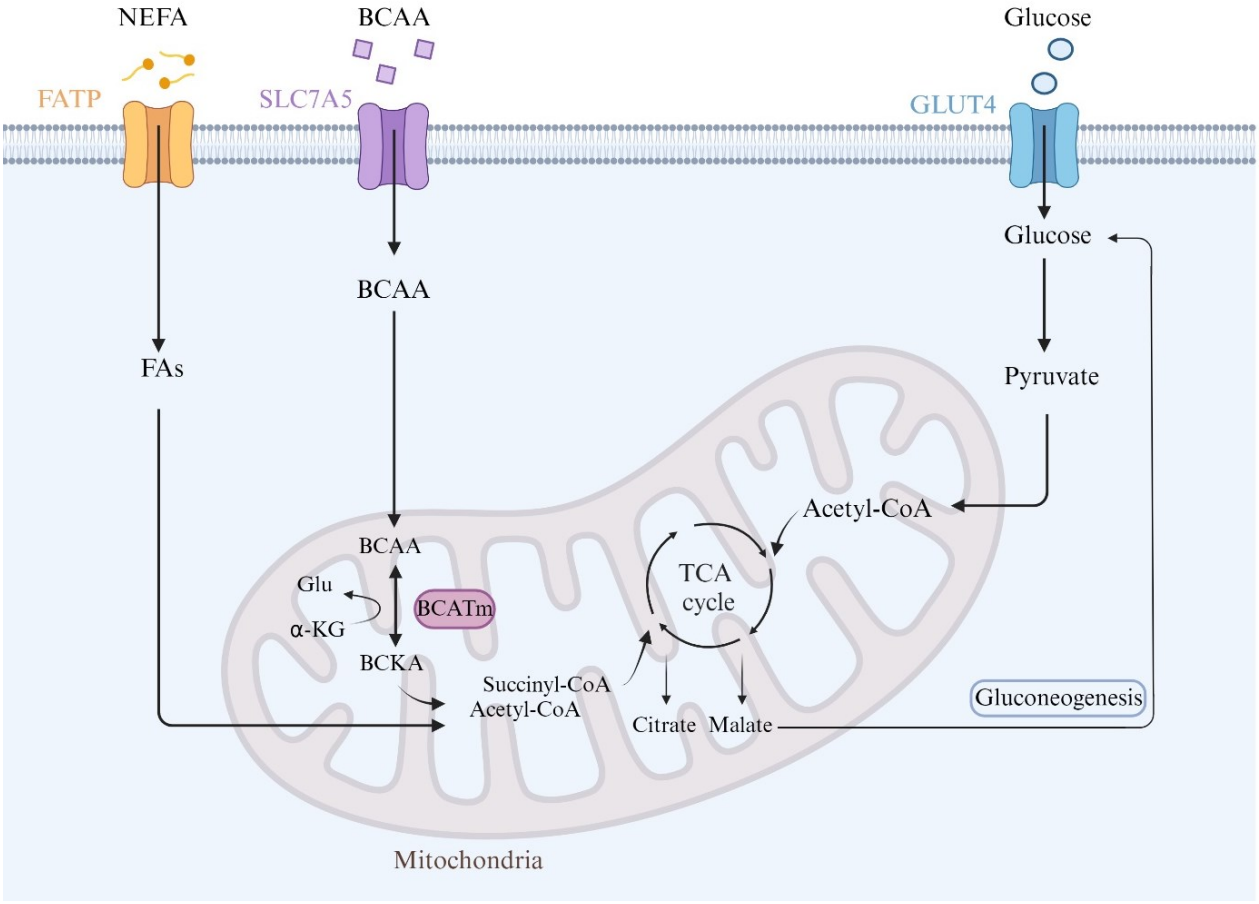

Figure 1: Interaction of energy substrates in skeletal muscle, adipose tissue and the liver. Following the ingestion of food, the following macronutrients are digested to provide energy substrates: carbohydrates, fat and protein. Carbohydrates are broken down into glucose, which is taken up by the cells in response to insulin, and provides pyruvate via glycolysis. In the mitochondrial matrix, pyruvate serves as a substrate for acetyl-CoA, which enters the TCA cycle to generate ATP. Fatty acids are taken up into the cells from circulating lipids or hydrolyzed from stored triglycerides via beta-oxidation and converted to acetyl-CoA in the mitochondrial matrix to enter the TCA cycle. Essential BCAAs from the diet or protein catabolism are taken up into the cells by specialized transporters and transaminated by branched-chain aminotransferase (BCAT) to branched-chain alpha-ketoacids (BCKAs). BCKAs are metabolized to acetyl-CoA or succinyl-CoA and enter the TCA cycle for oxidation. In addition to ATP synthesis, TCA cycle intermediates from energy substrates can also serve as substrates for gluconeogenesis [232]. α-KG: α-ketoglutarate, BCAA: Branched-chain amino acids, BCATm: mitochondrial branched-chain aminotransferase, BCKA: branched-chain alpha-ketoacids, CoA: Coenzyme-A, FA: fatty acids, FATP: fatty acid transporter protein, Glu: glutamate, GLUT4: glucose transporter type 4, NEFA: non-esterified fatty acid, SLC7A5: solute carrier family 7 member 5, TCA: tricarboxylic acid. Created by Biorender.com

1.4 The role of organ crosstalk in energy metabolism

Skeletal muscle accounts for approximately 40% of total body mass and thus plays a crucial role in energy metabolism [233]. Metabolic diseases are often associated with alterations in skeletal muscle metabolism [203]. Compared to lean individuals, individuals with obesity or T2DM show

impaired insulin-stimulated glucose uptake, oxidative metabolism, and TCA cycle flux in skeletal muscle [234]. However, accumulating evidence suggests that T2DM results from multiorgan insulin resistance and altered interorgan crosstalk via multiple metabolites acting as mediators [231].

1.4.1 Energy substrate-mediated crosstalk between skeletal muscle, adipose tissue and liver

Substrates and intermediates of energy substrate metabolism such as lipid species, AA, and ketoacids have been described to mediate organ crosstalk and to promote the development of insulin resistance [231].

One of the first signaling factors described to link obesity with insulin resistance and T2DM were FFA. FFA released from adipose tissue have been shown to induce lipotoxic effects and fat accumulation in liver and skeletal muscle and further lipotoxic effects in pancreatic β-cells [235, 236]. Specific circulating lipid species are biomarkers of ectopic lipid accumulation and T2DM [237]. FA such as palmitate impair oxidative glucose metabolism, non-oxidative glucose storage, and interfere with insulin signal transduction in skeletal muscle and liver [238, 239]. In addition to adipose tissue, the liver releases lipids into the circulation, contributing to organ crosstalk and potential peripheral insulin resistance [231].

Similar to FFA, AA have been shown to interfere with insulin signaling in both a direct (substrate-mediated) and indirect (hormone-mediated) manner [240, 241]. Studies have shown that increased plasma AA resulted in increased IRS-1 phosphorylation, but decreased PI3K activity in skeletal muscle in response to insulin as well as overactivated mTOR-mediated S6K phosphorylation. Similarly, the mTOR/S6K1 pathway is activated by AA in the liver [241]. Hepatic estrogen receptor α (ERα) is positively regulated by AA via mTOR signaling, which further leads to increased secretion of insulin-like growth factor-1 (IGF-1) [242]. Thus, studies highlight the contribution of AA to hepatic insulin resistance via estrogen and IGF-1 signaling [243]. Studies elucidating the effect of AA on adipose tissue showed no effect of AA on fasting FFA concentrations in lean individuals. However, in individuals with T2DM, AA positively correlated with adipose tissue sensitivity and decreased mTOR signaling. Furthermore, increased plasma AA concentrations have been associated with decreased expression of lipid storage enzymes in adipose tissue [244]. TCA cycle intermediates such as pyruvate, oxaloacetate, α-ketoglutarate as well as ketone bodies, β-ketoacid acetoacetate and β-hydroxybutyrate (βHB) are ketoacid derivatives of

AA and lipid metabolism that may additionally act as signaling factors for different tissues [245, 246].

1.4.2 The role of adipokines in interorgan-crosstalk

Adipose tissue accounts for approximately 10-15% of total body mass in normal-weight male adults and 20-30% in female adults, with variations due to age, ethnicity, genetics, and nutrition [247]. It is composed largely of adipocytes and preadipocytes, as well as endothelial cells, fibroblasts and immune cells such as macrophages and leukocytes [165].

In recent decades, adipose tissue has been recognized as a crucial endocrine organ secreting so-called adipokines, cytokines and chemokines [248]. These signaling factors allow communication between adipose tissue and other organs such as skeletal muscle, liver, pancreas and the brain [235]. Metabolically healthy adipose tissue secretes adipokines with insulin-like functions and potentially beneficial effects on glucose homeostasis during insulin resistance [249, 250]. Adipose tissue inflammation and the associated altered secretory profile are thought to contribute to the development of insulin resistance in obesity and T2DM [251]. Expanded adipose tissue has been shown to contribute to systemic insulin resistance by secreting pro-inflammatory cytokines such as TNFα, which has been shown to reduce adiponectin secretion, and IL-6, which decreases the effect of insulin on lipolysis and increases resistin release [235, 236, 252].

1.5 RabGAPs as key regulators of glucose and lipid metabolism

1.5.1 The impact of RabGAP-deficiency in humans

The closely related RabGAPs TBC1D1 and TBC1D4 have been described as key regulators of energy substrate utilization. The individual contribution and function of the two RabGAPs in metabolism has not yet been fully elucidated. While TBC1D1 has been suggested to play a crucial role in controlling exercise endurance, physical capacity and skeletal muscle development due to its association with meat production [253, 254], TBC1D4 has been suggested to regulate insulin sensitivity in skeletal muscle and adipose tissue [130, 131, 255].

To date, several RabGAP variants have been described in humans and linked to obesity, insulin resistance and T2DM. A TBC1D1 *R125W* variant was associated with susceptibility to obesity in humans [256]. Furthermore, severe insulin resistance was mediated by a TBC1D4 (*R363X*) mutation resulting in impaired GLUT4 translocation [257]. In addition, a common TBC1D4

p.Arg684Ter loss-of-function mutation was identified in Arctic populations in Greenland defining a specific T2DM subtype [258]. Homozygous carriers of the *p.Arg684Ter* variant present with postprandial hyperglycemia and reduced GLUT4 protein abundance in skeletal muscle. A high allele frequency of 17%, with 4% homozygous carriers indicates a positive selection for the *p.Arg684Ter* variant in these genetically isolated populations [259]. Interestingly, regular physical exercise has been shown to improve postprandial glycemia in homozygous carriers of the *p.Arg684Ter* variant [260], indicating lifestyle interventions as a potential non-pharmacological treatment in the prevention and management of T2DM.

1.5.2 RabGAP-deficient mouse models

Studies indicate that deficiency of either of the two RabGAPs, TBC1D1 or TBC1D4, in mice results in impaired insulin response and glucose tolerance. Furthermore, studies suggest a possible compensatory function of the remaining RabGAP in single RabGAP-deficient mice [130, 261, 262]. In contrast, double *Tbc1d1*- and *Tbc1d4*-deficient mice present with significantly impaired insulin- as well as AICAR (5-aminoimidazole-4-carboxamide ribonucleotide)-stimulated glucose uptake into skeletal muscle and primary white adipocytes. Consequently, the effect on whole-body glycemia is more severe compared to single RabGAP-deficient mice [131]. Studies in mice have proposed that TBC1D1 may affect fasting blood glucose concentrations by regulating β-cell function. Glucose-stimulated insulin secretion from β-cells was enhanced in response to TBC1D1-deficiency, indicating a possible negative regulation of TBC1D1 in insulin secretion [263, 264]. TBC1D4-deficiency in mice results in postprandial hyperglycemia, indicating distinct functions of the two RabGAPs in the regulation of whole-body glycemia [265, 266].

Despite high homology and overlapping functions, TBC1D1 and TBC1D4 have distinct expression patterns in skeletal muscle and adipose tissue [267]. In mice, *Tbc1d1* is highly expressed in skeletal muscle, predominantly in glycolytic skeletal muscle fibers as found in the *Extensor digitorum longus* (*EDL*) [261, 268, 269]. In contrast, *Tbc1d4* is highly expressed in adipose tissue and oxidative skeletal muscle fibers such as *Soleus* and the cardiac muscle [270, 271]. Consistent with the expression pattern, GLUT4 protein abundance in insulin-responsive tissues is reduced in response to RabGAP-deficiency [131]. Compared to mice, there are no differences in the expression pattern of the two RabGAPs described in human skeletal muscle [272]. Previous discussions postulate different effects of TBC1D1 and TBC1D4 regarding their regulation in substrate metabolism [273, 274]. RabGAP-deficient mice show a shift from glucose to FA

metabolism as indicated by enhanced FAO in skeletal muscle, which may be facilitated by increased SLC27A4/FATP4 abundance [130, 131, 261, 275].

To date, TBC1D1 and TBC1D4 have been shown to be crucial regulators of whole-body metabolism by controlling GLUT4-mediated glucose uptake in skeletal muscle and adipose tissue, as well as FAO in skeletal muscle. However, the exact functions of TBC1D1 and its close homologue TBC1D4 in glucose and lipid metabolism remain to be elucidated.

1.5.3 Regulators of cellular GLUT4 trafficking

GLUT4 translocation to the plasma membrane has been well described to require PI3K signaling followed by TBC1D4 phosphorylation in response to Akt activation [276]. TBC1D4 regulates the activity of Rab proteins, small GTPases that regulate intracellular trafficking events including vesicle budding, delivery, tethering and membrane fusion [134, 277]. Rab proteins cycle between an inactive guanosine 5'-diphosphate (GDP)-bound and an active guanosine 5'-triphosphate (GTP)-bound state and interact with three types of regulatory proteins. Guanine nucleotide exchange factor (GEF) and Rab GTPase-activating proteins (GAPs) and GDP dissociation inhibitor (GDI) enhance and inhibit Rab protein function, respectively. GEFs facilitate Rab activation by replacing GDP with GTP, whereas RabGAPs promote the hydrolysis of bound GTP to GDP, allowing Rab association with GDI, which induces Rab translocation to the cytosol [138]. Several Rab-GTPases have been described to regulate both exocytic and endocytic GLUT4 trafficking [278-280].

Additionally, the signaling architecture of GLUT4 trafficking involves assistance from cytoskeletal proteins such as filamentous actin (F-actin). Insulin induces the remodeling of actin filaments into a cortical network, which is required for GLUT4 translocation and involves PIP3 and downstream signaling components [281-283]. In addition, Cbl and Cbl-associated protein (CAP) are recruited by adaptor molecules containing pleckstrin homology (PH) and Src-homology 2 (SH2) (APS) domains [284]. Upon IR-mediated tyrosine phosphorylation of Cbl, CrkII and the GEF C3G are recruited to activate the GTP-binding protein TC10 [285, 286]. The downstream targets of TC10, neural Wiskott-Aldrich syndrome protein (N-WASP) and actin related protein-3 (Arp3), have been suggested to regulate actin polymerization [281], whereas GLUT4 vesicle attachment to the plasma membrane is regulated by the exocyst protein complex [287]. SNARE proteins subsequently mediate the fusion of GLUT4 vesicles with the plasma membrane to allow glucose uptake [288] (Figure 2).

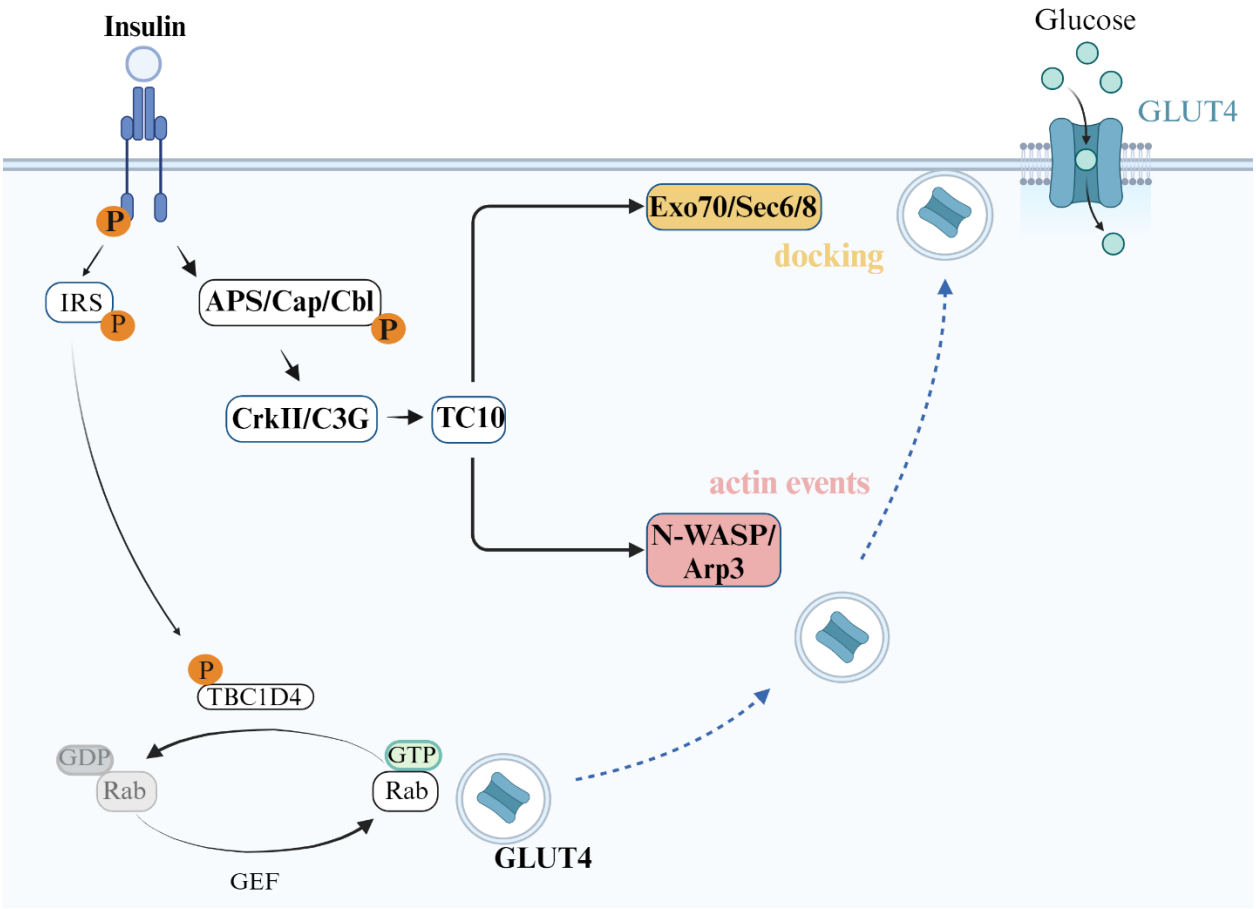

Figure 2: Insulin-mediated regulators of GLUT4 trafficking. In response to insulin, GLUT4 translocation to the plasma membrane requires IRS-mediated signaling for phosphorylation of TBC1D4 to initiate Rab-mediated trafficking of intracellular GLUT4-storage vesicles. Simultaneously, insulin initiates actin filament polymerization and GLUT4 vesicle tethering/docking to the plasma membrane. GLUT4 fusion with the plasma membrane allows glucose uptake. APS: adaptor molecules containing pleckstrin homology and Src-homology 2, Arp3: actin related protein-3, CAP: Cbl-associated protein, Exo70: Exocyst complex component, IRS: insulin receptor substrate, N-WASP: neural Wiskott-Aldrich syndrome protein. Created by Biorender.com

1.6 Aim of the study

Previous studies have demonstrated the regulatory function of the two RabGAPs TBC1D1 and TBC1D4 in whole-body glycemia. Studies indicate a strong association of TBC1D1 with the susceptibility to obesity and a role in skeletal muscle development [131, 132, 256], suggesting TBC1D1 as a candidate for lifestyle intervention studies. In Arctic populations, a common TBC1D4 *p.Arg684Ter* variant results in a loss-of-function mutation characterized by postprandial hyperglycemia and an increased risk of T2DM in homozygous carriers of the gene variant [258]. Similarly, *Tbc1d4*-deficient mice exhibit postprandial hyperglycemia and impaired insulin-stimulated glucose uptake in oxidative *Soleus* muscle and white adipose tissue [131, 266, 289, 290].

We hypothesized that the Arctic *p.Arg684Ter* gene variant represents an evolutionary adaptation to the traditional Arctic lifestyle characterized by a ketogenic diet, with a low-carbohydrate and high-protein and -fat content. Thus, a traditional Arctic diet may represent a potential approach to prevent the characteristic phenotype of *Tbc1d4*-deficient mice and present a possible treatment in precision medicine for homozygous carriers of the TBC1D4 *p.Arg684Ter* gene variant. To elucidate the impact of macronutrient ratios on whole-body glycemia, interorgan crosstalk, insulin resistance, and skeletal muscle development, the following key questions were addressed the in present study (Figure 3):

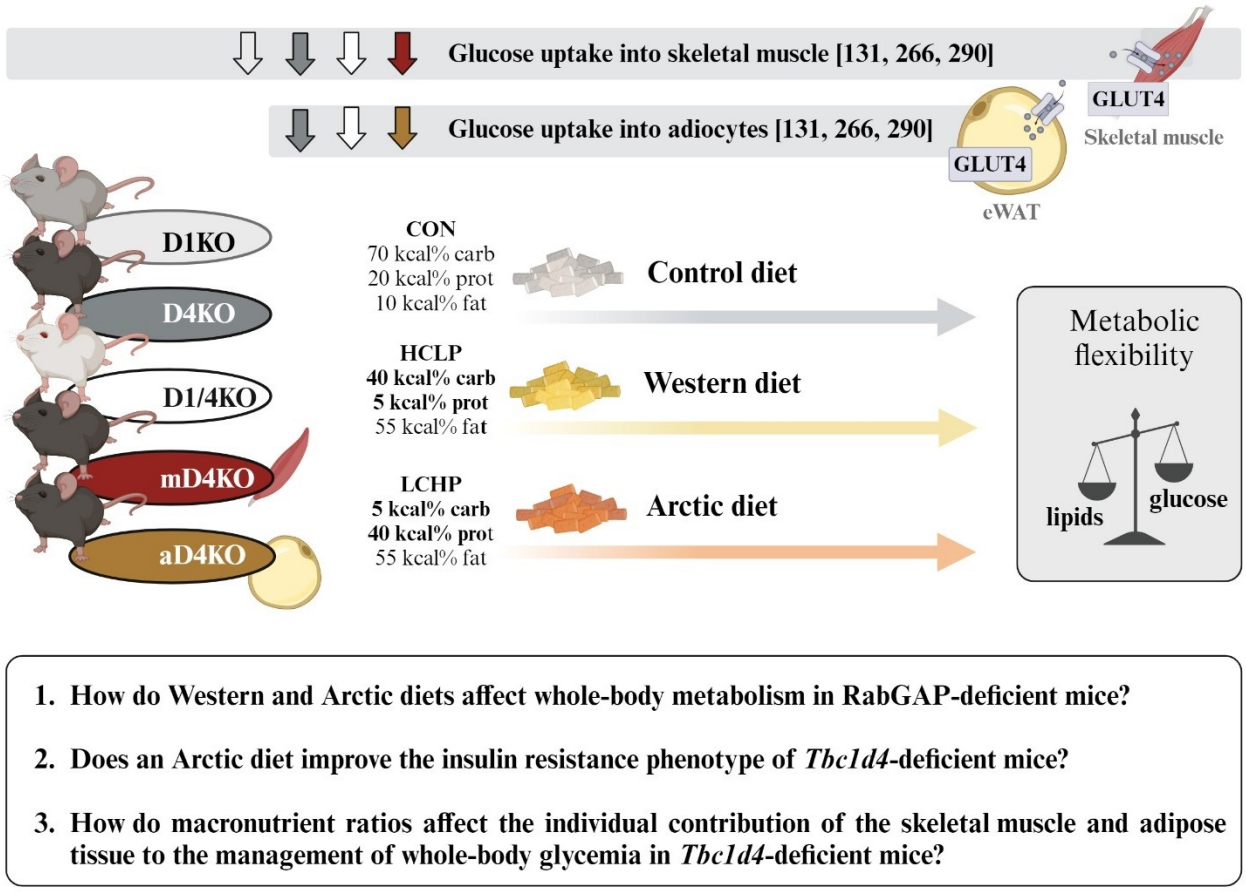

Figure 3: Study design for addressing key questions of the present study. In the present study, *Tbc1d1*- (D1KO), *Tbc1d4*- (D4KO) and *Tbc1d1/4*- deficient (D1/4KO) mice were metabolically characterized during dietary interventions to clarify the impact of Western and Arctic diets on whole-body glycemia. In addition, it was evaluated whether an Arctic diet is a potential approach to prevent the characteristic insulin resistance phenotype of D4KO mice. Lastly, muscle- (mD4KO) and adipocyte-specific (aD4KO) *Tbc1d4*-deficient mice were metabolically characterized to evaluate the individual contribution of skeletal muscle and adipose tissue to whole-body glycemia. Created by Biorender.com

2. Materials and methods

2.1 Materials

2.1.1Buffers and solutions

For the present study following buffers and solutions were used.

Table 1: Buffers and solutions

Buffer and solution	Composition
DNA isolation	
DNA lysis buffer	0.1 M Tris-HCl (pH 8.0), 0.2 M NaCl, 5 mM EDTA, 0.4% SDS
TE buffer	10 mM Tris-HCl (pH 8.0), 1 mM EDTA
Ex vivo glucose uptake into primary white adipocytes	
Krebs-Ringer-Bicarbonate HEPES buffer (KRBH)	Stock I: 118.5 mM NaCl, 4.7 mM KCl, 1.2 mM KH_2PO_4, 25 mM $NaHCO_3$, gassed with carbogen gas for 20 min on ice; Added Stock II: 2.5 mM $CaCl_2 \cdot 2 H_2O$, 1.2 mM $mgSO_4 \cdot 7 H_2O$, 5 mM HEPES, gassed with carbogen gas for 10 min on ice, 1% Bovine serum albumin (BSA) added
Lipid extract solution	78 Vol.% 2-propanol, 20 Vol.% heptane, 2 Vol.% sulphuric acid
Ex vivo glucose uptake into skeletal muscle	
Avertin solution	10mL MQ water, 250µL Avertin (10 g dissolved in 10mL 2-methyl-2-butanol)
Krebs-Henseleit buffer (KHB)	Stock I: 118.5 mM NaCl, 4.7 mM KCl, 1.2 mM KH_2PO_4, 25 mM $NaHCO_3$, gassed with carbogen gas for 20 min on ice; Added Stock II: 2.5 mM $CaCl_2 \cdot 2$ H_2O, 1.2 mM $mgSO_4 \cdot 7 H_2O$, 5 mM HEPES, gassed with carbogen gas for 10 min on ice, 1% BSA added
Hot incubation buffer	19 mM Mannitol, 1 mM 2-deoxyglucose

	+/- 120nM Insulin, 2.5 µCi/mL [^{3}H]-2-deoxyglucose, 0.7 µCi/mL [^{14}C]-mannitol (in KHB)
Incubation buffer	15 mM Mannitol, 5 mM Glucose +/-120nM Insulin (in KHB)
Recovery buffer	15 mM Mannitol, 5 mM Glucose (in KHB)
Rinse buffer	20 mM Mannitol, +/- 120nM Insulin (in KHB)
Western Blot	
Blocking solution	5% powdered milk, TBS-Tween (1x)
Electrophoresis buffer	25 mM Tris, 192 mM glycine, 0.1% SDS, 20 Vol% glycerol, 8% SDS, 10 mM EDTA
LaemmLi sample buffer (4x LSB)	0.25 M Tris, 6% DTT, 0.2% bromophenol blue (pH 6.8)
Separating gel buffer	1.5 M Tris, 0.4% SDS (pH 8.8)
Stacking gel buffer	0.5 M Tris, 0.4% SDS (pH 6.8)
TBS-Tween buffer (TBS-T, 1x)	10 mM Tris, 150 mM NaCl, 0.05 Vol.% Tween 20
Transfer buffer	25 mM Tris, 192 mM glycine, 20% methanol

2.1.2 Chemicals

Following chemicals were used throughout the present study.

Table 2: Chemicals

Chemical	Supplier
2-deoxyglucose	Sigma-Aldrich (St. Louis, MO, USA)
2-methyl-2-butanol	Sigma-Aldrich (St. Louis, MO, USA)
2-propanol	Applichem (Darmstadt, Germany)
5x HF Buffer	Mobidiag (Espo, Finland)
6x DNA Loading Dye	Thermo Scientific (Peqlab, Wilmington MA, USA)
10x Green Buffer	Thermo Scientific (Peqlab, Wilmington MA, USA)
Acrylamid 4K Solution (37. 5:1; 30%)	Applichem (Darmstadt, Germany)
Actraprid Penfill Insulin human	Novo Nordisk (Bagsværd, Denmark)
Adenosine	Sigma-Aldrich (St. Louis, MO, USA)

AICAR (5-Aminoimidazole-4-carboxamide ribonucleotide)	Toronto Research Chemicals Inc., (Toronto, Canada)
Albumin Fraction V (BSA)	Merck (Darmstadt, Germany)
Ammonium persulfate (APS)	Serva (Heidelberg, Germany)
Avertin (2,2, -Tribromoethanol)	Sigma-Aldrich (St. Louis, MO, USA)
Bromophenol blue	Applichem (Darmstadt, Germany)
Calcium chloride dehydrate ($CaCl_2$ 2 H_2O)	Merck (Darmstadt, Germany)
Chloroform	Applichem (Darmstadt, Germany)
Collagenase Type 1	Worthington Biochemical (Lakewood, NJ, USA)
Corn Oil	Sigma-Aldrich (St. Louis, MO, USA)
D-(+)-Glucose	Sigma-Aldrich (St. Louis, MO, USA)
Deoxynucleoside Triphosphate Set (dNTPs)	Roche (Mannheim, Germany
Dimethylsulfoxide (DMSO)	Applichem (Darmstadt, Germany)
Dinonyl Phthalate	PHYWE (Göttingen, Germany)
Dithiothreitol (DTT)	Carl Roth (Karlsruhe, Germany)
Dream Taq Polymerase	Thermo Scientific (Peqlab, Wilmington MA, USA)
Ethanol, absolute (EtOH)	Merck (Darmstadt, Germany)
Ethylenediaminetetraacetic acid (EDTA)	Carl Roth (Karlsruhe, Germany)
Ethylene glycol bis (2-aminoethylether)-N, N, N', N'-tetra acetic acid (EGTA)	Carl Roth (Karlsruhe, Germany)
Glucose (20%)	B Braun (Melsungen, Germany)
Glycerol	MP Biomedicals (Santa Ana, CA, USA)
Glycine	Applichem (Darmstadt, Germany)
HD Green fluorescent dye	Intas Science Imaging (Göttingen, Germany)
HEPES 4-(2-hydroxyethyl)-1-piperazineethanesulfonic acid	Sigma-Aldrich (St. Louis, MO, USA)
Heptane (Isomers)	Carl Roth (Karlsruhe, Germany)

Hydrochloric acid (HCL)	Carl Roth (Karlsruhe, Germany)
Magnesium sulfate heptahydrate ($MgSO_4$ 7 H_2O)	Merck (Darmstadt, Germany)
Mannitol	Applichem (Darmstadt, Germany)
Methanol	Carl Roth (Karlsruhe, Germany)
Phosphatase inhibitor tablets (PhosSTOP)	Roche (Mannheim, Germany)
Potassium chloride (KCl)	Merck (Darmstadt, Germany)
Potassium dihydrogen phosphate (KH_2PO_4)	Merck (Darmstadt, Germany)
Powdered milk	Carl Roth (Karlsruhe, Germany)
Proteinase Inhibitor Cocktail (cOmplete)	Roche (Mannheim, Germany)
Proteinase K	Carl Roth (Karlsruhe, Germany)
Rotiszint eco plus	Carl Roth (Karlsruhe, Germany)
Sodium acetate	Sigma-Aldrich (St. Louis, MO, USA)
Sodium chloride (NaCl)	Carl Roth (Karlsruhe, Germany)
Sodium dodecyl sulfate (SDS)	Carl Roth (Karlsruhe, Germany)
Sodium hydrogen carbonate ($NaHCO_3$)	Merck (Darmstadt, Germany)
Sodium sulfate (Na_2SO_4)	Merck (Darmstadt, Germany)
Sulphuric acid	Carl Roth (Karlsruhe, Germany)
N, N, N', N'-Tetramethylendiamine (TEMED)	Carl Roth (Karlsruhe, Germany)
Tris	Carl Roth (Karlsruhe, Germany)
Triton X-100	Sigma-Aldrich (St. Louis, MO, USA)
TRIzol™ RNA Isolation Reagent	Thermo Scientific (Peqlab, Wilmington MA, USA)
Tween 20	Applichem (Darmstadt, Germany)

2.1.3 Devices

Following devices were used throughout the present study.

Table 3: Devices

Device	Supplier
Centrifuge 5415 C	Eppendorf (Hamburg, Germany)
Centrifuge 5424 R	Eppendorf (Hamburg, Germany)
ChemiDoc XRS+	Bio-Rad Laboratories (Munich, Germany)
Contour Glucometer	Bayer (Leverkusen, Germany)
GelDoc XR+	Bio-Rad Laboratories (Munich, Germany)
iMARK Microplate Reader	Bio-Rad Laboratories (Munich, Germany)
Microbeta Counter	PerkinElmer (Waltham, MA, USA)
NanoDrop 2000	Thermo Scientific (Peqlab, Wilmington, MA, USA)
Shandon Excelsior	Thermo Fisher Scientific (Waltham, MA, USA)
Thermomixer Compact	Eppendorf (Hamburg, Germany)
TissueLyser II	Qiagen (Hilden, Germany)
Whole Body Composition Analyzer	Echo MRI (Houston, TX, USA)
TSE PhenoMaster, Indirect gas calorimetry	TSE systems (Berlin, Germany)

2.1.4 Primers

For the present study following primers were used.

Table 4: Primers for genotyping

Primer	Sequence 5'-3'
Tbc1d4	Fwd: AGTAGACTCAGAGTGGTCTTGG
	WT Rev: GTCTTCCGACTCCATATTTGC
	Geo Rev: GCAGCGCATCGCCTTCTATC
floxed	Tbc1d4fl_geno_Fwd9: CTGTGAAGCCAAGCAGAGGA
	CSD-loxF: GAGATGGCGCAACGCAATTAATG
	CSD-R: GTAGGGACCTAGTGATGGTGGTCTC

HSA-Cre	Fwd: GCGGTCTGGCAGTAAAAACTATC
	Rev: GTGAAACAGCATTGCTGTCACTT
Adiponectin-Cre	Fwd: CTAGGCCACAGAATTGAAAGATCT
	Rev: GTAGGTGGAAATTCTAGCATCATCC
	Col F: TCCAATTTACTGACCGTACACCAA
	Col R: CCTGATCCTGGCAATTTCGGCTA

2.1.5 Molecular weight size markers

Following molecular weight size markers were used throughout the present study for genotype (2.2.4.2–2.2.4.3) and Western Blot (2.2.3.8–2.2.3.10) analysis.

Table 5: Molecular weight size markers

Molecular weight size marker	Supplier
50 bp DNA ladder	Thermo Scientific (Peqlab, Wilmington MA, USA)
100 bp DNA ladder	Thermo Scientific (Peqlab, Wilmington MA, USA)
PageRuler Prestained Protein Ladder	Thermo Scientific (Peqlab, Wilmington MA, USA)

2.1.6 Mouse diets

Experimental diets used throughout the present study were purchased from Research Diets Inc. (New Brunswick, NJ, USA). Experimental animals were subjected to the diets after weaning at 3–4 weeks of age. The following table summarizes the dietary composition.

Table 6: Composition of mouse diets

	HCLP (D20092413)	LCHP (D20092414)	CON (20092415)
	kcal%		
Carbohydrate	**40**	**5**	70
Fat	55	55	10
Protein	**5**	**40**	20
kcal/gm	5.1	5.1	3.8

2.1.7 Mouse strains

The following mouse strains were used throughout the present study. B6.Tbc1d4^{tm1}-Tg(Adipoq-cre)$^{1Evdr/J}$ mice were kindly provided by Prof. Maria Grandoch (University Hospital, Düsseldorf, Germany)

Table 7: Mouse strains

Strain	Abbreviation	Supplier
C57BL/6J RCS.B6.SJL-Nob1.10$^{B6/SJL}$-*Tbc1d4*$^{+/+}$	WT	German Diabetes Center (DDZ), Düsseldorf, Germany
RCS.B6.SJL-Nob1.10B6/SJL-*Tbc1d4*$^{-/-}$	D4KO	DDZ, Düsseldorf, Germany
B6.Tbc1d4^{tm1}	floxed	DDZ, Düsseldorf, Germany
B6.Tbc1d4^{tm1}-Tg(ACTA1-cre)$^{79Jme/J}$	mD4KO	DDZ, Düsseldorf, Germany
B6.*Tbc1d4*^{tm1}-Tg(Adipoq-cre)$^{1Evdr/J}$	aD4KO	DDZ, Düsseldorf, Germany

2.1.8 Reaction Kits

Following reaction kits were used for the present study.

Table 8: Reaction Kits

Reaction kit	Supplier
Bio-Plex Pro Mouse Diabetes Adiponectin Assay	Bio-Rad Laboratories (Munich, Germany)
Bio-Plex Pro Mouse Diabetes 8-plex Assay	Bio-Rad Laboratories (Munich, Germany)
Bicinchoninic acid (BCA) Protein Assay Kit	Pierce (Rockford, IL, USA)
GoScript Reverse Transcription System	Promega (Madison, WI, USA)
GoTaq qPCR Master Mix	Promega (Madison, WI, USA)
Insulin (Mouse) Ultrasensitive ELISA	DRG Instruments (Marburg, Germany)
Autokit 3-HB (total ketone bodies)	Wako Chemicals (Neuss, Germany)
NEFA-HR (2) Assay Kit	Wako Chemicals (Neuss, Germany)
TGX^{TM} and TGX Stain-Free^{TM} FastCast^{TM} Acrylamide Kit	Bio-Rad Laboratories (Munich, Germany)
Western Lightning ECL Enhanced	PerkinElmer (Waltham, MA, USA)

Chemiluminescence Substrate	

2.1.9 Radioactive isotopes

Following radioactively labeled chemicals were used for determination of *ex vivo* insulin-stimulated glucose uptake into skeletal muscle (2.2.2.9) and primary white adipocytes (2.2.2.10).

Table 9: Radioactive isotopes

Isotope	Supplier
[^{3}H]-2-deoxyglucose	Hartmann Analytic (Brunswick, Germany)
[^{14}C]-D-glucose	Hartmann Analytic (Brunswick, Germany)
[^{14}C]-mannitol	PerkinElmer (Waltham, MA, USA)

2.1.10 Software

Following software were used throughout the present study for data analysis.

Table 10: Software

Software	Supplier
Bio-Plex-Manager 6.0	Bio-Rad Laboratories (Munich, Germany)
ConsensusPathDB	Max-Planck-Institute for Molecular Genetics (Berlin, Germany)
GraphPad Prism 10	GraphPad Software Inc (San Diego, CA, USA)
Image Lab 6.0.1	Bio-Rad Laboratories (Munich, Germany)
Microplate Manager 6	Bio-Rad Laboratories (Munich, Germany)
NanoDrop 2000	Thermo Scientific (Peqlab, Wilmington, MA, USA)
Proteome Discoverer 2.5	Thermo Fisher Scientific Inc. (Waltham, MA, USA)
Phenomaster	TSE Systems (Bad Homburg, Germany)

2.1.11 Antibodies

For the present study following antibodies were used for determination of protein abundance via Western blot (2.2.3.8–2.2.3.10).

Table 11: Antibodies

Antibody	Supplier, Catalog #	Dilution in TBS-T
Primary antibodies		
Anti-rabbit-AS160/TBC1D4	Abcam (Cambridge, UK), #ab189890	1:1000 + 5% milk powder
Anti-rabbit-FATP4	Abcam (Cambridge, UK), #ab200353	1:1000 + 5% milk powder
Anti-rabbit-GAPDH	Cell Signaling (Danvers, MA, USA), #2118	1:5000 + 5% milk powder
Anti-rabbit-GLUT4 Anti-rat-GLUT4	Custom-made (Sam Cushman, University of Oxford, UK) Custom-made (Helmholtz, Munich)	1:1000 + 5% milk powder 1:10 + 5% milk powder
Anti-rabbit-TBC1D1	Cell Signaling (Danvers, MA, USA), #4629S	1:1000 + 5% milk powder
Secondary antibodies		
Goat-anti-rabbit IgG	Dianova (Hamburg, Germany), #111-035-003	1:20.000 + 5% milk powder
Anti-rat	Custom-made (Helmholtz, Munich)	1:1000 + 5% milk powder

2.2 Methods

2.2.1 Study design

For the present study, experimental animals were subjected to a Control diet (CON) or two high-fat diets differing in their carbohydrate to protein ratio: a high-carbohydrate low-protein (HCLP) or a low-carbohydrate high-protein (LCHP) diet, after weaning. During the different dietary interventions, experimental animals underwent metabolic characterization.

2.2.2 Animal experiments

All experiments were approved by the Ethics Committee of the State Agency for Nature, Environment and Consumer Protection (LANUV, North Rhine-Westphalia, Germany; reference number 81-02.04.2019.A492).

2.2.2.1 General animal housing

Male mice were housed in Makrolon type III-cages (EBECO, Castrop-Rauxel, Germany) in groups of 2–6 animals at an environmental temperature of 22°C and a 12-hour light-dark cycle with lights off from 6 pm to 6 am. Animals had *ad libitum* access to their respective experimental diet (Table 6) and water and were kept in accordance with the National Institutes of Health guidelines for the care and use of laboratory animals.

2.2.2.2 Body composition via nuclear magnetic resonance (NMR)

Body composition of the animals was determined by NMR (Whole Body Composition Analyzer, Echo MRI, Houston, TX, USA). Body fat and lean mass were measured in duplicate with a 40-seconds interval between each measurement. Total body weight was determined using scales (Sartorius, Goettingen, Germany) and may differ from the sum of body fat and lean mass due to possible movement of the animal in then NMR tube and elimination of water content determination during the measurement.

2.2.2.3 Carbohydrate and fatty acid oxidation (indirect calorimetry)

The original technique of indirect calorimetry to measure carbohydrate and FAO was established in 1956 [291]. To measure the respiratory exchange ratio (RER) by indirect calorimetry the experimental animals are placed in individual cages in a calorimetric climate chamber system (TSE PhenoMaster, TSE Systems, Bad Homburg, Germany) for three days at a temperature of 22°C and a 12-hour light-dark cycle (lights turn on from 6 am to 6 pm) adapted to the general animal housing conditions. For data analysis, the 24-hour averages were calculated, excluding the first 24 hours of

acclimatization. The analysis of the calorimetric parameters includes VO_2, VCO_2, RER and voluntary activity, which are measured every 30 minutes at a constant flow rate of 0.4 L/min (sample flow rate of 0.38 L/min). CHO and FAO are calculated using the respiratory quotient and the corresponding equations: CHO = 4.585 x VCO_2 (L/min)–3.226 x VO_2; FAO = 1.695 x VO_2 (L/min)–1.701 x VCO_2 (L/min) [131, 292]. Voluntary activity is measured by the number of infrared light beam interruptions in the x/y axis using the Phenomaster system. Depending on the composition of the experimental diet, food intake is measured using the PhenoMaster software or manually by weighing the diet pellets before and after the measurement. To ensure a clear light/dark circle, the experimental animals are given an *ad libitum* excess of the experimental diet only during their naturally active phase (from 6 pm to 6 am).

2.2.2.4 Determination of blood glucose

To measure blood glucose concentrations, a small portion of the tail tip was cut off and glucose concentrations were assessed by using a glucose meter and glucose strips (Contour next blood glucose meter, Bayer, Leverkusen, Germany). Blood samples were collected in microvettes (Microvette CB 300 LH, Sarstedt, Nümbrecht, Germany) during the glucose tolerance tests (2.2.2.5), and 6 h fasted blood glucose (6 h FBG) measurements. Blood samples collected during a Fasting-Refeeding experiment (2.2.2.8) were collected in EDTA-covered microvettes (Microvette CB 300 K2 EDTA, Sarstedt, Nümbrecht, Germany). For further analysis, blood samples were centrifuged at 5000 xg for 5 minutes at 4°C. Blood plasma was then collected and stored at -80°C until further use.

2.2.2.5 Intraperitoneal glucose tolerance test (i.p. GTT)

To determine whole-body glucose tolerance, animals underwent an intraperitoneal glucose tolerance test (i.p. GTT) at 12 weeks of age. Animals were fasted overnight for 16 h prior to the experiment. Basal blood glucose levels were assessed, mice were weighed and injected with a sterile glucose solution (2 g/kg body weight, 20% solution). Blood glucose levels were then measured 15, 30, 60, 120, and 240 minutes after the injection. Blood samples were taken from the tail tip and processed for later analysis of plasma insulin levels. Blood glucose levels returned to basal levels after 240 minutes. During the experimental period, the animals were kept in individual cages without access to the experimental diet, but with *ad libitum* access to water.

2.2.2.6 Intraperitoneal insulin tolerance test (i.p. ITT)

To assess whole-body insulin sensitivity, random fed mice underwent an intraperitoneal insulin tolerance test (i.p. ITT). Basal blood glucose levels were measured and mice were injected with 1 U/kg body weight of insulin dissolved in 0.9% NaCl. Blood glucose concentrations were measured at 15, 30, and 60 minutes after the injection. During the test period, mice were individually caged without access to the experimental diet but with *ad libitum* access to water.

2.2.2.7 Intraperitoneal AICAR tolerance test (i.p. ATT)

To determine whole-body sensitivity to 5-aminoimidazole-4-carboxamide ribonucleotide (AICAR), intraperitoneal AICAR tolerance tests (i.p. ATT) were conducted in random fed 14-week-old mice. Basal blood glucose levels were measured and mice were injected with 250 mg/kg body weight of AICAR dissolved in 0.9% NaCl. Blood glucose concentrations were measured at 15, 30, and 60 minutes after the injection. During the test period, mice were individually caged without access to the experimental diet but with *ad libitum* access to water.

2.2.2.8 Fasting and Refeeding

To assess postprandial glycemia, a Fasting-Refeeding experiment was conducted in week 16 of the metabolic characterization. The animals were fasted overnight for 16 hours prior to the experiment. After 16 hours of fasting, body weight and basal blood glucose concentrations were measured. The mice were then refed with the respective experimental diets. Blood glucose concentrations were measured and blood samples were collected for later plasma analysis at 1, 2, and 4 hours after refeeding. Mice were housed in individual cages with *ad libitum* access to the experimental diet and water.

2.2.2.9 Ex vivo glucose uptake into isolated skeletal muscle

To assess glucose uptake into skeletal muscle *ex vivo,* the incorporation of radioactively labelled [^{3}H]-2-deoxyglucose (2-DOG) was measured. Animals were fasted for 4 hours prior to the experiment and anesthetized by intraperitoneal injection of 500 mg/kg body weight Avertin (Table 1). *Soleus* and *EDL* muscles were carefully isolated under anesthesia before animals were sacrificed by cervical dislocation to collect the remaining tissues. Isolated muscles were incubated in four different buffers (Table 1) at 30°C in a shaking water bath with a constant supply of carbogen gas (95% O_2, 5% CO_2). Muscles were incubated in small glass vials containing 1 mL of each buffer per muscle. Muscles were incubated with recovery buffer for 30 minutes. Thereafter, muscles were transferred to new glass vials containing incubation buffer for an additional 30 minutes. While one

muscle was incubated under basal conditions, the second muscle was incubated in buffer supplemented with 120 nM of insulin. Muscles were then incubated in basal or insulin supplemented rinse buffer for 10 minutes. Finally, *Soleus* and *EDL* muscles were incubated under basal or insulin-stimulated conditions in HOT buffer containing radioactively labelled [^{3}H]-2-DOG, and [^{14}C]-mannitol for 20 minutes. After the HOT incubation, tendons were removed from the muscles and frozen in liquid nitrogen before further processing.

For scintillation counting muscles were homogenized in 300 µL of lysis buffer (Table 1). 40 µL of the resulting protein lysate (2.2.3.5) were transferred to 1.5 mL of Rotiszint scintillation liquid (Table 2) to count the radioactivity of incorporated 2-DOG and [^{14}C]-mannitol in a scintillation counter (Beckman Coulter, Krefeld, Germany). 2-DOG uptake was calculated as counts per minute (cpm) that were normalized to protein concentrations as determined by BCA analysis (2.2.3.6). Glucose uptake values are given as nmol/ mg protein/20 min. The calculation considers extracellularly bound 2-DOG by the detection of the extracellular space with [^{14}C]-mannitol and subtraction from intracellular 2-deoxyglucose [293].

2.2.2.10 Ex vivo glucose uptake into isolated adipocytes

Glucose uptake into primary white adipocytes from epididymal WAT was assessed *ex vivo* by incorporation of radioactively labelled [^{14}C]-D-glucose. Adipocytes were isolated by dissecting epididymal WAT from mice followed by transfer to 3 mL of prewarmed (37°C) KRBH buffer containing 200 nM adenosine and 5% BSA (Table 1). 16 mg of collagenase diluted in 500 KRBH buffer were added to the sheared WAT and incubated for 1 hour at 37°C for collagenase digestion. The resulting cell lysate was filtered through 400 µm polyamide nylon mesh into a falcon tube and centrifuged at 50 xg for 1 minute at RT. After centrifugation the upper layer contained white adipocytes and the lower aqueous phase was discarded. The cells were shortly centrifuged for three times with 5 mL of freshly added KRBH buffer. After washing, equal volumes of adipocytes and KRBH buffer were combined to a final 6.25% adipocyte cell suspension. Subsequently, 200 µL of adipocyte suspension and KRBH buffer were incubated with or without 120nM of insulin shaking for 30 minutes at 37°C in a water bath. To assess glucose uptake, the adipocyte suspension was incubated with 0.1 µCi/µL [^{14}C]-D-glucose for 30 minutes at 37°C. After incubation, 280 µL of adipocyte suspension were transferred to small tubes supplemented with 125 µL of dinonyl phthalate oil and centrifuged at 9391 xg for 10 minutes at RT to remove excess radioactivity and stop glucose uptake. After centrifugation, the upper part of the tube containing the adipocytes was

cut off and transferred to counting vials containing 3 mL of Rotiszint scintillation liquid (Table 2). Vials were incubated for 30 minutes at RT, rotating overhead, before measuring the incorporated [^{14}C]-D-glucose in a scintillation counter (Beckman Coulter, Krefeld, Germany). The resulting values were given as counts per minute (cpm) and normalized to the lipid weight of the samples. For quantitative determination of lipid weight, 200 µL of adipocyte suspension were transferred to 2.7 mL of lipid extract solution (Table 1) and stored overnight at 4°C. After the addition of 1.2 mL heptane and 800 µL ddH_2O, samples were vortexed and centrifuged at 201 xg for 5 minutes at RT. Subsequently, 1mL of the supernatant was transferred to tared glass tubes (Rotilabo-test tubes, Carl Roth, Karlsruhe, Germany). Samples were dried and evaporated by heating and gassing with nitrogen for 15 minutes using a Reacti-Therm and Reacti-Vap Evaporating Unit (Pierce, Rockford, IL, USA). Samples were measured in quintuple for basal and insulin-stimulated conditions and final values were given as cpm/ mg lipid. This assay was kindly performed by Anette Kurowski and Heidrun Podini.

2.2.3 Biochemical methods

2.2.3.1 Determination of plasma insulin concentrations

For quantitative determination of plasma insulin concentration, the Insulin (Mouse) Ultrasensitive ELISA Kit (Table 8) was used according to the manufacturer's instructions. This method is based on an enzyme-linked immunoassay using a 96-well plate coated with anti-insulin antibody and a horseradish peroxidase (HRP)-coupled secondary antibody that catalyzes the oxidation of 3,3',5,5'-tetramethylbenzidine (TMB). TMB was additionally added to form a violet substrate that was read colorimetrically at 450 nm (iMark Microplate Absorbance Reader, Bio-Rad, Hercules, CA, USA). Samples were measured as a single measurement due to low sample volume and values were given as µg/l.

2.2.3.2 Determination of plasma ketone bodies

A photometrical assay kit was used for the quantitative determination of plasma ketone body concentrations, as a sum of acetoacetate (AcAc) and 3-hydroxybutyrat (3-HB) (Table 8). The method is based on the cyclic conversion of AcAc and 3-HB to 3-HB and AcAc, respectively, in the presence of 3-HB dehydrogenase, NADH, and thio-NAD. As a result, NAD and thio-NADH are produced. The total ketone body content is determined by spectrophotometrical measurement of Thio-NADH.

4 µL of each plasma sample were pipetted into a 96-well plate and incubated with 135 µL of enzymatic reagent R1 for 5 minutes at 37°C. Subsequently, 45 µL of enzymatic reagent R2 were added to each well and the samples were further incubated for 2 minutes at 37°C. The absorbance of the samples was measured at 415 and 595 nm (iMARK Microplate Absorbance Reader, Bio-Rad, Hercules, CA, USA) and the values were given as µmol/l.

2.2.3.3 Determination of plasma free fatty acids

To determine total concentration of plasma NEFAs, the NEFA-HR (2) Assay Kit (Table 8) was used according to the manufacturer's instructions. Plasma samples were diluted 1:2 with ddH_2O, incubated with 100 µL enzyme reagent A for 15 minutes at RT, followed by incubation of 15 minutes at RT with 50 µL of enzyme reagent B. By converting free fatty acids to Acyl-CoA, catalyzed by peroxidases, a blue colored substrate was generated. Samples were measured in technical duplicates and absorption was assessed at 560 nm (iMARK Microplate Absorbance Reader, Bio-Rad, Hercules, CA, USA). Total values were given as mmol/l.

2.2.3.4 Determination of plasma diabetes biomarker concentrations

For determination of plasma concentrations of diabetes biomarkers ghrelin, Glucose-dependent insulinotropic polypeptide (GIP), Glucagon-like peptide-1 (GLP-1), glucagon, insulin. leptin, Plasminogen activator inhibitor-1 (PAI-1) and resistin, the Bio-Plex Pro Mouse Diabetes 8-plex Assay (Table 8), a magnetic bead-based multiplex immunoassay, was used according to manufacturer's instructions. Analysis was performed using a Bio-Plex200 suspension array system (Biorad). Total concentrations were calculated with optimized standard curves using the Bio-Plex-Manager-Software version 6.0 (Biorad). This assay was kindly performed by Martina Schiller.

2.2.3.5 Preparation of protein lysates from murine tissue

Frozen muscle tissue (*EDL*, *Soleus*) was transferred into a 2 mL Safe-Lock tube with a steel ball and 300 µL of lysis buffer (Table 1) were added. Muscle and liver samples were homogenized for 5 minutes at 25 Hz using a TissueLyser (Qiagen, Hilden, Germany) and subsequently centrifuged at 15871 xg for 10 minutes at 4°C. The supernatant was transferred to a new 1.5mL Eppendorf tube and centrifuged again for 10 minutes at 4°C. The final supernatant was used immediately for quantitative determination of protein content via BCA (2.2.3.6) or stored at -80°C for later use.

2.2.3.6 Determination of protein concentration

For quantitative determination of protein content, the BCA Protein Assay Kit (Table 8) was used according to the manufacturer's instructions. This method is based on the Biuret reaction. A violet complex is formed by the reduction of Cu^{2+} ions interacting with proteins and BCA. Samples were diluted 1:20. Protein concentration was measured colorimetrically in technical duplicates at 560 nm (iMARK Microplate Absorbance Reader, Bio-Rad, Hercules, CA, USA).

2.2.3.8 Sodium-dodecylsulfate-polyacrylamide gel electrophoresis (SDS-page)

Proteins from lysates (2.2.3.5) were separated electrophoretically according to the molecular weight by denaturating sodium dodecylsulfate-polyacrylamide gel electrophoresis (SDS-PAGE). Thus, 20 µg of protein from lysates were diluted with ddH2O and 4x LSB (Table 2) to a total volume of 20 µL. Samples were shortly vortexed and denatured for 30 minutes at RT. Subsequently, *EDL* and *Soleus* samples were briefly centrifuged and loaded onto 10% SDS gels (Table 12) or stain-free gels (Table 13) (Protein Gels, Bio-Rad, Hercules, CA, USA), respectively. A pre-stained protein ladder (Table 5) was used to determine the molecular weight of separated proteins. Electrophoretic separation was performed at an initial 50 V for 15 minutes and 150 V for 45–60 minutes in electrophoresis buffer (Table 1) using the Mini-PROTEAN Tetra Vertical Electrophoresis Cell System (Bio-Rad, Hercules, CA, USA).

Table 12: Composition of SDS-gels

Compound	Separating gel (10%)	Stacking gel
Acrylamide (30%)	3 mL	390 µL
Ammonium persulfate (APS, 50%)	18 µL	6 µL
ddH_2O	3.66 mL	1.83 mL
Separation buffer (Table 1)	2.34 mL	
Stacking gel buffer (Table 1)		780 µL
TEMED	9 µL	3 µL

Table 13: Composition stain-free gels

Compound	Separating gel (10%)	Stacking gel
Resolver A	4mL	
Resolver B	4mL	
Stacker A		1.5mL
Stacker B		1.5mL
TEMED	4µL	3µL
Ammonium persulfate (APS, 10%)	40µL	15µL

2.2.3.9 Immunochemical protein detection

After electrophoresis, the separated proteins from the SDS gel were transferred to nitrocellulose membranes for 2 hours at 0.2 A using tank blots (Tankblot Eco-Mini, Biometra, Göttingen, Germany). Subsequently, non-specific antibody binding sites were covered by blocking the membrane for 1 hour with 5% fat-free powdered milk in TBS-T (Table 1). The membrane was briefly washed 3 times with TBS-T and incubated with the respective primary antibody (Table 11) overnight in cold at approximately 7°C shaking. After incubation, the membrane was shortly washed 3 times followed by TBS-T incubation for 30 minutes. After washing, the membranes were incubated with a primary antibody-dependent secondary antibody (Table 11) for 1 hour. After another incubation with TBS-T for 30 minutes, protein-bound antibodies were detected with Western Lightning ECL Pro or Ultra solution (Table 8) and visualized using the ChemiDoc Western Blot documentation system (Table 3). Quantitative analysis was performed using the Image Lab software (Table 10).

2.2.3.10 Immunochemical protein detection using stain-free gels

To normalize protein abundance to a non-heterogeneous housekeeping protein in *Soleus* muscle, normalization to the total protein content was performed. Therefore, proteins were separated in stain-free gels by SDS-PAGE (2.2.3.8). The total protein content was then detected by UV radiation using the ChemiDoc before transfer to nitrocellulose membranes. Subsequent antibody incubation and detection of proteins was performed as previously described (2.2.3.9).

2.2.4 Molecular biological methods

2.2.4.1 Isolation of genomic DNA from murine tail tips

To determine the genotype of the experimental animals, ear notches were collected from the animals after weaning. Genomic DNA was then isolated. Biopsies were incubated with 200 µL lysis buffer supplemented with 10 µL Proteinase K, at 1200 rpm and 55°C overnight in a Thermomixer (Table 3). To remove cell debris, samples were centrifuged at 9391 rcf for 1 minute at RT. 150 µL of the supernatant were transferred to a new 1.5 mL Eppendorf tube. For DNA extraction, 200 µL of isopropanol were added and samples were centrifuged at 9391 rcf for 10 minutes at RT. The supernatant was removed and the DNA-containing pellet was washed by adding 200 µL of 75% ethanol followed by centrifugation at 9391 rcf for 5 minutes, after which the supernatant was removed and the pellet was incubated at 55°C for 15 minutes to evaporate the remaining ethanol. Samples were eluted with 100 µL TE buffer (Table 1) for 5 minutes at 55°C in a Themomixer prior to DNA concentration determination using the Nanodrop (Table 3).

2.2.4.2 Polymerase Chain Reaction (PCR)

To verify the genotype of the experimental animals, the genetic region of interest was amplified by polymerase chain reaction (PCR). First, double-stranded DNA is denaturated at 98°C, breaking the hydrogen bonds between the nucleic bases to generate single-stranded DNA. Subsequently, forward and reverse primers anneal at 65°C to elongate and synthesize complementary strands with dNTPs. The following PCR reactions were performed to determine the genotype of whole-body *Tbc1d1/4*-deficient mice, muscle- or adipose tissue-specific *Tbc1d4*-deficient mice, overexpressing the HSA- and Adiponectin-Cre recombinase, as well as mice carrying floxed *Tbc1d4* alleles.

Table 14: PCR reaction setup for RCS-*Tbc1d1*

Compound	Volume (µL)	Stock concentration
MQ H2O	5.8	
HF Buffer 5x	4.0	
dNTPs	2.0	8 mM
SJL forward	1.0	10 nM
SJL reverse	1.0	10 nM
B6 forward	1.0	10 nM
B6 reverse	1.0	10 nM

Phusion-Taq	0.2	2 U/µL
DNA	4.0	10 ng/µL

Table 15: PCR reaction setup for the *Tbc1d4* knockout

Compound	Volume (µL)	Stock concentration
MQ H2O	5.8	
GreenGoTaq-Buffer 10x	4.0	
dNTPs	2.0	8 mM
Tbc1d4 forward	2.0	10 nM
Tbc1d4 WT reverse	1.0	10 nM
Tbc1d4 Geo reverse	1.0	10 nM
Dream Taq Green	0.2	2 U/µL
DNA	4.0	10 ng/µL

Table 16: PCR reaction setup for the HSA-Cre recombinase

Compound	Volume (µL)	Stock concentration
MQ H2O	7.8	
GreenGoTaq-Buffer 10x	4.0	
dNTPs	2.0	8 mM
Cre forward (oIMR1084)	1.0	10 nM
Cre reverse (oIMR1085)	1.0	10 nM
Dream Taq Green	0.2	2 U/µL
DNA	4.0	10 ng/µL

Table 17: PCR reaction setup for the Adiponectin-Cre recombinase

Compound	Volume (µL)	Stock concentration
MQ H2O	5.8	
HF Buffer 5x	4.0	

dNTPs	2.0	8 mM
iIMR7338	1.0	10 nM
iIMR7339	1.0	10 nM
Col 12249	1.0	10 nM
Col 12250	1.0	10 nM
Phusion-Polymerase	0.2	2 U/µL
DNA	4.0	10 ng/µL

Table 18: PCR reaction setup for the floxed *Tbc1d4* allele

Compound	Volume (µL)	Stock concentration
MQ H2O		
HF Buffer 5x		
DMSO		
dNTPs	0.5	8 mM
Tbc1d4fl_Geno_Fwd9	0.5	10 nM
CSD-loxF	0.5	10 nM
CSD-R	1.0	10 nM
Phusion-Polymerase	0.2	2 U/µL
DNA	2.0	10 ng/µL

2.2.4.3 Agarose gel electrophoresis

The resulting PCR products were separated and visualized by agarose gel electrophoresis with 1% (floxed) or 2% (*Tbc1d1*, *Tbc1d4*, *Cre*) agarose gels supplemented with 4.5µL/100mL of the fluorescent dye HD Green (Table 2). HD Green allows visualization of DNA fragments under UV irradiation by intercalating into the DNA double helix. For *Tbc1d1*, Adiponection-Cre and floxed PCR products, 4µL of 6x Loading dye was added after the PCR reaction. PCR products were separated in an electrophoresis chamber at 120 V for 30 minutes. PCR fragments were then visualized using the GelDoc UV gel imager (Table 3).

2.2.5 Histological methods

2.2.5.1 Paraffin embedding of murine white adipose tissue

Epididymal adipose tissue was collected from experimental animals and transferred to a cassette for overnight fixation in 4% paraformaldehyde. Subsequent embedding was performed using the Shandon Excelsior (Thermo Fisher Scientific., Waltham, MA, USA). Tissue dehydration under vacuum was kindly performed by Carmen Weidlich according to the following protocol:

Table 19: Paraffin embedding protocol

Process	Time
EtOH 70%	1 hour
EtOH 70%	1 hour
EtOH 96%	1 hour
EtOH 96%	1 hour
EtOH absolute	1 hour
EtOH absolute	2 hours
Xylol	1 hour
Xylol	1 hour
Xylol	1 hour
Paraffin	1 hour
Paraffin	1 hour
Paraffin	2 hours

2.2.5.2 Hematoxylin and eosin (HE) staining of white adipose tissue sections

To visualize adipocytes of epididymal adipose tissue, 10 µm thick sections were kindly prepared by Carmen Weidlich. For subsequent Hematoxylin and Eosin (HE) staining, tissue sections were deparaffinized and rehydrated to allow adipocyte staining according to the following steps:

Table 20: HE-staining protocol

Process	Time
Xylol	5 minutes
Xylol	5 minutes
EtOH absolute	5 minutes
EtOH absolute	5 minutes
EtOH 96%	5 minutes
EtOH 96%	5 minutes
EtOH 70%	5 minutes
EtOH 70%	5 minutes
H_2O (bidestilate)	shortly
Mayer's Hemalum solution	2 minutes
H_2O (bidestilate)	shortly
Tap water	10 minutes
EtOH 70%	2 minutes
0.1% eosin in EtOH 70% +50µL acetic acid 99%/ 100mL	30 seconds
EtOH 96%	shortly
EtOH 96%	2 minutes
EtOH absolute	2 minutes
EtOH absolute	2 minutes
Xylol	5 minutes
Xylol	5 minutes
EZ-Mount	

2.2.5.3 Imaging and quantification of adipocytes

HE staining allowed visualization of adipocytes. For quantification and determination of adipocyte size, images were taken with a VS200 Slide Scanner (Olympus, Tokyo, Japan) at a 40x resolution. Adipocyte size (μm^2) was analyzed using the open-source Software QuPath plugin with ImageJ

with the following settings Area min. (sq µm): 400; Area max (sq µm): 15,000; Circularity min: 0.4; Circularity max: 1.00; "Check if inversion is needed".

2.2.6 Proteome analysis

2.2.6.1 Proteomic profiling of skeletal muscle

For proteomic profiling, muscle tissue was ground on liquid nitrogen. Proteins were solubilized in denaturing SDS buffer (100 mM Tris-HCl, 4% SDS and 20 mM DTT, supplemented with CompleteTM (Roche) and Phosphatase Inhibitors (Sigma)), using a PrecellysTM (Bertin) homogenizer (soft program: 5,800 rpm for 2 x 15 s with 30 s pause; ceramic bead mix (#P000918-LYSKO-A.0, Bertin)). After sonication–2 x pulse 0.09sec_10sec (Sonoplus, Bandelin), samples were centrifuged at 75,000 xg for 30min at 4°C and the supernatants were transferred to new reaction tubes. Protein concentrations were determined by direct photometric measurements (NanoDrop, ThermoFisher Scientific). Subsequently, 200 µg of protein was digested with LysC/trypsin mix (1:25 w/w, Promega) using miniS-TrapTM columns (ProtiFi) according to the manufacturer's recommendations. 100 µg of the resulting peptides were fractionated (eight fractions; 5, 7.5, 10, 12.5, 15, 17.5, 20 and 50% ACN) by using the PierceTM High pH Reversed-Phase Peptide Fractionation Kit (#84868, ThermoFisher Scientific) according to the manufacturer's recommendations.

For MS analysis, lyophilized peptides were reconstituted in 1% TFA (v/v) and peptide concentrations were measured using a quantitative Colorimetric Peptide Assay (Pierce™, ThermoFisher Scientific). Samples (400 ng) were separated by liquid chromatography (Vanquish Neo, ThermoFisher Scientific) and measured on an Orbitrap Exploris OE480 (ThermoFisher Scientific).

Peptides were captured and desalted on an Acclaim PepMap C18-LC column (ID: 75 µm, 2 cm length; ThermoFisher Scientific) and then separated with an Aurora C18 column (AUR2-25075C18A, 25 cm x 75 µm C18 1.6 µm; IonOpticks) using a 2-hour, three-step gradient at a total flow rate of 300 nl/min with buffer A (0.1% formic acid) and buffer B (80% ACN, 0.1% formic acid). First, a linear gradient from 2–1% buffer B for 72 minutes, second, from 19–29% buffer B for 28 minutes, followed by 20 minutes from 29–41% buffer B and a 1 minute increasing buffer B to 95% was applied.

MS data were acquired in data dependent acquisition (DDA) mode at 120,000 resolution (2 seconds cycle time), m/z range of 350–1,200 and a normalized AGC target value of 300%. For fragmentation, precursor selection filters were set to charge state between 2 and 6 and dynamic exclusion of 45 seconds. Fragmentation of precursors was performed with an isolation window (m/z) of 1.6, Higher-energy collisional dissociation (HCD) energy of 30% at 15,000 resolution with automatic AGC target setting and an injection time of 22 ms.

Proteomic profiling and mass spectrometry analysis were kindly performed by Martina Schiller, Ulrike Kettel, Sonja Hartwig and Stefan Lehr.

2.2.6.2 Proteomic profiling of white adipose tissue

For proteomic profiling, adipose tissue was homogenized in two volumes (w/v) TES buffer (50 mM Tris-HCl, 1mM EDTA and 8.7% sucrose, supplemented with CompleteTM (Roche) and Phosphatase Inhibitors (Sigma)), using PrecellysTM (Bertin) homogenizer (soft program: 5,800 rpm for 2 x 15 seconds with 30 seconds pause; ceramic bead mix (#P000918-LYSKO-A.0, Bertin)). The homogenates were transferred to fresh reaction tubes and then sonicated twice (pulse 0.09seconds_10seconds (Sonoplus, Bandelin)). To remove the lipids, the samples were centrifuged at 1,000 xg for 5 minutes at 4°C and the aqueous phase was transferred to a fresh reaction tube. This procedure was repeated three times. SDS (final concentration 2%) was added to the clarified protein samples. After freezing (1 hour, liquid N2) and thawing, the samples were centrifuged at 4°C for 30 minutes at 75,000 xg. Protein concentrations were determined using the BCA protein assay (ThermoScientific). Subsequently, 30 µg of protein was digested with LysC/trypsin mix (1:25 w/w, Promega) using µS-TrapTM columns (ProtiFi) according to the manufacturer's recommendations.

Proteomic profiling and mass spectrometry analysis were kindly performed by Martina Schiller, Ulrike Kettel, Sonja Hartwig and Stefan Lehr.

2.2.6.3 Analysis of mass spectrometry data

Mass spectrometry raw files, were analyzed using Proteome DiscovererTM 3.0 software (ThermoFisher Scientific). The SpectrumRC node was used with the FASTA database (reviewed SwissProt, Mus musculus canonical (v2023-03-01) to recalibrate spectra. For quantification, the Minora feature detector node was used with default settings (minimum trace length 5, maximum delta RT of isoptope pattern multiplets of 0.2 minutes, and only high confident PSMs were used

for feature-ID linking). For identification, search was performed with Chimerys (inferys_2.1_fragmentation) against the UniProtKB database (reviewed SwissProt, Mus musculus with isoforms (v2023-03-01) and an in-house contaminant FASTA file). Enzymatic digest was set to trypsin with a maximum of 2 missed cleavage sites allowed. Carbamidomethylation of cysteine was set as static modification and methionine oxidation were allowed as dynamic modifications. Percolator was used to validate the FDR data. Label-free quantification was performed on precursor intensity present in at least 20% of the replicates. Protein ratios were calculated on a pairwise ratio basis (t-test, background based).

The analysis of the mass spectrometry data was kindly performed by Sonja Hartwig and Stefan Lehr.

2.2.6.4 Filtering criteria for mass spectrometry data

To identify candidate proteins, the following filtering criteria were applied to the mass spectrometry data obtained using Proteome DiscovererTM 3.0 software (ThermoFisher Scientific): Master is equal to Master - Protein FDR Confidence has level High in Protein FDR Confidence Combined - Species Map is true in species Mus musculus - #Unique peptides is greater than or equal to 1.

Canonical pathways over-representation analyses were then conducted using ConsensusPathDB [294] for differentially regulated proteins ($p < 0.05$).

2.2.7 Statistical analysis

All experiments were performed with n = 8–12 animals per group and are presented as mean values ± SEM. Significant differences were determined by one- or two-way ANOVA (post hoc test, Bonferroni multiple comparison test) or two-tailed Student's t-test using GraphPad Prism 10 software. P-values < 0.05 were considered statistically significant. Exact conditions and tests are indicated in the figure legends.

3. Results

Similar to humans, RabGAP-deficiency in mice has previously been associated with impaired glucose tolerance, reduced insulin sensitivity, postprandial hyperglycemia and severely impaired insulin-stimulated glucose uptake to skeletal muscle and white adipose tissue [131, 262, 266, 270, 290]. To further elucidate the impact of nutrition on whole-body glycemia and the regulatory functions of the two RabGAP TBC1D1 and TBC1D4, RabGAP-deficient mice were subjected to different dietary interventions. In addition, mice with a skeletal muscle-specific *Tbc1d4*-deficiency (mD4KO) were metabolically characterized to resemble the Arctic muscle-specific TBC1D4-variant. Furthermore, adipocyte-specific D4KO (aD4KO) mice were metabolically characterized to evaluate the individual contribution of adipose tissue to whole-body glycemia. For the present study, the following dietary interventions were performed: 1. a control (CON) diet, indicated in white below; 2. a high-carbohydrate low-protein (HCLP) diet, indicated in yellow below; or 3. a low-carbohydrate high-protein (LCHP) diet, indicated in orange below (Figure 4).

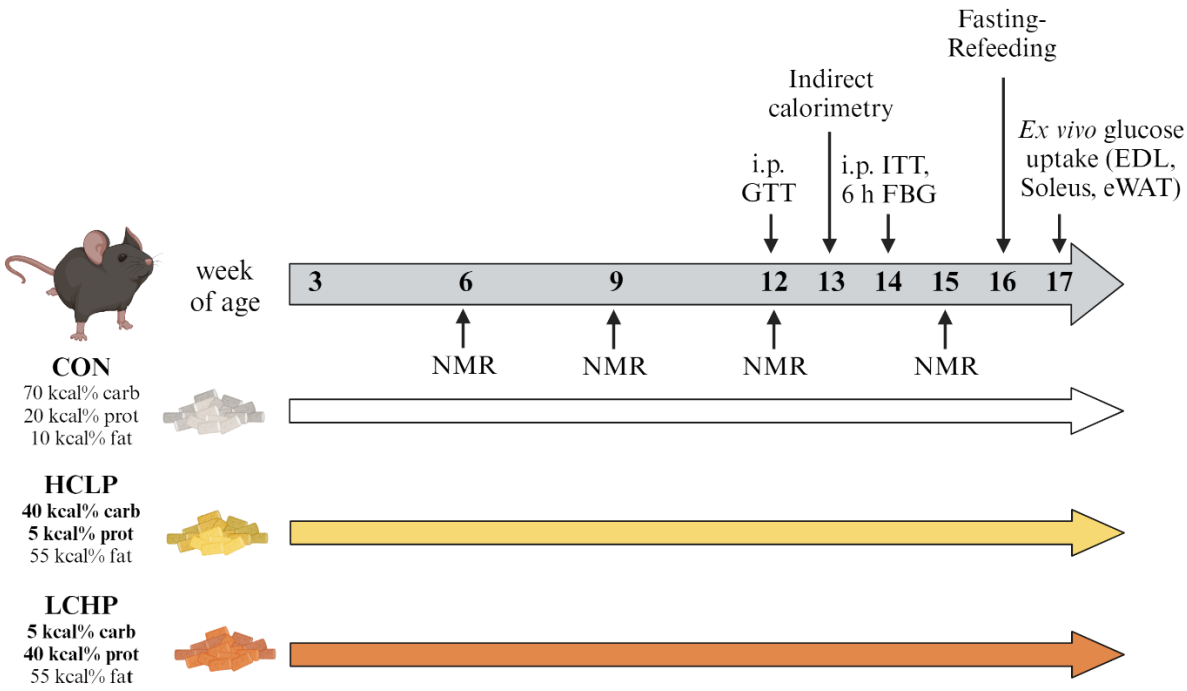

Figure 4: Study design for the experimental dietary interventions and metabolic characterization of experimental animals. After weaning, male mice were subjected to chronic dietary interventions and undergo metabolic characterization. CON: control, EDL: Extensor digitorum longus, eWAT: epididymal white adipose tissue, FBG: fasted blood glucose, HCLP: high-carbohydrate low-protein, i.p. GTT: intraperitoneal glucose tolerance test, i.p. ITT: intraperitoneal insulin tolerance test, LCHP: Low-carbohydrate high-protein,nMR: nuclear magnetic resonance. Created with Biorender.com

3.1 Impact of dietary macronutrient ratios on the energy metabolism of mice with a global RabGAP-deficiency

TBC1D1 has been shown to convey susceptibility to obesity and to play a role in skeletal muscle development [131, 253, 254], suggesting that nutrition may affect its regulatory function. In addition, TBC1D4-regulated glycemia, has been suggested to be influenced by nutrition [295]. Therefore, the present study aimed to investigate the regulatory function of the two RabGAPs TBC1D1 and TBC1D4 as molecular switches of energy substrate utilization and the impact of Arctic and Western diets on whole-body glycemia in *Tbc1d1- and Tbc1d4*-deficiency.

3.1.1 Body weight and body composition of RabGAP-deficient mice on HCLP and LCHP diets

To evaluate the impact of dietary macronutrient ratios on body composition, total body weight was assessed via weighing experimental animals to analyze body lean and body fat mass by NMR (2.2.2.2). Therefore, *Tbc1d1*- (D1KO), *Tbc1d4*- (D4KO) and *Tbc1d1/4*-knockout (D1/4KO) mice were subjected to a CON (indicated by a white background), a HCLP (indicated by a yellow background) or a LCHP (indicated by an orange background) diet and body composition was assessed at 6, 9 12 and 15 weeks of age.

In the present study, body weight of RabGAP-deficient mice was unaltered compared to wildtype (WT) littermates when subjected to the CON diet (Figure 5 A.1). On the HCLP diet, however, total body weight was significantly reduced in D1/4KO mice compared to D4KO mice at 6, 9, 12 and 15 weeks of age. Furthermore, total body weight of D4KO mice tended to be increased compared to WT and D1KO littermates (Figure 5 B.1). On the LCHP diet, total body weight remained unaltered between RabGAP-deficient mice and WT mice, whereas *Tbc1d1*-deficiency in mice tendentially resulted in reduced total body weight (Figure 5 C.1). Body fat mass was unaltered between the genotypes on a CON diet (Figure 5 A.2) and significantly elevated in D4KO and D1/4KO mice compared to WT and D1KO littermates at 6 and 9 weeks of age and in D4KO mice compared to WT and D1KO mice at 12 and 15 weeks of age when subjected to a HCLP diet (Figure 5 B.2). When subjected to a LCHP diet, body fat mass was tendentially elevated in D4KO mice at 6, 9 and 12 weeks of age and significantly elevated compared to D1KO mice at 15

weeks of age (Figure 5 C.2). Body lean mass was unaltered between the genotypes on a CON diet (Figure 5 A.3), but was significantly reduced in D1/4KO mice compared to the other genotypes at 6, 9 and 12 weeks of age and significantly lower compared to D4KO mice at 15 weeks of age on a HCLP diet (Figure 5 B.3). On the LCHP diet, body lean mass was tendentially increased in D1KO mice at 6 and 9 weeks of age and significantly elevated compared to D4KO mice at 12 and 15 weeks of age (Figure 5 C.3).

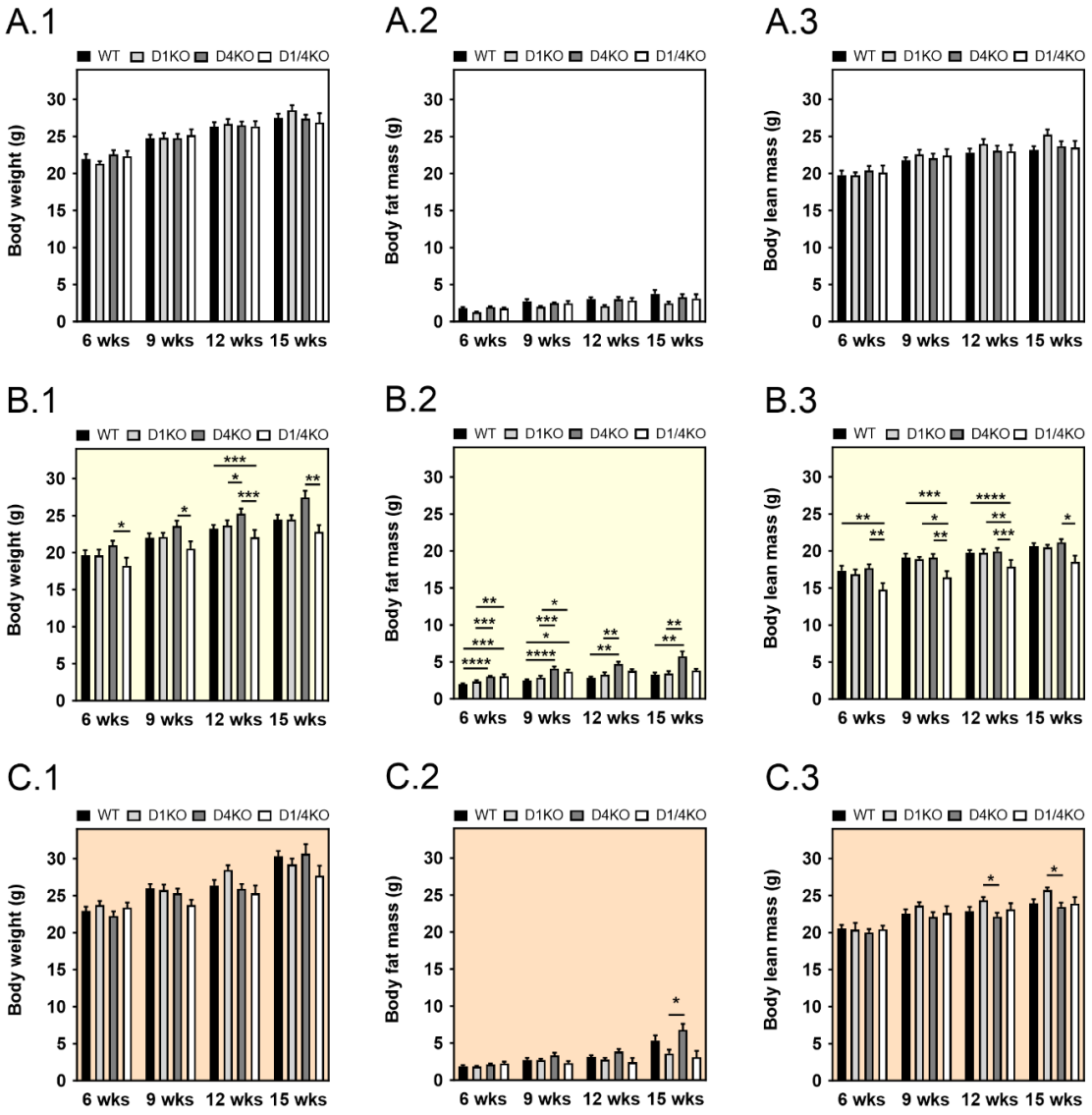

Figure 5: Impact of dietary macronutrient ratios on body composition of RabGAP-deficient mice. Determination of body composition in total body weight (A.1–C.1), body fat mass (A.2–C.2) and lean mass (A.3–C.3) in *Tbc1d1*- (D1KO), *Tbc1d4*- (D4KO) and *Tbc1d1/4*-deficient (D1/4KO) mice and WT littermates subjected to a CON (A), HCLP (B) or LCHP (C) diet at 6, 9, 12 and 15 weeks of age. Data are

presented as mean ± SEM (n = 8–13). *p < 0.05, **p < 0.01, ***p < 0.001, ****p < 0.0001, WT vs. D1KO, D4KO, D1/4KO (One-way ANOVA with Bonferroni correction).

3.1.2 Whole-body glycemia in RabGAP-deficient mice on HCLP and LCHP diets

3.1.2.1 Blood glucose levels in RabGAP-deficient mice on HCLP and LCHP diets

Moreover, random fed and fasted blood glucose concentrations were assessed (2.2.2.4). Random fed blood glucose concentrations remained unaltered between the genotypes when subjected to the CON diet (Figure 6 A.1). When subjected to the HCLP diet, random fed blood glucose concentrations were significantly reduced in D4KO and D1/4KO mice compared to D1KO littermates (Figure 6 B.1), but were unchanged between the genotypes on the LCHP diet (Figure 6 C.1).

After 6 h of fasting, blood glucose concentrations of D4KO and D1/4KO mice were significantly reduced compared to D1KO and WT littermates on the CON diet (WT: 126 ± 7 mg/dL, D1KO: 141 ± 8 mg/dL, D4KO: 103 ± 3 mg/dL, D1/4KO: 108 ± 3 mg/dL, Figure 6 A.2). When subjected to a HCLP diet, 6 h fasted blood glucose concentrations were significantly reduced in D4KO and D1/4KO mice compared to D1KO and WT mice (WT: 168 ± 9 mg/dL, D1KO: 165 ± 10 mg/dL, D4KO: 93 ± 4 mg/dL, D1/4KO: 101 ± 7 mg/dL, Figure 3 B.2) and remained unaltered between the genotypes on the LCHP diet (Figure 6 C.2)

After an overnight fast of 16 h, blood glucose concentrations were unchanged between the genotypes when fed the CON (Figure 6 A.3), the HCLP (Figure 6 B.3) or the LCHP diet (Figure 6 C.3).

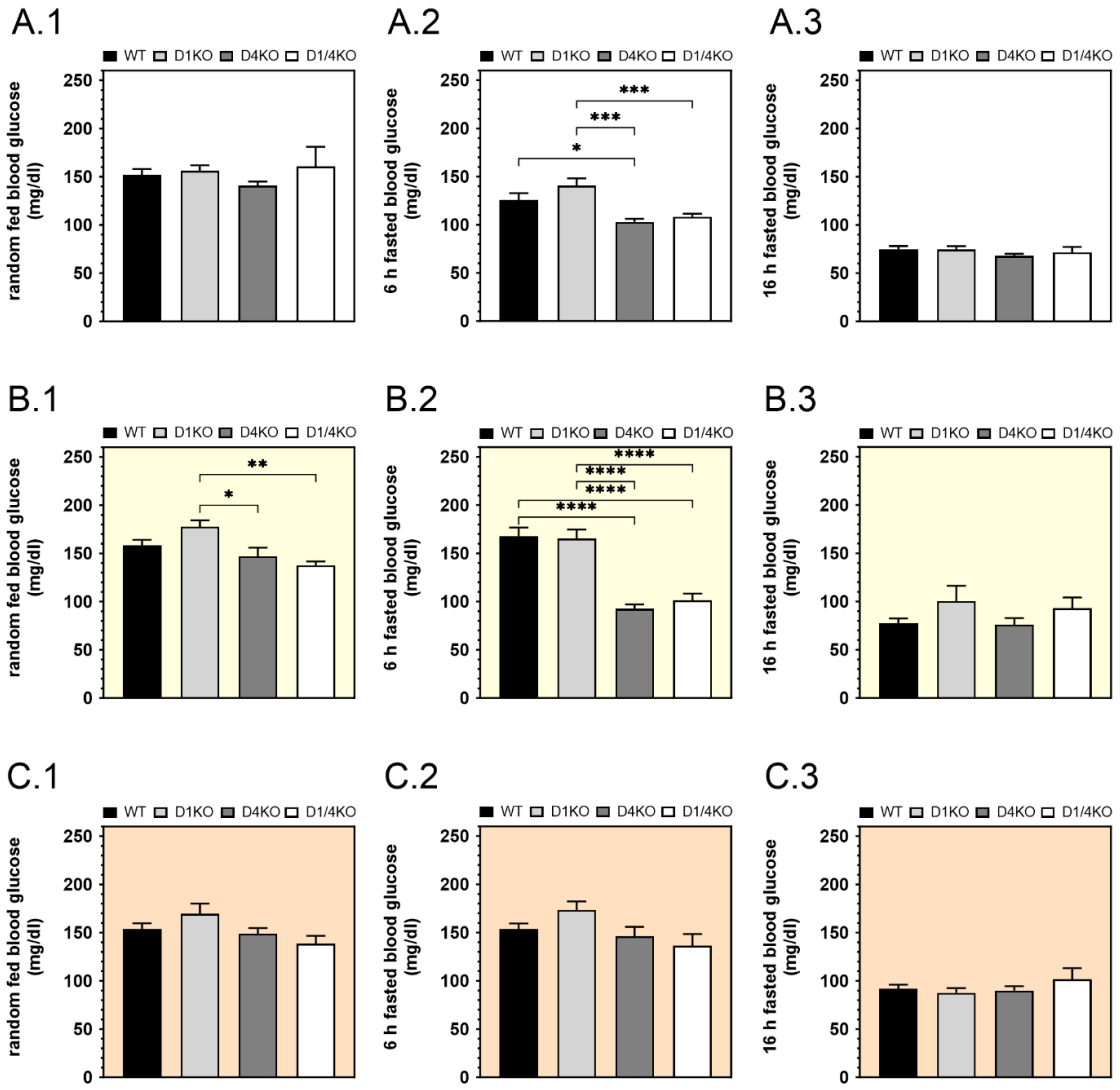

Figure 6: Impact of dietary macronutrient ratios on blood glucose of RabGAP-deficient mice. Determination of random fed (A.1–C.1), 6 h fasted (A.2–C.2) and 16 h fasted (A.3–C.3) blood glucose concentrations of male *Tbc1d1*-, *Tbc1d4*- and *Tbc1d1/4*-deficient (D4KO) mice and WT littermates aged 12–14 weeks subjected to a CON (A), HCLP (B) or LCHP (C) diet. Data are presented as mean ± SEM (n = 7–12). *p < 0.05, **p < 0.01, ***p < 0.001, ****p < 0.0001 (One-way ANOVA with Bonferroni correction).

3.1.2.2 Glucose, insulin and AICAR tolerance in RabGAP-deficient mice on HCLP and LCHP diets

To determine whole-body glycemia, glucose tolerance by i.p. GTT (2.2.2.5, Figure 7 A.1–C.1), insulin tolerance by i.p. ITT (2.2.2.6, Figure 7 A.2–C.2), and AICAR tolerance (2.2.2.7, Figure 7 A.3–C.3) were assessed.

While glucose tolerance on each experimental diet remained unaltered between the genotypes, absolute blood glucose concentrations were elevated when mice were subjected to the LCHP diet, as indicated by the area under the curve (AUC) (WT: 45217 ± 1277 (CON) vs. 37037 ± 1736 (HCLP) vs. 57119 ± 3161 (LCHP), D1KO: 43724 ± 1410 (CON) vs. 41191 ± 2116 (HCLP) vs. 51554 ± 1175 (LCHP), D4KO: 41279 ± 2672 (CON) vs. 34850 ± 1576 (HCLP) vs. 56085 ± 2492 (LCHP), D1/4KO: 49229 ± 3412 (CON) vs. 33502 ± 2183 (HCLP) vs. 62628 ± 1884 (LCHP)).

Similarly, insulin tolerance was unaffected by the genotype when mice were fed the CON (Figure 7 A.2) or the HCLP (Figure 7 B.2) diet. However, when fed the LCHP diet (Figure 7 B.2), insulin tolerance was impaired in D1/4KO mice compared to D1KO mice. Moreover, the AUC was higher in mice fed the LCHP diet compared to the CON or HCLP diet (WT: 5435 ± 167 (CON) vs. 5277 ± 253 (HCLP) vs. 7191 ± 312 (LCHP), D1KO: 5870 ± 238 (CON) vs. 4846 ± 123 (HCLP) vs. 6506 ± 214 (LCHP), D4KO: 5852 ± 183 (CON) vs. 5428 ± 152 (HCLP) vs. 7435 ± 260 (LCHP), D1/4KO: 6181 ± 589 (CON) vs. 5088 ± 188 (HCLP) vs. 8003 ± 180 (LCHP)).

Interestingly, AICAR tolerance was significantly elevated in D4KO and D1/4KO mice compared to WT and D1KO littermates when subjected to a CON diet, as indicated by a reduced AUC (WT: 8427 ± 1588, D1KO: 8596 ± 258, D4KO: 4585 ± 279, D1/4KO: 6009 ± 559, Figure 4 A.3), or a HCLP diet (WT: 9116 ± 283, D1KO: 8878 ± 472, D4KO: 4664 ± 272, D1/4KO: 4671 ± 337, Figure 7 B.3). When subjected to a LCHP diet, AICAR tolerance was significantly enhanced in D4KO compared to the other genotypes as indicated by a reduced AUC (WT: 7051 ± 318, D1KO: 7335 ± 361, D4KO: 5030 ± 145, D1/4KO: 6851 ± 428, Figure 7 C.3).

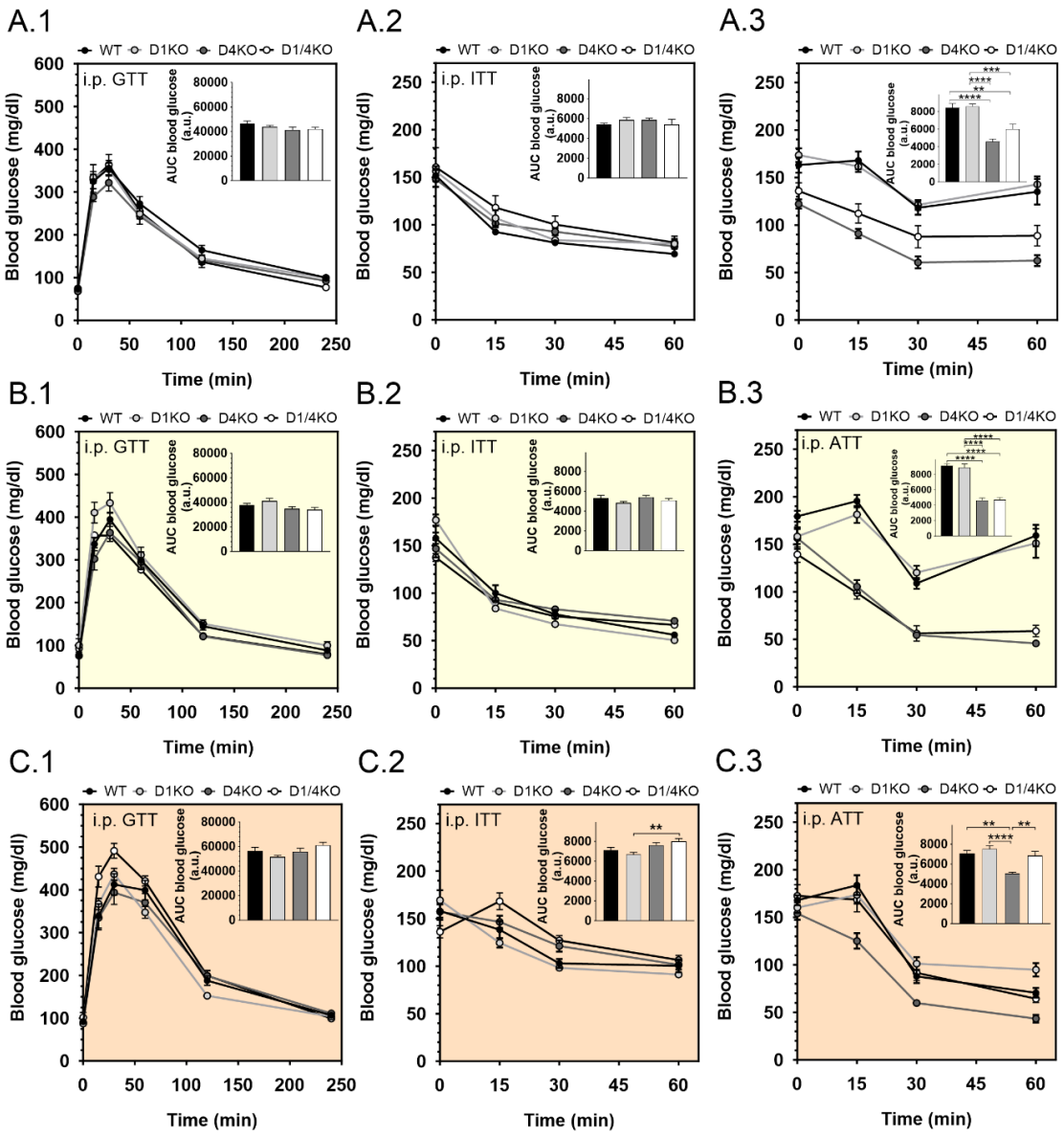

Figure 7: Impact of dietary macronutrient ratios on glucose, insulin and AICAR tolerance in RabGAP-deficient mice. Determination of intraperitoneal tolerance for glucose (GTT), insulin (ITT), and AICAR (ATT) of male *Tbc1d1*- (D1KO), *Tbc1d4*- (D4KO) and *Tbc1d1/4*-deficient (D1/4KO) mice and WT littermates aged 12–14 weeks. Blood glucose concentrations in D1KO, D4KO and D1/4KO mice after intraperitoneal injection of glucose (2 g/kg) subjected to a CON (A.1), HCLP (B.1) or LCHP (C.1) diet. Blood glucose concentrations after intraperitoneal injection of insulin (1 IU/kg) subjected to a CON (A.2), HCLP (B.2) or LCHP (C.2) diet. Blood glucose concentrations after intraperitoneal injection of AICAR (250 mg/kg) subjected to a CON (A.3), HCLP (B.3) or LCHP (C.3) diet. Data are presented as mean ± SEM

(n = 8–12). *p < 0.05, **p < 0.01, ***p < 0.001, ****p < 0.0001, AUC (One-way ANOVA with Bonferroni correction).

3.1.2.3 Postprandial glycemia in RabGAP-deficient mice on HCLP and LCHP diets

To determine the impact of dietary macronutrient ratios on postprandial glycemia, experimental animals were fasted overnight and refed with the respective experimental diets after blood withdrawal (2.2.2.8). Over the course of four hours, blood glucose (2.2.2.4) and plasma insulin concentrations (2.2.3.1) were assessed, as was food intake.

Postprandial blood glucose concentrations were significantly elevated in D4KO and D1/4KO mice compared to WT and D1KO littermates 1 h and 2 h after refeeding with the CON (Figure 8 A.1) and HCLP (Figure 8 B.1) diets. Interestingly, blood glucose concentrations in D4KO mice on the LCHP diet tended to be lower than in WT littermates at all time points examined, as reflected by a significantly lower AUC (WT:33171 ± 1042, D4KO: 29270 ± 664, Figure 8 C.1). Plasma insulin concentrations were unchanged between the genotypes when refed with the CON diet (Figure 8 A.2), but showed a strong tendency to be elevated in D4KO and D1/4KO mice compared to WT and D1KO littermates 1 h after refeeding with a HCLP diet (WT: 2.88 ± 0.62 µg/l, D1KO: 3.62 ± 0.74 µg/l, D4KO: 5.85 ± 1.11 µg/l, D1/4KO: 6.85 ± 1.3 µg/l, Figure 8 B.2). Similarly, when mice were refed with a LCHP, plasma insulin concentrations were tendentially elevated 1 h after refeeding in D4KO and D1/4KO mice compared to WT and D1KO mice (Figure 8 C.2). Food intake was unaltered between the genotypes regardless of the diet (Figure 8 A.3–C.3). However, when refed with a CON diet, food intake of D1KO and D4KO was significantly reduced 2 h after refeeding compared to 1 h and significantly increased after 4 h of refeeding compared to 2 h. Moreover, after 4 h food intake was significantly increased in WT and D1/4KO mice compared to 2 h after refeeding (Figure 8 A.3). On the HCLP diet intervention, food intake at 2 h of refeeding was significantly reduced in WT mice and tendentially reduced in RabGAP-deficient mice compared to 1 h after refeeding. Moreover, food intake was significantly elevated in D1KO mice and tendentially increased in WT, D4KO and D1/4KO mice 4 h after refeeding with a HCLP diet compared to 2 h (Figure 8 B.3). When subjected to the LCHP diet, food intake was significantly decreased in WT mice and tendentially decreased in RabGAP-deficient

littermates 2 h compared to 1 h after refeeding. 4 h after refeeding, food intake was tendentially increased in all genotypes compared to 2 h after refeeding (Figure 8 C.3).

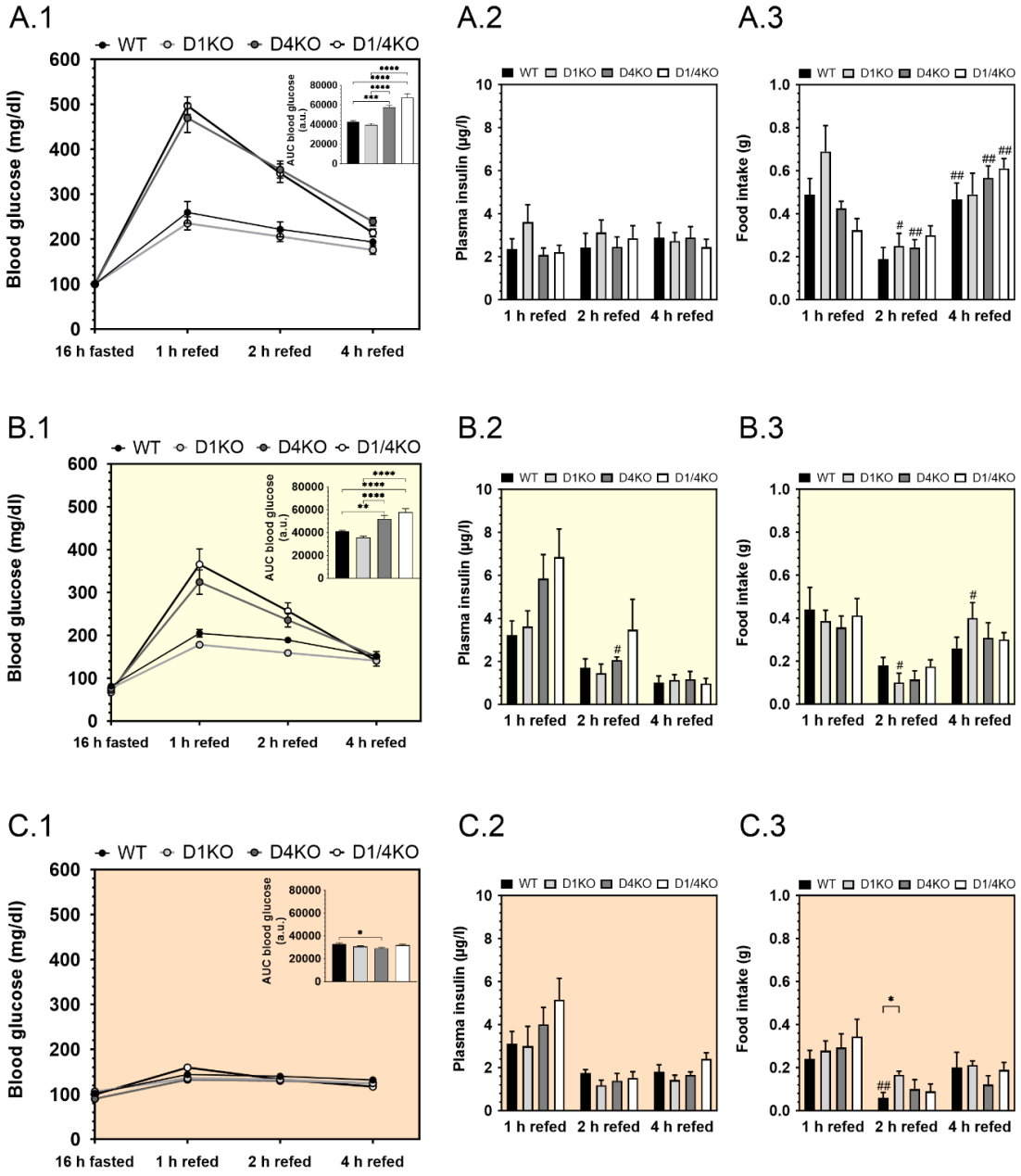

Figure 8: Impact of dietary macronutrient ratios on postprandial glycemia, plasma insulin concentrations and food intake of RabGAP-deficient mice. Determination of fasted and postprandial blood glucose concentrations and AUC (A.1–C.1), postprandial plasma insulin concentrations (A.2–C.2) and food intake (A.3–C.3) from *Tbc1d1*- (D1KO), *Tbc1d4*- (D4KO) and *Tbc1d1/4*-deficient (D1/4KO) mice and WT littermates aged 16–17 weeks subjected to a CON (A), HCLP (B) or LCHP (C) diet. Data are presented as mean ± SEM (n = 8-13). *p < 0.05, **p < 0.01, ***p < 0.001, AUC WT vs. D1KO, D4KO,

D1/4KO (One-way ANOVA), #p < 0.05, ##p < 0.01, 1 h refed vs. 2 h refed, 2 h refed vs. 4 h refed (Two-way ANOVA with Bonferroni correction).

3.1.2.4 Postprandial incretin concentrations in RabGAP-deficient mice on HCLP and LCHP diets

Besides insulin, incretins are crucial in the regulation of postprandial glycemia. Alterations in incretin secretion are associated with insulin resistance [296, 297]. Therefore, plasma concentrations of ghrelin, GIP, GLP, glucagon, PAI-1 and resistin were determined in the postprandial state (2.2.3.4, Figure 9 A–F).

Fasted plasma ghrelin concentrations were significantly elevated in RabGAP-deficient mice subjected to a HCLP or LCHP compared to a CON diet. Further, plasma ghrelin concentrations were significantly elevated in D1KO and D1/4KO mice compared to WT littermates when subjected to a HCLP diet (Figure 9 A). Postprandial GIP concentrations were significantly increased in mice subjected to a CON diet compared to a HCLP or LCHP diet. Moreover, plasma GIP concentrations were significantly elevated in D1/4KO mice compared to WT littermates on a CON diet, but remained unchanged on a HCLP and LCHP diet between the genotypes (Figure 9 B). Plasma GLP concentrations in response to different dietary interventions were unchanged between genotypes (Figure 9 C). Postprandial plasma glucagon concentrations were unchanged between the genotypes, however, were significantly elevated in mice subjected to a HCLP diet compared to a CON and a LCHP diet (Figure 9 D). PAI-1 concentrations were unaltered between the genotypes after refeeding, but were significantly elevated in response to the HCLP diet compared to the CON or LCHP diets (Figure 9 E). Postprandial resistin concentrations were 2- to 3- fold higher in mice subjected to a HCLP and LCHP diet compared to a CON diet. Tendentially plasma resistin concentrations were lower in D4KO and D1/4KO mice compared to WT littermates, however remained otherwise unaltered between the genotypes (Figure 9 F).

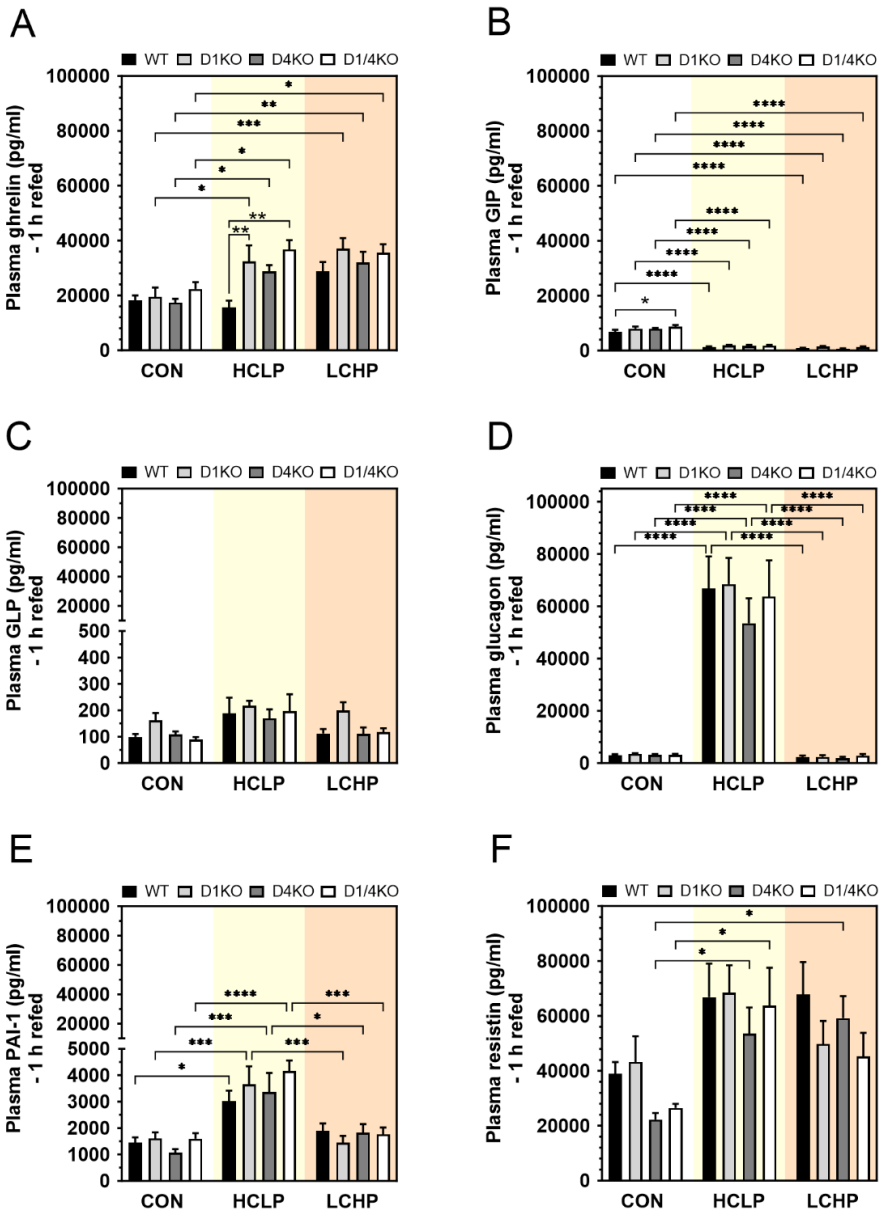

Figure 9: Impact of dietary macronutrient ratios on postprandial incretin concentrations of RabGAP-deficient mice. Determination of postprandial plasma concentrations of ghrelin (A), GIP (B), GLP (C), glucagon (D), PAI-1 (E), resistin (F) from *Tbc1d1*- (D1KO), *Tbc1d4*- (D4KO) and *Tbc1d1/4*-deficient (D1/4KO) mice and WT littermates aged 16–17 weeks subjected to a CON (indicated in white), HCLP (indicated in yellow) or LCHP (indicated in orange) diet. Data are presented as mean ± SEM (n = 3-8). *p < 0.05, **p < 0.01, ***p < 0.001, ****p < 0.0001 (Two-way ANOVA with Bonferroni correction).

3.1.3 Plasma parameters in RabGAP-deficient mice on HCLP and LCHP diets

Moreover, 6 h fasted plasma concentrations of insulin (2.2.3.1), ketone bodies (2.2.3.2) and NEFAs (2.2.3.3) were determined. Fasted plasma insulin concentrations were

tendentially increased in D4KO compared to WT, D1KO and D1/4KO mice on the CON diet (WT: 0.32 ± 0.05 µg/l, D1KO: 0.33 ± 0.02 µg/l, D4KO: 0.46 ± 0.06 µg/l, D1/4KO: 0.28 ± 0.09 µg/l, Figure 10 A.1) but remained unchanged on the HCLP (Figure 10 B.1) and LCHP (Figure 10 C.1) diets.

Fasted plasma ketone body concentrations were significantly increased in D4KO and D1/4KO mice compared to WT and D1KO littermates when fed the CON (WT: 416 ± 24 µmol/l, D1KO: 331 ± 22 µmol/l, D4KO: 756 ± 124 µmol/l, D1/4KO: 714 ± 45 µmol/l, Figure 10 A.2) and a HCLP (WT: 327 ± 88 µmol/l, D1KO: 333 ± 47 µmol/l, D4KO: 1264 ± 95 µmol/l, D1/4KO: 896 ± 66 µmol/l). In addition, fasted plasma ketone bodies were significantly higher in D4KO compared to D1/4KO mice on the HCLP diet (Figure 10 B.2). Moreover, fasted plasma ketone bodies were significantly increased in D4KO and D1/4KO mice compared to WT and D1KO mice when subjected to a LCHP diet (WT: 307 ± 49 µmol/l, D1KO: 204 ± 19 µmol/l, D4KO: 443 ± 35 µmol/l, D1/4KO: 402 ± 46 µmol/l, Figure 10 C.2).

When subjected to a CON diet, fasted plasma NEFAs concentrations were significantly elevated in D1/4KO mice compared to WT and D1KO mice (WT: 1.20 ± 0.06 mmol/l, D1KO: 1.14 ± 0.12 mmol/l, D4KO: 1.29 ± 0.08 mmol/l, D1/4KO: 1.56 ± 0.09 mmol/l, Figure 10 A.3) and compared to D1KO mice when subjected to a HCLP. Further, fasted plasma NEFA concentrations were markedly increased in D4KO mice compared to D1KO mice when subjected to a HCLP diet (WT: 0.91 ± 0.09 mmol/l, D1KO: 0.63 ± 0.02 mmol/l, D4KO: 1.15 ± 0.14 mmol/l, D1/4KO: 1.22 ± 0.09 mmol/l, Figure 10 B.3) and a LCHP diet (WT: 0.81 ± 0.1 mmol/l, D1KO: 0.64 ± 0.04 mmol/l, D4KO: 0.78 ± 0.06 mmol/l, D1/4KO: 1.01 ± 0.07 mmol/l, Figure 10 C.3) diet.

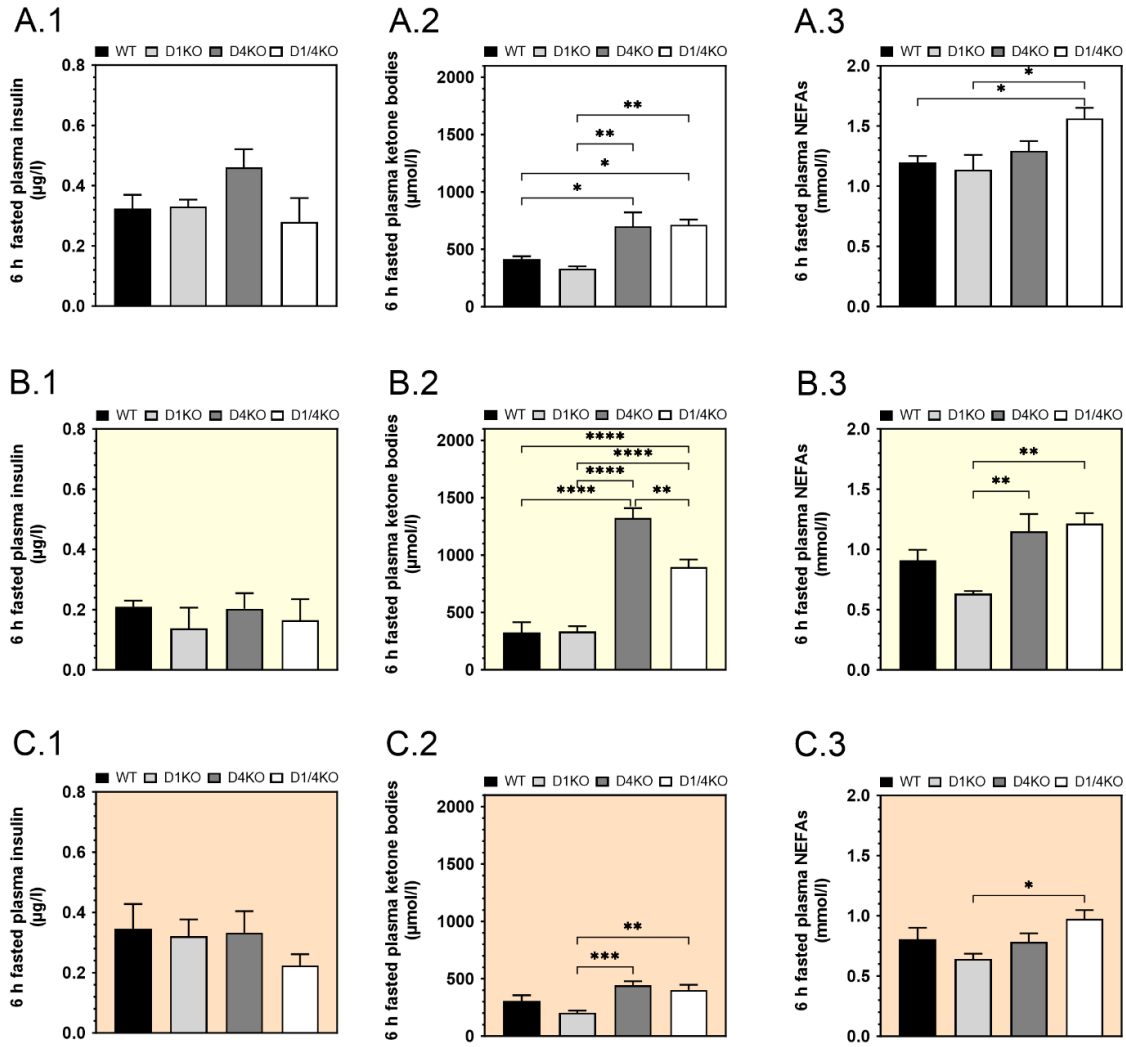

Figure 10: Impact of dietary macronutrient ratios on fasted plasma parameters of RabGAP-deficient mice. Determination of 6 h fasted plasma insulin (A.1–C.1), ketone bodies (A.2–C.2) and NEFA (A.3–C.3) concentrations of male *Tbc1d1*-(D1KO), *Tbc1d4*- (D4KO) and *Tbc1d1/4*-deficient (D1/4KO) mice and WT littermates aged 14 weeks subjected to a CON (A), HCLP (B) or LCHP (C) diet. Data are presented as mean ± SEM (n = 8–12). *p < 0.05, **p < 0.01, ***p < 0.001, ****p < 0.0001 (One-way ANOVA with Bonferroni correction).

3.1.4 Energy substrate utilization in RabGAP-deficient mice on HCLP and LCHP diets

Energy substrate utilization and preference may affect whole-body glycemia. Therefore, the respiratory quotient was assessed (Figure 11 A.1–C.1) to determine whole-body CHO and FAO over two consecutive days (2.2.2.3). In all genotypes whole-body CHO was significantly increased (Figure 11 A.2) and whole-body FAO was significantly decreased

(Figure 11 A.3) in the dark phase compared to the light phase, when mice were fed the CON diet.

On the HCLP diet, whole-body CHO (Figure 11 B.2) was significantly increased in the dark phase compared to the light phase, while whole-body FAO (Figure 11 B.3) was significantly decreased in the dark phase compared to the light phase in all genotypes. Interestingly, in the dark phase, whole-body CHO was significantly lower in RabGAP-deficient mice compared to WT littermates. Moreover, in the light phase, whole-body FAO was significantly lower in D1/4KO mice compared to WT and D1KO mice, and in the dark phase, whole-body FAO was significantly higher in D4KO compared to WT mice (WT: 0.27 ± 0.02 mg/min, D4KO: 0.4 ± 0.03 mg/min).

Interestingly, on the LCHP diet, whole-body CHO (Figure 11 C.2) in the dark phase was significantly elevated in all genotypes as well as whole-body FAO (Figure 11 C.3) in WT, D4KO and D1/4KO mice compared to the light phase.

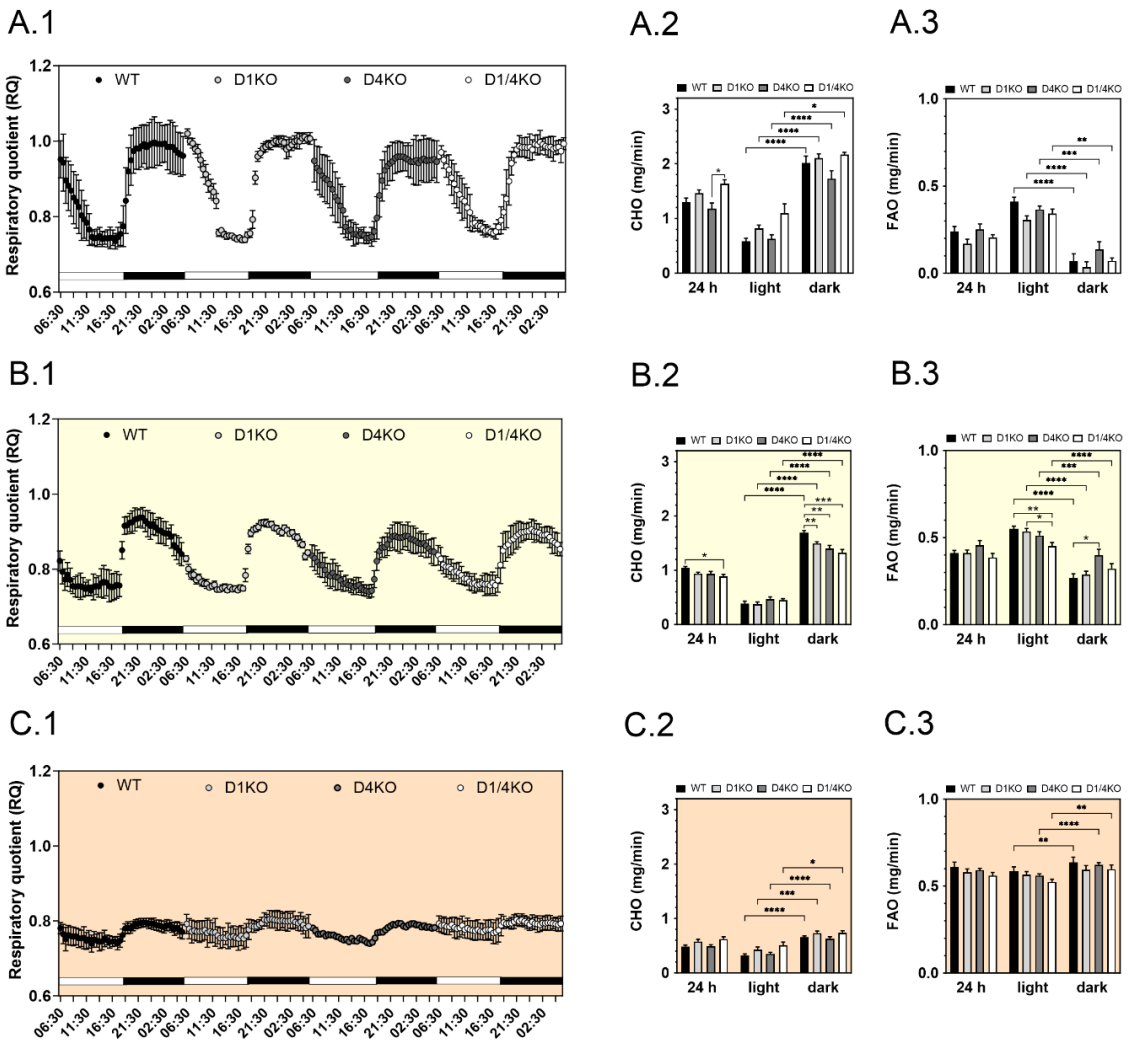

Figure 11: Impact of dietary macronutrient ratios on energy substrate preference in RabGAP-deficient mice. Determination of respiratory quotient (A.1–C.1), whole body carbohydrate oxidation (A.2–C.2) and whole-body fatty acid oxidation (A.3–C.3) during light and dark phase in male *Tbc1d1*- (D1KO), *Tbc1d4*-(D4KO) and *Tbc1d1/4*-deficient (D1/4KO) mice and WT littermates aged 12–13 weeks subjected to a CON (A), HCLP (B) or LCHP (C) diet. Data are presented as mean ± SEM (n = 8–12). *p < 0.05, **p < 0.01, ***p < 0.001, ****p < 0.0001 (Two-way ANOVA with Bonferroni correction).

3.1.5 Ex vivo substrate utilization in RabGAP-deficient mice on HCLP and LCHP diets

3.1.5.1 Insulin-stimulated glucose uptake into skeletal muscle from RabGAP-deficient mice on HCLP and LCHP diets

Skeletal muscle presents the predominant site of postprandial glucose uptake. Therefore, insulin-stimulated glucose uptake was assessed in oxidative *Soleus* and glycolytic *EDL* muscle (2.2.2.9). Basal glucose uptake into *Soleus* muscle was significantly decreased in

D1/4KO mice and tendentially decreased in D4KO mice compared to WT littermates when subjected to a CON diet (Figure 12 A.1). On the other hand, when subjected to a HCLP diet (Figure 12 A.2), basal glucose uptake was tendentially decreased in D1KO and D4KO mice, and significantly reduced in D1/4KO mice compared to WT littermates. Furthermore, when fed the LCHP diet (Figure 12 A.3), basal glucose uptake was tendentially decreased in D1KO and D1/4KO mice compared to WT littermates.

Insulin-stimulated glucose uptake into *Soleus* muscle was significantly impaired in D4KO and D1/4KO mice compared to WT and D1KO mice on a CON diet (Figure 12 A.1) as well as on a HCLP diet (Figure 12 A.2). Interestingly, when fed the LCHP diet, insulin-stimulated glucose uptake in *Soleus* muscle of D4KO mice was similar to that of WT littermates (WT: 2.97 ± 0.42 nmol/ mg/ 20 min, D4KO: 3.03 ± 0.21 nmol/ mg/ 20 min), whereas insulin-stimulated glucose uptake in *Soleus* muscle of D1KO and D1/4KO mice tended to be reduced (Figure 12 A.3).

In *EDL* muscle, basal glucose uptake was significantly reduced in D1KO and D1/4KO mice compared to D4KO and WT mice regardless of the diet. Similarly, insulin-stimulated glucose uptake in *EDL* muscle of D1KO and D1/4KO mice was significantly impaired compared to D4KO and WT mice (Figure 12 B.1–B.3). Surprisingly, insulin-stimulated glucose uptake in *EDL* muscle of D4KO mice was significantly elevated compared to WT mice when fed the LCHP diet (WT: 3.19 ± 0.26 nmol/ mg/ 20 min, D4KO: 4.18 ± 0.42 nmol/ mg/ 20 min, Figure 12 B.3)

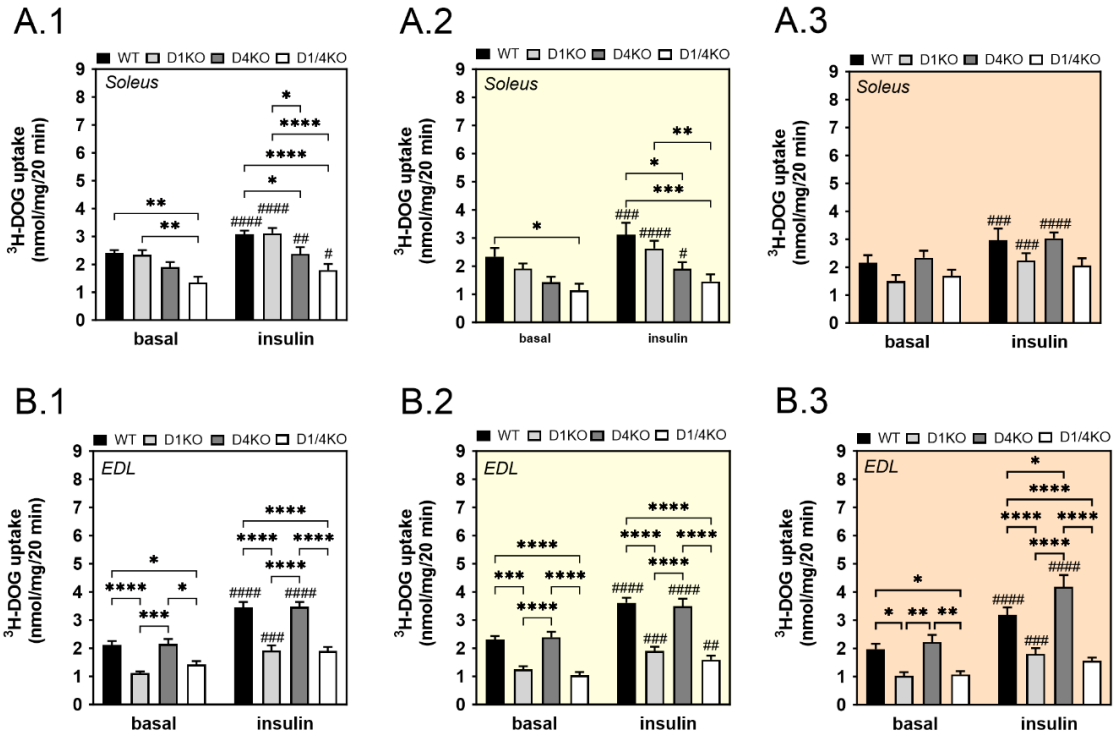

Figure 12: Impact of dietary macronutrient ratios on glucose uptake into skeletal muscle of RabGAP-deficient mice. Insulin-stimulated [^{3}H]-deoxyglucose uptake into oxidative Soleus muscle from *Tbc1d1*- (D1KO), *Tbc1d4*- (D4KO) and *Tbc1d1/4*-deficient (D1/4KO) mice aged 17–19 weeks (n = 7–12) subjected to a CON (A.1), HCLP (A.2) or LCHP (A.3) diet. Insulin-stimulated [^{3}H]-deoxyglucose uptake into glycolytic *Extensor digitorum longus* (*EDL*) muscle (n = 8–13) of mice subjected to a CON (B.1), HCLP (B.2) or LCHP (B.3) diet (n = 9–12). Data are presented as mean ± SEM. *p < 0.05, **p < 0.01, ***p < 0.001, ****p < 0.0001 WT vs. D1KO, D4KO, D1/4KO and #p < 0.05, ##p < 0.01, ###p < 0.001, ####p < 0.0001 basal vs. insulin (Two-way ANOVA with Bonferroni correction).

3.1.5.2 Insulin-stimulated glucose uptake into white adipocytes from RabGAP-deficient mice on HCLP and LCHP diets

Besides skeletal muscle, adipose tissue contributes to postprandial glucose uptake. Previous studies have shown that TBC1D4 ablation in white adipose tissue is associated with severely impaired insulin-stimulated glucose uptake in primary white adipocytes from epididymal adipose tissue. Chronic exercise training resulted in enhanced insulin-stimulated glucose uptake in primary white adipocytes from D4KO mice subjected to a high-fat diet [290]. Therefore, the effects of different dietary interventions on insulin-stimulated glucose uptake into primary white adipocytes were determined (2.2.2.10).

Under basal conditions, glucose uptake was unchanged between the genotypes on a CON diet (Figure 13 A). On the HCLP diet, basal glucose uptake tended to be reduced in D4KO and D1/4KO mice compared to D1KO and WT mice (Figure 13 B) and remained unaltered between the genotypes on the LCHP diet (Figure 13 C). Insulin-stimulated glucose uptake was significantly impaired in D4KO and D1/4KO mice compared to D1KO and WT mice when fed the CON (Figure 13 A) or the HCLP (Figure 13 B) diet. Interestingly, on the LCHP diet, insulin-stimulated glucose uptake in primary white adipocytes was significantly enhanced in D1KO and D1/4KO mice (Figure 13 C). While insulin-stimulated glucose uptake in WAT of D1KO mice was significantly increased compared to WT littermates, insulin-stimulated glucose uptake into WAT of D1/4KO mice was significantly higher compared to D4KO and similar to WT mice (WT: 67.5 ± 9.5 cpm/ mg lipid, D1KO: 108.6 ± 48 cpm/ mg lipid, D4KO: 31.9 ± 15.7 cpm/ mg lipid, D1/4KO: 73.8 ± 31.2 cpm/ mg lipid).

In addition, insulin-stimulated glucose uptake in WAT of WT mice fed the LCHP diet was 56% lower compared to the CON diet, and 61% lower compared to the HCLP diet (CON: 153.3 ± 17.2 cpm/ mg lipid; HCLP: 174.2 ± 26.6 cpm/ mg lipid, LCHP: 67.5 ± 9.5 cpm/ mg lipid).

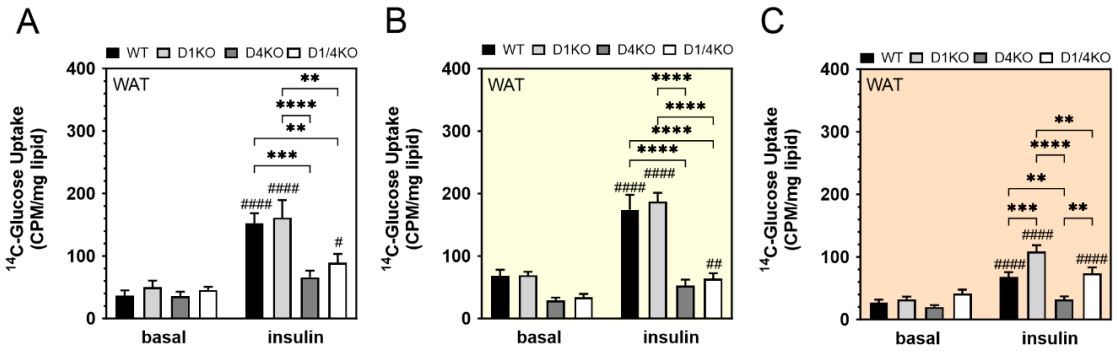

Figure 13: Impact of dietary macronutrient ratios on glucose uptake into primary white adipocytes of RabGAP-deficient mice Insulin-stimulated [^{14}C]-D-glucose (U) uptake into primary adipocytes (A) from epididymal WAT of *Tbc1d1*- (D1KO), *Tbc1d4*- (D4KO) and *Tbc1d1/4*-deficient (D1/4KO) mice and WT littermates aged 17–19 weeks subjected to a CON (A), HCLP (B) or LCHP (A.4) diet (n = 10–13). Data are presented as mean ± SEM. *p < 0.05, **p < 0.01, ***p < 0.001, ****p < 0.0001, WT vs. D1KO, D4KO,

D1/4KO and #p < 0.05, ##p < 0.01, ###p < 0.001, ####p < 0.0001 basal vs. insulin (Two-way ANOVA with Bonferroni correction).

3.1.6 In-depth analyses on the phenotype of Tbc1d4-deficient mice in response to HCLP and LCHP diets

3.1.6.1 Impact of an acute carbohydrate challenge on postprandial glycemia in Tbc1d4-deficient mice on HCLP and LCHP diets

To distinguish between possible chronic and acute effects of different macronutrient ratios on postprandial glycemia, experimental animals were subjected to a chronic HCLP or LCHP dietary interventions. Only during the Fasting-Refeeding experiment (2.2.2.8), D4KO and WT mice were refed with the LCHP or HCLP diet, respectively, for an acute dietary challenge.

Similar to D4KO mice that received the HCLP dietary intervention and were refed with the HCLP diet (Figure 14 B.1), D4KO mice that received the LCHP dietary intervention but refed with the HCLP diet exhibited significantly higher blood glucose concentrations 1 h after refeeding compared to WT mice. Interestingly, 2 h after refeeding, blood glucose concentrations were unaltered between D4KO and WT mice that were subjected to the LCHP dietary intervention and refed with a HCLP diet (Figure 14 A). Postprandial blood glucose concentrations after refeeding with the LCHP diet tended to be lower in D4KO compared to WT mice subjected to the HCLP dietary intervention, resulting in a significantly lower AUC in D4KO compared to WT mice (Figure 14 B).

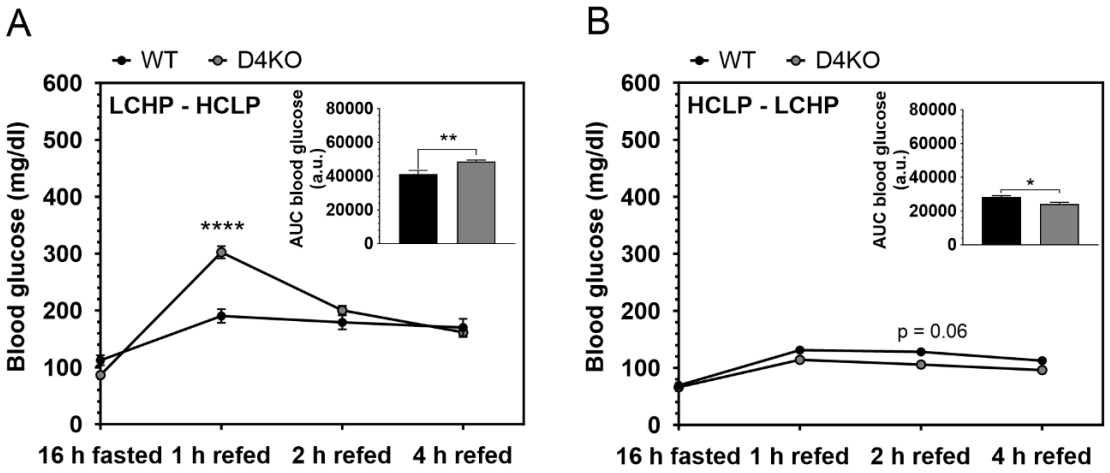

Figure 14: Impact of an acute carbohydrate challenge on postprandial glycemia of *Tbc1d4*-deficient mice after chronic dietary intervention. Determination of postprandial blood glucose concentrations and AUC from *Tbc1d4*-deficient (D4KO) mice and WT littermates aged 16–17 weeks subjected to a chronic intervention with a LCHP (A) or a HCLP (B) diet when acutely subjected to a HCLP and LCHP diet, respectively. Data are presented as mean ± SEM (n = 6–11). *p < 0.05, **p < 0.01, ***p < 0.001, ***p < 0.0001, WT vs. D4KO (Student's t-test).

3.1.6.2 Adipocyte size in Tbc1d4-deficient mice on HCLP and LCHP diets

Body composition analysis (2.2.2.2) revealed a differential effect of macronutrient ratios on body fat mass of D4KO mice compared to WT littermates. Therefore, adipocyte size was determined in epididymal adipose tissue (2.2.5.3) following the different dietary interventions by HE-staining (2.2.5.2, Figure 15 A). Adipocyte size remained unaltered between the genotypes in response to all dietary interventions. However, adipocyte size was increased by 2-fold in both D4KO and WT mice when fed the HCLP diet and by 3- to 4-fold in those fed the LCHP diet compared to the CON diet (Figure 15 B). Similar to adipocyte size, plasma leptin concentrations (2.2.3.4) were significantly increased in D4KO and WT mice after 16 h of fasting (Figure 15 C) and 1 h of refeeding (Figure 15 D) when fed the LCHP diet compared to the CON and HCLP diets.

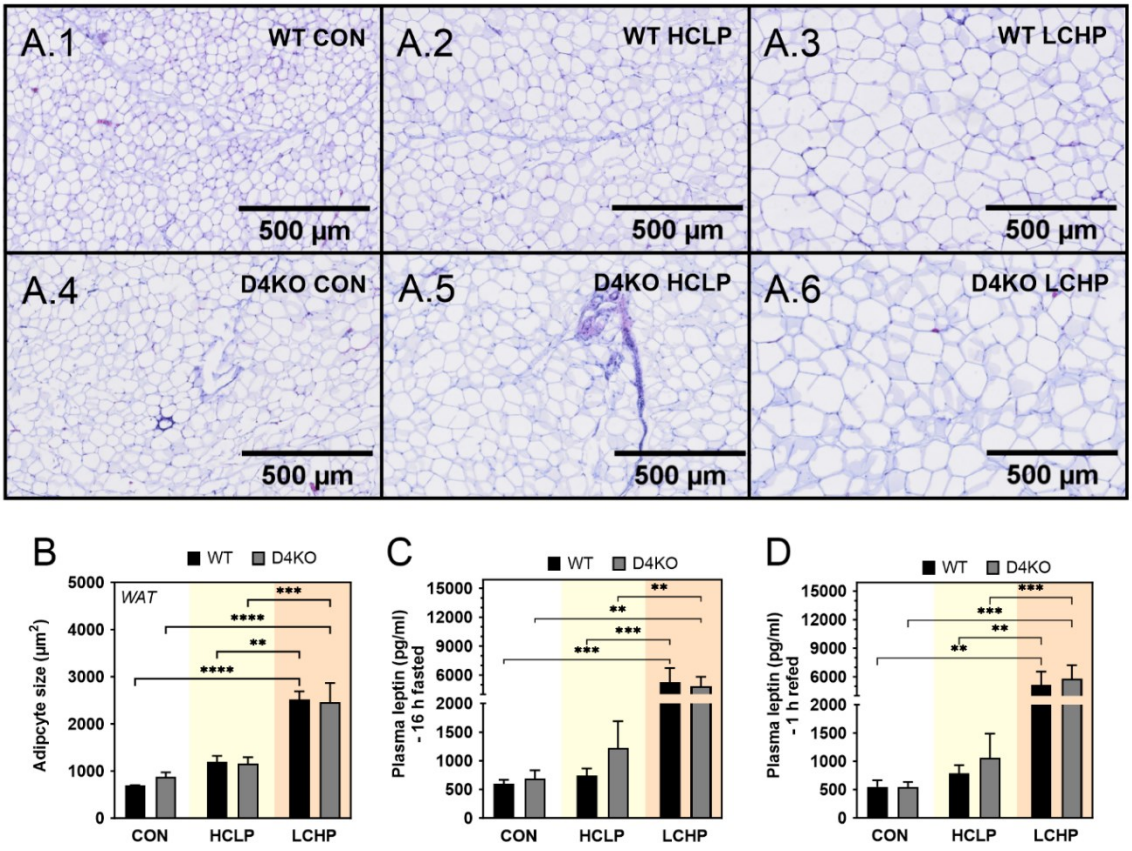

Figure 15: Impact of dietary macronutrient ratios on adipocyte size in *Tbc1d4*-deficient mice. Representative images of HE-staining of epididymal adipose tissue, resolution: 40x, scale bar: 500 µm (A). Determination of adipocyte size (B) (n = 3–4). Determination of plasma leptin concentrations after 16 h fasting (C) and 1 h refeeding (D) of *Tbc1d4*-deficient (D4KO) mice and WT littermates aged 17–19 weeks subjected to a CON (indicated in white), HCLP (indicated in yellow) or LCHP (indicated in orange) diet (n = 6–8). Data are presented as mean ± SEM. *p < 0.05, **p < 0.01, ***p < 0.001, ****p < 0.0001 (Two-way ANOVA with Bonferroni correction).

3.1.6.2 GLUT4 and FATP4 protein abundance in skeletal muscle of Tbc1d4-deficient mice on HCLP and HCLP diets

Previous studies have observed alterations in the abundance of the glucose transporter GLUT4 and the FA transporter FATP4 in skeletal muscle in response to TBC1D4 deficiency [266, 275, 290]. GLUT4 presents the primary transporter regulating insulin-stimulated glucose uptake in skeletal muscle. Therefore, the impact of different macronutrient ratios on GLUT4 and FATP4 abundance was determined in skeletal muscle of D4KO and WT mice (2.2.3.8). TBC1D4 ablation was validated in *Soleus* (Figure 16 A.1) and *EDL* (Figure 16 B.1) muscles. Interestingly, TBC1D4 abundance tended to be

increased in *Soleus* muscle and was significantly elevated in *EDL* muscle of WT mice subjected to the HCLP diet compared to the CON diet. GLUT4 abundance was significantly reduced in D4KO mice compared to WT littermates regardless of the diet (Figure 16 A.2), and remained unchanged between the genotypes in *EDL* muscle on the CON and the LCHP diets. However, on the HCLP diet, GLUT4 abundance tended to be decreased in D4KO mice compared to WT mice (Figure 16 B.2). FATP4 abundance was unchanged in *Soleus* (Figure 16 A.3) and *EDL* (Figure 16 B.3) muscles between D4KO and WT mice in response to the CON, the HCLP and the LCHP dietary intervention.

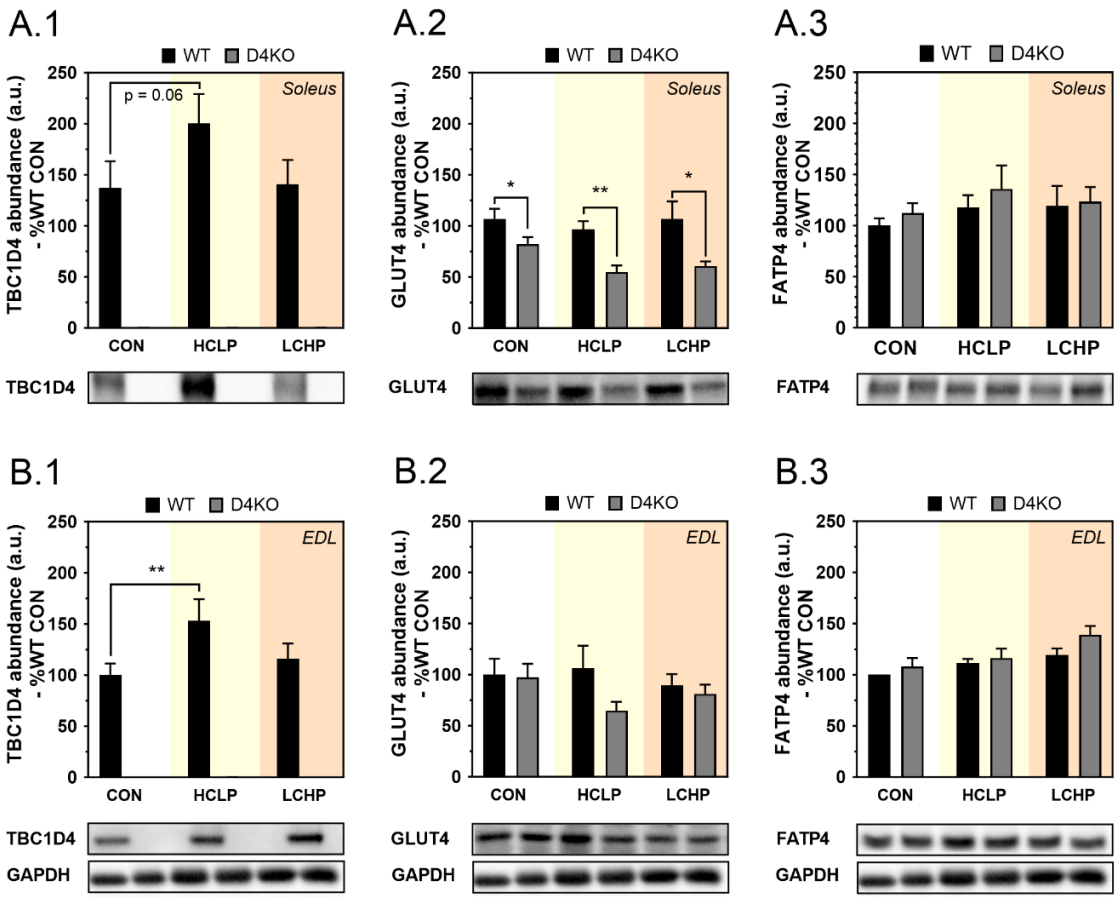

Figure 16: Impact of dietary macronutrient ratios on GLUT4 and FATP4 protein abundance in skeletal muscle of *Tbc1d4*-deficient mice. Representative Western blots and quantification of TBC1D4 (A.1, B.1), GLUT4 (A.2, B.2) and FATP4 (A.3, B.3) protein abundances in *Soleus* (A) and *EDL* (B) muscle of *Tbc1d4*-deficient (D4KO) mice and WT littermates aged 17–19 weeks subjected to a CON (indicated in white), HCLP (indicated in yellow) or LCHP (indicated in orange) diet (n = 10–13). Protein abundance in *Soleus* muscle was normalized to total protein via stain-free gels and protein abundance in *EDL* muscle was normalized to GAPDH. Data are presented as mean ± SEM. *p < 0.05, **p < 0.01, WT vs. D4KO (unpaired Student's t-test), *p < 0.05, **p < 0.01, CON vs. HCLP (Two-way ANOVA with Bonferroni correction).

3.2 Impact of dietary macronutrient ratios on the energy metabolism of mice with a muscle-specific Tbc1d4-deficiency

In Arctic populations, a nonsense mutation leading to loss of TBC1D4 in skeletal muscle results in impaired glycemic control, postprandial hyperglycemia, and has been associated with a significantly elevated risk of T2DM [258, 298]. Interestingly, enhanced physical activity correlates with improved glycemia in individuals with muscular TBC1D4-deficiency [260]. Previously, mice with a skeletal muscle *Tbc1d4*-deficiency (mD4KO) were generated to elucidate the individual contribution of skeletal muscle to whole-body glycemia. Therefore, mice carrying floxed *Tbc1d4* alleles were crossed with mice overexpressing a Cre recombinase regulated by a human skeletal muscle actin (HSA) promotor [266]. To elucidate the impact of nutrition on skeletal muscle and its contribution to whole-body glycemia, mD4KO mice were metabolically characterized during dietary interventions. In the following, mice carrying floxed *Tbc1d4* alleles lacking HSA-Cre recombinase, termed floxed, were used as control mice.

3.2.1 Body weight and body composition of mD4KO mice on HCLP and LCHP diets

In the present study, body composition (2.2.2.2) was unaltered in mD4KO mice compared to floxed mice when subjected to the CON diet (Figure 17 A.1–A.3), the HCLP diet (Figure 17 B.1–B.3) or the LCHP diet (Figure 17 C.1–C.3). In contrast to whole-body D4KO mice, the body fat mass of mD4KO mice on the HCLP diet was unchanged compared to floxed mice (Figure 17 B.2). Moreover, mice fed the HCLP diet had lower total body weight (Figure 17 B.1) and lean mass (Figure 17 B.3) compared to littermates on the CON or LCHP diets.

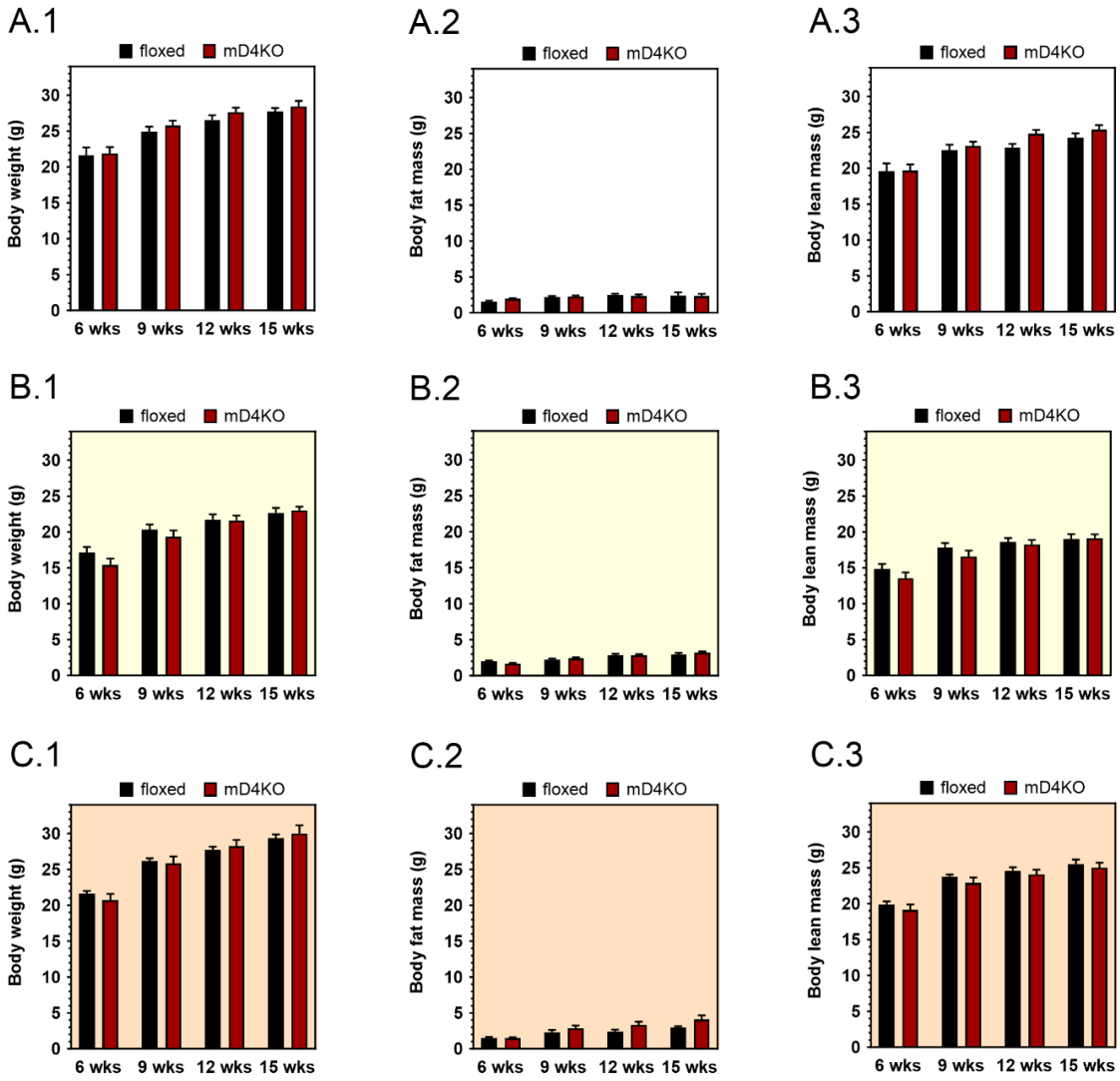

Figure 17: Impact of dietary macronutrient ratios on body composition of muscle-specific *Tbc1d4*-deficient mice. Determination of body composition in total body weight (A.1–C.1), body fat mass (A.2–C.2) and lean mass (A.3–C.3) in muscle-specific *Tbc1d4*-deficient (mD4KO) and floxed control mice subjected to a CON (A), HCLP (B) or LCHP (C) diet at 6, 9, 12 and 15 weeks of age. Data are presented as mean ± SEM (n = 7–10).

3.2.2 Whole-body glycemia in mD4KO mice on HCLP and HCLP diets

3.2.2.1 Blood glucose levels in mD4KO mice on HCLP and LCHP diets

In addition, random fed and fasted blood glucose concentrations were assessed (2.2.2.4). Similar to whole-body D4KO mice, random fed blood glucose concentrations remained unaltered between mD4KO and floxed mice during the CON (Figure 18 A.1), the HCLP (Figure 18 B.1) and the LCHP (Figure 18 C.1) dietary intervention. However, in contrast

to whole-body D4KO mice, 6 h fasted blood glucose concentrations of mD4KO mice were unaltered compared to floxed control mice on all diets (Figure 18 A.2–C.2). Moreover, after an overnight fast of 16 h, blood glucose concentrations were unchanged between mD4KO and floxed mice on all diets (Figure 18 A.3–C.3).

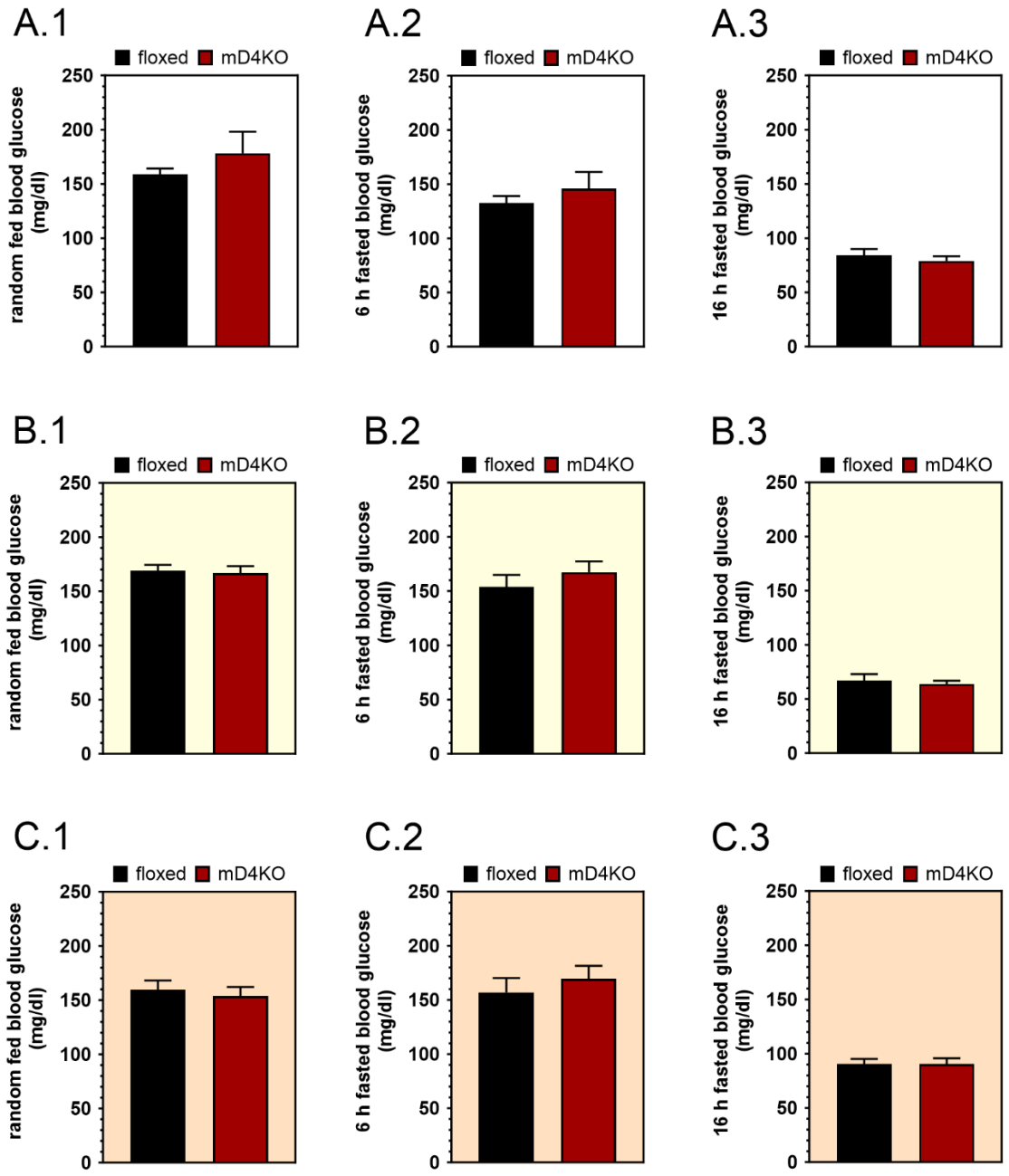

Figure 18: Impact of dietary macronutrient ratios on blood glucose of muscle-specific *Tbc1d4*-deficient mice. Determination of random fed (A.1–C.1), 6 h fasted (A.2–C.2) and 16 h fasted (A.3–C.3) blood glucose concentrations of male muscle-specific *Tbc1d4*-deficient (mD4KO) and floxed control mice

aged 12–14 weeks subjected to a CON (A), HCLP (B) or LCHP (C) diet. Data are presented as mean ± SEM (n = 7–10).

3.2.2.2 Glucose and insulin tolerance in mD4KO mice on HCLP and LCHP diets

To determine the impact of skeletal muscle *Tbc1d4*-deficiency on whole-body glycemia, glucose tolerance via i.p. GTT (2.2.2.5, Figure 19 A.1–C.1) and insulin tolerance via i.p. ITT (2.2.2.6, Figure 19 A.2–C.2) were determined in mD4KO mice. Similar to whole-body D4KO mice, glucose tolerance on each experimental diet remained unaltered between mD4KO and floxed mice, however, absolute blood glucose concentrations were elevated when mice were fed the LCHP diet, as indicated by the AUC (floxed: 42968 ± 2010 (CON), 44480 ± 2504 (HCLP), 65315 ± 3458 (LCHP), mD4KO: 42260 ± 1563 (CON), 43233 ± 2435 (HCLP), 62495 ± 3884 (LCHP), Figure 19 A.1–C.1).

Insulin tolerance was also unaffected by the genotype. However, absolute blood glucose concentrations were lower when mice were fed the HCLP diet, as indicated by the AUC (floxed: 5434 ± 382 (CON), 4436 ± 215 (HCLP), 6135 ± 193 (LCHP), mD4KO: 5981 ± 437 (CON), 4803 ± 225 (HCLP), 6625 ± 445 (LCHP), Figure 19 A.2–C.2).

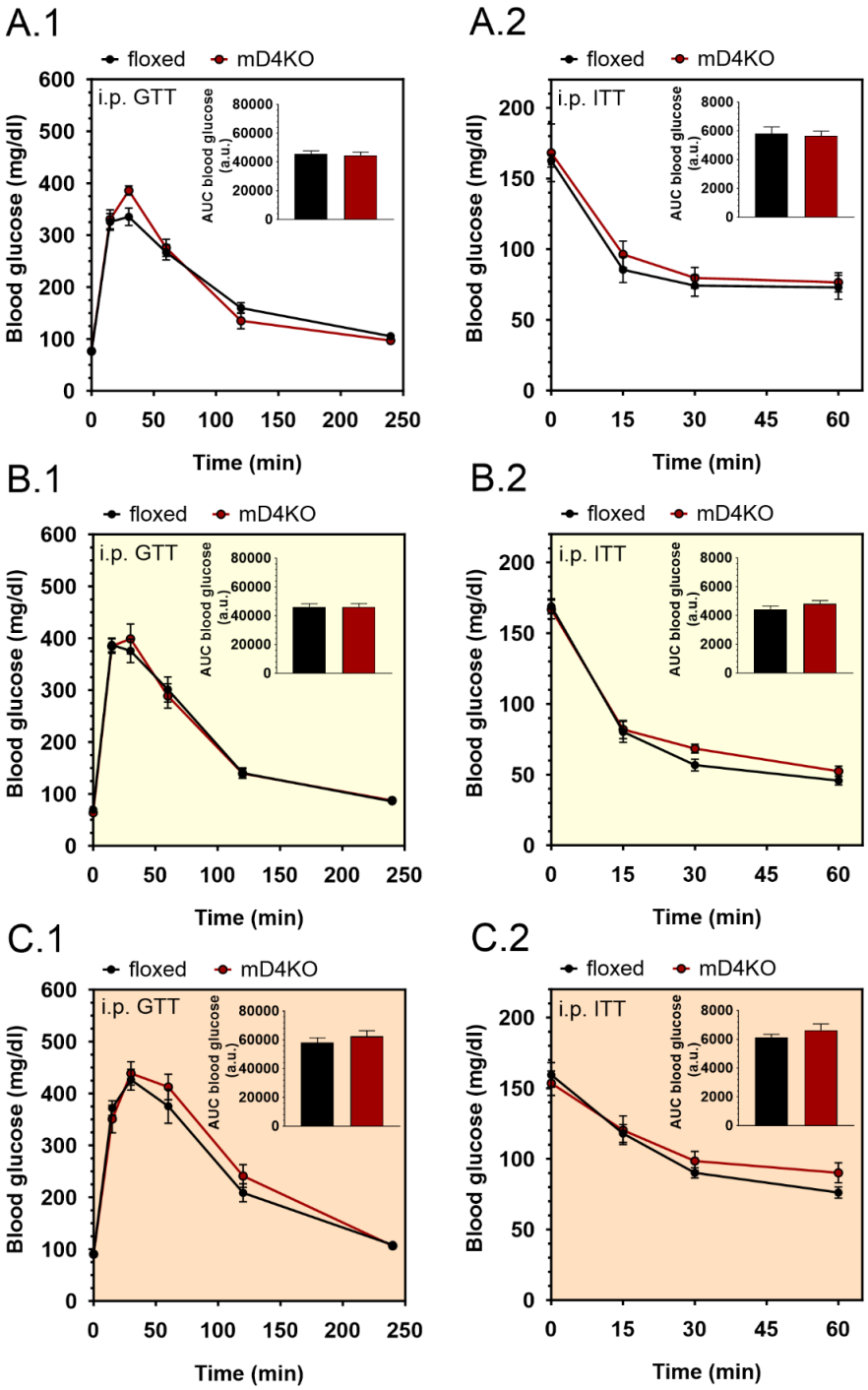

Figure 19: Impact of dietary macronutrient ratios on glucose and insulin tolerance in muscle-specific *Tbc1d4*-deficient mice. Determination of intraperitoneal tolerance for glucose (GTT) and insulin (ITT) of male muscle-specific *Tbc1d4*-deficient (mD4KO) and floxed control mice aged 12–14 weeks. Blood glucose concentrations in mD4KO mice after intraperitoneal injection of glucose (2 g/kg) subjected to a CON (A.1), HCLP (B.1) or LCHP (C.1) diet. Blood glucose concentrations after intraperitoneal injection of insulin (1 IU/kg) subjected to a CON (A.2), HCLP (B.2) or LCHP (C.2) diet. Data are presented as mean ± SEM (n = 7–10).

3.2.2.3 Postprandial glycemia in mD4KO mice on HCLP and LCHP diets

In addition, the impact of dietary macronutrient ratios on postprandial glycemia was determined in mD4KO mice (2.2.2.8). Similar to whole-body D4KO mice, postprandial blood glucose concentrations in mD4KO mice were significantly elevated compared to floxed control mice 1 h and 2 h after refeeding with the CON diet (Figure 20 A.1). Interestingly, postprandial blood glucose concentrations remained unchanged between mD4KO and floxed mice when subjected and refed with a HCLP diet (Figure 20 B.1). Consistent with whole-body D4KO mice, when subjected to and refed with a LCHP diet, blood glucose concentrations were unaltered between the genotypes (Figure 20 C.1). Plasma insulin concentrations (2.2.3.1) were unchanged between mD4KO and floxed mice on a CON diet (Figure 20 A.2). However, mD4KO mice fed the HCLP diet, showed tendentially elevated plasma insulin concentrations compared to floxed control mice, but remained unchanged on the LCHP diet (Figure 20 C.2). In addition, there was no significant difference in food intake between mD4KO and floxed mice regardless of the diet (Figure 20 A.3–C.3).

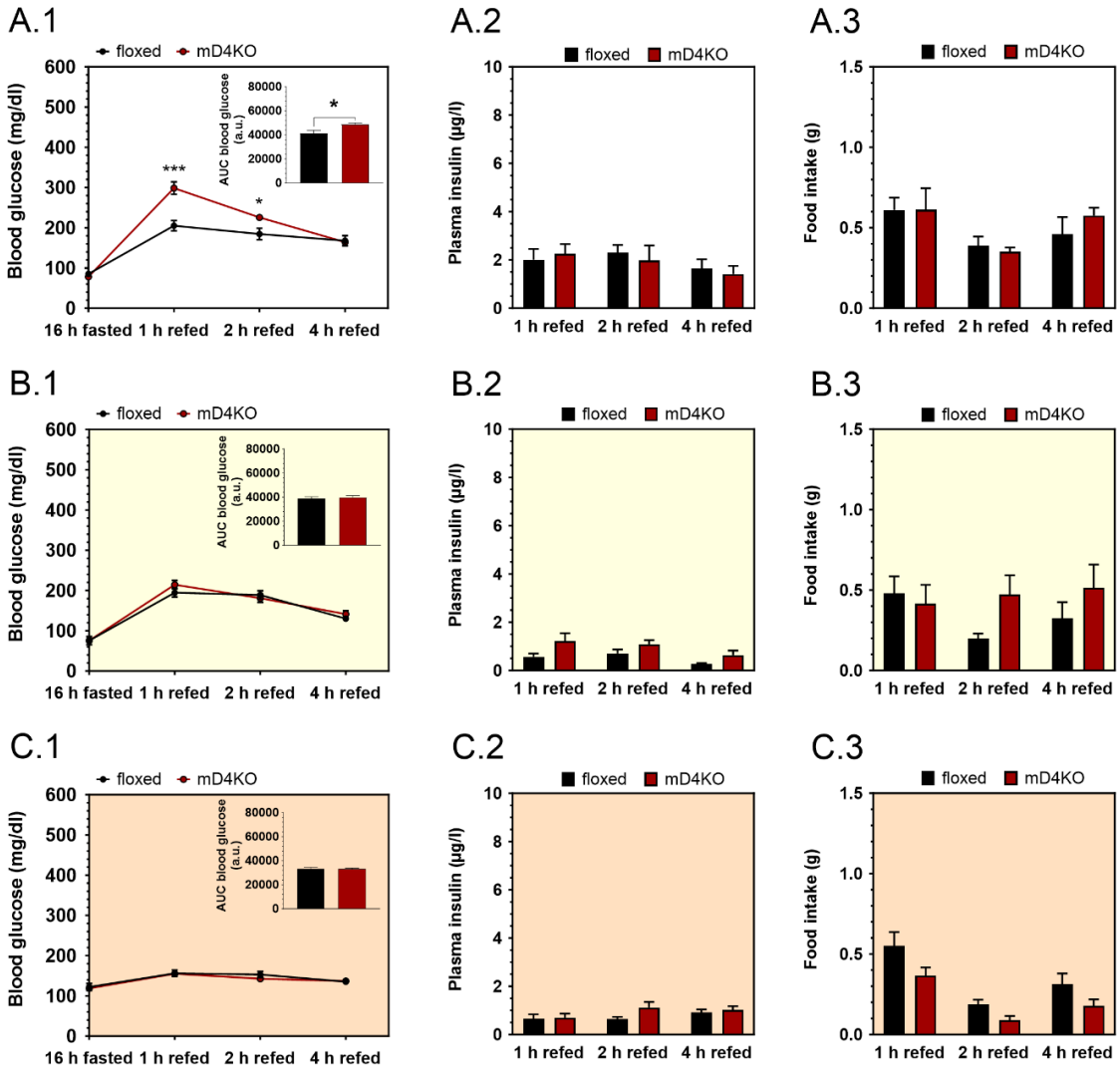

Figure 20: Impact of dietary macronutrient ratios on fasted and postprandial glycemia, plasma insulin concentrations and food intake of muscle-specific *Tbc1d4*-deficient mice. Determination of fasted and postprandial blood glucose concentrations and AUC (A.1–C.1), postprandial plasma insulin concentrations (A.2–C.2) and food intake (A.3–C.3) from muscle-specific Tbc1d4-deficient (mD4KO) and floxed control mice aged 16–17 weeks subjected to a CON (A), HCLP (B) or LCHP (C) diet. Data are presented as mean ± SEM (n = 7–10). *p < 0.05, **p < 0.01, ***p < 0.001 (Student's t-test).

3.2.4 Plasma parameters in mD4KO mice on HCLP and LCHP diets

Moreover, 6 h fasted plasma concentrations of insulin (2.2.3.1), ketone bodies (2.2.3.2), and NEFAs (2.2.3.3) were determined. Fasted plasma insulin concentrations were tendentially decreased in mD4KO compared to floxed mice on a CON diet (Figure 21 A.1) and tendentially increased on a LCHP diet (Figure 21 C.1). Interestingly, 6 h fasted plasma insulin concentrations were 4- to 6-fold higher in mD4KO and floxed mice fed the

CON or LCHP diets compared to a HCLP diet (Figure 21 B.1). Fasted plasma ketone body concentrations were unchanged in mD4KO mice compared to floxed control mice on all diets (Figure 21 A.2–C.2). Fasted plasma NEFA concentrations were unaltered between the two genotypes on the CON (Figure 21 A.3), but significantly elevated in mD4KO mice compared to floxed mice on the HCLP diet (floxed: 0.58 ± 0.06 mmol/l, mD4KO: 0.90 ± 0.12 mmol/l, Figure 21 B.3) and unchanged on the LCHP diet (Figure 21 C.3).

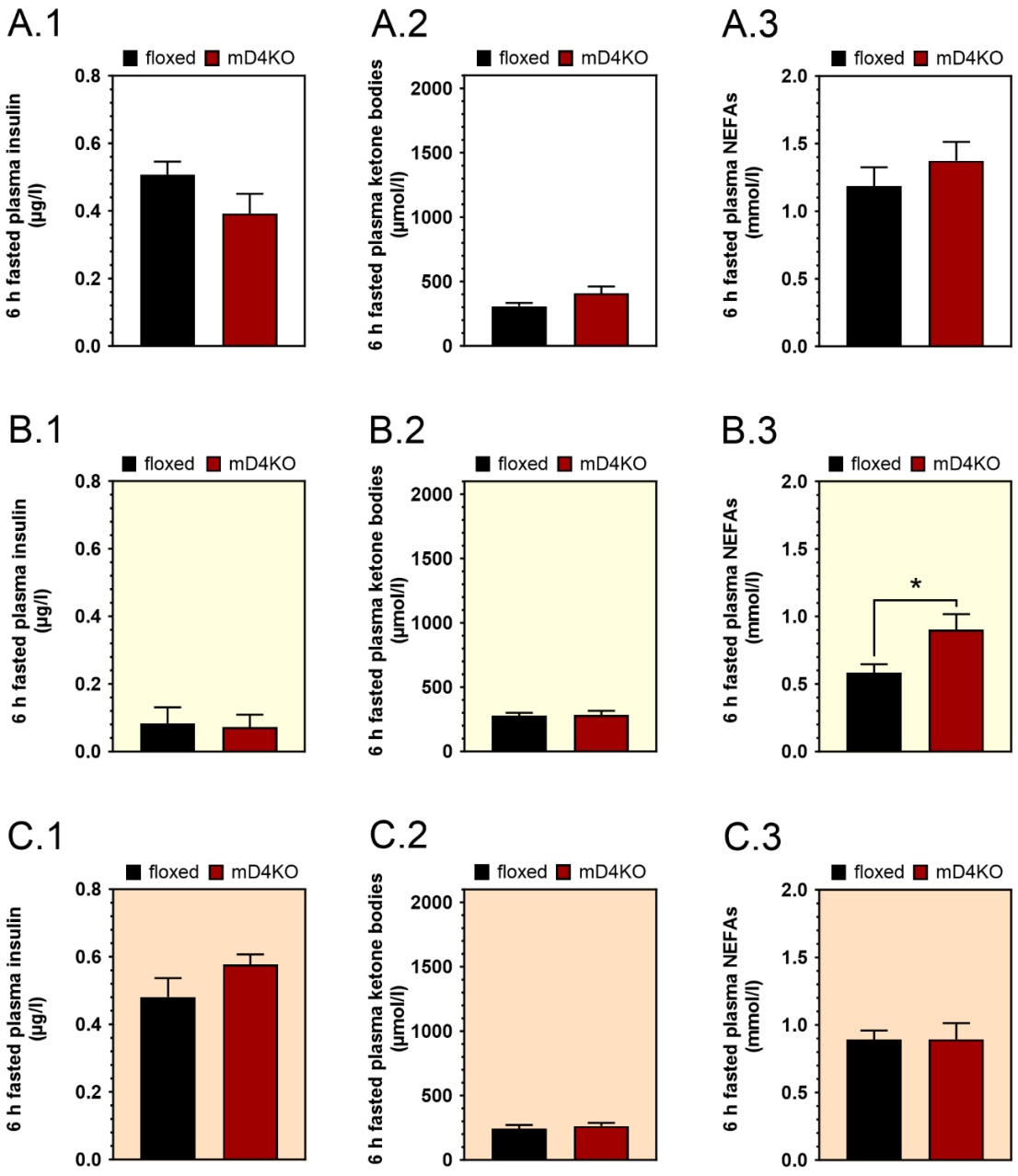

Figure 21: Impact of dietary macronutrient ratios on fasted plasma parameters of muscle-specific *Tbc1d4*-deficient mice. Determination of 6 h fasted plasma insulin (A.1–C.1), ketone bodies (A.2–C.2) and NEFA (A.3–C.3) concentrations of male muscle-specific *Tbc1d4*-deficient (mD4KO) and floxed control mice aged 14 weeks subjected to a CON (A), HCLP (B) or LCHP (C) diet. Data are presented as mean ± SEM (n = 7–9). *p < 0.05, **p < 0.01, ***p < 0.001, ****p < 0.0001 (Student's t-test).

3.2.5 Ex vivo substrate utilization in mD4KO mice on HCLP and LCHP diets

3.2.5.1 Insulin-stimulated glucose uptake into skeletal muscle from mD4KO mice on HCLP and LCHP diets

Additionally, glucose uptake in oxidative *Soleus* muscle was determined *ex vivo* (2.2.2.9). Consistent with data from whole-body D4KO mice, basal glucose uptake was unaltered between the genotypes regardless of the diet (Figure 22 A–C). However, when fed the CON diet basal glucose uptake was tendentially lower in mD4KO mice compared to floxed control mice. Furthermore, insulin-stimulated glucose uptake was significantly impaired in mD4KO compared to floxed mice fed the CON diet (Figure 22 A). Interestingly, insulin-stimulated glucose uptake in *Soleus* muscle of mD4KO mice remained unchanged compared to floxed mice when subjected to HCLP (Figure 22 B) and LCHP (Figure 22 C) diets.

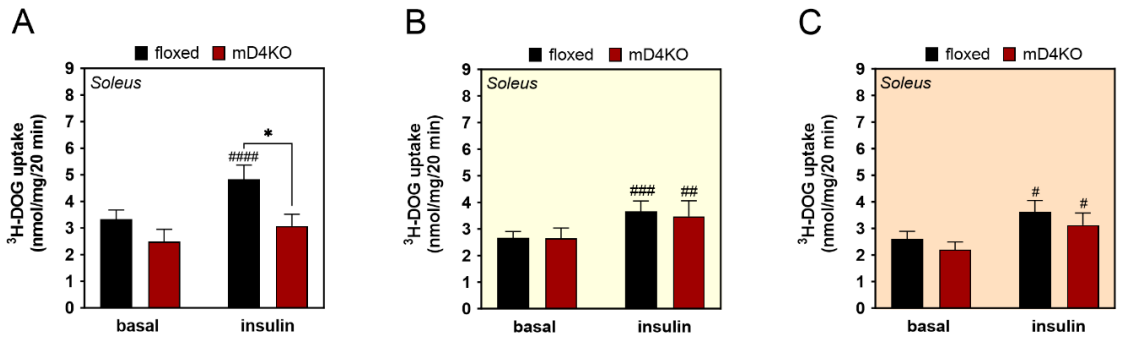

Figure 22: Impact of dietary macronutrient ratios on glucose uptake into oxidative *Soleus* muscle of muscle-specific *Tbc1d4*-deficient mice. Insulin-stimulated [^{3}H]-deoxyglucose uptake into oxidative Soleus muscle from muscle-specific *Tbc1d4*-deficient (mD4KO) and floxed control mice aged 17–19 weeks subjected to a CON (A), HCLP (B) or LCHP (C) diet (n = 7–9). Data are presented as mean ± SEM. *p < 0.05, floxed vs. mD4KO and #p < 0.05, ##p < 0.01, ###p < 0.001, ####p < 0.0001 basal vs. insulin (Two-way ANOVA with Bonferroni correction).

3.2.5.2 Insulin-stimulated glucose uptake into white adipocytes from mD4KO mice on HCLP and LCHP diets

Glucose uptake was also determined in primary white adipocytes from mD4KO mice (2.2.2.10). Both basal and insulin-stimulated glucose uptake were unchanged between the genotypes regardless of the diet. While basal glucose uptake was similar between the diets, insulin-stimulated glucose uptake in primary white adipocytes was higher in both genotypes when fed the CON (Figure 23 A) diet compared to a HCLP (Figure 23 B) or

LCHP (Figure 23 C) diet (floxed: 299.3 ± 69.7 cpm/ mg lipid (CON), 182.3 ± 25.5 cpm/ mg lipid (HCLP), 197.5 ± 47.6 cpm/ mg lipid (LCHP); mD4KO: 283.6 ± 35.7 cpm/ mg lipid (CON), 160.1 ± 11.8 cpm/ mg lipid (HCLP), 124.4 ± 23 cpm/ mg lipid (LCHP)).

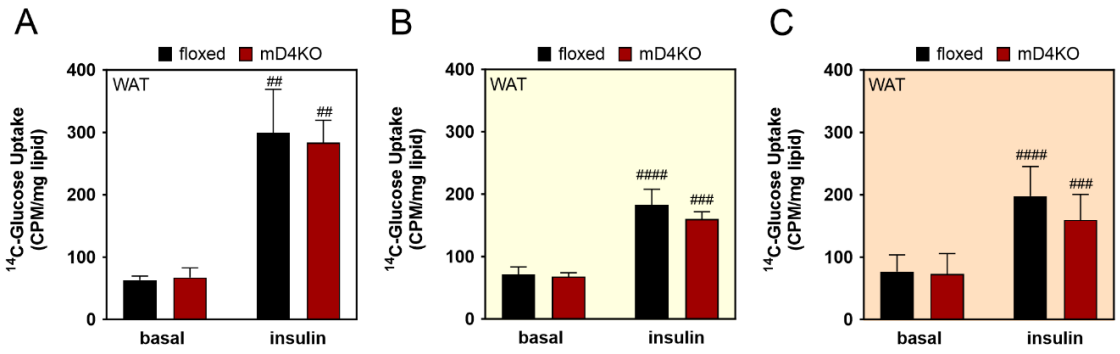

Figure 23: Impact of dietary macronutrient ratios on glucose uptake into primary white adipocytes of muscle-specific *Tbc1d4*-deficient mice Insulin-stimulated [^{14}C]-D-glucose (U) uptake into primary adipocytes from epididymal WAT of muscle-specific *Tbc1d4*-deficient (mD4KO) and floxed control mice aged 17–19 weeks subjected to a CON (A), HCLP (B) or LCHP (A.4) diet (n = 7–10). Data are presented as mean ± SEM. #p < 0.05, ##p < 0.01, ###p < 0.001, ####p < 0.0001 basal vs. insulin (Two-way ANOVA with Bonferroni correction).

3.3 Impact of dietary macronutrient ratios on the energy metabolism of mice with an adipose tissue-specific Tbc1d4-deficiency

Besides skeletal muscle, TBC1D4 further presents a key regulator of insulin-stimulated glucose uptake in adipose tissue. Recent findings from our group indicate differential contributions of skeletal muscle and adipose tissue to whole-body glycemia in *Tbc1d4*-deficient mice [266, 290]. To elucidate the individual contribution of the adipose tissue to whole-body glycemia, mice deficient in *Tbc1d4* in adipocytes (aD4KO) were generated by crossing mice carrying floxed *Tbc1d4* alleles with mice overexpressing a Cre recombinase regulated by an adiponectin promotor [266]. To evaluate the impact of macronutrient ratios on the adipose tissue and its contribution to whole-body glycemia, aD4KO mice were metabolically characterized during dietary interventions. In the following, mice carrying floxed *Tbc1d4* alleles lacking adiponectin-Cre recombinase, termed floxed, were used as control mice.

3.3.1 Body weight and body composition of aD4KO mice on HCLP and LCHP diets

In the present study, body composition was determined in aD4KO mice (2.2.2.2). Total body weight was unaltered in aD4KO mice compared to floxed mice when subjected to a CON (Figure 24 A.1), a HCLP (Figure 24 B.1), or a LCHP (Figure 24 C.1) diet. Similar to mD4KO mice, the body fat mass of aD4KO mice was unchanged compared to floxed control mice when fed the CON diet (Figure 24 A.2). However, when fed the HCLP diet, aD4KO mice showed tendentially elevated body fat mass at 6, 9, and 12 weeks of age and significantly elevated body fat mass at 15 weeks of age compared to floxed control mice (Figure 24 B.2). When fed the LCHP diet, body fat mass was unchanged between the genotypes (Figure 24 C.2). Moreover, total body lean mass tended to be elevated in aD4KO mice compared to floxed control mice on all diet (Figure 24 A.3–C.3).

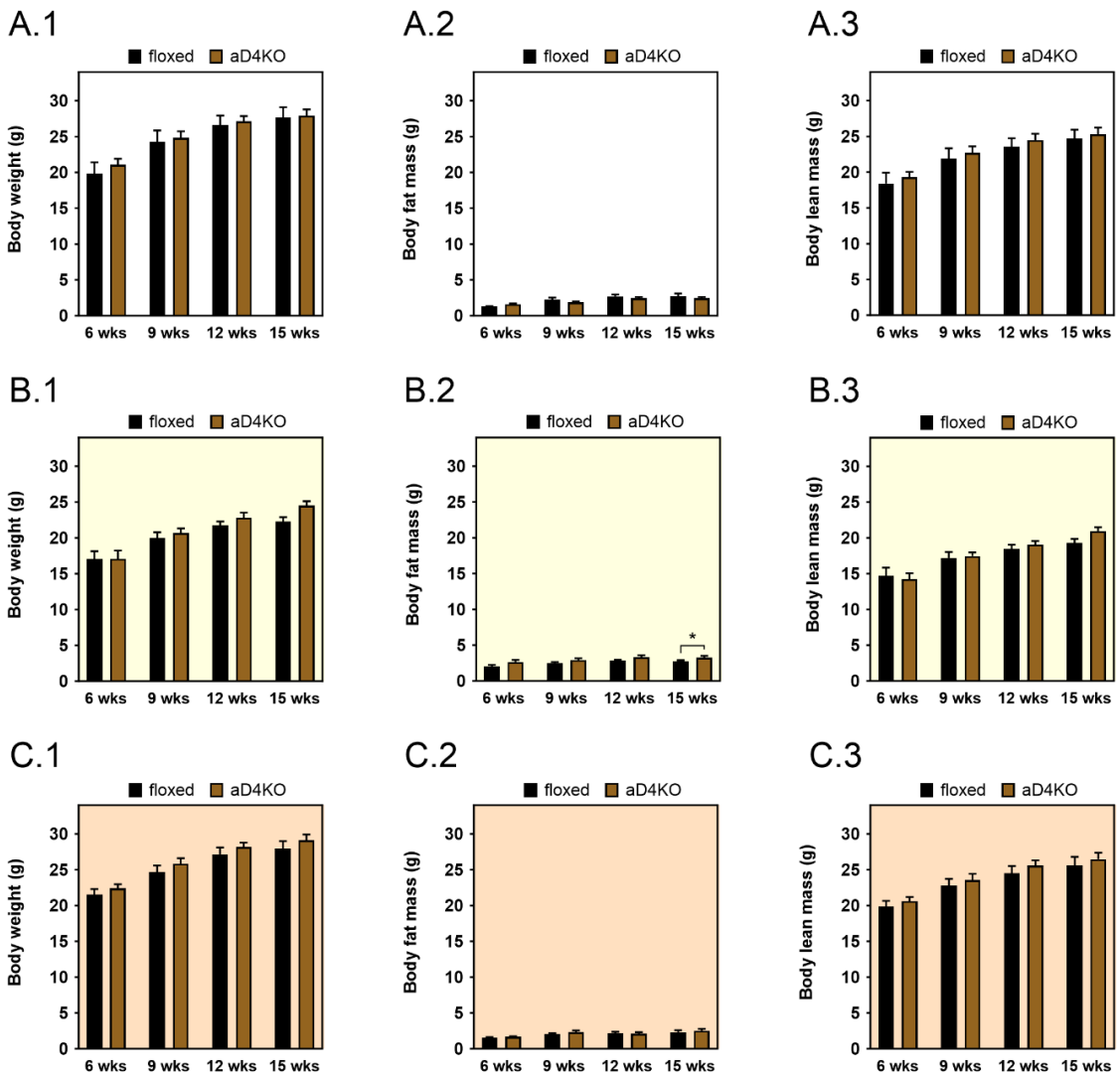

Figure 24: Impact of dietary macronutrient ratios on body composition of adipocyte-specific *Tbc1d4*-deficient mice. Determination of body composition in total body weight (A.1–C.1), body fat mass (A.2–C.2) and lean mass (A.3–C.3) in adipocyte-specific *Tbc1d4*-deficient (aD4KO) and floxed control mice subjected to a CON (A), HCLP (B) or LCHP (C) diet at 6, 9, 12 and 15 weeks of age. Data are presented as mean ± SEM (n = 7–9).

3.3.2 Whole-body glycemia in aD4KO mice on HCLP and HCLP diets

3.3.2.1 Blood glucose concentrations in aD4KO mice on HCLP and HCLP diets

In addition, random fed and fasted blood glucose concentrations were determined (2.2.2.4). Interestingly, in contrast to whole-body D4KO and mD4KO mice, random fed blood glucose concentrations were significantly reduced in aD4KO compared to floxed mice when subjected to the CON (Figure 25 A.1) and the HCLP (Figure 25 B.1), but not

the LCHP (Figure 25 C.1) dietary intervention. 6 h fasted blood glucose concentrations of aD4KO mice tended to be decreased compared to floxed control mice on the CON diet (Figure 25 A.2). However, when fed the HCLP diet, 6 h fasted blood glucose concentrations were significantly decreased in aD4KO mice compared to floxed control mice (Figure 25 B.2), but remained unaltered on the LCHP diet (Figure 25 C.2). Moreover, after an overnight fast of 16 h, blood glucose concentrations were unchanged between aD4KO and floxed mice during all dietary interventions (Figure 25 A.3–C.3), but were increased in both genotypes on a LCHP compared to a CON or HCLP diet (floxed: 73 ± 2 mg/dL (CON), 61 ± 3 mg/dL (HCLP), 105 ± 7 mg/dL (LCHP), aD4KO: 74 ± 3 mg/dL (CON), 63 ± 2 mg/dL (HCLP), 94 ± 5 mg/dL (LCHP)).

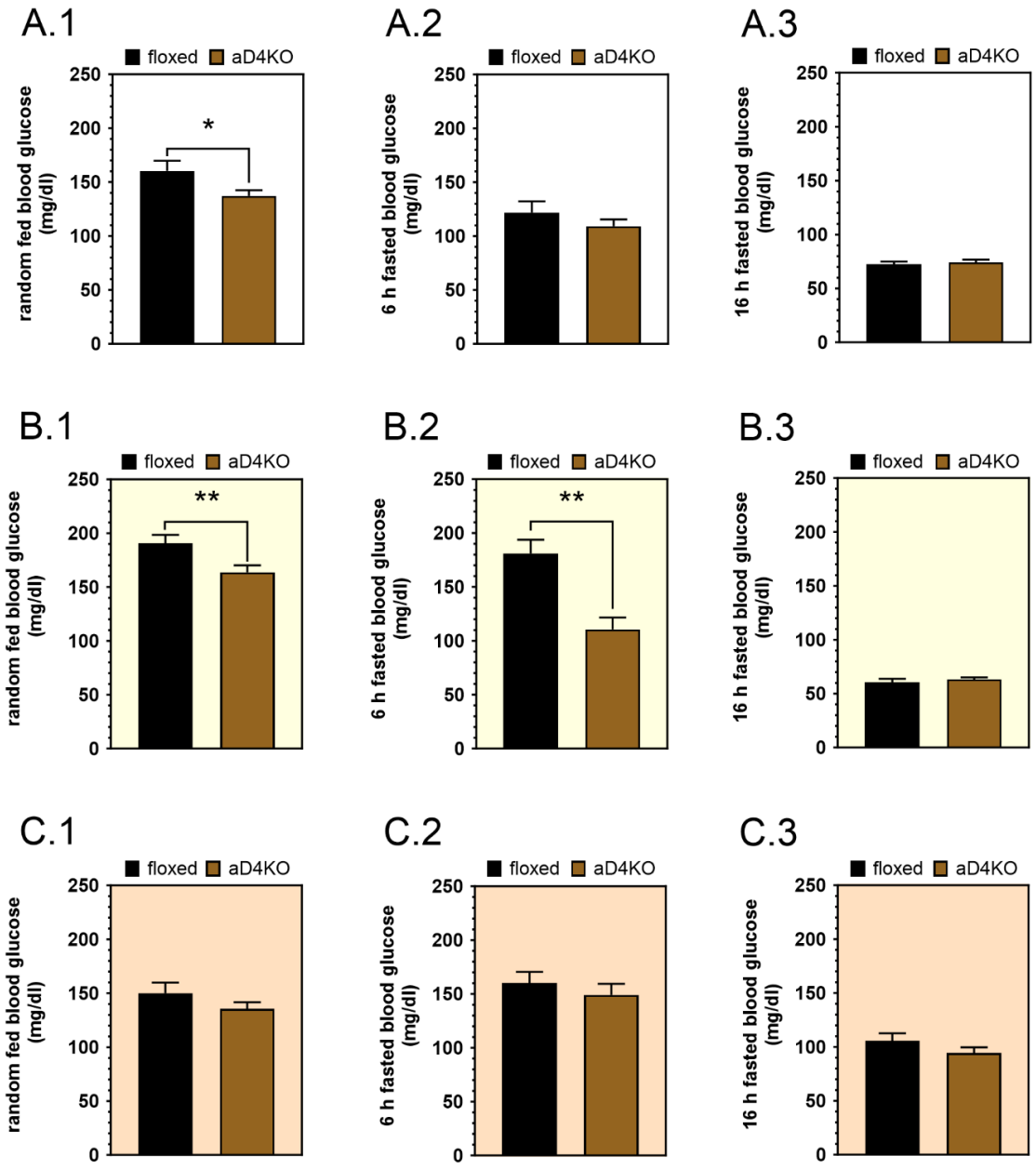

Figure 25: Impact of dietary macronutrient ratios on blood glucose of adipocyte-specific *Tbc1d4*-deficient mice. Determination of random fed (A.1–C.1), 6 h fasted (A.2–C.2) and 16 h fasted (A.3–C.3) blood glucose concentrations of male adipocyte-specific *Tbc1d4*-deficient (aD4KO) and floxed control mice aged 12–14 weeks subjected to a CON (A), HCLP (B) or LCHP (C) diet. Data are presented as mean ± SEM (n = 7–10). *p < 0.05, **p < 0.01 (Student's t-test).

3.3.2.2 Glucose and insulin tolerance in aD4KO mice on HCLP and LCHP diets

To evaluate the impact of adipose tissue on whole-body glycemia, glucose tolerance by i.p. GTT (2.2.2.5, Figure 26 A.1–C.1) and insulin tolerance by i.p. ITT (2.2.2.6, Figure 26 A.2–C.2) were determined in aD4KO mice.

Similar to whole-body D4KO and mD4KO mice, glucose tolerance remained unaltered between aD4KO and floxed mice when subjected to a CON diet (Figure 26 A.1). However, when fed the HCLP diet (Figure 26 B.1), glucose tolerance tended to be elevated in a aD4KO mice compared to floxed control mice, and was significantly elevated when subjected to the LCHP diet as indicated by the AUC (HCLP: 48060 ± 3946 (floxed), 45597 ± 3324 (aD4KO), LCHP: 64406 ± 3218 (floxed), 56247 ± 2038 (aD4KO), Figure 26 C.1). Similar to whole-body D4KO and mD4KO mice, absolute blood glucose concentrations were elevated when mice were subjected to the LCHP diet compared to the CON or HCLP diets as indicated by the AUC (floxed: 46123 ± 1291 (CON), 48060 ± 3946 (HCLP), 64406 ± 3218 (LCHP), aD4KO: 44576 ± 959 (CON), 45597 ± 3324 (HCLP), 56247 ± 2038 (LCHP)).

Insulin tolerance was also unaltered between the genotypes. However, absolute blood glucose concentrations were lowest when mice were fed the HCLP diet compared to the CON or LCHP diets as indicated by the AUC (floxed: 6454 ± 387 (CON), 5514 ± 304 (HCLP), 6364 ± 492 (LCHP), aD4KO: 5763 ± 252 (CON), 5338 ± 222 (HCLP), 6508 ± 343 (LCHP), Figure 26 A.2–C.2).

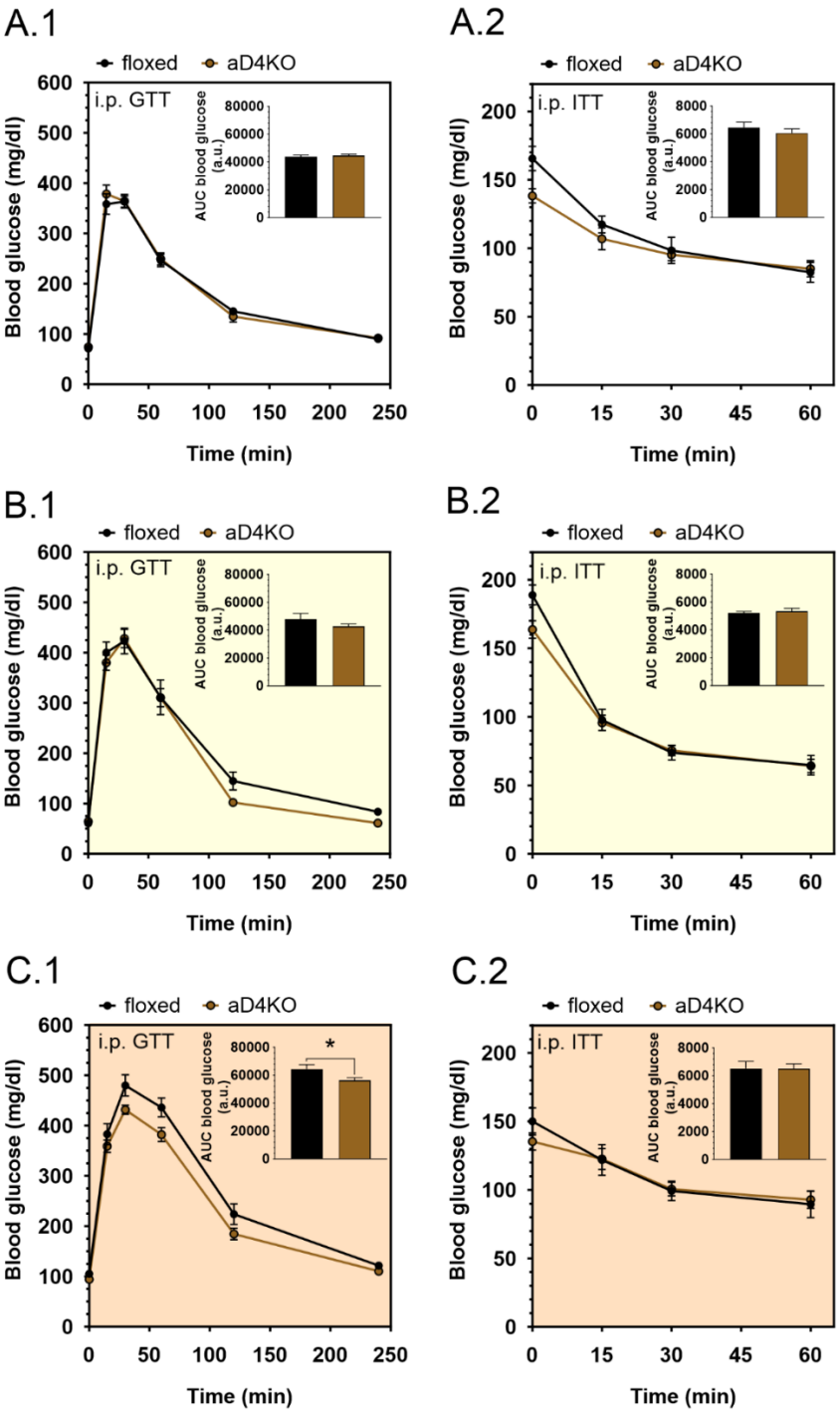

Figure 26: Impact of dietary macronutrient ratios on glucose and insulin tolerance in adipocyte-specific *Tbc1d4*-deficient mice. Determination of intraperitoneal tolerance for glucose (GTT) and insulin (ITT) of male adipocyte-specific *Tbc1d4*-deficient (aD4KO) and floxed control mice aged 12–14 weeks. Blood glucose concentrations in aD4KO mice after intraperitoneal injection of glucose (2 g/kg) subjected to a CON (A.1), HCLP (B.1) or LCHP (C.1) diet. Blood glucose concentrations after intraperitoneal injection of insulin (1 IU/kg) subjected to a CON (A.2), HCLP (B.2) or LCHP (C.2) diet. Data are presented as mean ± SEM (n = 7–9). *p < 0.05, (Student's t-test).

3.3.2.3 Postprandial glycemia in aD4KO mice on HCLP and LCHP diets

Subsequently, the impact of dietary macronutrient ratios on postprandial glycemia was determined in aD4KO mice (2.2.2.8). Unlike whole-body D4KO and mD4KO mice, postprandial blood glucose concentrations in aD4KO mice were unchanged compared to floxed control mice when subjected and refed with the CON diet (Figure 27 A.1). However, when subjected and refed with the HCLP diet, postprandial blood glucose concentrations were significantly increased in aD4KO compared to floxed mice 1 h, 2 h, and 4 h after refeeding (Figure 27 B.1). Consistent with whole-body D4KO and mD4KO mice, blood glucose concentrations were unaltered between the genotypes when subjected and refed with the LCHP diet (Figure 27 C.1). Plasma insulin concentrations were tendentially increased in aD4KO compared to floxed mice 1 h and 2 h after refeeding and significantly increased 4 h after refeeding on a CON diet (Figure 27 A.2). However, when subjected to a HCLP (Figure 27 B.2) or LCHP (Figure 27 C.2) diets, plasma insulin concentrations remained unaltered between aD4KO and floxed control mice. Furthermore, there was no significant difference in food intake between aD4KO and floxed mice regardless of the diet (Figure 27 A.3–C.3).

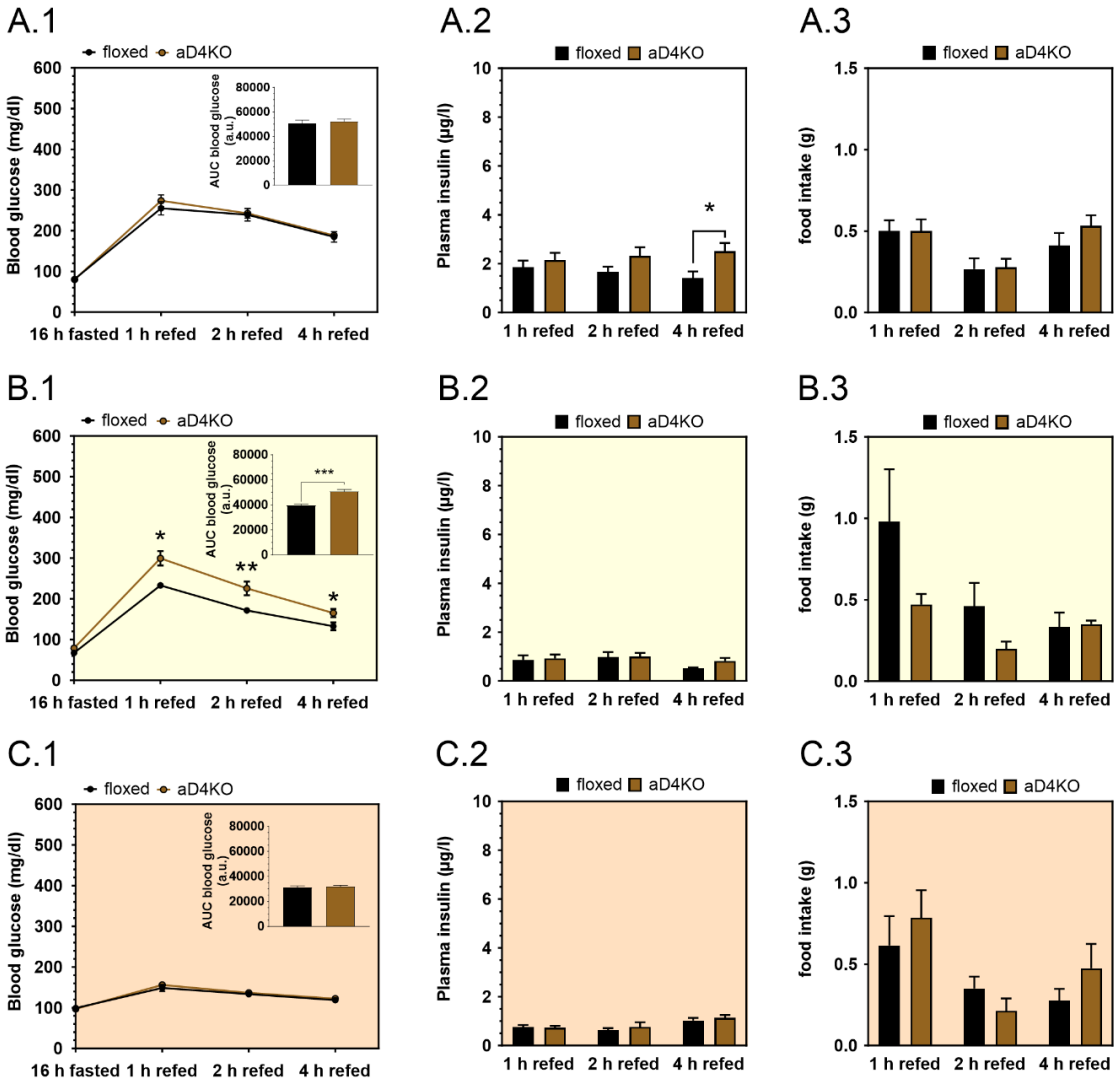

Figure 27: Impact of dietary macronutrient ratios on fasted and postprandial glycemia, plasma insulin concentrations and food intake of adipocyte-specific *Tbc1d4*-deficient mice. Determination of fasted and postprandial blood glucose concentrations and AUC (A.1–C.1), postprandial plasma insulin concentrations (A.2–C.2) and food intake (A.3–C.3) from adipocyte-specific *Tbc1d4*-deficient (aD4KO) and floxed control mice aged 16–17 weeks subjected to a CON (A), HCLP (B) or LCHP (C) diet. Data are presented as mean ± SEM (n = 7-9). *p < 0.05, **p < 0.01, ***p < 0.001 (Student's t-test).

3.3.4 Plasma parameters in aD4KO mice on HCLP and LCHP diets

In addition, 6 h fasted plasma concentrations of insulin (2.2.3.1), ketone bodies (2.2.3.2), and NEFAs (2.2.3.3) were analyzed. Fasted plasma insulin concentrations were similar between the genotypes on CON (Figure 28 A.1), HCLP (Figure 28 B.1), and LCHP (Figure 28 C.1) diets. Similar to the whole-body D4KO and mD4KO cohorts, 6 h fasted plasma insulin concentrations were lowest when mice were subjected to the HCLP diet.

Similar to whole-body D4KO, but not mD4KO mice, concentrations of fasted plasma ketone body concentrations were significantly increased in aD4KO mice compared to floxed control mice on all diets (Figure 28 A.2–C.2). Fasted plasma NEFA concentrations were unaltered between the genotypes when subjected to a CON diet (Figure 28 A.3), but were significantly elevated in aD4KO mice compared to floxed control mice when subjected to the HCLP diet (floxed: 0.62 ± 0.06 mmol/l, aD4KO: 0.86 ± 0.09 mmol/l, Figure 24 B.3), similar to the concentrations observed in mD4KO mice. When subjected to the LCHP diet, fasted plasma NEFA concentrations were unchanged (Figure 28 C.3).

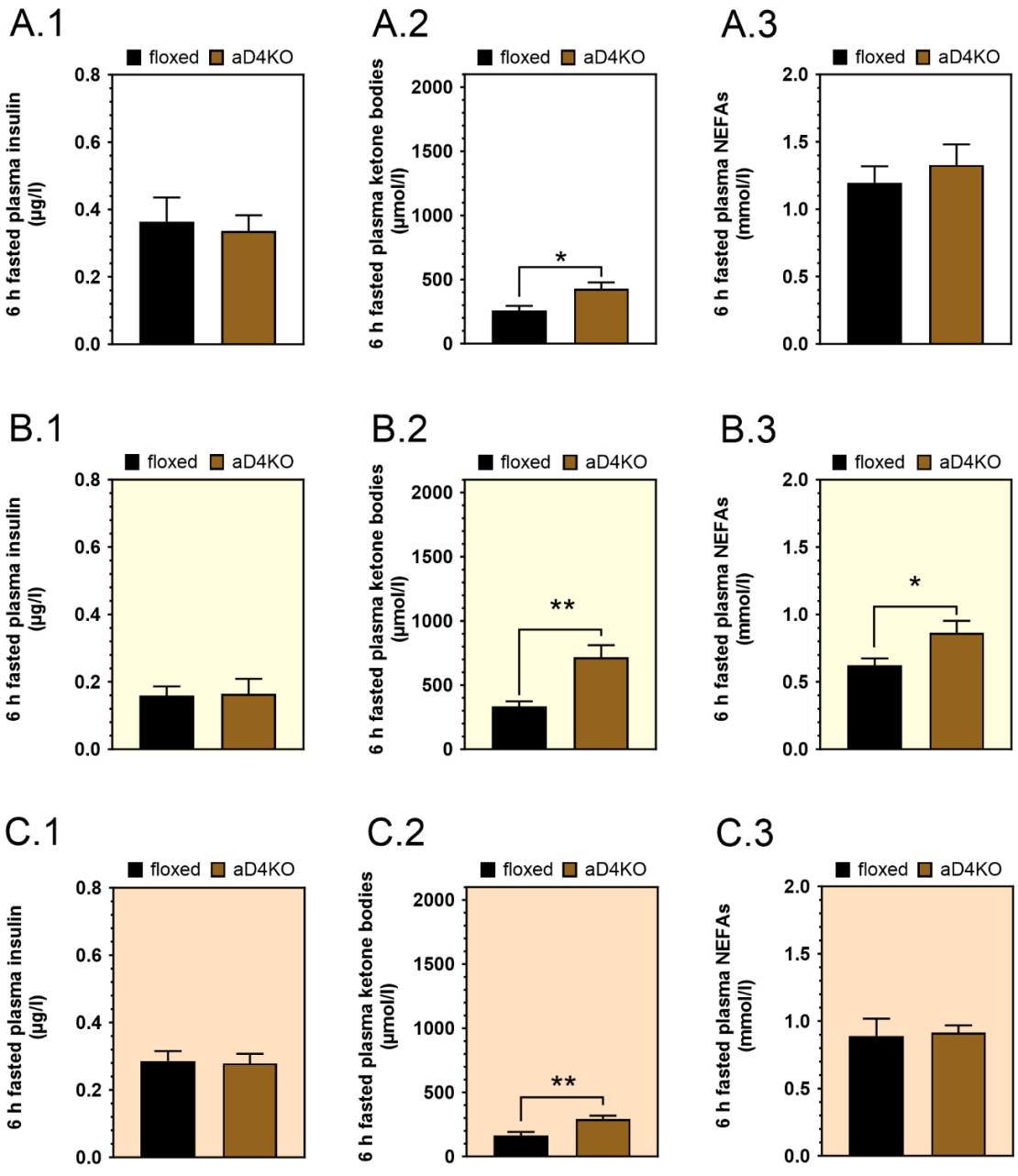

Figure 28: Impact of dietary macronutrient ratios on fasted plasma parameters of adipocyte-specific *Tbc1d4*-deficient mice. Determination of 6 h fasted plasma insulin (A.1–C.1), ketone bodies (A.2–C.2) and NEFA (A.3–C.3) concentrations of male adipocyte-specific *Tbc1d4*-deficient (aD4KO) and floxed control mice aged 14 weeks subjected to a CON (A), HCLP (B) or LCHP (C) diet. Data are presented as mean ± SEM (n = 7–9). *p < 0.05, **p < 0.01, (Student's t-test).

3.3.5 Ex vivo substrate utilization in aD4KO mice on HCLP and LCHP diets

3.3.5.1 Insulin-stimulated glucose uptake into skeletal muscle from aD4KO mice on HCLP and LCHP diets

Subsequently, *ex vivo* glucose uptake in oxidative *Soleus* muscle was determined (2.2.2.9). Basal and insulin-stimulated glucose uptake into *Soleus* muscle indicated no significant differences between the genotypes (Figure 29 A–C). However, when subjected to the HCLP diet, basal and insulin-stimulated glucose uptake tended to be lower in aD4KO mice compared to floxed control mice (Figure 29 B). Interestingly, basal and insulin-stimulated glucose uptake in *Soleus* muscle of aD4KO mice was lowest when subjected to a LCHP diet (Figure 29 C).

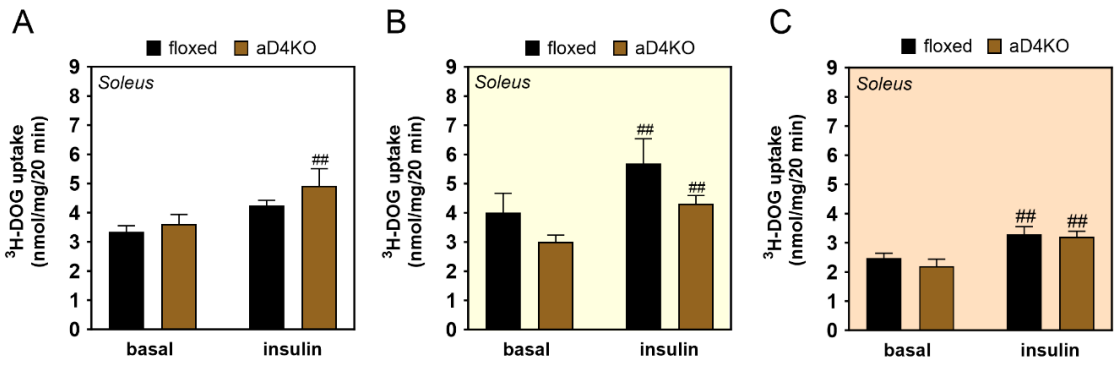

Figure 29: Impact of dietary macronutrient ratios on glucose uptake into oxidative *Soleus* muscle of adipocyte-specific *Tbc1d4*-deficient mice. Insulin-stimulated [^{3}H]-deoxyglucose uptake into oxidative *Soleus* muscle from adipocyte-specific *Tbc1d4*-deficient (aD4KO) and floxed control mice aged 17–19 weeks subjected to a CON (A), HCLP (B) or LCHP (C) diet (n = 6–9). Data are presented as mean ± SEM. #p < 0.05, ##p < 0.01, basal vs. insulin (Two-way ANOVA).

3.3.5.2 Insulin-stimulated glucose uptake into white adipocytes from aD4KO mice on HCLP and LCHP diets

Additionally, glucose uptake was determined in primary white adipocytes from aD4KO mice (2.2.2.10). Basal glucose uptake was altered between the genotypes on all diets. However, similar to whole-body D4KO mice, insulin-stimulated glucose uptake into WAT was impaired in aD4KO mice compared to floxed control mice when subjected to

a CON diet (Figure 30 A) and significantly decreased in aD4KO when subjected to a HCLP (Figure 30 B) and LCHP (Figure 30 C) diets.

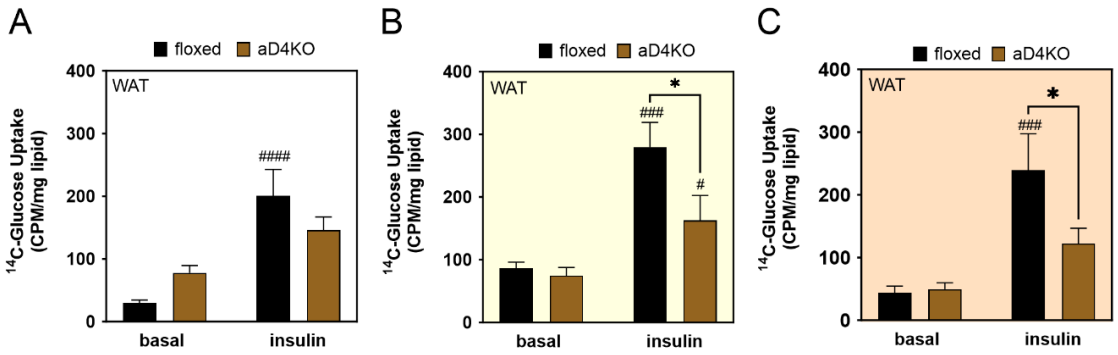

Figure 30: Impact of dietary macronutrient ratios on glucose uptake into primary white adipocytes of adipocyte-specific *Tbc1d4*-deficient mice Insulin-stimulated [^{14}C]-D-glucose (U) uptake into primary adipocytes from epididymal WAT of adipocyte-specific *Tbc1d4*-deficient (aD4KO) and floxed control mice aged 17–19 weeks subjected to a CON (A), HCLP (B) or LCHP (A.4) diet (n = 6–9). Data are presented as mean ± SEM. *p < 0.05 floxed vs. aD4KO and #p < 0.05, ##p < 0.01, ###p < 0.001, ####p < 0.0001 basal vs. insulin (Two-way ANOVA with Bonferroni correction).

3.4 Chronic adaptations in skeletal muscle and white adipose tissue of D4KO mice

Data obtained from metabolic characterization of whole-body D4KO and tissue-specific D4KO mice revealed differential effects of different macronutrient ratios on skeletal muscle and adipose tissue. In addition, the results indicate distinct contributions of skeletal muscle and adipose tissue to whole-body glycemia. Although TBC1D4 was shown to be an acute regulator of postprandial blood glucose concentrations, further results indicated chronic adaptations in skeletal muscle and adipose tissue in response to dietary intervention. Therefore, a bottom-up proteomics approach (2.2.6) was used to elucidate chronic changes in the proteome of whole-body D4KO mice and WT littermates induced by a HCLP and LCHP dietary intervention.

3.4.1 Impact of a nutrition on skeletal muscle proteome of D4KO mice

To investigate the chronic adaptations in skeletal muscle of whole-body D4KO mice, an untargeted proteomic analysis was performed on *Gastrocnemius* muscle of WT and D4KO subjected to chronic dietary intervention with HCLP or LCHP diets (2.2.6.1). Mass spectrometry analysis (2.2.6.4) revealed a total of 366 proteins significantly regulated in the *Gastrocnemius* muscle of D4KO mice compared to WT littermates on the HCLP diet, of which 160 proteins were up-regulated and 206 were down-regulated. When subjected to the LCHP diet, 313 proteins were differentially regulated in D4KO compared to WT mice, of which 164 were up-regulated and 149 down-regulated. In WT mice, a total of 293 proteins were differentially regulated on a LCHP vs. a HCLP diet. While 134 proteins were up-regulated, 159 proteins were down-regulated in WT mice subjected to a LCHP vs. a HCLP diet. In D4KO mice, 386 proteins were shown to be differentially regulated on a LCHP vs. a HCLP diet, including 202 up-regulated and 184 down-regulated proteins (Figure 31).

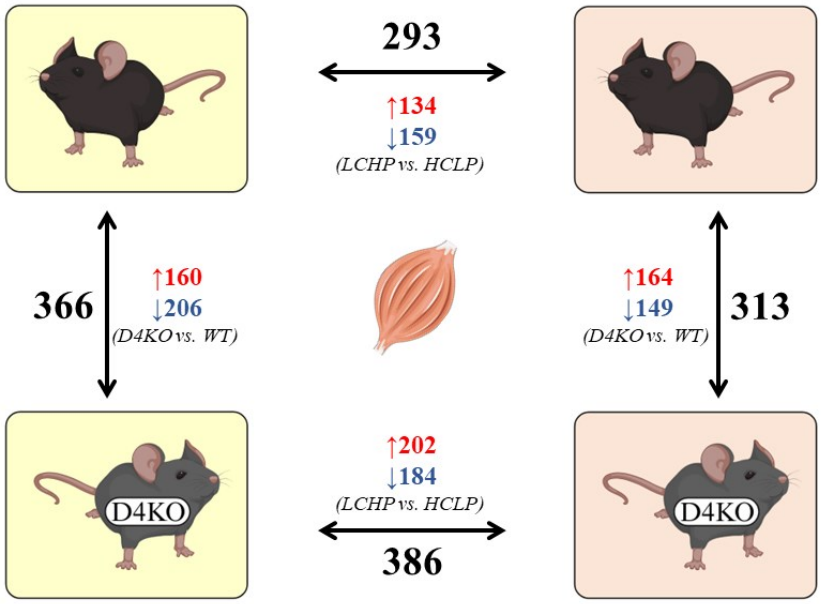

Figure 31: Impact of nutrition on proteome of *Gastrocnemius* muscle of *Tbc1d4*-deficient mice. Overview of differentially regulated proteins (indicated by black arrows) in *Gastrocnemius* muscle of *Tbc1d4*-deficient mice and WT littermates aged 17–19 weeks subjected to a HCLP (indicated in yellow) or LCHP (indicated in orange) diet. Red arrows indicate up-regulated and blue arrows indicate down-regulated proteins. Significance threshold was set at $p < 0.05$ ($n = 6$). Created with Biorender.com

3.4.1.1 Differentially regulated proteins in Gastrocnemius muscle in response to a LCHP vs. a HCLP diet in Tbc1d4-deficient mice

To evaluate potential proteins involved in regulation of postprandial glycemia and improvement of insulin sensitivity in skeletal muscle of *Tbc1d4*-deficient mice in response to a LCHP diet, the proteome of *Gastrocnemius* muscle was visualized in volcano plots. In addition, unregulated and differentially down- and up-regulated proteins were revealed, indicated in black, blue and red, respectively. Proteome analysis highlighted differentially regulated proteins in D4KO vs. WT mice subjected to a HCLP (Figure 32 A) or a LCHP (Figure 32 B) as well as in WT (Figure 32 C) and D4KO (Figure 32 D) mice subjected to a LCHP vs. a HCLP diets.

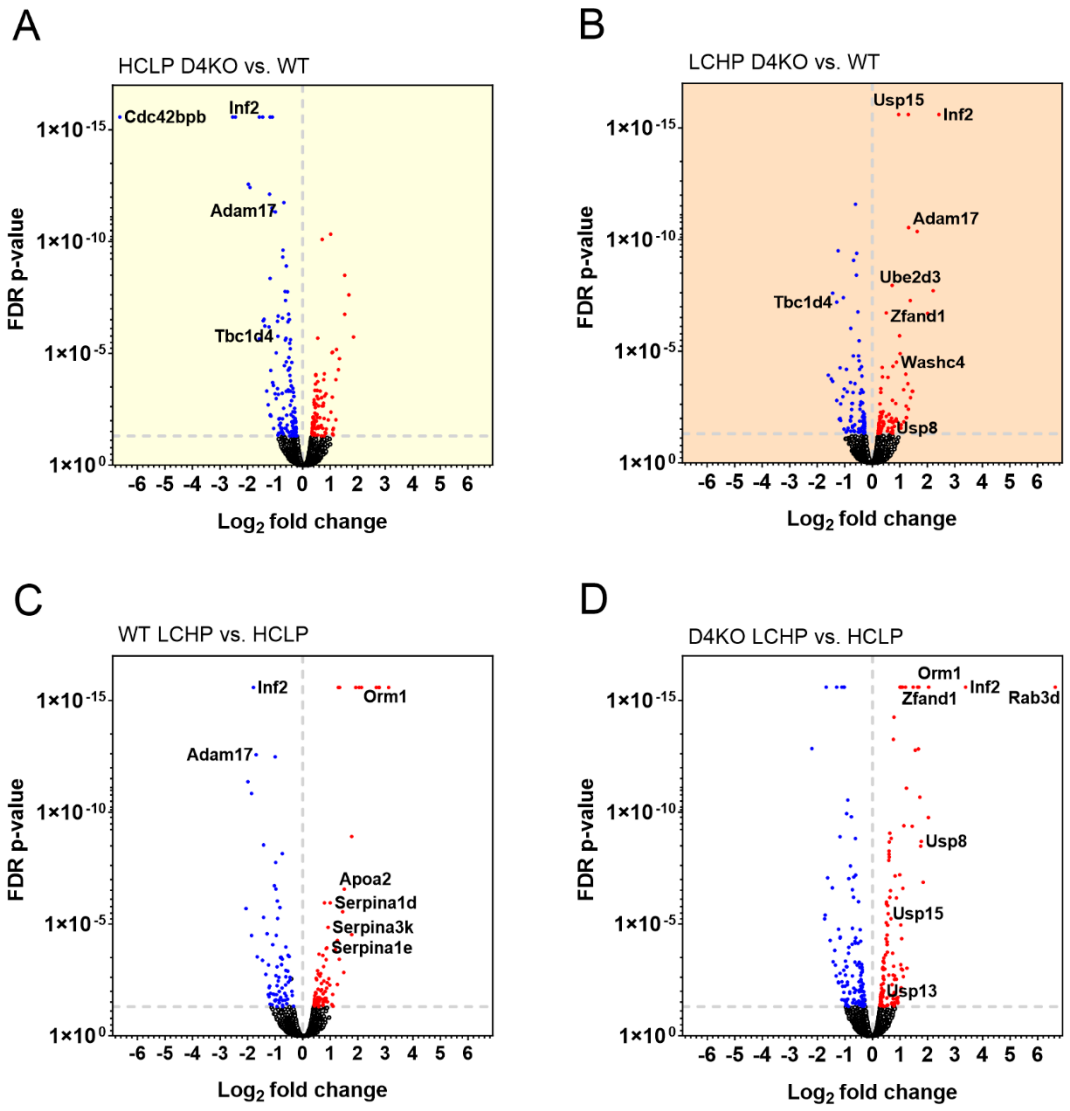

Figure 32: Impact of nutrition on regulation of proteins in *Gastrocnemius* muscle of *Tbc1d4*-deficient mice. Volcano plots of differentially regulated proteins in *Gastrocnemius* muscle of *Tbc1d4*-deficient vs. WT mice in response to a LCHP diet (A) and in D4KO mice on a LCHP vs. HCLP diet (B) diet displaying the size of differential regulation and significance. Significance threshold was set at $p < 0.05$ ($n = 6$).

Subsequently, correction for multiple testing (adjusted p-value < 0.05) and the effect size estimation (log2 fold change) revealed top regulated proteins, as listed in (Table 21). According to KEGG and Reactome database, selected differentially regulated proteins in D4KO vs. WT subjected to a HCLP diet included proteins associated with signal transduction that were down-regulated in D4KO vs. WT mice. In D4KO vs. WT subjected

to a LCHP diet, proteins associated with transport and signal transduction were up-regulated and proteins associated with endosomal sorting were down-regulated.

In WT mice, proteins associated with stress response were up-regulated, whereas in D4KO mice, proteins associated with signal transduction were up-regulated on a LCHP vs. a HCLP diet.

Inf2 was the top regulated candidate protein, which was significantly down-regulated in D4KO vs. WT mice subjected to a HCLP diet (adjusted p-value = 2.63719E-16, Log2 fold change = -2.44) and in WT mice subjected to a LCHP vs a HCLP diet (adjusted p-value = 2.5671E-16, Log2 fold change = -1.79). In D4KO vs. WT mice subjected to a LCHP diet, Inf2 was significantly up-regulated (adjusted p-value = 2.4782E-16, Log2 fold change = 2.42) as well as in D4KO mice subjected to a LCHP vs. a HCLP diet (adjusted p-value = 2.4921E-16, Log2 fold change = 3.38).

Table 21: Selected differentially regulated proteins in *Gastrocnemius* muscle

Gene Symbol	Adjusted p-value	log2 fold change	Gene Symbol	Adjusted p-value	log2 fold change
HCLP D4KO vs. WT			*LCHP D4KO vs. WT*		
Inf2	2.63719E-16	-2.44	Tmub1	2.4782E-16	-2.77
Usp8	5.90805E-07	-1.37	Tbc1d4	6.2663E-08	-1.29
Smad2	6.52999E-07	-1.22	Cdc42ep1	0.01	-1.17
Adam17	4.20582E-12	-1.11	Vps37a	0.00048	-1.02
Tbc1d4	1.6953E-06	-0.90	Ubap1	0.00065	-0.91
Uchl5	0.03650602	-0.72	Usp8	0.027	0.71
Plin5	0.00223504	0.71	Ube2d3	1.1152E-08	0.72
Pdk4	7.89647E-11	0.71	Washc4	3.0636E-05	0.88
Ankfy1	0.00080279	0.80	Usp15	2.4782E-16	0.96
Ranbp9	2.38E+06	1.68	Cdc26	1.9209E-08	2.21
Them4	2.64E-02	2.27	Inf2	2.4782E-16	2.42
WT LCHP vs. HCLP			*D4KO LCHP vs. HCLP*		
Inf2	2.5671E-16	-1.79	Leprotl1	3.91395E-06	-1.72
Adam17	2.6429E-13	-1.69	Cdc42ep1	5.3766E-05	-1.54

Rab8a	0.033	-0.85	Vps18	0.0001	-0.86
Aldoc	0.005	-0.62	Akt1s1	7.92742E-08	-0.68
Fasn	0.004	-0.52	Pik3c3	0.024907347	-0.67
Akt2	0.0028	-0.42	Rab5b	0.0058	-0.43
Fabp3	0.025	0.61	Adam17	0.042	0.55
Pdk4	0.008569437	0.69	Usp15	3.4436E-06	0.57
Ormdl1	0.00014	1.18	Vps51	4.4894E-05	1.06
Orm1	2.5671E-16	2.05	Usp8	2.0073E-09	1.77
Them4	2.5671E-16	2.67	Orm1	2.4921E-16	2.04
Pik3cb	2.5671E-16	2.78	Inf2	2.4921E-16	3.38

3.4.1.2 Differentially regulated canonical pathways in Gastrocnemius muscle of Tbc1d4-deficient mice in response to a LCHP vs. a HCLP diet

To investigate the differential effects of macronutrient ratios on canonical pathways in skeletal muscle, a ConsensusPathDB (CPDB) (2.2.6.3) was performed for differentially regulated proteins ($p < 0.05$). Selected differentially regulated canonical pathways in *Gastrocnemius* muscle of D4KO and WT mice in response to a HCLP and LCHP diets are shown in Table 22.

CPDB analysis highlighted over-represented Reactome and KEGG canonical pathways in *Gastrocnemius* muscle of D4KO vs. WT mice in response to a HCLP diet, which showed significant regulation of pathways associated with inflammation and immune response such as “Toll-like receptor cascades” and insulin signaling such as “Insulin receptor signalling cascade”, “PI3K cascade” and “IRS-mediated signalling”. In addition, canonical pathways associated with lipid metabolism such as “Mitochondrial fatty acid beta-oxidation” and “Fatty acid elongation” were significantly regulated in D4KO vs. WT mice subjected to the HCLP diet.

When subjected to the LCHP diet, CPDB analysis of *Gastrocnemius* muscle revealed differential regulation of canonical pathways associated with ubiquitin signaling such as “Ub-specific processing proteases” and “Deubiquitination” as well as signal transduction

and metabolic pathways such as “RHO GTPase Effectors”, “Utilization of Ketone Bodies” and “mTOR signaling pathway” in D4KO vs. WT mice.

Furthermore, pathways associated with insulin signaling were significantly regulated in WT mice subjected to a LCHP vs HCLP diet such as “PI3K Cascade” and “IRS-mediated signalling”. In addition, pathways associated with lipid metabolism “Biosynthesis of unsaturated fatty acids” were differentially regulated in WT subjected to a LCHP diet vs a HCLP diet.

Significantly regulated canonical pathways in D4KO mice subjected to a LCHP vs a HCLP diet included pathways associated with immunity such as “Complement and coagulation cascades” and “Toll-like Receptor Cascades” and lipid metabolism “Plasma lipoprotein assembly” as well as signaling pathways “Integrin cell surface interactions” and “Signaling by Interleukins” (Table 22).

Table 22: Over-represented Reactome and KEGG canonical pathways in *Gastrocnemius* muscle

Canonical pathway	p-value	Candidates contained (%)
HCLP D4KO vs. WT		
Toll-like Receptor Cascades	0.0024131	15.87
Insulin receptor signalling cascade	0.00328842	26.32
PI3K Cascade	0.00467837	30.77
Mitochondrial Fatty Acid Beta-Oxidation	0.00566591	20.00
Activation of AKT2	0.00911752	66.67
Fatty acid elongation	0.01042026	25.00
LCHP D4KO vs. WT		
RHO GTPase Effectors	2.00E-05	7.69
Toll-like Receptor Cascades	0.00195828	14.29
Ub-specific processing proteases	0.00230138	4.27
Signal Transduction	0.00534448	5.37

Utilization of Ketone Bodies	0.00600506	66.67
Deubiquitination	0.0147868	3.42
mTOR signaling pathway	0.0279732	10.00
Branched-chain amino acid catabolism	0.03946502	17.65
Ketone body metabolism	0.04819678	25.00
PI3K-Akt signaling pathway	0.04842812	7.97
WT LCHP vs. HCLP		
Biosynthesis of unsaturated fatty acids	0.00146249	33.33
PI3K Cascade	0.00203899	30.77
IRS-mediated signalling	0.00275541	28.57
Activation of AKT2	0.00582767	66.67
Deubiquitination	0.01314463	3.42
D4KO LCHP vs. HCLP		
Complement and coagulation cascades	5.18E-13	38.18
Integrin cell surface interactions	0.00013675	25.00
Post-translational protein phosphorylation	0.00068717	18.87
Regulation of Insulin-like Growth Factor (IGF) transport and uptake by Insulin-like Growth Factor Binding Proteins (IGFBPs)	0.00068717	18.87
Toll-like Receptor Cascades	0.00074471	17.46
Plasma lipoprotein assembly	0.00076912	35.71
Signaling by Interleukins	0.01492142	12.50
Ketone oxidation	0.02905674	40.00

3.4.2 Impact of nutrition on white adipose tissue proteome of D4KO mice

To determine the impact of nutrition on white adipose tissue proteome of whole-body D4KO mice, untargeted proteomic analysis of epididymal WAT from WT and D4KO mice subjected to chronic dietary intervention with a HCLP or a LCHP diets was performed (2.2.6.2–2.2.6.4). Mass spectrometry analysis revealed a total of 181 proteins significantly regulated in epididymal WAT of D4KO mice compared to WT littermates

on the HCLP diet, including 75 up-regulated and 106 down-regulated proteins. When subjected to a LCHP diet, 188 proteins were differentially regulated in D4KO compared to WT mice, of which 101 were up-regulated and 87 down-regulated. In WT mice, a total of 237 proteins were differentially regulated on a LCHP vs. a HCLP diet. While 84 proteins were up-regulated, 159 proteins were down-regulated in WT mice subjected to a LCHP vs. a HCLP diet. In D4KO mice, 279 proteins were shown to be differentially regulated on a LCHP vs. a HCLP diet, including 118 up-regulated and 161 down-regulated proteins (Figure 33).

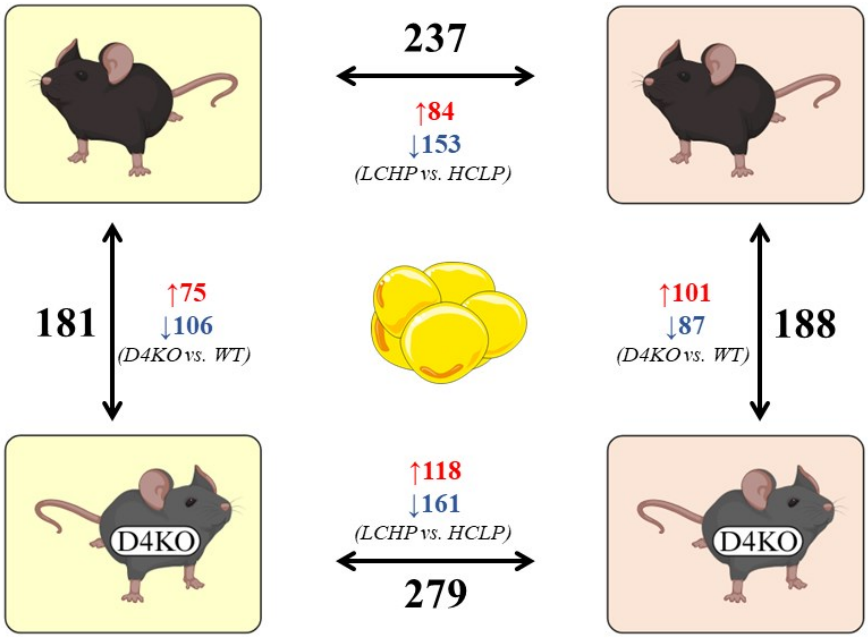

Figure 33: Impact of nutrition on proteome of white adipose tissue of *Tbc1d4*-deficient mice. Overview of differentially regulated proteins (indicated by black arrows) in epididymal adipose tissue of *Tbc1d4*-deficient mice and WT littermates aged 17–19 weeks subjected to a HCLP (indicated in yellow) or LCHP (indicated in orange) diet. Red arrows indicate up-regulated and blue arrows indicate down-regulated proteins. Significance threshold was set at $p < 0.05$ ($n = 6$). Created with Biorender.com

3.4.2.1 Differentially regulated proteins in white adipose tissue in response to a LCHP vs. a HCLP diet in Tbc1d4-deficient mice

To elucidate potential proteins involved in the regulation of whole-body glycemia and insulin sensitivity in white adipose tissue of *Tbc1d4*-deficient and WT mice in response to different macronutrient ratios, the proteome of epididymal white adipose tissue was visualized in volcano plots. In addition, unregulated and differentially down- and up-regulated proteins were revealed, indicated in black, blue and red, respectively. Proteome

analysis identified differentially regulated proteins in D4KO vs. WT mice subjected to a HCLP (Figure 34 A) or a LCHP (Figure 34 B) as well as in WT (Figure 34 C) and D4KO (Figure 34 D) mice subjected to a LCHP vs a HCLP diet.

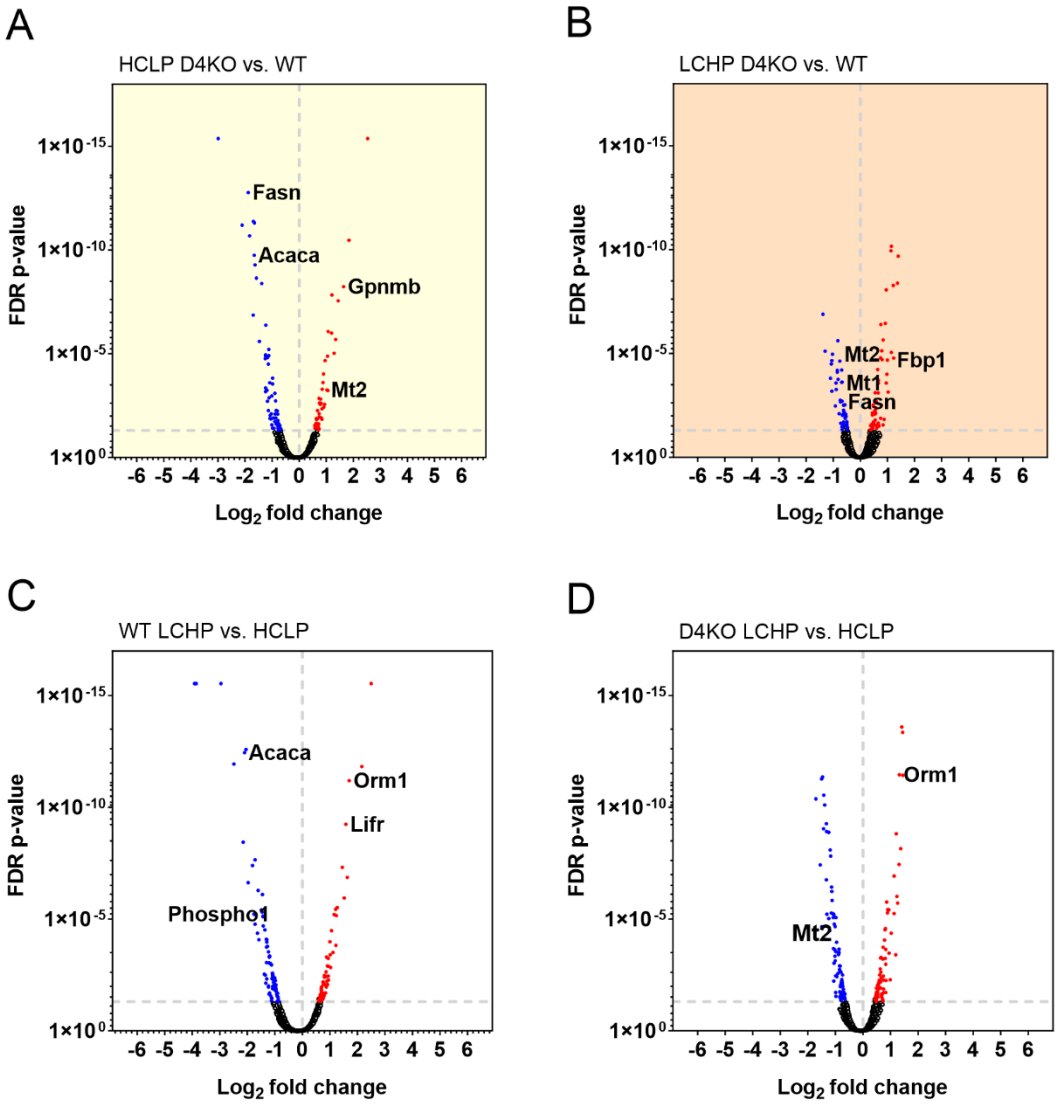

Figure 34: Impact of nutrition on regulation of proteins in white adipose tissue of *Tbc1d4*-deficient mice. Volcano plots of differentially regulated proteins in epididymal adipose tissue of *Tbc1d4*-deficient vs. WT mice in response to a LCHP diet (A) and in D4KO mice on a LCHP vs. HCLP diet (B) diet displaying the size of differential regulation and significance. Significance threshold was set at $p < 0.05$ ($n = 6$).

Subsequent correction for multiple testing (adjusted p-value < 0.05) and the effect size estimation (log2 fold change) revealed top regulated proteins, as listed in Table 23.

According to KEGG and Reactome database, selected differentially down-regulated proteins in D4KO vs. WT mice subjected to a HCLP diet included proteins associated with FA biosynthesis, while proteins associated with stress response were up-regulated. On a LCHP diet, proteins associated with stress response and signal transduction were down-regulated in D4KO vs. WT mice, while proteins associated with protein metabolism were up-regulated.

In WT mice, proteins associated with FA biosynthesis were down-regulated on a LCHP vs. HCLP diet, whereas proteins associated with stress response were up-regulated. In D4KO mice, several proteins associated with enzyme regulator activity and stress response were differentially regulated.

Table 23: Selected differentially regulated proteins in white adipose tissue

Gene Symbol	Adjusted p-value	log2 fold change	Gene Symbol	Adjusted p-value	log2 fold change
HCLP D4KO vs. WT			*LCHP D4KO vs. WT*		
Phospho1	0.003	-2.99	Faf1	2.1643E-05	-1.05
Fasn	0.002	-1.88	Vars2	0.0006	-1.05
Gde1	0.002	-1.83	Mt2	1.0837E-05	-1.03
Acaca	0.001	-1.66	Mt1	0.00026174	-0.9
Acly	0.001	-1.63	Acly	0.0002	-0.82
Acsm3	0.0003	-1.23	Pgam2	0.0002	-0.69
Acss2	2.04E-06	-1.01	Itga3	1.5991E-05	0.75
Fabp1	4.1665E-16	0.59	Apoa2	1.9475E-05	0.8
Plin2	4.1665E-16	0.85	Wwtr1	0.0003	0.96
Mt2	4.1665E-16	1.03	Mrpl49	9.9679E-05	0.98
Bicd1	4.1665E-16	1.29	Fbp1	2.0542E-05	1
Gpnmb	4.1665E-16	1.64	Eng	0.0007	1.03
WT LCHP vs. HCLP			*D4KO LCHP vs. HCLP*		
Asap2	2.8529E-16	-2.96	Asap2	2.8371E-16	-3.51
Acaca	3.5043E-13	-2.1	Hsd11b1	2.8371E-16	-2.23
Phospho1	5.9857E-06	-1.76	Stx6	2.8371E-16	-1.95

Eng	1.6728E-05	-1,72	Serpina7	5.3285E-12	-1.5
Ptges	7.6967E-06	-1.43	Apoa4	1.1958E-09	-1.32
Acly	0.0001	-1.29	Ptges	1.3069E-09	-1.24
Serpina1e	0.004	0.87	Ctrb1	0.00552877	0.84
Mt2	0.0084	0.91	Serpina1d	3.7701E-06	0.9
Fbn1	0.001	0.94	Phospho1	0.00511519	0.99
Lifr	5.6812E-10	1.58	Orm1	3.4526E-12	1.32
Orm1	6.2877E-12	1.7	Gpnmb	3.6425E-12	1.45
Gpnmb	1.4898E-12	2.16	Lifr	2.8371E-16	1.56

3.4.2.2 Differentially regulated canonical pathways in white adipose tissue of Tbc1d4-deficient mice in response to a LCHP vs. a HCLP diet

For differentially regulated proteins ($p < 0.05$) in WAT from D4KO and WT mice in response to a HCLP and LCHP diet, differentially regulated canonical pathways were highlighted using ConsensusPathDB analysis (2.2.6.3). Selected differentially regulated canonical pathways in WAT from D4KO and WT mice in response to a HCLP and LCHP diets are shown in Table 24.

CPDB analysis highlighted over-represented Reactome and KEGG canonical pathways, in D4KO vs. WT mice in response to the HCLP diet associated with “Metabolism of lipids” such as “Fatty acid biosynthesis”, “Triglyceride catabolism” and “PPAR signaling pathway” and signal transduction “RHO GTPases Activate Formins” as well as “AMPK signaling pathway”.

When subjected to a LCHP diet, CPDB analysis of differentially regulated proteins revealed differential regulation of canonical pathways associated with lipid “HDL clearance” and glucose “Glycolysis” metabolism as well as transport processes “Transport of small molecules” and “ABC transporters in lipid homeostasis”.

Further, lipid metabolism associated pathways were significantly regulated in WT mice subjected to a LCHP vs HCLP diet such as “Fat digestion and absorption”, “Plasma lipoprotein assembly” and “PPAR signaling pathway”.

Overrepresented canonical pathways in D4KO mice subjected to a LCHP vs a HCLP diet included pathways associated with fatty acid metabolism “Peroxisomal lipid metabolism”, “Biosynthesis of unsaturated fatty acids”, immunity “Terminal pathway of complement”, “Complement cascade” and Ubiquitionation “Ub-specific processing proteases”.

Table 24: Over-represented Reactome and KEGG canonical pathways in white adipose tissue

Canonical pathway	p-value	Candidates contained (%)
HCLP D4KO vs. WT		
Fatty acid biosynthesis	2.92E-04	30,77
Valine, leucine and isoleucine degradation	6.61E-03	11.11
PPAR signaling pathway	9.48E-03	10.20
Triglyceride catabolism	9.98E-03	33.33
Synthesis of Ketone Bodies	9.98E-03	33.33
RHO GTPases Activate Formins	2.15E-02	8.33
AMPK signaling pathway	3.67E-02	7.25
Beta-oxidation of VLCFA	3.95E-02	16.67
LCHP D4KO vs. WT		
HDL clearance	2.34E-03	66.67
Plasma lipoprotein assembly	6.40E-03	21.43
Glycolysis	1.18E-02	10.20
Transport of small molecules	1.40E-02	5.56
Plasma lipoprotein assembly, remodeling, and clearance	2.14E-02	10,53
ABC transporters in lipid homeostasis	2.51E-02	22.22
Synthesis of PIPs at the plasma membrane	2.59E-02	13.04
WT LCHP vs. HCLP		
Triglyceride metabolism	1.65E-03	28.57
Fat digestion and absorption	1.11E-02	17.39

Plasma lipoprotein assembly	1.55E-02	21.43
Synthesis of PC	1.55E-02	21.43
AMPK signaling pathway	1.71E-02	10.14
Synthesis of PE	2.05E-02	33.33
PPAR signaling pathway	4.07E-02	10.20
D4KO LCHP vs. HCLP		
Peroxisomal lipid metabolism	5.58E-06	34.78
Terminal pathway of complement	2.30E-05	80.00
Complement cascade	1.32E-04	23.53
Metabolism of lipids	6.25E-04	8.92
Biosynthesis of unsaturated fatty acids	1.14E-03	27.78
Beta-oxidation of VLCFA	1.75E-03	33.33
PPAR signaling pathway	1.79E-03	16.33
Ub-specific processing proteases	2.49E-02	1.90

4. Discussion

The RabGTPase-activating proteins (RabGAPs) TBC1D1 and TBC1D4 represent non-redundant key proteins in GLUT4-mediated glucose uptake, and are therefore crucial regulators of whole-body glycemia. Studies from our group have shown that FAO is favored over carbohydrate utilization in RabGAP-deficient mice, suggesting an additional role for TBC1D1 and TBC1D4 as metabolic switches regulating energy substrate utilization [131]. In humans, a mutation in *TBC1D1* was associated with severe obesity [256], while *TBC1D4* variants were associated with insulin resistance and T2DM [257, 258]. In Arctic populations, homozygosity for a muscle-specific loss-of-function mutation in the *TBC1D4* gene was shown to convey postprandial hyperglycemia and an increased risk for T2DM. This *TBC1D4* variant has been proposed to represent an evolutionary adaptation to the indigenous lifestyle characterized by a high degree of physical activity and a traditional Arctic diet high in protein and (unsaturated) lipids but being low in carbohydrates [258, 295]. Similarly, whole-body *Tbc1d4*-deficient (D4KO) mice are characterized by postprandial hyperglycemia due to impaired insulin-stimulated glucose uptake in skeletal muscle and white adipose tissue accompanied by decreased GLUT4 protein abundance in these tissues [131]. The present study aims to elucidate the impact of macronutrient ratios on whole-body glycemia and insulin resistance in RabGAP-deficient mice. We hypothesize that a low-carbohydrate high-protein diet (LCHP), representing a traditional Arctic diet, will restore insulin sensitivity in D4KO mice.

4.1 The impact of Western and Arctic diets on whole-body metabolism of RabGAP-deficient mice

4.1.1 An Arctic diet impairs whole-body glycemia in WT mice

Traditional diets of hunter-gatherer populations, such as the Arctic diet, are typically ketogenic [93]. Since 1921, the beneficial effects of a “ketogenic” diet have been suggested by mimicking a state of fasting [299]. However, since then, studies have shown that a ketogenic diet is mechanistically very different from fasting and have argued for its beneficial effects on metabolic health [300-302]. Previous studies demonstrated the effects of amino acids (AA) and dietary protein on glucose homeostasis and have associated increased dietary protein intake with improved insulin sensitivity in healthy individuals and individuals with insulin resistance [303-306]. However, in these studies, improved insulin sensitivity was associated with reduced body weight due to hypocaloric diets. Therefore, it remained unclear whether the improved insulin sensitivity was due to the reduction in body weight or to the effect of a high dietary

protein content. The present study showed that mice fed the LCHP diet had an increased body weight compared to mice fed the HCLP diet, thus ruling out the possibility that any improvements in insulin sensitivity were due to weight loss. Mice fed the LCHP diet showed impaired insulin tolerance in response to insulin injection compared to mice fed the HCLP diet. In WT mice, the LCHP diet resulted in decreased insulin-stimulated glucose uptake into primary white adipocytes, which was associated with increased adipocyte size compared to the HCLP diet. These results indicate that the LCHP diet promoted insulin resistance in WT mice, which is consistent with other studies linking elevated plasma BCAA concentrations with insulin resistance and T2DM [106, 228, 307-309].

In addition to the controversy regarding the effects of ketogenic diets on insulin sensitivity, the effects of ketogenic diets on lipid metabolism have also been debated. While some studies have shown that a ketogenic diet ameliorates lipid metabolism [310, 311], others have suggested that ketogenic diets may increase circulating lipid concentrations, due to high dietary lipid content, which potentially affects hepatic metabolism [312]. In the present study, mice showed elevated fasting blood glucose concentrations in response to a LCHP diet, indicating alterations in hepatic glucose metabolism. It was shown that in individuals with prediabetes and T2DM, excessive hepatic glucose production during post-absorptive conditions contributes to elevated fasted blood glucose concentrations [313-316]. Moreover, a short-term ketogenic diet intervention induced hepatic insulin resistance [317], whereas long-term effects may include glucose intolerance and reduced β- and α-cell mass despite initial weight loss [104]. The present study showed that mice fed the LCHP diet had elevated blood glucose concentrations and reduced glucose clearance during a glucose tolerance test. These results may indicate impaired insulin-mediated suppression of endogenous glucose production in response to a LCHP diet, which is common in individuals with T2DM [318, 319].

4.1.2 An Arctic diet improves glycemia in whole-body RabGAP-deficient mice

4.1.2.1 RabGAPs regulate adipose tissue expansion in response to different macronutrient ratios

Previous studies indicate regulatory roles of TBC1D1 and TBC1D4 in lipid metabolism showing that deficiency of TBC1D1 and TBC1D4 increases the transport of long-chain fatty acids (LCFAs) into muscle and human fat cells via fatty acid handling proteins [275, 320].

In the current study, D1KO mice presented with reduced adipose tissue mass when fed the HCLP or the LCHP diet. Contrary to *Tbc1d1*-deficiency, *Tbc1d4*-deficiency appears to induce an increase in adipose tissue mass when mice are subjected to a high-fat diet (Figure 35), which

is consistent with previous findings from our research group [290]. The current study further suggests that predominantly *Tbc1d4*-deficiency in adipose tissue is responsible for the increased expansion of adipose tissue in whole-body D4KO mice since in contrast to muscle-specific (m)D4KO mice, only adipose tissue-specific (a)D4KO mice exhibited increased fat mass. TBC1D4 deficiency has been shown to result in increased FATP4 and CD36 abundance accompanied by increased LCFA uptake into adipocytes and increased FAO [321]. However, in the current study, adipocyte size remained unchanged in D4KO compared to WT mice, suggesting that *Tbc1d4*-deficiency in mice may enhance adipogenesis in response to high-fat diets.

Interestingly, the present study showed that *Tbc1d4*-deficiency in mice resulted in significantly elevated plasma leptin concentrations compared to *Tbc1d1*-deficiency when subjected to a LCHP. Elevated plasma leptin concentrations are commonly associated with obesity and adipocyte hypertrophy [322, 323]. Previously, it was shown that in obese leptin-deficient mice, *Tbc1d1*-deficiency did not affect feeding behavior but was associated with reduced body weight due to increased energy expenditure and skeletal muscle FAO [261, 324]. Contrary to these findings, whole-body FAO was unaltered in D1KO mice in the current study. Therefore, in this study, the reduced adipose tissue mass and protection against diet-induced changes in fat mass due to *Tbc1d1*-deficiency appear to be independent of FAO. Additionally, food intake was unchanged between D1KO and WT mice during a fasting refeeding experiment, indicating that reduced fat mass is also independent of feeding behavior. This may indicate, as previously suggested [130], that TBC1D4 compensates for a defect in TBC1D1 signaling. Interestingly, in D1/4KO mice adipose tissue mass was unaltered on the HCLP diet and reduced on the LCHP diet, which indicates, as previously suggested [256, 324], a possible role of TBC1D1 during the development of obesity that dominates the potential increase in adipose tissue mass due to *Tbc1d4*-deficiency. However, it remains to be determined whether *Tbc1d1*-deficiency is associated with reduced adipogenesis, adipocyte hypertrophy or both.

Hyperinsulinemia is associated with insulin resistance, increased plasma FFA concentrations, increased lipogenesis and consequently elevated fat mass [325, 326]. D4KO mice exhibited postprandial hyperinsulinemia when fed the HCLP diet and elevated postprandial plasma insulin concentrations in response to feeding the LCHP diet. This correlates with a significantly increased fat mass in D4KO subjected to the HCLP and a tendentially elevated fat mass on a LCHP diet compared to WT littermates. In conclusion, while D1KO mice showed reduced adipose tissue mass, D4KO mice showed increased fat mass (Figure 35). Contrary to previous

findings in skeletal muscle [275], the results of the present study indicate rather opposite roles of TBC1D1 and TBC1D4 in adipose tissue lipid metabolism.

4.1.2.2 RabGAPs regulate lipid metabolism in response to different macronutrient ratios

Studies have demonstrated the impact of TBC1D1 and TBC1D4 as regulators of glucose and lipid metabolism in skeletal muscle and adipose tissue [131, 264, 327]. The current study further introduces the two RabGAPs as potential regulators of hepatic lipid metabolism.

Ketone bodies are produced by the liver via fatty acid catabolism as an alternative energy source when glucose supply is insufficient [328, 329]. The present study revealed that *Tbc1d4*-deficiency resulted in reduced blood glucose accompanied by increased ketone body concentrations when mice were subjected to high-carbohydrate diets, especially a HCLP diet (Figure 35). This indicates that despite adequate glucose and fat availability, *Tbc1d4*-deficiency results in inadequate glucose utilization inducing hepatic ketogenesis. Moreover, plasma NEFA concentrations were elevated in D4KO mice when fed the HCLP diet, consistent with previous findings [270], and remained unchanged when fed the LCHP diet. Furthermore, aD4KO but not mD4KO mice had elevated plasma NEFA concentrations when fed the HCLP diet. These findings are consistent with previous studies, suggesting that increased adipose tissue mass is associated with increased plasma NEFA concentrations [330] and that *Tbc1d4*-deficiency in adipose tissue might promote ectopic fat accumulation in peripheral tissues and consequently promote metabolic complications.

Consistent with these findings, studies have shown that fasted plasma FFA concentrations were reduced in individuals with T2DM in response to a 6-week high-protein diet intervention, accompanied by decreased hepatic lipid content [244]. However, as mentioned above, the findings on the impact of ketogenic diets on hepatic lipid metabolism are controversial, as other studies have shown no change of FFA concentrations in individuals with T2DM after a 5-week or an 8-week high-protein diet intervention [331, 332]. Considering the different study characteristics, including individuals with untreated T2DM as well as obese individuals, the findings are not exactly comparable [244, 331, 332]. Nevertheless, studies agree that elevated plasma NEFA concentrations are associated with insulin resistance [330]. Moreover, similar to whole-body D4KOs, aD4KOs showed reduced random fed plasma glucose concentrations in response to high carbohydrate diets, which appears to be independent of plasma insulin. Insulin-independent random hypoglycemia may be caused by malnutrition or inadequate glycogen storage and mobilization [333, 334]. Furthermore, 6 h fasting blood glucose concentrations were reduced in aD4KOs. As previously discussed, reduced plasma glucose accompanied by

elevated plasma ketone body concentrations in the fasted state, indicate inadequate glucose utilization leading to hepatic ketogenesis [328, 334]. Therefore, the current study demonstrates that HCLP diet feeding promotes insulin resistance in D4KO mice, presumably due to alterations in adipose tissue lipid metabolism.

Contrary, *Tbc1d1*-deficiency in mice resulted in reduced plasma ketone bodies, which correlated with decreased plasma NEFA concentrations. Interestingly, when fed the HCLP diet, D1/4KO compared to D4KO mice showed decreased plasma ketone bodies but increased NEFA concentrations. This suggests, non-redundant regulatory roles of TBC1D1 and TBC1D4 in hepatic lipid metabolism. While knockout of both RabGAPs appears to further impair lipid metabolism in adipocytes compared to single RabGAP-deficiency, ablation of both RabGAPs proposes possible protection from altered hepatic lipid metabolism compared to *Tbc1d4*-deficiency likely due to compensation by TBC1D1. Several studies describe a protective function of TBC1D1 in obesity by mediating leanness [261, 335]. To date, no studies have demonstrated a direct impact of TBC1D1 on hepatic lipid metabolism. However, it has been shown that D1KO, D4KO and D1/4KO mice have elevated triglyceride concentrations in the liver [131]. Nevertheless, it remains to be determined whether alterations in hepatic lipid metabolism are a direct consequence of RabGAP-deficiency or a secondary consequence of altered lipid metabolism in adipose tissue and skeletal muscle.

4.1.2.3 An Arctic diet enhances insulin-stimulated glucose uptake into white adipose tissue of Tbc1d1-deficient mice

Skeletal muscle represents the predominant site of postprandial glucose uptake [53], whereas the contribution of adipose tissue is significantly lower [336]. However, a study revealed that adipose tissue-specific GLUT4-deficiency promotes the development of insulin resistance and increases the risk of T2DM in mice [337], indicating the critical role of the adipose tissue in the regulation of whole-body glycemia. Previous studies have shown that *Tbc1d4*-deficiency results in impaired GLUT4-mediated glucose uptake in adipose tissue [131, 266, 290]. Similarly, in the present study D4KO mice showed significantly impaired insulin-stimulated glucose uptake regardless of the diet. Previous findings from our research groups demonstrated that insulin-stimulated glucose uptake into primary white adipocytes is rescued in D4KO mice in response to a chronic exercise intervention, which was associated with increased expression of browning markers in subcutaneous adipose tissue [290]. In contrast to these findings, the dietary interventions of the present study did not appear to have a beneficial effect on adipose tissue insulin sensitivity in D4KO mice.

Contrary to *Tbc1d4*-deficiency, *Tbc1d1*-deficiency has not been associated with impaired insulin-stimulated glucose uptake in adipose tissue [131], which correlates with the tissue-specific expression of TBC1D1 and TBC1D4 in mice [132]. In 3T3-L1 adipocytes the abundance of TBC1D1 compared to TBC1D4 has been shown to be 1:20 [338], indicating that TBC1D1 plays a minor role in adipocyte glucose uptake. Surprisingly, when mice were subjected to the LCHP diet, insulin-stimulated glucose uptake in primary white adipocytes was significantly enhanced in D1KO compared to WT mice. Furthermore, D1/4KO mice, previously shown to have impaired insulin-stimulated glucose uptake on a standard Chow diet [131], showed increased insulin-stimulated glucose uptake in WAT compared to D4KO mice. As discussed above, *Tbc1d1*-deficiency resulted in reduced leptin concentrations on the LCHP diet (Supplemental figure 1), which is hypothesized to be associated with reduced adipocyte size. Studies have shown that increased adipocyte size correlates with decreased insulin sensitivity [339, 340]. In conclusion, *Tbc1d4*-deficiency results in impaired insulin-stimulated glucose uptake into adipose tissue independent of macronutrient rations. In adipose tissue from *Tbc1d1*-deficient mice, insulin-stimulated glucose uptake is unaltered in response to diets rich in carbohydrates but is enhanced in response to the LCHP diet (Figure 35). In this study, diet-induced adipocytes enlargement in WT correlated with decreased adipocyte insulin sensitivity. The results further indicate that in D1KO mice, adipocyte insulin sensitivity is maintained possibly due to reduced adipocyte size.

4.2 Carbohydrate restriction improves the insulin resistance phenotype of Tbc1d4-deficient mice

4.2.1 An Arctic diet restores postprandial glycemia and skeletal muscle insulin sensitivity in Tbc1d4-deficient mice

Postprandial glycemia presents a crucial predictor of diabetes [341]. In individuals with T2DM, postprandial hyperglycemia has been shown to correlate with oxidative stress and inflammation, and is often accompanied by hyperinsulinemia and elevated FFA concentrations. Therefore, it's difficult to elucidate the individual impact of each metabolic abnormality [342].

In Arctic populations, a loss-of-function mutation in the *TBC1D4* gene is characterized by postprandial hyperglycemia and an increased risk to developing T2DM [258]. Previous studies from our research group have shown that *Tbc1d4*-deficiency in mice resembles the human phenotype and is associated with postprandial hyperglycemia accompanied by impaired insulin-stimulated glucose uptake into skeletal muscle and adipose tissue [266, 290]. Similar to

these findings, in the current study, *Tbc1d4*-deficiency resulted in postprandial hyperglycemia when mice were subjected to high-carbohydrate diets, CON and HCLP. Surprisingly, postprandial hyperglycemia was accompanied by hyperinsulinemia only on the HCLP diet, indicating that feeding the HCLP diet exacerbates insulin resistance in D4KO and D1/4KO mice compared to the CON diet. Interestingly, postprandial glycemia was restored when D4KO and D1/4KO mice were fed the LCHP diet. As shown in other studies, high dietary protein intake reduces postprandial hyperglycemia in individuals with T2DM and in rodent models [343-345]. It has been suggested that excess AA from high dietary protein intake may overactivate mTOR, resulting in reduced insulin-mediated glucose uptake [346]. Others suggest that high dietary protein leads to enhanced insulin secretion [303-305, 347]. In the current study, plasma insulin concentrations of D4KO mice on the LCHP were unchanged compared WT littermates, indicating that the improved postprandial hyperglycemia is independent of plasma insulin concentrations.

Previous studies have shown that *Tbc1d4*-deficiency in mice results in impaired insulin-stimulated glucose uptake in oxidative *Soleus* muscle [290]. This is consistent with the results of the present study, in which D4KO mice subjected to a CON or HCLP diet had impaired insulin-stimulated glucose uptake in *Soleus* muscle. However, when fed the LCHP diet, insulin-stimulated glucose uptake in *Soleus* muscle was rescued. Furthermore, the present study for the first time that insulin-stimulated glucose uptake into glycolytic *EDL* muscle is additionally enhanced and significantly higher in D4KO compared to WT mice when subjected to a LCHP diet. Previously, it has been shown that insulin-stimulated glucose uptake into *EDL* muscle is unaltered in D4KO mice [131]. In conclusion, the present study demonstrated that *Tbc1d4*-, but not *Tbc1d1*-deficiency results in postprandial hyperglycemia in response to diets rich in carbohydrate, which is accompanied by impaired insulin-stimulated glucose uptake in skeletal muscle and adipose tissue (Figure 35).

TBC1D4 regulates glycemia via GLUT4-mediated glucose uptake in skeletal muscle and adipose tissue [348]. Previous studies have shown that impaired insulin-stimulated glucose uptake in D4KO mice is accompanied by decreased GLUT4 protein abundance [131, 266, 290] presumably due missorting and lysosomal degradation promoted by *Tbc1d4*-deficiency [131, 265]. Interestingly, GLUT4 protein abundance in adipose tissue, but not skeletal muscle, was shown to be restored in response to chronic exercise resulting in rescued insulin-stimulated glucose uptake in white adipose tissue [290]. Surprisingly, in the current study, improved insulin-stimulated glucose uptake in skeletal muscle, which likely contributes to improved

postprandial glycemia in D4KO mice on the LCHP diet, was not accompanied by an increase in GLUT4 protein abundance. Studies have shown that glucose uptake in skeletal muscle is unaltered in mice with a skeletal muscle GLUT4-deficiency [349], presumably due to compensation by other transporters such as GLUT12 [350, 351]. However, more recent studies rather indicate distinct roles for GLUT4 and GLUT12, showing that similar to GLUT1, GLUT12-mediated glucose transport is suppressed by glucose-1-phosphate and glucose-6-phosphate [352]. In conclusion, the present study indicates that the enhanced glucose uptake in skeletal muscle in D4KO in response to LCHP diet feeding (Figure 35) is independent of total GLUT4 protein abundance.

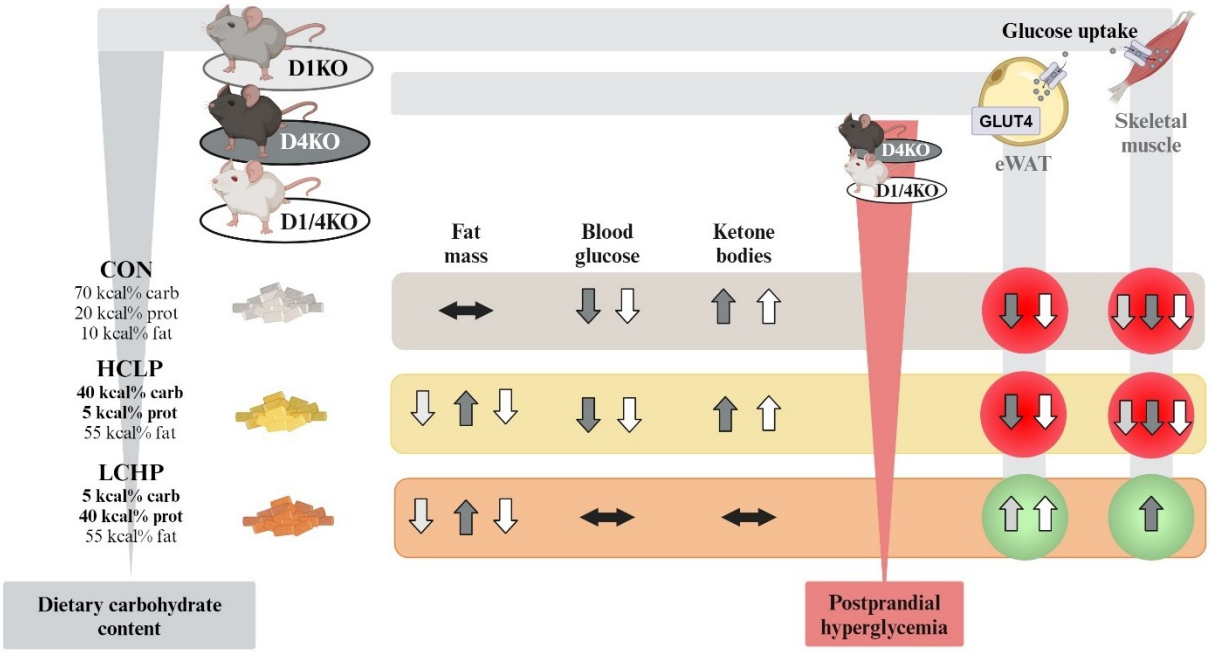

Figure 35: Key findings of the impact of macronutrient rations in whole-body RabGAP-deficient mice. When fed a CON diet, fat mass was unchanged between RabGAP-deficient mice, whereas when fed the HCLP or the LCHP diet, *Tbc1d4*-deficient (D4KO, indicated in dark gray) mice showed elevated fat mass and *Tbc1d1*-(D1KO, indicated in light gray) and *Tbc1d1/4*-deficient (D1/4KO, indicated in white) mice showed reduced fat mass. Fasted blood glucose concentrations were reduced in D4KO and D1/4KO mice, which was accompanied by increased plasma ketone bodies in response to the CON and the HCLP diets. D4KO and D1/4KO mice exhibited a carbohydrate-dependent postprandial hyperglycemia associated with impaired insulin-stimulated glucose uptake in epididymal WAT and skeletal muscle. When fed the LCHP diet, insulin-stimulated glucose uptake in adipose tissue was enhanced in D1KO and D1/4KO mice, whereas insulin-stimulated glucose uptake in skeletal muscle was enhanced in D4KO mice. Carb: carbohydrates, CON: control diet, HCLP: high-carbohydrate low-protein diet, LCHP: low-carbohydrate high-protein diet, prot: protein. Created with Biorender.com

4.2.2 An Arctic diet affects endosomal sorting in skeletal muscle of Tbc1d4-deficient mice

Proteomic profiling of skeletal muscle revealed significant regulation of deubiquitinating enzymes (Usp8, Usp,13, Usp15) and proteins associated with ubiquitination (Vps37a, Smad2, Ubap1, Ube2d3, Cdc26) in D4KO compared to WT mice in response to a LCHP diet.

Previously, the impact of dietary AA and interventions on ubiquitination have been demonstrated [353, 354]. Ubiquitination is a reversible post-translational modification that regulates protein trafficking by regulating lysosomal trafficking and degradation of plasma membrane proteins upon endocytosis from the cell surface [355, 356]. It has been suggested to induce plasma membrane internalization by promoting the incorporation of membrane receptors into intralumenal vesicles and subsequent sorting for lysosomal degradation [357]. Deubiquitinating enzymes (DUBs) have been shown to rescue membrane receptors from lysosomal degradation and enhance receptor recycling to the plasma membrane [358]. Ubiquitination by Usp25 was shown to be critical for GLUT4 sorting into GLUT4 storage vesicles [359], whereas depletion reduced GLUT4 abundance in adipocytes [360]. Furthermore, Usp25 was shown to regulate the endoproteolytic cleavage of ubiquitin-like processing of TUG (Tether, containing a UBX domain, for GLUT4) proteins in adipocytes and muscle cells, which promotes GLUT4 trafficking from the Golgi matrix to the plasma membrane [361, 362]. Moreover, GLUT4 trafficking in insulin-sensitive tissues is regulated by Endosomal Sorting Complex Required for Transport (ESCRT)-dependent sorting [363], which has been linked to ubiquitination cycles involving Usp8 [364]. These studies highlight the importance of (de-) ubiquitination processes in insulin-dependent GLUT4 trafficking.

In the present study, proteomic profiling of skeletal muscle identified inverted formin 2 (Inf2) as the most significantly up-regulated protein in skeletal muscle of D4KO mice after the LCHP diet intervention. Recent studies demonstrate the localization of Inf2 to early and recycling endosomes and its requirement for endosomal transport, indicating a putative role of Inf2 in membrane trafficking and endosomal recycling [365-368]. Consistent with this, it has been shown that Inf2 mutation enhances trafficking to proteolytic pathways and decreases recycling [369].

As discussed above, in the current study, total GLUT4 protein abundance was unaltered by the LCHP diet, whereas insulin-stimulated glucose uptake into skeletal muscle was significantly improved in D4KO mice. Thus, due to reduced GLUT4 protein abundance, D4KO animals exhibited postprandial hyperglycemia in response to high-carbohydrate diets. However, proteomic profiling indicated a potential role for DUBs and Inf2-mediated mechanisms, induced by LCHP diet feeding in D4KO mice, which could promote a shift from missorting and lysosomal GLUT4 degradation, induced by *Tbc1d4*-deficiency [131, 265], to GLUT4 recycling. Furthermore, this could compensate for the reduced GLUT4 protein abundance,

resulting in elevated glucose clearance by skeletal muscle and consequently improved postprandial glycemia.

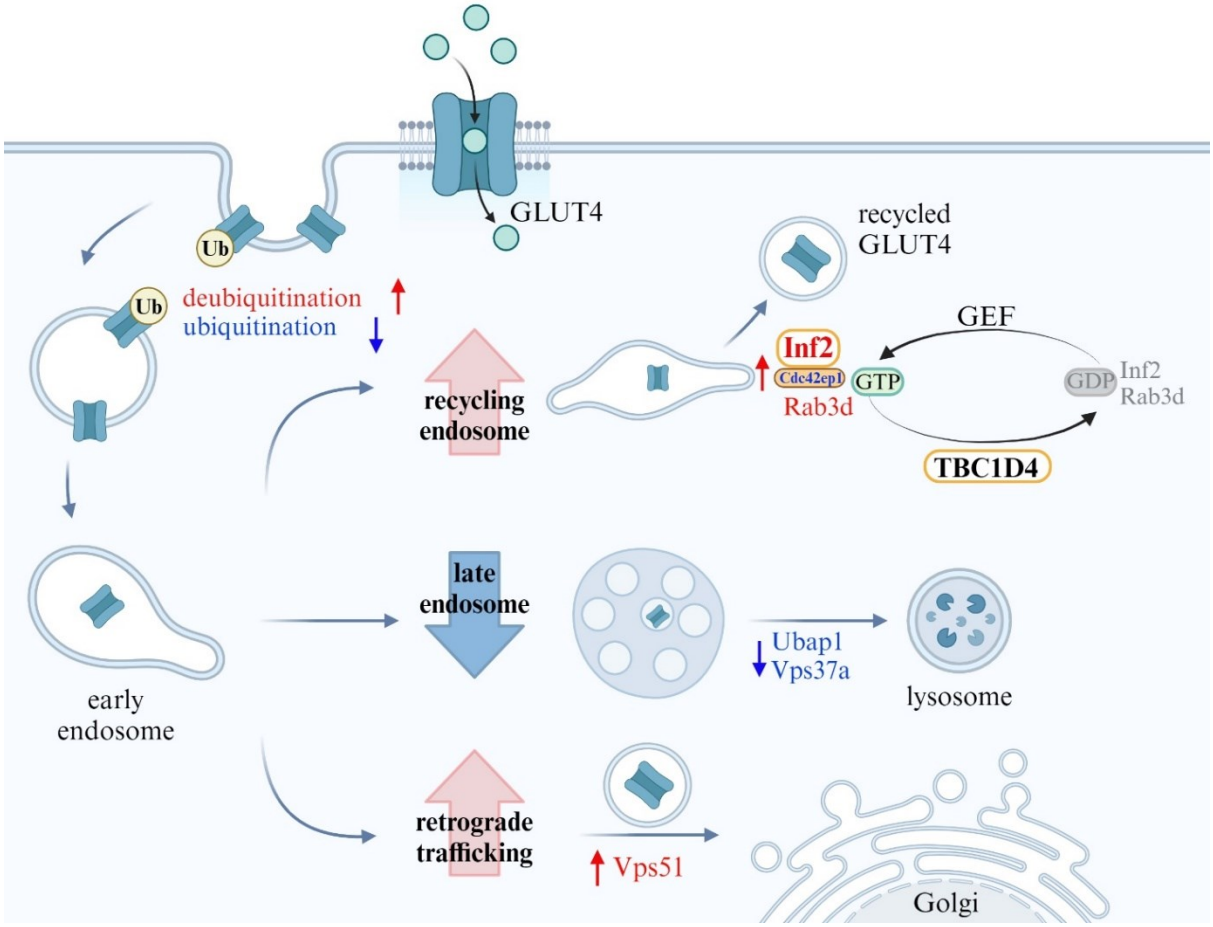

Figure 36: Putative mechanism of enhanced GLUT4 recycling in skeletal muscle of *Tbc1d4*-deficient mice on an Arctic diet. In addition to the well-described regulatory role of TBC1D4 in GLUT4 trafficking from GSVs to the plasma membrane to allow glucose uptake, TBC1D4 presumably has a function in GLUT4 recycling. In response to an Arctic diet, proteins associated with deubiquitination are up-regulated, while proteins associated with ubiquitination are down-regulated, determining degradation of target proteins. An Arctic diet may enhance GLUT4 recycling and retrograde trafficking to the Golgi apparatus, while decreasing protein degradation via late endosomes. In response to an Arctic diet, GTP-associated Inf2 and Rab3d are upregulated in skeletal muscle of D4KO mice resulting in enhanced GLUT4 recycling and subsequent improved glucose clearance and insulin-stimulated glucose uptake. Red indicates up-regulation, while blue indicates down-regulation. GEF = guanosine exchange factor, Ub = Ubiquitin, Created with Biorender.com

4.2.3 An Arctic diet enhances glucose clearance in Tbc1d4-deficient mice

Since GLUT4 protein abundance in skeletal muscle of D4KO mice was unaltered in response to different dietary interventions, it further remained to be clarified whether postprandial normoglycemia on the LCHP diet was solely due to the lack of dietary carbohydrates. Therefore, D4KO mice were subjected to a chronic LCHP diet intervention and postprandial glycemia was assessed in response to acute feeding with a high carbohydrate diet.

D4KO mice that underwent a chronic LCHP dietary intervention showed postprandial hyperglycemia in response to an acute carbohydrate challenge 1h after refeeding. This is likely due to reduced GLUT4 protein abundance in oxidative muscle as well as adipose tissue. However, postprandial glycemia was restored in these mice as early as 2 h after refeeding compared to 4 h after chronic high-carbohydrate dietary interventions. As suggested by others [370], the results of the present study indicate that the LCHP diet improves glucose clearance and therefore enhance postprandial glycemia presumably through a putative enhanced GLUT4 recycling.

4.3 The impact of macronutrient ratios on insulin-responsive tissues

4.3.1 Macronutrient ratios differentially affect skeletal muscle and adipose tissue of Tbc1d4-deficient mice

In the present study, mD4KO mice resembled homozygous allele carriers of an Arctic *TBC1D4* loss-of-function variant resulting in postprandial hyperglycemia and an increased risk for T2DM [258]. Interestingly, a previous study revealed that mD4KO mice only partially resemble the human phenotype, exhibiting less pronounced postprandial hyperglycemia compared to whole-body D4KO mice [266, 290]. However, similar to whole-body D4KO mice, mD4KO presented with postprandial hyperglycemia, accompanied by impaired insulin-stimulated glucose uptake into oxidative *Soleu*s muscle, when subjected to a CON diet. The CON diet consists of 70% carbohydrates mainly in the form of complex carbohydrates derived from corn starch. Interestingly, the postprandial blood glucose concentration of mD4KO mice remained unchanged when subjected to an HCLP diet with 40% carbohydrates, which mainly derive form sucrose. Thus, in the present study, muscle-specific *Tbc1d4*-deficiency resulted in less pronounced postprandial hyperglycemia in a carbohydrate-dependent manner. These results are consistent with previous observations, which indicate that mice with a TBC1D4^{R691X} mutation affecting the long isoform of *TBC1D4,* resembling the Arctic *TBC1D4* loss-of-function variant in humans, resulted in postprandial normoglycemia. This study further demonstrated that insulin-stimulated glucose uptake in skeletal muscle was unaltered presumably due to compensatory up-regulation of a short *TBC1D4* splice isoform [371]. Contrary, rats with a *TBC1D4*^{R693X} mutation, analogous to the murine *TBC1D4*^{R691X} variant, exhibited postprandial hyperglycemia associated with impaired GLUT4-mediated glucose uptake possibly due to the lack of compensatory up-regulation of the short *TBC1D4* variant [371].

Interestingly, studies suggest that a high-sucrose diet may induce greater blood glucose oscillations than high-starch diets [372]. Obese mice fed a high-starch diet remained glucose and insulin tolerant similar to lean mice [373]. Therefore, the postprandial hyperglycemia induced by muscle-specific *Tbc1d4*-deficiency appears to be due to total carbohydrate content rather than carbohydrate complexity, supporting the previously discussed impaired ability of *Tbc1d4*-deficient mice to utilize glucose. However, it appears that intact TBC1D4-regulated glucose uptake in adipose tissue may compensate for muscle-specific *Tbc1d4*-deficiency to maintain postprandial normoglycemia when subjected to the HCLP diet.

Contrary to mD4KO mice, aD4KO mice exhibited postprandial hyperglycemia when fed the HCLP diet, but not when subjected to the CON diet. This is consistent with the previously discussed observations that a HCLP diet predominately leads to alterations in glucose and lipid metabolism in aD4KO mice compared to a CON diet. Interestingly, similar to whole-body and mD4KO mice, postprandial hyperglycemia in aD4KO mice was accompanied by reduced insulin-stimulated glucose uptake into oxidative *Soleus* muscle. Despite intact functionality of TBC1D4 in skeletal muscle of aD4KO, glucose uptake was reduced in response to HCLP diet feeding. Therefore, additional impairment of insulin-stimulated glucose uptake in primary white adipocytes may lead to postprandial hyperglycemia in aD4KO mice on a HCLP diet. While insulin-stimulated glucose uptake in primary white adipocytes was impaired regardless of the diet, postprandial normoglycemia was likely maintained in aD4KO mice on the CON and the LCHP diet due to unaltered glucose uptake in skeletal muscle.

These findings indicate that on the one hand the HCLP diet, which represents a westernized diet, affects predominately the adipose tissue and exacerbates the impaired glucose metabolism caused by *Tbc1d4*-deficiency. Therefore, adipocyte metabolism of D4KO mice on high-carbohydrate diets appears to be maintained to some extent despite the indicated lack of glucose utilization, possibly due to compensation by skeletal muscle. On the other hand, impaired skeletal muscle glucose metabolism due to *Tbc1d4*-deficiency is predominantly affected by carbohydrates and exacerbated by the high-carbohydrate CON diet, but not by the reduced-carbohydrate HCLP diet, possibly due to compensation by adipose tissue. Thus, the observed postprandial hyperglycemia in whole-body D4KO mice appears to be diet-dependent and caused by a combined *Tbc1d4*-deficiency in skeletal muscle and adipose tissue. Similar to previous findings of our research group [266], the present study indicates that improved whole-body glycemia in response to certain macronutrient rations depends on interorgan crosstalk between *Tbc1d4*-deficient adipose tissue and skeletal muscle.

4.3.2 Macronutrient rations determine chronic alterations in skeletal muscle and adipose tissue of Tbc1d4-deficient mice

The current study presents alterations in glucose and lipid metabolism in response to different dietary interventions in *Tbc1d4*-deficient mice. *In vivo* measurements demonstrated milder phenotypes in muscle- and adipose tissue-specific compared to whole-body D4KO mice. However, the different diets appeared to have distinct effects on the two tissues resulting in an additive effect in whole-body D4KO mice. The LCHP diet, representing an Arctic diet, significantly enhanced insulin-stimulated glucose uptake in oxidative and glycolytic muscle. To identify possible chronic adaptations in skeletal muscle of D4KO mice in response to a LCHP diet, which presumably enhances insulin-stimulated glucose uptake, mass spectrometry-based analysis of the mixed-fiber type *Gastrocnemius* muscle was conducted. Analysis of over-represented canonical pathways highlighted that several canonical pathways associated with insulin signaling were significantly regulated in D4KO compared to WT mice. Mass spectrometry-based analysis further showed that candidates included in CPDB highlighted canonical pathways were down-regulated in D4KO compared to WT mice (Supplemental table 1). This is consistent with the present *in vivo* measurements showing that D4KO mice fed the HCLP diet, resembling a Western diet, show impaired insulin-stimulated glucose uptake, presumably leading to postprandial hyperglycemia accompanied by hyperinsulinemia. Similarly, previous studies have suggested the impact of a Western diet on insulin signaling [374]. Moreover, Westernization accompanied by a characteristic HCLP diet promotes the development of T2DM, especially in individuals with a genetic predisposition [83, 84]. On the other hand, indigenous diets, as represented by the LCHP diet, are hypothesized to improve metabolic health in individuals with genetic predisposition as identified in indigenous populations [375, 376], but are controversial when applied to individuals without a genetic predisposition for T2DM [317, 377]. CPDB analysis revealed that in WT mice several canonical pathways associated with insulin signaling were differentially regulated when exposed to the LCHP compared to the HCLP diet. Mass spectrometry-based analysis further demonstrated that candidates, included in insulin signaling-associated canonical pathways were down-regulated in WT mice on a LCHP (Supplemental table 2). Thus, the present study supports the hypothesis that an Arctic diet may impair metabolic health in individuals without genetic predisposition.

In skeletal muscle, *Tbc1d4*-deficiency was accompanied by alterations in canonical pathways associated with insulin signaling in response to a Western diet. Although insulin-stimulated glucose uptake was significantly impaired in white adipose tissue of D4KO mice regardless of

the diet, CPDB analysis revealed that fatty acid metabolism was differentially regulated in white adipose tissue of D4KO compared to WT mice fed the Western diet. Consistent with this, others have demonstrated the impact of a Western diet on lipid metabolism in multiple organs [378-380]. Mass spectrometry-based analysis revealed that metallothioneins (Mt)1 and 2 are differentially regulated in D4KO compared to WT mice in an opposite manner with respect to the different diets. While zinc-binding metallothioneins were up-regulated on a Western diet in D4KO, they were down-regulated in response to the LCHP diet. Dysfunctional zinc signaling has been implicated with metabolic diseases, including T2DM [381]. Metallothioneins have been suggested to regulate adipogenesis. Mt1 and Mt2 are upregulated during adipocyte differentiation and MT1 and MT2-deficient mice show increased adipocyte size and fat mass. Furthermore, alterations in metallothionein expression are associated with insulin signaling [382]. Similar to the current study, Mt1 and Mt2 have been shown to be regulated in response to nutrition in white adipose tissue [383] and to be associated with Rab5a, Rab8a and Rab14-mediated exocytosis [384, 385], suggesting a regulatory role for TBC1D4 in metallothionein-associated adipocyte differentiation.

Interestingly, the dietary interventions differentially affected white adipose tissue in WT compared to D4KO mice. While in WT mice predominantly fatty acid metabolism was regulated in response to the diets, in D4KO mice canonical pathways associated with immune response and peroxisomal metabolism were differentially regulated. Leukemia inhibitory factor receptor (Lifr) was the most up-regulated protein in D4KO mice in response to the LCHP diet compared to the HCLP diet. LIFR binds IL-6 family member leukemia inhibitory factor and is associated with PI3Ks signaling [386]. These results may suggest a link between adipocyte inflammation and insulin resistance as a result of *Tbc1d4*-deficiency.

4.4 Conclusion

In conclusion, the present study showed that an Arctic diet resulted in reduced insulin sensitivity and adiposity in WT mice. *Tbc1d1*-deficiency resulted in reduced adipocyte mass and presumably adipocyte size on an Arctic diet, indicating that *Tbc1d1*-deficiency is associated with the maintenance of adipose tissue insulin sensitivity during diet-induced obesity. Contrary, *Tbc1d4*-deficiency elevated adipocyte mass in response to high-fat diets accompanied by alterations in lipid metabolism in adipose tissue and skeletal muscle. In conclusion, both TBC1D1 and TBC1D4 were shown to be critical regulators of lipid metabolism. While *Tbc1d1*-deficiency conveys leanness and maintains insulin sensitivity of adipocytes, *Tbc1d4*-deficiency

in mice results in marked alterations in lipid metabolism and potentially promotes ectopic fat accumulation, which consequently affects insulin sensitivity of peripheral tissues.

Tissue-specific *Tbc1d4*-deficiency results in less pronounced alterations in glucose and lipid metabolism compared to systemic TBC1D4 ablation. More specifically, muscle-specific *Tbc1d4*-deficiency resulted in impaired insulin-stimulated glucose uptake in oxidative *Soleus* muscle leading to postprandial hyperglycemia in a carbohydrate-dependent manner. Contrary, adipose tissue-specific *Tbc1d4*-deficiency resulted in reduced insulin-stimulated glucose uptake in white adipose tissue and oxidative *Soleus* muscle leading to postprandial hyperglycemia when subjected to a Western diet. In conclusion, an additive phenotype was observed in whole-body D4KO mice as a result of *Tbc1d4*-deficiency in both tissues, but likely additionally due to interorgan crosstalk. Presumably, this interorgan crosstalk is critical to enhance insulin-stimulated glucose uptake in skeletal muscle induced by an Arctic diet in whole-body D4KO mice. This was shown to be independent of total GLUT4 protein abundance, but may result from alterations in endosomal GLUT4 sorting that suppress lysosomal degradation and favor GLUT4 recycling.

5. Outlook

The present study highlighted TBC1D1 and TBC1D4 as crucial regulators of adipocyte metabolism, however, providing evidence for rather opposite roles in the development of adipose tissue mass and insulin sensitivity. To evaluate the results of the present study, it would be interesting to clarify the impact of *Tbc1d1*-deficiency on adipocyte size in response to the dietary interventions. Additionally, the impact of *Tbc1d1*- and *Tbc1d4*-deficiency on adipogenesis could be clarified via gene expression analysis.

Moreover, this study provides evidence that *Tbc1d4*-deficiency alters lipid metabolism, possibly promoting ectopic fat accumulation in peripheral organs, which consequently impairs insulin sensitivity due to certain lipid species. Therefore, it would be interesting to analyze triglyceride content in skeletal muscle and liver. Additionally, lipid profiling of these tissues would clarify if certain lipid species accumulate in response to different macronutrient ratios in D4KO mice and enhance or diminish insulin signaling.

Mass spectrometry-based analysis revealed the impact of nutrition on the skeletal muscle proteome of D4KO mice. The present thesis highlighted the crucial role of TBC1D4 in energy substrate metabolism and firstly demonstrated that an Arctic diet enhances insulin-stimulated glucose uptake into skeletal muscle of D4KO mice. Various proteins were differentially regulated in D4KO mice in response to the dietary interventions, providing evidence that an Arctic diet alters GLUT4 ubiquitination presumably via ubiquitin specific peptidase (Usp) 8, 13 and 15. This potentially favors GLUT4 recycling via Inf2, which regulates actin filament polymerization and therefore potentially GLUT4 trafficking. In order to evaluate these finding, deubiquitinating proteins or Inf2 could be overexpressed in oxidative *Soleus* muscle of D4KO mice and analyze the impact on insulin-stimulated glucose uptake. Additionally, it would be interesting to localize endosomal GLUT4 subsequent to insulin associated endocytosis. To clarify the association of TBC1D4 to Inf2, an *in vitro* GAP assay could be performed to evaluate if the Rho GTPase Cdc42, a key regulator of Inf2, presents a substrate of TBC1D4.

6. References

1. *Diagnosis and classification of diabetes mellitus.* Diabetes Care, 2009. 32 Suppl 1(Suppl 1): p. S62-7.
2. Cole, J.B. and J.C. Florez, *Genetics of diabetes mellitus and diabetes complications.* Nat Rev Nephrol, 2020. 16(7): p. 377-390.
3. Federation., I.D., t.e.B. IDF Diabetes Atlas, and Belgium, 2021.
4. *2. Classification and Diagnosis of Diabetes: Standards of Medical Care in Diabetes-2019.* Diabetes Care, 2019. 42(Suppl 1): p. S13-s28.
5. Mobasseri, M., et al., *Prevalence and incidence of type 1 diabetes in the world: a systematic review and meta-analysis.* Health Promot Perspect, 2020. 10(2): p. 98-115.
6. Dabelea, D., et al., *Trends in the prevalence of ketoacidosis at diabetes diagnosis: the SEARCH for diabetes in youth study.* Pediatrics, 2014. 133(4): p. e938-45.
7. Rewers, A., et al., *Presence of diabetic ketoacidosis at diagnosis of diabetes mellitus in youth: the Search for Diabetes in Youth Study.* Pediatrics, 2008. 121(5): p. e1258-66.
8. Rewers, A., et al., *Incidence of Diabetic Ketoacidosis at Diagnosis of Type 1 Diabetes in Colorado Youth, 1998-2012.* JAMA, 2015. 313(15): p. 1570-1572.
9. Usher-Smith, J.A., et al., *Factors associated with the presence of diabetic ketoacidosis at diagnosis of diabetes in children and young adults: a systematic review.* 2011. 343: p. d4092.
10. Khawandanah, J., *Double or hybrid diabetes: A systematic review on disease prevalence, characteristics and risk factors.* Nutr Diabetes, 2019. 9(1): p. 33.
11. *2. Classification and Diagnosis of Diabetes: Standards of Medical Care in Diabetes-2018.* Diabetes Care, 2018. 41(Suppl 1): p. S13-s27.
12. Udler, M.S., et al., *Type 2 diabetes genetic loci informed by multi-trait associations point to disease mechanisms and subtypes: A soft clustering analysis.* PLOS Medicine, 2018. 15(9): p. e1002654.
13. Ahlqvist, E., et al., *Novel subgroups of adult-onset diabetes and their association with outcomes: a data-driven cluster analysis of six variables.* Lancet Diabetes Endocrinol, 2018. 6(5): p. 361-369.
14. Morris, A.P., et al., *Large-scale association analysis provides insights into the genetic architecture and pathophysiology of type 2 diabetes.* Nat Genet, 2012. 44(9): p. 981-90.
15. Scott, R.A., et al., *Large-scale association analyses identify new loci influencing glycemic traits and provide insight into the underlying biological pathways.* Nat Genet, 2012. 44(9): p. 991-1005.
16. Kahn, S.E., M.E. Cooper, and S. Del Prato, *Pathophysiology and treatment of type 2 diabetes: perspectives on the past, present, and future.* Lancet, 2014. 383(9922): p. 1068-83.
17. Klein, S., et al., *Why does obesity cause diabetes?* Cell Metabolism, 2022. 34(1): p. 11-20.
18. Tchoukalova, Y.D., et al., *Regional differences in cellular mechanisms of adipose tissue gain with overfeeding.* 2010. 107(42): p. 18226-18231.
19. WHO, *Obesity: preventing and managing the global epidemic: report of a WHO consultation.* 2000.
20. WHO, *Obesity and overweight* 2021.
21. Hardy, O.T., M.P. Czech, and S. Corvera, *What causes the insulin resistance underlying obesity?* Curr Opin Endocrinol Diabetes Obes, 2012. 19(2): p. 81-7.
22. Reaven, G.M., *Banting lecture 1988. Role of insulin resistance in human disease.* Diabetes, 1988. 37(12): p. 1595-607.
23. Petersen, K.F., et al., *The role of skeletal muscle insulin resistance in the pathogenesis of the metabolic syndrome.* Proc Natl Acad Sci U S A, 2007. 104(31): p. 12587-94.
24. Boden, G., *Obesity and free fatty acids.* Endocrinol Metab Clin North Am, 2008. 37(3): p. 635-46, viii-ix.
25. Boden, G. and G.I. Shulman, *Free fatty acids in obesity and type 2 diabetes: defining their role in the development of insulin resistance and beta-cell dysfunction.* Eur J Clin Invest, 2002. 32 Suppl 3: p. 14-23.
26. Consitt, L.A., J.A. Bell, and J.A. Houmard, *Intramuscular lipid metabolism, insulin action, and obesity.* IUBMB Life, 2009. 61(1): p. 47-55.
27. van Ommen, B., et al., *Phenotypic flexibility as key factor in the human nutrition and health relationship.* Genes Nutr, 2014. 9(5): p. 423.
28. Smith, R.L., et al., *Metabolic Flexibility as an Adaptation to Energy Resources and Requirements in Health and Disease.* Endocr Rev, 2018. 39(4): p. 489-517.
29. Goodpaster, B.H. and L.M. Sparks, *Metabolic Flexibility in Health and Disease.* Cell Metabolism, 2017. 25(5): p. 1027-1036.

30. Randle, P.J., et al., *The glucose fatty-acid cycle. Its role in insulin sensitivity and the metabolic disturbances of diabetes mellitus.* Lancet, 1963. 1(7285): p. 785-9.
31. Kelley, D.E. and J.A. Simoneau, *Impaired free fatty acid utilization by skeletal muscle in non-insulin-dependent diabetes mellitus.* J Clin Invest, 1994. 94(6): p. 2349-56.
32. Kelley, D.E., et al., *Interaction between glucose and free fatty acid metabolism in human skeletal muscle.* J Clin Invest, 1993. 92(1): p. 91-8.
33. Kelley, D.E. and L.J. Mandarino, *Hyperglycemia normalizes insulin-stimulated skeletal muscle glucose oxidation and storage in noninsulin-dependent diabetes mellitus.* The Journal of Clinical Investigation, 1990. 86(6): p. 1999-2007.
34. Perry, R.J., et al., *Leptin Mediates a Glucose-Fatty Acid Cycle to Maintain Glucose Homeostasis in Starvation.* Cell, 2018. 172(1-2): p. 234-248.e17.
35. Cahill, G.F., Jr., *Starvation in man.* N Engl J Med, 1970. 282(12): p. 668-75.
36. Rothman, D.L., et al., *Quantitation of hepatic glycogenolysis and gluconeogenesis in fasting humans with 13CnMR.* Science, 1991. 254(5031): p. 573-6.
37. Browning, J.D., et al., *The effect of short-term fasting on liver and skeletal muscle lipid, glucose, and energy metabolism in healthy women and men.* J Lipid Res, 2012. 53(3): p. 577-586.
38. Soeters, M.R., et al., *Adaptive reciprocity of lipid and glucose metabolism in human short-term starvation.* Am J Physiol Endocrinol Metab, 2012. 303(12): p. E1397-407.
39. Veech, R.L., *The therapeutic implications of ketone bodies: the effects of ketone bodies in pathological conditions: ketosis, ketogenic diet, redox states, insulin resistance, and mitochondrial metabolism.* Prostaglandins Leukot Essent Fatty Acids, 2004. 70(3): p. 309-19.
40. Yancy, W.S., et al., *A low-carbohydrate, ketogenic diet to treat type 2 diabetes.* Nutrition & Metabolism, 2005. 2(1): p. 34.
41. Meessen, E.C.E., et al., *Human Postprandial Nutrient Metabolism and Low-Grade Inflammation: A Narrative Review.* Nutrients, 2019. 11(12).
42. Schaap, F.G., M. Trauner, and P.L. Jansen, *Bile acid receptors as targets for drug development.* Nat Rev Gastroenterol Hepatol, 2014. 11(1): p. 55-67.
43. Kuipers, F., V.W. Bloks, and A.K. Groen, *Beyond intestinal soap--bile acids in metabolic control.* Nat Rev Endocrinol, 2014. 10(8): p. 488-98.
44. Waseem, T., et al., *Exogenous ghrelin modulates release of pro-inflammatory and anti-inflammatory cytokines in LPS-stimulated macrophages through distinct signaling pathways.* Surgery, 2008. 143(3): p. 334-42.
45. Lee, Y.S. and H.S. Jun, *Anti-Inflammatory Effects of GLP-1-Based Therapies beyond Glucose Control.* Mediators Inflamm, 2016. 2016: p. 3094642.
46. Zhang, Y., et al., *Positional cloning of the mouse obese gene and its human homologue.* Nature, 1994. 372(6505): p. 425-32.
47. Fantuzzi, G. and R. Faggioni, *Leptin in the regulation of immunity, inflammation, and hematopoiesis.* J Leukoc Biol, 2000. 68(4): p. 437-46.
48. Considine, R.V., et al., *Serum immunoreactive-leptin concentrations in normal-weight and obese humans.* N Engl J Med, 1996. 334(5): p. 292-5.
49. Maffei, M., et al., *Leptin levels in human and rodent: measurement of plasma leptin and ob RNA in obese and weight-reduced subjects.* Nat Med, 1995. 1(11): p. 1155-61.
50. Iikuni, N., et al., *Leptin and Inflammation.* Curr Immunol Rev, 2008. 4(2): p. 70-79.
51. Ferrannini, E., et al., *The disposal of an oral glucose load in patients with non-insulin-dependent diabetes.* Metabolism, 1988. 37(1): p. 79-85.
52. Merz, K.E. and D.C. Thurmond, *Role of Skeletal Muscle in Insulin Resistance and Glucose Uptake.* Compr Physiol, 2020. 10(3): p. 785-809.
53. DeFronzo, R.A. and D. Tripathy, *Skeletal muscle insulin resistance is the primary defect in type 2 diabetes.* Diabetes Care, 2009. 32 Suppl 2(Suppl 2): p. S157-63.
54. Kumar, A.A., et al., *Postprandial Metabolism is Impaired in Overweight Normoglycemic Young Adults without Family History of Diabetes.* Sci Rep, 2020. 10(1): p. 353.
55. Strassburg, K., et al., *Postprandial fatty acid specific changes in circulating oxylipins in lean and obese men after high-fat challenge tests.* Mol Nutr Food Res, 2014. 58(3): p. 591-600.
56. Bozzetto, L., et al., *Insulin resistance, postprandial GLP-1 and adaptive immunity are the main predictors of NAFLD in a homogeneous population at high cardiovascular risk.* Nutr Metab Cardiovasc Dis, 2016. 26(7): p. 623-629.

57. Services., U.D.o.H.a.H., *"US Department of Agriculture. 2015–2020 dietary guidelines for Americans. December 2015."* 2015.
58. de Souza, R.J., et al., *Alternatives for macronutrient intake and chronic disease: a comparison of the OmniHeart diets with popular diets and with dietary recommendations.* Am J Clin Nutr, 2008. 88(1): p. 1-11.
59. Carey, V.J., et al., *Rationale and design of the Optimal Macro-Nutrient Intake Heart Trial to Prevent Heart Disease (OMNI-Heart).* Clin Trials, 2005. 2(6): p. 529-37.
60. Ungvari, Z., et al., *Mechanisms underlying caloric restriction and lifespan regulation: implications for vascular aging.* Circ Res, 2008. 102(5): p. 519-28.
61. Solon-Biet, S.M., et al., *Macronutrients and caloric intake in health and longevity.* J Endocrinol, 2015. 226(1): p. R17-28.
62. Mair, W., M.D. Piper, and L. Partridge, *Calories do not explain extension of life span by dietary restriction in Drosophila.* PLoS Biol, 2005. 3(7): p. e223.
63. Garralda-Del-Villar, M., et al., *Healthy Lifestyle and Incidence of Metabolic Syndrome in the SUN Cohort.* Nutrients, 2018. 11(1).
64. Galaviz, K.I., et al., *Lifestyle and the Prevention of Type 2 Diabetes: A Status Report.* Am J Lifestyle Med, 2018. 12(1): p. 4-20.
65. Rakhra, V., et al., *Obesity and the Western Diet: How We Got Here.* Mo Med, 2020. 117(6): p. 536-538.
66. Hunter, J.E., J. Zhang, and P.M. Kris-Etherton, *Cardiovascular disease risk of dietary stearic acid compared with trans, other saturated, and unsaturated fatty acids: a systematic review.* Am J Clin Nutr, 2010. 91(1): p. 46-63.
67. Esmaillzadeh, A., et al., *Dietary patterns, insulin resistance, and prevalence of the metabolic syndrome in women.* Am J Clin Nutr, 2007. 85(3): p. 910-8.
68. Muoio, D.M., *Metabolic inflexibility: when mitochondrial indecision leads to metabolic gridlock.* Cell, 2014. 159(6): p. 1253-62.
69. Dhindsa, S., et al., *Differential effects of glucose and alcohol on reactive oxygen species generation and intranuclear nuclear factor-kappaB in mononuclear cells.* Metabolism, 2004. 53(3): p. 330-4.
70. Deopurkar, R., et al., *Differential effects of cream, glucose, and orange juice on inflammation, endotoxin, and the expression of Toll-like receptor-4 and suppressor of cytokine signaling-3.* Diabetes Care, 2010. 33(5): p. 991-7.
71. Gregersen, S., et al., *Inflammatory and oxidative stress responses to high-carbohydrate and high-fat meals in healthy humans.* J Nutr Metab, 2012. 2012: p. 238056.
72. Ghanim, H., et al., *Increase in plasma endotoxin concentrations and the expression of Toll-like receptors and suppressor of cytokine signaling-3 in mononuclear cells after a high-fat, high-carbohydrate meal: implications for insulin resistance.* Diabetes Care, 2009. 32(12): p. 2281-7.
73. Lee, J.J., et al., *High-fat diet induces toll-like receptor 4-dependent macrophage/microglial cell activation and retinal impairment.* Invest Ophthalmol Vis Sci, 2015. 56(5): p. 3041-50.
74. Calder, P.C., et al., *Dietary factors and low-grade inflammation in relation to overweight and obesity.* Br J Nutr, 2011. 106 Suppl 3: p. S5-78.
75. Minihane, A.M., et al., *Low-grade inflammation, diet composition and health: current research evidence and its translation.* Br J Nutr, 2015. 114(7): p. 999-1012.
76. Libby, P., *Inflammation in atherosclerosis.* Arterioscler Thromb Vasc Biol, 2012. 32(9): p. 2045-51.
77. Boyden, S.V. and A.A.o. Science, *The Impact of Civilisation on the Biology of Man*. 1970: Australian National University Press.
78. O'Dea, K., N.G. White, and A.J. Sinclair, *An investigation of nutrition-related risk factors in an isolated Aboriginal community in northern Australia: advantages of a traditionally-orientated life-style.* Med J Aust, 1988. 148(4): p. 177-80.
79. Carrera-Bastos, P., et al., *The Western diet and lifestyle and diseases of civilization.* Research Reports in Clinical Cardiology, 2011. 2: p. 2-15.
80. Lindeberg, S., et al., *Low serum insulin in traditional Pacific Islanders--the Kitava Study.* Metabolism, 1999. 48(10): p. 1216-9.
81. Cordain, L., et al., *Origins and evolution of the Western diet: health implications for the 21st century.* Am J Clin Nutr, 2005. 81(2): p. 341-54.
82. Singh, A. and D. Singh, *The Paleolithic Diet.* Cureus, 2023. 15(1): p. e34214.
83. Kopp, W., *How Western Diet And Lifestyle Drive The Pandemic Of Obesity And Civilization Diseases.* Diabetes Metab Syndr Obes, 2019. 12: p. 2221-2236.

84. Qi, L., et al., *Genetic predisposition, Western dietary pattern, and the risk of type 2 diabetes in men.* Am J Clin Nutr, 2009. 89(5): p. 1453-8.
85. Ioannidis, J.P.A., *The Challenge of Reforming Nutritional Epidemiologic Research.* Jama, 2018. 320(10): p. 969-970.
86. *5. Lifestyle Management: Standards of Medical Care in Diabetes-2019.* Diabetes Care, 2019. 42(Suppl 1): p. S46-s60.
87. Hamdy, O., et al., *Fat Versus Carbohydrate-Based Energy-Restricted Diets for Weight Loss in Patients With Type 2 Diabetes.* Curr Diab Rep, 2018. 18(12): p. 128.
88. Brouns, F., *Overweight and diabetes prevention: is a low-carbohydrate–high-fat diet recommendable?* European Journal of Nutrition, 2018. 57(4): p. 1301-1312.
89. Adam-Perrot, A., P. Clifton, and F. Brouns, *Low-carbohydrate diets: nutritional and physiological aspects.* Obes Rev, 2006. 7(1): p. 49-58.
90. O'Dea, K., *Marked improvement in carbohydrate and lipid metabolism in diabetic Australian aborigines after temporary reversion to traditional lifestyle.* Diabetes, 1984. 33(6): p. 596-603.
91. Lindeberg, S., et al., *A Palaeolithic diet improves glucose tolerance more than a Mediterranean-like diet in individuals with ischaemic heart disease.* Diabetologia, 2007. 50(9): p. 1795-1807.
92. Paoli, A., et al., *Beyond weight loss: a review of the therapeutic uses of very-low-carbohydrate (ketogenic) diets.* Eur J Clin Nutr, 2013. 67(8): p. 789-96.
93. Cordain, L., et al., *Plant-animal subsistence ratios and macronutrient energy estimations in worldwide hunter-gatherer diets.* Am J Clin Nutr, 2000. 71(3): p. 682-92.
94. Wolever, T.M. and C. Bolognesi, *Prediction of glucose and insulin responses of normal subjects after consuming mixed meals varying in energy, protein, fat, carbohydrate and glycemic index.* J Nutr, 1996. 126(11): p. 2807-12.
95. Björck, I., H. Liljeberg, and E. Ostman, *Low glycaemic-index foods.* Br J Nutr, 2000. 83 Suppl 1: p. S149-55.
96. Ren, W.-K., et al., *Glutamine on Intestinal Inflammation: A Mechanistic Perspective.* 2013. 11(2): p. 315-326.
97. Wang, W., et al., *Glycine stimulates protein synthesis and inhibits oxidative stress in pig small intestinal epithelial cells.* J Nutr, 2014. 144(10): p. 1540-8.
98. Uehara, K., et al., *The lower intestinal tract-specific induction of heme oxygenase-1 by glutamine protects against endotoxemic intestinal injury.* Crit Care Med, 2005. 33(2): p. 381-90.
99. Kabir, M., et al., *Dietary amylose-amylopectin starch content affects glucose and lipid metabolism in adipocytes of normal and diabetic rats.* J Nutr, 1998. 128(1): p. 35-43.
100. Kabir, M., et al., *A high glycemic index starch diet affects lipid storage-related enzymes in normal and to a lesser extent in diabetic rats.* J Nutr, 1998. 128(11): p. 1878-83.
101. Lerer-Metzger, M., et al., *Effects of long-term low-glycaemic index starchy food on plasma glucose and lipid concentrations and adipose tissue cellularity in normal and diabetic rats.* Br J Nutr, 1996. 75(5): p. 723-32.
102. Pawlak, D.B., J.A. Kushner, and D.S. Ludwig, *Effects of dietary glycaemic index on adiposity, glucose homoeostasis, and plasma lipids in animals.* Lancet, 2004. 364(9436): p. 778-85.
103. Roberts, M.N., et al., *A Ketogenic Diet Extends Longevity and Healthspan in Adult Mice.* Cell Metab, 2017. 26(3): p. 539-546.e5.
104. Ellenbroek, J.H., et al., *Long-term ketogenic diet causes glucose intolerance and reduced β- and α-cell mass but no weight loss in mice.* 2014. 306(5): p. E552-E558.
105. Perng, W., et al., *Metabolomic profiles and childhood obesity.* Obesity (Silver Spring), 2014. 22(12): p. 2570-8.
106. Newgard, C.B., *Interplay between lipids and branched-chain amino acids in development of insulin resistance.* Cell Metab, 2012. 15(5): p. 606-14.
107. Carreiro, A.L., et al., *The Macronutrients, Appetite, and Energy Intake.* 2016. 36(1): p. 73-103.
108. Coyle, E.F., *Physical activity as a metabolic stressor.* Am J Clin Nutr, 2000. 72(2 Suppl): p. 512s-20s.
109. Wells, G.D., H. Selvadurai, and I. Tein, *Bioenergetic provision of energy for muscular activity.* Paediatr Respir Rev, 2009. 10(3): p. 83-90.
110. Kwon, Y.J., et al., *Associating Intake Proportion of Carbohydrate, Fat, and Protein with All-Cause Mortality in Korean Adults.* Nutrients, 2020. 12(10).
111. Alghannam, A.F., M.M. Ghaith, and M.H. Alhussain, *Regulation of Energy Substrate Metabolism in Endurance Exercise.* Int J Environ Res Public Health, 2021. 18(9).
112. Matschinsky, F.M. and D.F. Wilson, *The Central Role of Glucokinase in Glucose Homeostasis: A Perspective 50 Years After Demonstrating the Presence of the Enzyme in Islets of Langerhans.* Front Physiol, 2019. 10: p. 148.

113. Ganapathy-Kanniappan, S. and J.-F.H. Geschwind, *Tumor glycolysis as a target for cancer therapy: progress and prospects.* Molecular Cancer, 2013. 12(1): p. 152.
114. Sousa, J.S., E. D'Imprima, and J. Vonck, *Mitochondrial Respiratory Chain Complexes.* Subcell Biochem, 2018. 87: p. 167-227.
115. Martínez-Reyes, I. and N.S. Chandel, *Mitochondrial TCA cycle metabolites control physiology and disease.* Nat Commun, 2020. 11(1): p. 102.
116. Granchi, C., et al., *Inhibitors of lactate dehydrogenase isoforms and their therapeutic potentials.* Curr Med Chem, 2010. 17(7): p. 672-97.
117. Lenzen, S., *A fresh view of glycolysis and glucokinase regulation: history and current status.* J Biol Chem, 2014. 289(18): p. 12189-94.
118. Jha, M.K., I.K. Lee, and K. Suk, *Metabolic reprogramming by the pyruvate dehydrogenase kinase-lactic acid axis: Linking metabolism and diverse neuropathophysiologies.* Neurosci Biobehav Rev, 2016. 68: p. 1-19.
119. Emhoff, C.A., et al., *Gluconeogenesis and hepatic glycogenolysis during exercise at the lactate threshold.* J Appl Physiol (1985), 2013. 114(3): p. 297-306.
120. Adeva-Andany, M.M., et al., *Glycogen metabolism in humans.* BBA Clin, 2016. 5: p. 85-100.
121. Tadaishi, M., et al., *Adenosine stimulates hepatic glycogenolysis via adrenal glands-liver crosstalk in mice.* PLoS One, 2018. 13(12): p. e0209647.
122. Sherman, W.M., *Metabolism of sugars and physical performance.* Am J Clin Nutr, 1995. 62(1 Suppl): p. 228s-241s.
123. Kahn, C.R., *The molecular mechanism of insulin action.* Annu Rev Med, 1985. 36: p. 429-51.
124. Saltiel, A.R. and C.R. Kahn, *Insulin signalling and the regulation of glucose and lipid metabolism.* Nature, 2001. 414(6865): p. 799-806.
125. Sesti, G., et al., *Defects of the insulin receptor substrate (IRS) system in human metabolic disorders.* Faseb j, 2001. 15(12): p. 2099-111.
126. Fruman, D.A., R.E. Meyers, and L.C. Cantley, *Phosphoinositide kinases.* Annu Rev Biochem, 1998. 67: p. 481-507.
127. Rameh, L.E. and L.C. Cantley, *The role of phosphoinositide 3-kinase lipid products in cell function.* J Biol Chem, 1999. 274(13): p. 8347-50.
128. Cho, H., et al., *Insulin resistance and a diabetes mellitus-like syndrome in mice lacking the protein kinase Akt2 (PKB beta).* Science, 2001. 292(5522): p. 1728-31.
129. Yang, G., et al., *A Positive Feedback Loop between Akt and mTORC2 via SIN1 Phosphorylation.* Cell Rep, 2015. 12(6): p. 937-43.
130. Dokas, J., et al., *Conventional knockout of Tbc1d1 in mice impairs insulin- and AICAR-stimulated glucose uptake in skeletal muscle.* Endocrinology, 2013. 154(10): p. 3502-14.
131. Chadt, A., et al., *"Deletion of both Rab-GTPase–activating proteins TBC1D1 and TBC1D4 in mice eliminates insulin- and AICAR-stimulated glucose transport [corrected].* Diabetes, 2015. 64(3): p. 746-59.
132. Espelage, L., H. Al-Hasani, and A. Chadt, *RabGAPs in skeletal muscle function and exercise.* J Mol Endocrinol, 2020. 64(1): p. R1-r19.
133. Sano, H., et al., *Insulin-stimulated phosphorylation of a Rab GTPase-activating protein regulates GLUT4 translocation.* J Biol Chem, 2003. 278(17): p. 14599-602.
134. Grosshans, B.L., D. Ortiz, and P. Novick, *Rabs and their effectors: achieving specificity in membrane traffic.* Proc Natl Acad Sci U S A, 2006. 103(32): p. 11821-7.
135. Joost, H.G., et al., *Nomenclature of the GLUT/SLC2A family of sugar/polyol transport facilitators.* Am J Physiol Endocrinol Metab, 2002. 282(4): p. E974-6.
136. Thorens, B. and M. Mueckler, *Glucose transporters in the 21st Century.* Am J Physiol Endocrinol Metab, 2010. 298(2): p. E141-5.
137. Huang, S. and M.P. Czech, *The GLUT4 glucose transporter.* Cell Metab, 2007. 5(4): p. 237-52.
138. Satoh, T., *Molecular Mechanisms for the Regulation of Insulin-Stimulated Glucose Uptake by Small Guanosine Triphosphatases in Skeletal Muscle and Adipocytes.* 2014. 15(10): p. 18677-18692.
139. Khan, A. and J. Pessin, *Insulin regulation of glucose uptake: a complex interplay of intracellular signalling pathways.* Diabetologia, 2002. 45(11): p. 1475-1483.
140. Dohm, G.L., et al., *An in vitro human muscle preparation suitable for metabolic studies. Decreased insulin stimulation of glucose transport in muscle from morbidly obese and diabetic subjects.* J Clin Invest, 1988. 82(2): p. 486-94.
141. Goodyear, L.J., et al., *Insulin receptor phosphorylation, insulin receptor substrate-1 phosphorylation, and phosphatidylinositol 3-kinase activity are decreased in intact skeletal muscle strips from obese subjects.* J Clin Invest, 1995. 95(5): p. 2195-204.

142. Bell, J.A., et al., *Lipid partitioning, incomplete fatty acid oxidation, and insulin signal transduction in primary human muscle cells: effects of severe obesity, fatty acid incubation, and fatty acid translocase/CD36 overexpression.* J Clin Endocrinol Metab, 2010. 95(7): p. 3400-10.
143. Warram, J.H., et al., *Slow glucose removal rate and hyperinsulinemia precede the development of type II diabetes in the offspring of diabetic parents.* Ann Intern Med, 1990. 113(12): p. 909-15.
144. Moore, M.C., et al., *Sources of carbon for hepatic glycogen synthesis in the conscious dog.* J Clin Invest, 1991. 88(2): p. 578-87.
145. Rizza, R.A., *Pathogenesis of fasting and postprandial hyperglycemia in type 2 diabetes: implications for therapy.* Diabetes, 2010. 59(11): p. 2697-707.
146. Hatting, M., et al., *Insulin regulation of gluconeogenesis.* Ann N Y Acad Sci, 2018. 1411(1): p. 21-35.
147. I, O.S., et al., *FoxO1 integrates direct and indirect effects of insulin on hepatic glucose production and glucose utilization.* Nat Commun, 2015. 6: p. 7079.
148. Gastaldelli, A., et al., *Effect of physiological hyperinsulinemia on gluconeogenesis in nondiabetic subjects and in type 2 diabetic patients.* Diabetes, 2001. 50(8): p. 1807-12.
149. Girard, J., *Insulin's effect on the liver: "direct or indirect?" continues to be the question.* J Clin Invest, 2006. 116(2): p. 302-4.
150. Sharabi, K., et al., *Molecular pathophysiology of hepatic glucose production.* Mol Aspects Med, 2015. 46: p. 21-33.
151. Puigserver, P., et al., *Insulin-regulated hepatic gluconeogenesis through FOXO1–PGC-1α interaction.* Nature, 2003. 423(6939): p. 550-555.
152. Haeusler, R.A., K.H. Kaestner, and D. Accili, *FoxOs function synergistically to promote glucose production.* J Biol Chem, 2010. 285(46): p. 35245-8.
153. Li, X., et al., *Akt/PKB regulates hepatic metabolism by directly inhibiting PGC-1alpha transcription coactivator.* Nature, 2007. 447(7147): p. 1012-6.
154. Lin, H.V. and D. Accili, *Hormonal regulation of hepatic glucose production in health and disease.* Cell Metab, 2011. 14(1): p. 9-19.
155. Lochhead, P.A., et al., *Inhibition of GSK-3 selectively reduces glucose-6-phosphatase and phosphatase and phosphoenolypyruvate carboxykinase gene expression.* Diabetes, 2001. 50(5): p. 937-46.
156. Petersen, K.F., et al., *Mechanism by which glucose and insulin inhibit net hepatic glycogenolysis in humans.* J Clin Invest, 1998. 101(6): p. 1203-9.
157. Magnusson, I., et al., *Increased rate of gluconeogenesis in type II diabetes mellitus. A 13C nuclear magnetic resonance study.* The Journal of Clinical Investigation, 1992. 90(4): p. 1323-1327.
158. Perry, R.J., et al., *The role of hepatic lipids in hepatic insulin resistance and type 2 diabetes.* Nature, 2014. 510(7503): p. 84-91.
159. Roden, M. and G.I. Shulman, *The integrative biology of type 2 diabetes.* Nature, 2019. 576(7785): p. 51-60.
160. Benhamed, F., et al., *The lipogenic transcription factor ChREBP dissociates hepatic steatosis from insulin resistance in mice and humans.* J Clin Invest, 2012. 122(6): p. 2176-94.
161. Kumashiro, N., et al., *Cellular mechanism of insulin resistance in nonalcoholic fatty liver disease.* 2011. 108(39): p. 16381-16385.
162. Michelotti, G.A., M.V. Machado, and A.M. Diehl, *NAFLD, NASH and liver cancer.* Nat Rev Gastroenterol Hepatol, 2013. 10(11): p. 656-65.
163. Zhang, T., et al., *Acetylation negatively regulates glycogen phosphorylase by recruiting protein phosphatase 1.* Cell Metab, 2012. 15(1): p. 75-87.
164. Rui, L., *Energy metabolism in the liver.* Compr Physiol, 2014. 4(1): p. 177-97.
165. Luo, L. and M. Liu, *Adipose tissue in control of metabolism.* J Endocrinol, 2016. 231(3): p. R77-r99.
166. Reddy, P., et al., *Metabolic syndrome is an inflammatory disorder: A conspiracy between adipose tissue and phagocytes.* Clin Chim Acta, 2019. 496: p. 35-44.
167. Alkhouli, N., et al., *The mechanical properties of human adipose tissues and their relationships to the structure and composition of the extracellular matrix.* 2013. 305(12): p. E1427-E1435.
168. Manolopoulos, K.N., F. Karpe, and K.N. Frayn, *Gluteofemoral body fat as a determinant of metabolic health.* Int J Obes (Lond), 2010. 34(6): p. 949-59.
169. Piya, M.K., P.G. McTernan, and S. Kumar, *Adipokine inflammation and insulin resistance: the role of glucose, lipids and endotoxin.* J Endocrinol, 2013. 216(1): p. T1-t15.
170. Björntorp, P., *"Portal" adipose tissue as a generator of risk factors for cardiovascular disease and diabetes.* 1990. 10(4): p. 493-496.
171. Mittal, B., *Subcutaneous adipose tissue & visceral adipose tissue.* Indian J Med Res, 2019. 149(5): p. 571-573.

172. Townsend, K. and Y.H. Tseng, *Brown adipose tissue: Recent insights into development, metabolic function and therapeutic potential.* Adipocyte, 2012. 1(1): p. 13-24.
173. Ikeda, K., P. Maretich, and S. Kajimura, *The Common and Distinct Features of Brown and Beige Adipocytes.* Trends Endocrinol Metab, 2018. 29(3): p. 191-200.
174. Pfeifer, A. and L.S. Hoffmann, *Brown, beige, and white: the new color code of fat and its pharmacological implications.* Annu Rev Pharmacol Toxicol, 2015. 55: p. 207-27.
175. Nedergaard, J., T. Bengtsson, and B. Cannon, *Unexpected evidence for active brown adipose tissue in adult humans.* Am J Physiol Endocrinol Metab, 2007. 293(2): p. E444-52.
176. Cypess, A.M., et al., *Identification and importance of brown adipose tissue in adult humans.* N Engl J Med, 2009. 360(15): p. 1509-17.
177. Scheel, A.K., L. Espelage, and A. Chadt, *Many Ways to Rome: Exercise, Cold Exposure and Diet—Do They All Affect BAT Activation and WAT Browning in the Same Manner?* 2022. 23(9): p. 4759.
178. Rolland, C., M. Hession, and I. Broom, *Effect of weight loss on adipokine levels in obese patients.* Diabetes Metab Syndr Obes, 2011. 4: p. 315-23.
179. Raghow, R., *Bariatric surgery-mediated weight loss and its metabolic consequences for type-2 diabetes.* World J Diabetes, 2013. 4(3): p. 47-50.
180. Frayn, K.N., P. Arner, and H. Yki-Järvinen, *Fatty acid metabolism in adipose tissue, muscle and liver in health and disease.* Essays Biochem, 2006. 42: p. 89-103.
181. Kersten, S., *Mechanisms of nutritional and hormonal regulation of lipogenesis.* EMBO Rep, 2001. 2(4): p. 282-6.
182. Assimacopoulos-Jeannet, F., et al., *In vivo effects of hyperinsulinemia on lipogenic enzymes and glucose transporter expression in rat liver and adipose tissues.* Metabolism, 1995. 44(2): p. 228-33.
183. Watt, M.J. and A.J. Hoy, *Lipid metabolism in skeletal muscle: generation of adaptive and maladaptive intracellular signals for cellular function.* Am J Physiol Endocrinol Metab, 2012. 302(11): p. E1315-28.
184. Strawford, A., et al., *Adipose tissue triglyceride turnover, de novo lipogenesis, and cell proliferation in humans measured with 2H2O.* Am J Physiol Endocrinol Metab, 2004. 286(4): p. E577-88.
185. Coleman, R.A. and D.P. Lee, *Enzymes of triacylglycerol synthesis and their regulation.* Prog Lipid Res, 2004. 43(2): p. 134-76.
186. Jump, D.B., et al., *Coordinate regulation of glycolytic and lipogenic gene expression by polyunsaturated fatty acids.* J Lipid Res, 1994. 35(6): p. 1076-84.
187. Kersten, S., et al., *Peroxisome proliferator-activated receptor alpha mediates the adaptive response to fasting.* J Clin Invest, 1999. 103(11): p. 1489-98.
188. Lass, A., et al., *Lipolysis–a highly regulated multi-enzyme complex mediates the catabolism of cellular fat stores.* Prog Lipid Res, 2011. 50(1): p. 14-27.
189. Zimmermann, R., et al., *Fat mobilization in adipose tissue is promoted by adipose triglyceride lipase.* Science, 2004. 306(5700): p. 1383-6.
190. Holm, C., *Molecular mechanisms regulating hormone-sensitive lipase and lipolysis.* Biochem Soc Trans, 2003. 31(Pt 6): p. 1120-4.
191. Liang, Q., et al., *FGF21 maintains glucose homeostasis by mediating the cross talk between liver and brain during prolonged fasting.* Diabetes, 2014. 63(12): p. 4064-75.
192. Ma, Y., et al., *Fatty acid oxidation: An emerging facet of metabolic transformation in cancer.* Cancer Lett, 2018. 435: p. 92-100.
193. Kershaw, E.E., et al., *Adipose triglyceride lipase: function, regulation by insulin, and comparison with adiponutrin.* Diabetes, 2006. 55(1): p. 148-57.
194. Duncan, R.E., et al., *Regulation of lipolysis in adipocytes.* Annu Rev Nutr, 2007. 27: p. 79-101.
195. Choi, S.M., et al., *Insulin regulates adipocyte lipolysis via an Akt-independent signaling pathway.* Mol Cell Biol, 2010. 30(21): p. 5009-20.
196. Chakrabarti, P., et al., *Mammalian target of rapamycin complex 1 suppresses lipolysis, stimulates lipogenesis, and promotes fat storage.* Diabetes, 2010. 59(4): p. 775-81.
197. Morigny, P., et al., *Adipocyte lipolysis and insulin resistance.* Biochimie, 2016. 125: p. 259-66.
198. Badin, P.M., et al., *Altered skeletal muscle lipase expression and activity contribute to insulin resistance in humans.* Diabetes, 2011. 60(6): p. 1734-42.
199. Kase, E.T., et al., *Primary defects in lipolysis and insulin action in skeletal muscle cells from type 2 diabetic individuals.* Biochim Biophys Acta, 2015. 1851(9): p. 1194-201.
200. Kelley, D.E., et al., *Skeletal muscle fatty acid metabolism in association with insulin resistance, obesity, and weight loss.* Am J Physiol, 1999. 277(6): p. E1130-41.

201. Boushel, R., et al., *Patients with type 2 diabetes have normal mitochondrial function in skeletal muscle.* Diabetologia, 2007. 50(4): p. 790-6.
202. Mogensen, M., et al., *Mitochondrial respiration is decreased in skeletal muscle of patients with type 2 diabetes.* Diabetes, 2007. 56(6): p. 1592-9.
203. Mengeste, A.M., A.C. Rustan, and J. Lund, *Skeletal muscle energy metabolism in obesity.* 2021. 29(10): p. 1582-1595.
204. Bonen, A., et al., *Triacylglycerol accumulation in human obesity and type 2 diabetes is associated with increased rates of skeletal muscle fatty acid transport and increased sarcolemmal FAT/CD36.* Faseb j, 2004. 18(10): p. 1144-6.
205. Chandel, N.S., *Amino Acid Metabolism.* Cold Spring Harb Perspect Biol, 2021. 13(4).
206. Nurjhan, N., et al., *Glutamine: a major gluconeogenic precursor and vehicle for interorgan carbon transport in man.* J Clin Invest, 1995. 95(1): p. 272-7.
207. Stumvoll, M., et al., *Role of glutamine in human carbohydrate metabolism in kidney and other tissues.* Kidney Int, 1999. 55(3): p. 778-92.
208. Gerich, J.E., et al., *Renal gluconeogenesis: its importance in human glucose homeostasis.* Diabetes Care, 2001. 24(2): p. 382-91.
209. Agostini, F., et al., *Physical inactivity decreases whole body glutamine turnover independently from changes in proteolysis.* J Physiol, 2008. 586(19): p. 4775-81.
210. Marliss, E.B., et al., *Muscle and splanchnic glutmine and glutamate metabolism in postabsorptive andstarved man.* J Clin Invest, 1971. 50(4): p. 814-7.
211. Ling, Z.-N., et al., *Amino acid metabolism in health and disease.* Signal Transduction and Targeted Therapy, 2023. 8(1): p. 345.
212. White, P.J., et al., *Insulin action, type 2 diabetes, and branched-chain amino acids: A two-way street.* Mol Metab, 2021. 52: p. 101261.
213. Isanejad, M., et al., *Branched-chain amino acid, meat intake and risk of type 2 diabetes in the Women's Health Initiative.* Br J Nutr, 2017. 117(11): p. 1523-1530.
214. Würtz, P., et al., *Branched-chain and aromatic amino acids are predictors of insulin resistance in young adults.* Diabetes Care, 2013. 36(3): p. 648-55.
215. Flores-Guerrero, J.L., et al., *Plasma Branched-Chain Amino Acids and Risk of Incident Type 2 Diabetes: Results from the PREVEND Prospective Cohort Study.* J Clin Med, 2018. 7(12).
216. Eagle, H., et al., *Protein turnover in mammaliar cell cultures.* J Biol Chem, 1959. 234(3): p. 592-7.
217. Lerin, C., et al., *Defects in muscle branched-chain amino acid oxidation contribute to impaired lipid metabolism.* Mol Metab, 2016. 5(10): p. 926-936.
218. Cheng, S., et al., *Adipose Tissue Dysfunction and Altered Systemic Amino Acid Metabolism Are Associated with Non-Alcoholic Fatty Liver Disease.* PLoS One, 2015. 10(10): p. e0138889.
219. Lake, A.D., et al., *Branched chain amino acid metabolism profiles in progressive human nonalcoholic fatty liver disease.* Amino Acids, 2015. 47(3): p. 603-15.
220. Riazi, R., et al., *The total branched-chain amino acid requirement in young healthy adult men determined by indicator amino acid oxidation by use of L-[1-13C]phenylalanine.* J Nutr, 2003. 133(5): p. 1383-9.
221. Wolfson, R.L., et al., *Sestrin2 is a leucine sensor for the mTORC1 pathway.* Science, 2016. 351(6268): p. 43-8.
222. Louard, R.J., et al., *Insulin sensitivity of protein and glucose metabolism in human forearm skeletal muscle.* J Clin Invest, 1992. 90(6): p. 2348-54.
223. Chevalier, S., et al., *The greater contribution of gluconeogenesis to glucose production in obesity is related to increased whole-body protein catabolism.* Diabetes, 2006. 55(3): p. 675-81.
224. Felig, P., E. Marliss, and G.F. Cahill, Jr., *Plasma amino acid levels and insulin secretion in obesity.* N Engl J Med, 1969. 281(15): p. 811-6.
225. Abdulla, H., et al., *Role of insulin in the regulation of human skeletal muscle protein synthesis and breakdown: a systematic review and meta-analysis.* Diabetologia, 2016. 59(1): p. 44-55.
226. Everman, S., et al., *Insulin does not stimulate muscle protein synthesis during increased plasma branched-chain amino acids alone but still decreases whole body proteolysis in humans.* Am J Physiol Endocrinol Metab, 2016. 311(4): p. E671-e677.
227. Mahendran, Y., et al., *Genetic evidence of a causal effect of insulin resistance on branched-chain amino acid levels.* Diabetologia, 2017. 60(5): p. 873-878.
228. Newgard, C.B., et al., *A branched-chain amino acid-related metabolic signature that differentiates obese and lean humans and contributes to insulin resistance.* Cell Metab, 2009. 9(4): p. 311-26.

229. Krebs, M., et al., *Mechanism of amino acid-induced skeletal muscle insulin resistance in humans.* Diabetes, 2002. 51(3): p. 599-605.
230. Nie, C., et al., *Branched Chain Amino Acids: Beyond Nutrition Metabolism.* Int J Mol Sci, 2018. 19(4).
231. Gancheva, S., et al., *Interorgan Metabolic Crosstalk in Human Insulin Resistance.* Physiol Rev, 2018. 98(3): p. 1371-1415.
232. Ye, Z., et al., *Coordinated Modulation of Energy Metabolism and Inflammation by Branched-Chain Amino Acids and Fatty Acids.* Front Endocrinol (Lausanne), 2020. 11: p. 617.
233. Frontera, W.R. and J. Ochala, *Skeletal muscle: a brief review of structure and function.* Calcif Tissue Int, 2015. 96(3): p. 183-95.
234. Friedman, J.E., et al., *Glucose metabolism in incubated human muscle: effect of obesity and non-insulin-dependent diabetes mellitus.* Metabolism, 1994. 43(8): p. 1047-54.
235. Qatanani, M. and M.A. Lazar, *Mechanisms of obesity-associated insulin resistance: many choices on the menu.* Genes Dev, 2007. 21(12): p. 1443-55.
236. Kahn, S.E., R.L. Hull, and K.M. Utzschneider, *Mechanisms linking obesity to insulin resistance and type 2 diabetes.* Nature, 2006. 444(7121): p. 840-6.
237. Markgraf, D.F., H. Al-Hasani, and S. Lehr, *Lipidomics-Reshaping the Analysis and Perception of Type 2 Diabetes.* Int J Mol Sci, 2016. 17(11).
238. Thiébaud, D., et al., *Effect of long chain triglyceride infusion on glucose metabolism in man.* Metabolism, 1982. 31(11): p. 1128-36.
239. Samuel, V.T., K.F. Petersen, and G.I. Shulman, *Lipid-induced insulin resistance: unravelling the mechanism.* Lancet, 2010. 375(9733): p. 2267-77.
240. Krebs, M., et al., *The Mammalian target of rapamycin pathway regulates nutrient-sensitive glucose uptake in man.* Diabetes, 2007. 56(6): p. 1600-7.
241. Tremblay, F., et al., *Overactivation of S6 kinase 1 as a cause of human insulin resistance during increased amino acid availability.* Diabetes, 2005. 54(9): p. 2674-84.
242. Della Torre, S., et al., *Amino acid-dependent activation of liver estrogen receptor alpha integrates metabolic and reproductive functions via IGF-1.* Cell Metab, 2011. 13(2): p. 205-14.
243. Jelenik, T. and M. Roden, *How estrogens prevent from lipid-induced insulin resistance.* Endocrinology, 2013. 154(3): p. 989-92.
244. Markova, M., et al., *Isocaloric Diets High in Animal or Plant Protein Reduce Liver Fat and Inflammation in Individuals With Type 2 Diabetes.* Gastroenterology, 2017. 152(3): p. 571-585.e8.
245. Gall, W.E., et al., *alpha-hydroxybutyrate is an early biomarker of insulin resistance and glucose intolerance in a nondiabetic population.* PLoS One, 2010. 5(5): p. e10883.
246. McGarry, J.D. and D.W. Foster, *Ketogenesis and its regulation.* Am J Med, 1976. 61(1): p. 9-13.
247. Ojha, S., H. Budge, and M. Symonds, *Adipocytes in Normal Tissue Biology*. 2014. p. 2003-2013.
248. Ahima, R.S. and M.A. Lazar, *Adipokines and the peripheral and neural control of energy balance.* Mol Endocrinol, 2008. 22(5): p. 1023-31.
249. Harwood, H.J., Jr., *The adipocyte as an endocrine organ in the regulation of metabolic homeostasis.* Neuropharmacology, 2012. 63(1): p. 57-75.
250. Falcão-Pires, I., et al., *Physiological, pathological and potential therapeutic roles of adipokines.* Drug Discov Today, 2012. 17(15-16): p. 880-9.
251. Burhans, M.S., et al., *Contribution of Adipose Tissue Inflammation to the Development of Type 2 Diabetes Mellitus.* Compr Physiol, 2018. 9(1): p. 1-58.
252. Swarbrick, M.M. and P.J. Havel, *Physiological, pharmacological, and nutritional regulation of circulating adiponectin concentrations in humans.* Metab Syndr Relat Disord, 2008. 6(2): p. 87-102.
253. Rubin, C.-J., et al., *Whole-genome resequencing reveals loci under selection during chicken domestication.* Nature, 2010. 464(7288): p. 587-591.
254. Wang, Y., et al., *Detection of SNPs in the TBC1D1 gene and their association with carcass traits in chicken.* Gene, 2014. 547(2): p. 288-94.
255. Stöckli, J., et al., *The RabGAP TBC1D1 plays a central role in exercise-regulated glucose metabolism in skeletal muscle.* Diabetes, 2015. 64(6): p. 1914-22.
256. Stone, S., et al., *TBC1D1 is a candidate for a severe obesity gene and evidence for a gene/gene interaction in obesity predisposition.* Hum Mol Genet, 2006. 15(18): p. 2709-20.
257. Dash, S., et al., *A truncation mutation in TBC1D4 in a family with acanthosis nigricans and postprandial hyperinsulinemia.* Proc Natl Acad Sci U S A, 2009. 106(23): p. 9350-5.
258. Moltke, I., et al., *A common Greenlandic TBC1D4 variant confers muscle insulin resistance and type 2 diabetes.* Nature, 2014. 512(7513): p. 190-3.

259. Overvad, M., et al., *The effect of diabetes and the common diabetogenic TBC1D4 p.Arg684Ter variant on cardiovascular risk in Inuit in Greenland.* Sci Rep, 2020. 10(1): p. 22081.
260. Schnurr, T.M., et al., *Physical activity attenuates postprandial hyperglycaemia in homozygous TBC1D4 loss-of-function mutation carriers.* Diabetologia, 2021. 64(8): p. 1795-1804.
261. Chadt, A., et al., *Tbc1d1 mutation in lean mouse strain confers leanness and protects from diet-induced obesity.* Nat Genet, 2008. 40(11): p. 1354-9.
262. Lansey, M.N., et al., *Deletion of Rab GAP AS160 modifies glucose uptake and GLUT4 translocation in primary skeletal muscles and adipocytes and impairs glucose homeostasis.* Am J Physiol Endocrinol Metab, 2012. 303(10): p. E1273-86.
263. Paglialunga, S., et al., *The Rab-GTPase activating protein, TBC1D1, is critical for maintaining normal glucose homeostasis and β-cell mass.* Appl Physiol Nutr Metab, 2017. 42(6): p. 647-655.
264. Stermann, T., et al., *Deletion of the RabGAP TBC1D1 Leads to Enhanced Insulin Secretion and Fatty Acid Oxidation in Islets From Male Mice.* Endocrinology, 2018. 159(4): p. 1748-1761.
265. Xie, B., et al., *The Inactivation of RabGAP Function of AS160 Promotes Lysosomal Degradation of GLUT4 and Causes Postprandial Hyperglycemia and Hyperinsulinemia.* Diabetes, 2016. 65(11): p. 3327-3340.
266. Espelage, L., *The mechanisms of exercise-induced improvements in whole-body glycemia in RabGAP-deficient mice (Dissertation).* 2023.
267. Park, S.Y., et al., *Crystal structures of human TBC1D1 and TBC1D4 (AS160) RabGTPase-activating protein (RabGAP) domains reveal critical elements for GLUT4 translocation.* J Biol Chem, 2011. 286(20): p. 18130-8.
268. An, D., et al., *TBC1D1 regulates insulin- and contraction-induced glucose transport in mouse skeletal muscle.* Diabetes, 2010. 59(6): p. 1358-65.
269. Szekeres, F., et al., *The Rab-GTPase-activating protein TBC1D1 regulates skeletal muscle glucose metabolism.* Am J Physiol Endocrinol Metab, 2012. 303(4): p. E524-33.
270. Wang, H.Y., et al., *AS160 deficiency causes whole-body insulin resistance via composite effects in multiple tissues.* Biochem J, 2013. 449(2): p. 479-89.
271. Binsch, C., et al., *Deletion of Tbc1d4/As160 abrogates cardiac glucose uptake and increases myocardial damage after ischemia/reperfusion.* Cardiovasc Diabetol, 2023. 22(1): p. 17.
272. Jensen, T.E., et al., *E MG-normalised kinase activation during exercise is higher in human gastrocnemius compared to soleus muscle.* PLoS One, 2012. 7(2): p. e31054.
273. Bonen, A., M.H. Tan, and W.M. Watson-Wright, *Insulin binding and glucose uptake differences in rodent skeletal muscles.* Diabetes, 1981. 30(8): p. 702-4.
274. James, D.E., A.B. Jenkins, and E.W. Kraegen, *Heterogeneity of insulin action in individual muscles in vivo: euglycemic clamp studies in rats.* Am J Physiol, 1985. 248(5 Pt 1): p. E567-74.
275. Benninghoff, T., et al., *The RabGAPs TBC1D1 and TBC1D4 Control Uptake of Long-Chain Fatty Acids Into Skeletal Muscle via Fatty Acid Transporter SLC27A4/FATP4.* Diabetes, 2020. 69(11): p. 2281-2293.
276. Kane, S., et al., *A method to identify serine kinase substrates. Akt phosphorylates a novel adipocyte protein with a Rab GTPase-activating protein (GAP) domain.* J Biol Chem, 2002. 277(25): p. 22115-8.
277. Zerial, M. and H. McBride, *Rab proteins as membrane organizers.* Nat Rev Mol Cell Biol, 2001. 2(2): p. 107-17.
278. Stein, M.P., J. Dong, and A. Wandinger-Ness, *Rab proteins and endocytic trafficking: potential targets for therapeutic intervention.* Adv Drug Deliv Rev, 2003. 55(11): p. 1421-37.
279. Sano, H., et al., *Rab10, a target of the AS160 Rab GAP, is required for insulin-stimulated translocation of GLUT4 to the adipocyte plasma membrane.* Cell Metab, 2007. 5(4): p. 293-303.
280. Kaddai, V., Y. Le Marchand-Brustel, and M. Cormont, *Rab proteins in endocytosis and Glut4 trafficking.* Acta Physiol (Oxf), 2008. 192(1): p. 75-88.
281. Jiang, Z.Y., et al., *A phosphatidylinositol 3-kinase-independent insulin signaling pathway to N-WASP/Arp2/3/F-actin required for GLUT4 glucose transporter recycling.* J Biol Chem, 2002. 277(1): p. 509-15.
282. Kanzaki, M. and J.E. Pessin, *Insulin-stimulated GLUT4 translocation in adipocytes is dependent upon cortical actin remodeling.* J Biol Chem, 2001. 276(45): p. 42436-44.
283. Brozinick, J.T., Jr., et al., *Disruption of cortical actin in skeletal muscle demonstrates an essential role of the cytoskeleton in glucose transporter 4 translocation in insulin-sensitive tissues.* J Biol Chem, 2004. 279(39): p. 40699-706.
284. Liu, J., et al., *APS facilitates c-Cbl tyrosine phosphorylation and GLUT4 translocation in response to insulin in 3T3-L1 adipocytes.* Mol Cell Biol, 2002. 22(11): p. 3599-609.

285. Chiang, S.H., et al., *Insulin-stimulated GLUT4 translocation requires the CAP-dependent activation of TC10.* Nature, 2001. 410(6831): p. 944-8.
286. Watson, R.T., et al., *Lipid raft microdomain compartmentalization of TC10 is required for insulin signaling and GLUT4 translocation.* J Cell Biol, 2001. 154(4): p. 829-40.
287. Inoue, M., et al., *The exocyst complex is required for targeting of Glut4 to the plasma membrane by insulin.* Nature, 2003. 422(6932): p. 629-33.
288. Brozinick, J.T., Jr., B.A. Berkemeier, and J.S. Elmendorf, *"Actin"g on GLUT4: membrane & cytoskeletal components of insulin action.* Curr Diabetes Rev, 2007. 3(2): p. 111-22.
289. de Wendt, C., et al., *Contraction-Mediated Glucose Transport in Skeletal Muscle Is Regulated by a Framework of AMPK, TBC1D1/4, and Rac1.* Diabetes, 2021. 70(12): p. 2796-2809.
290. Springer, C., *Impact of exercise on glucose homeostasis in different mouse models for impaired insulin sensitivity (Dissertation).* 2019.
291. Andres, R., G. Cader, and K.L. Zierler, *The quantitatively minor role of carbohydrate in oxidative metabolism by skeletal muscle in intact man in the basal state; measurements of oxygen and glucose uptake and carbon dioxide and lactate production in the forearm.* J Clin Invest, 1956. 35(6): p. 671-82.
292. Péronnet, F. and D. Massicotte, *Table of nonprotein respiratory quotient: an update.* Can J Sport Sci, 1991. 16(1): p. 23-9.
293. Mackrell, J.G. and G.D. Cartee, *A novel method to measure glucose uptake and myosin heavy chain isoform expression of single fibers from rat skeletal muscle.* Diabetes, 2012. 61(5): p. 995-1003.
294. Kamburov, A., et al., *ConsensusPathDB: toward a more complete picture of cell biology.* Nucleic Acids Res, 2011. 39(Database issue): p. D712-7.
295. Møller, G., et al., *The role of a traditional and western diet on glucose homeostasis in Greenlandic Inuit carriers and non-carriers of type 2 diabetes variant in the TBC1D4 gene: A protocol for a randomized clinical trial.* Contemp Clin Trials Commun, 2021. 21: p. 100734.
296. Juntunen, K.S., et al., *Postprandial glucose, insulin, and incretin responses to grain products in healthy subjects.* Am J Clin Nutr, 2002. 75(2): p. 254-62.
297. Holst, J.J., et al., *Loss of incretin effect is a specific, important, and early characteristic of type 2 diabetes.* Diabetes Care, 2011. 34 Suppl 2(Suppl 2): p. S251-7.
298. Manousaki, D., et al., *Toward Precision Medicine: TBC1D4 Disruption Is Common Among the Inuit and Leads to Underdiagnosis of Type 2 Diabetes.* Diabetes Care, 2016. 39(11): p. 1889-1895.
299. BARBORKA, C.J., *EPILEPSY IN ADULTS: RESULTS OF TREATMENT BY KETOGENIC DIET IN ONE HUNDRED CASES.* Archives of Neurology & Psychiatry, 1930. 23(5): p. 904-914.
300. Hartman, A.L., et al., *Seizure tests distinguish intermittent fasting from the ketogenic diet.* Epilepsia, 2010. 51(8): p. 1395-402.
301. Hartman, A.L., J.E. Rubenstein, and E.H. Kossoff, *Intermittent fasting: a "new" historical strategy for controlling seizures?* Epilepsy Res, 2013. 104(3): p. 275-9.
302. Zhu, H., et al., *Ketogenic diet for human diseases: the underlying mechanisms and potential for clinical implementations.* Signal Transduct Target Ther, 2022. 7(1): p. 11.
303. Galbreath, M., et al., *Effects of Adherence to a Higher Protein Diet on Weight Loss, Markers of Health, and Functional Capacity in Older Women Participating in a Resistance-Based Exercise Program.* Nutrients, 2018. 10(8).
304. Morell, P. and S. Fiszman, *Revisiting the role of protein-induced satiation and satiety.* Food Hydrocolloids, 2017. 68: p. 199-210.
305. Parker, B., et al., *Effect of a high-protein, high-monounsaturated fat weight loss diet on glycemic control and lipid levels in type 2 diabetes.* Diabetes Care, 2002. 25(3): p. 425-30.
306. Tettamanzi, F., et al., *A High Protein Diet Is More Effective in Improving Insulin Resistance and Glycemic Variability Compared to a Mediterranean Diet-A Cross-Over Controlled Inpatient Dietary Study.* Nutrients, 2021. 13(12).
307. Huffman, K.M., et al., *Relationships between circulating metabolic intermediates and insulin action in overweight to obese, inactive men and women.* Diabetes Care, 2009. 32(9): p. 1678-83.
308. Chen, T., et al., *Branched-chain and aromatic amino acid profiles and diabetes risk in Chinese populations.* Scientific Reports, 2016. 6(1): p. 20594.
309. Knebel, B., et al., *Specific Metabolic Profiles and Their Relationship to Insulin Resistance in Recent-Onset Type 1 and Type 2 Diabetes.* J Clin Endocrinol Metab, 2016. 101(5): p. 2130-40.
310. Yuan, X., et al., *Effect of the ketogenic diet on glycemic control, insulin resistance, and lipid metabolism in patients with T2DM: a systematic review and meta-analysis.* Nutr Diabetes, 2020. 10(1): p. 38.
311. Rusek, M., et al., *Ketogenic Diet in Alzheimer's Disease.* Int J Mol Sci, 2019. 20(16).

312. Crabtree, C.D., et al., *Comparison of Ketogenic Diets with and without Ketone Salts versus a Low-Fat Diet: Liver Fat Responses in Overweight Adults.* Nutrients, 2021. 13(3).
313. Basu, R., W.F. Schwenk, and R.A. Rizza, *Both fasting glucose production and disappearance are abnormal in people with "mild" and "severe" type 2 diabetes.* Am J Physiol Endocrinol Metab, 2004. 287(1): p. E55-62.
314. Firth, R.G., et al., *Postprandial hyperglycemia in patients with noninsulin-dependent diabetes mellitus. Role of hepatic and extrahepatic tissues.* J Clin Invest, 1986. 77(5): p. 1525-32.
315. Basu, R., et al., *Obesity and type 2 diabetes impair insulin-induced suppression of glycogenolysis as well as gluconeogenesis.* Diabetes, 2005. 54(7): p. 1942-8.
316. Sheehan, J.P., *Fasting hyperglycemia: etiology, diagnosis, and treatment.* Diabetes Technol Ther, 2004. 6(4): p. 525-33.
317. Grandl, G., et al., *Short-term feeding of a ketogenic diet induces more severe hepatic insulin resistance than an obesogenic high-fat diet.* J Physiol, 2018. 596(19): p. 4597-4609.
318. Rao, S.S., P. Disraeli, and T. McGregor, *Impaired glucose tolerance and impaired fasting glucose.* Am Fam Physician, 2004. 69(8): p. 1961-8.
319. Bhatt, H.B. and R.J. Smith, *Fatty liver disease in diabetes mellitus.* Hepatobiliary Surg Nutr, 2015. 4(2): p. 101-8.
320. Mikłosz, A., et al., *Does TBC1D4 (AS160) or TBC1D1 Deficiency Affect the Expression of Fatty Acid Handling Proteins in the Adipocytes Differentiated from Human Adipose-Derived Mesenchymal Stem Cells (ADMSCs) Obtained from Subcutaneous and Visceral Fat Depots?* Cells, 2021. 10(6).
321. Mikłosz, A., et al., *RabGAP AS160/TBC1D4 deficiency increases long-chain fatty acid transport but has little additional effect on obesity and metabolic syndrome in ADMSCs-derived adipocytes of morbidly obese women.* Front Mol Biosci, 2023. 10: p. 1232159.
322. Perakakis, N., O.M. Farr, and C.S. Mantzoros, *Leptin in Leanness and Obesity: JACC State-of-the-Art Review.* J Am Coll Cardiol, 2021. 77(6): p. 745-760.
323. Skurk, T., et al., *Relationship between adipocyte size and adipokine expression and secretion.* J Clin Endocrinol Metab, 2007. 92(3): p. 1023-33.
324. Dokas, J., et al., *Tbc1d1 deletion suppresses obesity in leptin-deficient mice.* Int J Obes (Lond), 2016. 40(8): p. 1242-9.
325. Fryk, E., et al., *Hyperinsulinemia and insulin resistance in the obese may develop as part of a homeostatic response to elevated free fatty acids: A mechanistic case-control and a population-based cohort study.* EBioMedicine, 2021. 65: p. 103264.
326. Choi, J.H., et al., *Effects of hyperinsulinemia on lipolytic function of three-dimensional adipocyte/endothelial co-cultures.* Tissue Eng Part C Methods, 2010. 16(5): p. 1157-65.
327. Hargett, S.R., et al., *Deletion of the Rab GAP Tbc1d1 modifies glucose, lipid, and energy homeostasis in mice.* Am J Physiol Endocrinol Metab, 2015. 309(3): p. E233-45.
328. Laffel, L., *Ketone bodies: a review of physiology, pathophysiology and application of monitoring to diabetes.* Diabetes Metab Res Rev, 1999. 15(6): p. 412-26.
329. Veneti, S., et al., *Ketone Bodies in Diabetes Mellitus: Friend or Foe?* Nutrients, 2023. 15(20).
330. Karpe, F., J.R. Dickmann, and K.N. Frayn, *Fatty acids, obesity, and insulin resistance: time for a reevaluation.* Diabetes, 2011. 60(10): p. 2441-9.
331. Gannon, M.C. and F.Q. Nuttall, *Effect of a high-protein, low-carbohydrate diet on blood glucose control in people with type 2 diabetes.* Diabetes, 2004. 53(9): p. 2375-82.
332. Sargrad, K.R., et al., *Effect of high protein vs high carbohydrate intake on insulin sensitivity, body weight, hemoglobin A1c, and blood pressure in patients with type 2 diabetes mellitus.* J Am Diet Assoc, 2005. 105(4): p. 573-80.
333. Kimura, Y., N. Kimura, and M. Akazawa, *Nutrition-related risk and severe hypoglycemia in older adult outpatients with and without diabetes.* Clin Case Rep, 2022. 10(1): p. e05317.
334. Wilson, V., *Non-diabetic hypoglycaemia: causes and pathophysiology.* Nurs Stand, 2011. 25(46): p. 35-9.
335. Chiang, P.M., et al., *Deletion of TDP-43 down-regulates Tbc1d1, a gene linked to obesity, and alters body fat metabolism.* Proc Natl Acad Sci U S A, 2010. 107(37): p. 16320-4.
336. Chadt, A. and H. Al-Hasani, *Glucose transporters in adipose tissue, liver, and skeletal muscle in metabolic health and disease.* Pflugers Arch, 2020. 472(9): p. 1273-1298.
337. Kotani, K., et al., *GLUT4 glucose transporter deficiency increases hepatic lipid production and peripheral lipid utilization.* J Clin Invest, 2004. 114(11): p. 1666-75.

338. Chavez, J.A., et al., *Inhibition of GLUT4 translocation by Tbc1d1, a Rab GTPase-activating protein abundant in skeletal muscle, is partially relieved by AMP-activated protein kinase activation.* J Biol Chem, 2008. 283(14): p. 9187-95.
339. Salans, L.B., J.L. Knittle, and J. Hirsch, *The role of adipose cell size and adipose tissue insulin sensitivity in the carbohydrate intolerance of human obesity.* J Clin Invest, 1968. 47(1): p. 153-65.
340. Franck, N., et al., *Insulin-induced GLUT4 translocation to the plasma membrane is blunted in large compared with small primary fat cells isolated from the same individual.* Diabetologia, 2007. 50(8): p. 1716-22.
341. Bonora, E., et al., *Plasma glucose levels throughout the day and HbA(1c) interrelationships in type 2 diabetes: implications for treatment and monitoring of metabolic control.* Diabetes Care, 2001. 24(12): p. 2023-9.
342. Blaak, E.E., et al., *Impact of postprandial glycaemia on health and prevention of disease.* Obes Rev, 2012. 13(10): p. 923-84.
343. Gannon, M.C., et al., *An increase in dietary protein improves the blood glucose response in persons with type 2 diabetes.* Am J Clin Nutr, 2003. 78(4): p. 734-41.
344. Blázquez, R. and C. López Quijada, *The effect of a high-protein diet on plasma glucose concentration, insulin sensitivity and plasma insulin in rats.* J Endocrinol, 1970. 46(4): p. 445-51.
345. Siegel, E.G., et al., *Beneficial effects of low-carbohydrate-high-protein diets in long-term diabetic rats.* Metabolism, 1980. 29(5): p. 421-428.
346. Ancu, O., et al., *Does high dietary protein intake contribute to the increased risk of developing prediabetes and type 2 diabetes?* 2021. 46(1): p. 1-9.
347. Pasiakos, S.M., et al., *Effects of high-protein diets on fat-free mass and muscle protein synthesis following weight loss: a randomized controlled trial.* Faseb j, 2013. 27(9): p. 3837-47.
348. Sakamoto, K. and G.D. Holman, *Emerging role for AS160/TBC1D4 and TBC1D1 in the regulation of GLUT4 traffic.* Am J Physiol Endocrinol Metab, 2008. 295(1): p. E29-37.
349. Stuart, C.A., et al., *Insulin-stimulated translocation of glucose transporter (GLUT) 12 parallels that of GLUT4 in normal muscle.* J Clin Endocrinol Metab, 2009. 94(9): p. 3535-42.
350. Purcell, S.H., et al., *Improved insulin sensitivity by GLUT12 overexpression in mice.* Diabetes, 2011. 60(5): p. 1478-82.
351. Fam, B.C., et al., *Normal muscle glucose uptake in mice deficient in muscle GLUT4.* J Endocrinol, 2012. 214(3): p. 313-27.
352. Matsuo, S., M. Hiasa, and H. Omote, *Functional characterization and tissue localization of the facilitative glucose transporter GLUT12.* J Biochem, 2020. 168(6): p. 611-620.
353. Nagarajan, S.R., et al., *Insulin and diet-induced changes in the ubiquitin-modified proteome of rat liver.* PLoS One, 2017. 12(3): p. e0174431.
354. Zhang, Y., et al., *Amelioration of hepatic steatosis by dietary essential amino acid-induced ubiquitination.* Mol Cell, 2022. 82(8): p. 1528-1542.e10.
355. Hicke, L. and H. Riezman, *Ubiquitination of a yeast plasma membrane receptor signals its ligand-stimulated endocytosis.* Cell, 1996. 84(2): p. 277-87.
356. Kölling, R. and C.P. Hollenberg, *The ABC-transporter Ste6 accumulates in the plasma membrane in a ubiquitinated form in endocytosis mutants.* Embo j, 1994. 13(14): p. 3261-71.
357. Duan, L., et al., *Cbl-mediated ubiquitinylation is required for lysosomal sorting of epidermal growth factor receptor but is dispensable for endocytosis.* J Biol Chem, 2003. 278(31): p. 28950-60.
358. Berthouze, M., et al., *The deubiquitinases USP33 and USP20 coordinate beta2 adrenergic receptor recycling and resensitization.* Embo j, 2009. 28(12): p. 1684-96.
359. Lamb, C.A., et al., *Insulin-regulated trafficking of GLUT4 requires ubiquitination.* Traffic, 2010. 11(11): p. 1445-54.
360. Sadler, J.B.A., et al., *The deubiquitinating enzyme USP25 binds tankyrase and regulates trafficking of the facilitative glucose transporter GLUT4 in adipocytes.* Sci Rep, 2019. 9(1): p. 4710.
361. Bogan, J.S., *Ubiquitin-like processing of TUG proteins as a mechanism to regulate glucose uptake and energy metabolism in fat and muscle.* Front Endocrinol (Lausanne), 2022. 13: p. 1019405.
362. Belman, J.P., E.N. Habtemichael, and J.S. Bogan, *A proteolytic pathway that controls glucose uptake in fat and muscle.* Rev Endocr Metab Disord, 2014. 15(1): p. 55-66.
363. Koumanov, F., et al., *GLUT4 traffic through an ESCRT-III-dependent sorting compartment in adipocytes.* PLoS One, 2012. 7(9): p. e44141.
364. Komander, D., M.J. Clague, and S. Urbé, *Breaking the chains: structure and function of the deubiquitinases.* Nat Rev Mol Cell Biol, 2009. 10(8): p. 550-63.
365. Capitani, N. and C.T. Baldari, *F-Actin Dynamics in the Regulation of Endosomal Recycling and Immune Synapse Assembly.* Front Cell Dev Biol, 2021. 9: p. 670882.

366. Andrés-Delgado, L., et al., *Formin INF2 regulates MAL-mediated transport of Lck to the plasma membrane of human T lymphocytes.* Blood, 2010. 116(26): p. 5919-29.
367. Antón, O.M., et al., *MAL protein controls protein sorting at the supramolecular activation cluster of human T lymphocytes.* J Immunol, 2011. 186(11): p. 6345-56.
368. Madrid, R., et al., *The formin INF2 regulates basolateral-to-apical transcytosis and lumen formation in association with Cdc42 and MAL2.* Dev Cell, 2010. 18(5): p. 814-27.
369. Sun, H., et al., *Dysregulated Dynein-Mediated Trafficking of Nephrin Causes INF2-related Podocytopathy.* J Am Soc Nephrol, 2021. 32(2): p. 307-322.
370. Rietman, A., et al., *High dietary protein intake, reducing or eliciting insulin resistance?* Eur J Clin Nutr, 2014. 68(9): p. 973-9.
371. Yang, X., et al., *Tissue-Specific Splicing and Dietary Interaction of a Mutant As160 Allele Determine Muscle Metabolic Fitness in Rodents.* Diabetes, 2021. 70(8): p. 1826-1842.
372. Daly, M.E., et al., *Acute effects on insulin sensitivity and diurnal metabolic profiles of a high-sucrose compared with a high-starch diet.* Am J Clin Nutr, 1998. 67(6): p. 1186-96.
373. Brandon, A.E., et al., *Insulin sensitivity is preserved in mice made obese by feeding a high starch diet.* Elife, 2022. 11.
374. Prada, P.O., et al., *Western diet modulates insulin signaling, c-Jun N-terminal kinase activity, and insulin receptor substrate-1ser307 phosphorylation in a tissue-specific fashion.* Endocrinology, 2005. 146(3): p. 1576-87.
375. Westman, E.C., et al., *Low-carbohydrate nutrition and metabolism.* Am J Clin Nutr, 2007. 86(2): p. 276-84.
376. Lewis, J.I., et al., *The effect of traditional diet on glucose homoeostasis in carriers and non-carriers of a common TBC1D4 variant in Greenlandic Inuit: a randomised crossover study.* Br J Nutr, 2023. 130(11): p. 1-14.
377. Park, S., et al., *A ketogenic diet impairs energy and glucose homeostasis by the attenuation of hypothalamic leptin signaling and hepatic insulin signaling in a rat model of non-obese type 2 diabetes.* Exp Biol Med (Maywood), 2011. 236(2): p. 194-204.
378. Gabbia, D., et al., *Western Diet-Induced Metabolic Alterations Affect Circulating Markers of Liver Function before the Development of Steatosis.* Nutrients, 2019. 11(7).
379. Akki, A. and A.M. Seymour, *Western diet impairs metabolic remodelling and contractile efficiency in cardiac hypertrophy.* Cardiovasc Res, 2009. 81(3): p. 610-7.
380. Heo, J., et al., *Differential effects of Western diet and traumatic muscle injury on skeletal muscle metabolic regulation in male and female mice.* J Cachexia Sarcopenia Muscle, 2023. 14(6): p. 2835-2850.
381. Norouzi, S., et al., *Zinc transporters and insulin resistance: therapeutic implications for type 2 diabetes and metabolic disease.* J Biomed Sci, 2017. 24(1): p. 87.
382. Kadota, Y., et al., *Metallothioneins regulate the adipogenic differentiation of 3T3-L1 cells via the insulin signaling pathway.* PLoS One, 2017. 12(4): p. e0176070.
383. Szrok, S., et al., *Metallothioneins 1 and 2, but not 3, are regulated by nutritional status in rat white adipose tissue.* Genes Nutr, 2016. 11: p. 18.
384. Wiesner, C., K. El Azzouzi, and S. Linder, *A specific subset of RabGTPases controls cell surface exposure of MT1-MMP, extracellular matrix degradation and three-dimensional invasion of macrophages.* J Cell Sci, 2013. 126(Pt 13): p. 2820-33.
385. Bravo-Cordero, J.J., et al., *MT1-MMP proinvasive activity is regulated by a novel Rab8-dependent exocytic pathway.* Embo j, 2007. 26(6): p. 1499-510.
386. Graf, U., E.A. Casanova, and P. Cinelli, *The Role of the Leukemia Inhibitory Factor (LIF)–Pathway in Derivation and Maintenance of Murine Pluripotent Stem Cells.* Genes (Basel), 2011. 2(1): p. 280-97.

7. Supplement

7.1 Contribution to manuscripts

1. De Wendt C, Espelage L, Eickelschulte S, Springer C, Toska L, **Scheel A**, Bedou Awovi Didi, Benninghoff T, Cames S, Stermann T, Chadt A, Al-Hasani H (2021). Contraction-Mediated Glucose Transport in Skeletal Muscle Is Regulated by a Framework of AMPK, TBC1D1/4, and Rac1. Diabetes. doi: 10.2337/db21-0587

   Contribution: I was involved in the interpretation of the data.

2. **Scheel AK**, Espelage L, Chadt A (2022). Many Ways to Rome: Exercise, Cold Exposure and Diet-Do They All Affect BAT Activation and WAT Browning in the Same Manner? International journal of molecular sciences. doi: 10.3390/ijms23094759

   Contribution: I wrote the review.

Parts of this thesis are planned to be published in a separate paper. The manuscript is currently in preparation.

3. **Scheel AK**, Binsch C, Pirseyedi S, Espelage L, Springer C, de Wendt C, Knobloch B, Jeruschke K, Weidlich C, Hartwig S, Lehr S, Al-Hasani H, Chadt A. Carbohydrate restriction overcomes genetic skeletal muscle insulin resistance in *Tbc1d4* null mice (in preparation)

7.2 Abbreviations

AA	Amino acid
Acetyl-CoA	Acetyl coenzyme A
aD4KO	adipocyte-specific *Tbc1d4*-deficient mouse
AICAR	5-Aminoimidazole-4-carboxamide ribonucleotide
AMPK	AMP-activated protein kinase
APS	Ammonium persulfate
AS160	Akt substrate of 160 kDa
ATP	Adenosine triphosphate
ATT	AICAR tolerance test
AUC	Area under the curve
BAT	Brown adipose tissue
BCA	Bicinchonic acid assay
BCAA	Branched-chain amino acid
Bp	Base pair
BSA	Bovine serum albumin
CHO	Carbohydrate oxidation
CON	control diet
CPDB	ConsensusPathDB
Cpm	Counts per minute
D1KO	*Tbc1d1*-deficient mouse
D4KO	*Tbc1d4*-deficient mouse
D1/4KO	*Tbc1d1*- *Tbc1d4*-deficient mouse
DNL	*de novo* lipogenesis
dNTP	Deoxynucleoside triphosphate
DUB	deubiquitinating enzyme
EDTA	Ethylenediaminetetraacetic acid
EGTA	Ethylene glycol bis (2-aminoethylether)-N, N, N’, N’-tetra acetic acid

EtOH	Ethanol
eWAT	epididymal WAT
FADH2	Flavin adenine dinucleotide
FABPpm	Fatty acid-binding protein
FAO	Fatty acid oxidation
FAT/CD36	Fatty acid translocase
FATP1	Fatty acid transporter protein 1
FATP4	Fatty acid transporter protein 4
FA	Fatty acid
FFA	Free fatty acids
G1P	Glucose-1-phosphate
G6P	Glucose-6-phosphate
GAP	GTPase activating protein
GAPDH	Glyceraldehyde 3-phosphate dehydrogenase
GEF	Guanine nucleotide exchange factor
GIP	Glucose-dependent insulinotropic polypeptide
GLP-1	Glucagon-like peptide-1
GLUT4	Glucose transporter type 4
GSV	GLUT4 containing storage vesicle
GTT	Glucose tolerance test
HCLP	high-carbohydrate low-protein
HEPES	4-(2-hydroxyethyl)-1-piperazineethanesulfonic acid
HRP	horseradish-peroxidase
HSA	Human-skeletal actin
IL	Interleukin
IMCL	Intramyocellular lipids
Inf2	Inverted formin 2
I.p.	Intraperitoneal
IR	Insulin receptor

IRS	Insulin receptor substrate
ITT	Insulin tolerance test
KB	Ketone bodies
KD	ketogenic diet
KHB	Krebs-Henseleit buffer
KO	Knockout
KRBH	Krebs-Ringer-Bicarbonate HEPES buffer
LCFA	Long-chain fatty acids
LCHP	low-carbohydrate high-protein
mD4KO	Muscle-specific *Tbc1d4*-deficient mouse
Mt	Metallothionein
NADH	Nicotinamide adenine dinucleotide
NEFA	Non-esterified free fatty acids
NMR	Nuclear magnetic resonance
PAI-1	Plasminogen activator inhibitor-1
PCR	Polymerase chain reaction
PDH	Pyruvate dehydrogenase
PI3K	Phosphatidylinositol-3'-kinase
PIP3	Phosphatidylinositol (3,4,5)-trisphosphate
PPAR	Peroxisome proliferator-activated receptor
PTB	Phosphotyrosine binding domain
Rab	Ras related in brain
RabGAP	GTPase-activating protein
RER	Respiratory exchange ratio
scWAT	Subcutaneous white adipose tissue
SDS	Sodium dodecyl sulfate
SEM	Standard error of the mean
T1DM	Type 1 diabetes mellitus
T2DM	Type 2 diabetes mellitus

TCA	tricarboxylic acid
TEMED	N, N, N', N'-Tetramethylendiamine
TGN	Trans-Golgi-Network
TUG	Tether, containing a UBX domain, for GLUT4
Ub	Ubiquitin
UCP1	Uncoupling protein 1
UDP	Uridine diphoshate
Usp	ubiquitin specific peptidase
visWAT	Visceral white adipose tissue
WAT	White adipose tissue
WHO	World Health Organization
WT	Wildtype

7.3 Supplemental figures

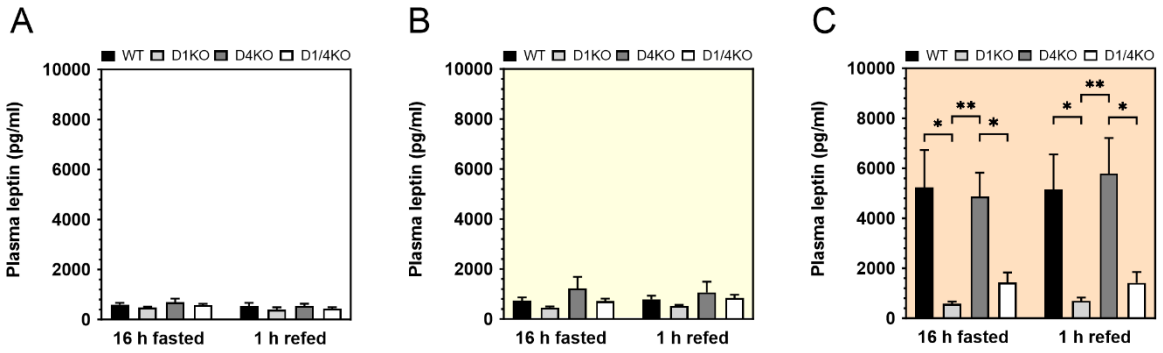

Supplemental figure 1: Impact of dietary macronutrient ratios on postprandial incretin concentrations of RabGAP-deficient mice. Determination of 16 h fasted and postprandial plasma leptin concentrations from *Tbc1d1*- (D1KO), *Tbc1d4*- (D4KO) and *Tbc1d1/4*-deficient (D1/4KO) mice and WT littermates aged 16–17 weeks subjected to a CON (A), HCLP (B) or LCHP (C) diet. Data are presented as mean ± SEM (n = 5-8). *p < 0.05, **p < 0.01, WT vs. D1KO, D4KO, D1/4KO (Two-way ANOVA).

7.4 Supplemental tables

Supplemental table 1: Differentially regulated proteins in *Gastrocnemius* muscle of D4KO vs. WT mice on HCLP diet and LCHP diets

Gene symbol	Adjusted p-value	log2 fold change	Gene symbol	Adjusted p-value	log2 fold change
HCLP D4KO vs. WT			*LCHP D4KO vs. WT*		
Ythdc2	2.63719E-16	6.64	Sfn	2.47822E-16	-6.64
Nt5c3b	2.63719E-16	-6.64	Dph2	2.47822E-16	-6.64
Them4	2.63719E-16	2.27	Acbd5	2.47822E-16	6.64
Retsat	2.63719E-16	-6.64	Ces2c	2.47822E-16	-6.64
Adh7	2.63719E-16	-6.64	Alpk2	2.47822E-16	-6.64
Txlna	2.63719E-16	-6.64	Asb12	2.47822E-16	-6.64
Asb12	2.63719E-16	-6.64	Ankrd40	2.47822E-16	6.64
Apom	2.63719E-16	6.64	Apom	2.47822E-16	6.64
Nat1	2.63719E-16	6.64	Glb1	2.47822E-16	-6.64
Bet1	2.63719E-16	-6.64	Borcs5	2.47822E-16	-6.64
Glb1	2.63719E-16	-6.64	Calhm5	2.47822E-16	-6.64
Abcb11	2.63719E-16	-6.64	Calm4	2.47822E-16	6.64
Borcs5	2.63719E-16	-6.64	Slc7a2	2.47822E-16	6.64
Borcs6	2.63719E-16	-6.64	Cnot11	2.47822E-16	6.64
Clec10a	2.63719E-16	-6.64	Cd2bp2	2.47822E-16	6.64
Micu2	2.63719E-16	-6.64	Cd59a	2.47822E-16	-6.64
Pde4d	2.63719E-16	6.64	Cd99l2	2.47822E-16	6.64
Ceacam1	2.63719E-16	6.64	Cemip2	2.47822E-16	6.64
Ctnna3	2.63719E-16	-6.64	Cers2	2.47822E-16	6.64
Cnot10	2.63719E-16	6.64	Cntf	2.47822E-16	-6.64
Cd59a	2.63719E-16	6.64	Cstf2t	2.47822E-16	6.64
Cemip2	2.63719E-16	-6.64	F13b	2.47822E-16	6.64
Zw10	2.63719E-16	-6.64	Crtc2	2.47822E-16	6.64
Cntf	2.63719E-16	6.64	Tmem63b	2.47822E-16	6.64
Cpsf1	2.63719E-16	-6.64	Nubp1	2.47822E-16	-6.64
Cstf2t	2.63719E-16	6.64	Dera	2.47822E-16	6.64
Ccdc12	2.63719E-16	6.64	Dnmt3b	2.47822E-16	-3.33
Cpne2	2.63719E-16	-6.64	Polr2d	2.47822E-16	-6.64
Cuedc1	2.63719E-16	1.35	Dnajc1	2.47822E-16	6.64
Cox6a1	2.63719E-16	-2.54	Dusp26	2.47822E-16	6.64
Cyp20a1	2.63719E-16	6.64	Ltn1	2.47822E-16	6.64
Agbl1	2.63719E-16	6.64	Entpd4	2.47822E-16	6.64
Nubp1	2.63719E-16	6.64	Enpp3	2.47822E-16	-6.64
Bdh2	2.63719E-16	-6.64	Efhd1	2.47822E-16	-1.57
Dera	2.63719E-16	-6.64	Ehbp1	2.47822E-16	-6.64
Polb	2.63719E-16	6.64	Elp2	2.47822E-16	-6.64
Polr2a	2.63719E-16	6.64	Emcn	2.47822E-16	6.64
Dnajc1	2.63719E-16	6.64	Ergic2	2.47822E-16	6.64
Dnajc24	2.63719E-16	-6.64	Ece1	2.47822E-16	-6.64
Dnajc30	2.63719E-16	6.64	Kdelr1	2.47822E-16	-6.64
Dolk	2.63719E-16	6.64	Eif4e2	2.47822E-16	6.64
Dctn5	2.63719E-16	6.64	Eif4ebp2	2.47822E-16	6.64
Itch	2.63719E-16	-6.64	Ecm1	2.47822E-16	6.64
Znf598	2.63719E-16	-6.64	Supt16h	2.47822E-16	-6.64
Efhd1	2.63719E-16	6.64	Far1	2.47822E-16	-6.64
Ehbp1	2.63719E-16	-6.64	Fhip1a	2.47822E-16	6.64
Elp2	2.63719E-16	-6.64	Ptk2	2.47822E-16	6.64
Ergic2	2.63719E-16	6.64	Gprc5c	2.47822E-16	-6.64
Kdelr1	2.63719E-16	-6.64	Pofut1	2.47822E-16	-6.64

Akr1c6	2.63719E-16	6.64	Ghdc	2.47822E-16	6.64
Fcho2	2.63719E-16	-6.64	Gnpda2	2.47822E-16	6.64
Flg2	2.63719E-16	-6.64	Glipr2	2.47822E-16	6.64
Ptk2	2.63719E-16	6.64	Grb10	2.47822E-16	6.64
Fbp1	2.63719E-16	6.64	Gtpbp4	2.47822E-16	-6.64
Pofut1	2.63719E-16	-6.64	H2-K1	2.47822E-16	-6.64
Gnpnat1	2.63719E-16	-6.64	Tsc1	2.47822E-16	6.64
Grb10	2.63719E-16	6.64	Hbb-y	2.47822E-16	1.31
Gtpbp4	2.63719E-16	-6.64	H mgn5	2.47822E-16	6.64
H2-K1	2.63719E-16	6.64	H mgb3	2.47822E-16	6.64
H1-2	2.63719E-16	-1.1	H mga1	2.47822E-16	6.64
Htt	2.63719E-16	-6.64	H2ac7	2.47822E-16	-6.64
	2.63719E-16	-6.64	H2bc21	2.47822E-16	6.64
	2.63719E-16	-6.64	Htt	2.47822E-16	-6.64
	2.63719E-16	-1.45	Ighv3-6	2.47822E-16	-6.64
Ighm	2.63719E-16	-1.18	Ig heavy chain V region 5-84	2.47822E-16	-6.64
Igkv9-120	2.63719E-16	6.64	Igkv9-120	2.47822E-16	-6.64
Inf2	2.63719E-16	-2.44	Itpr1	2.47822E-16	-6.64
Mff	2.63719E-16	6.64	Gpr180	2.47822E-16	6.64
Syne1	2.63719E-16	6.64	Inf2	2.47822E-16	2.42
Nrip2	2.63719E-16	-6.64	Kcnj2	2.47822E-16	-6.64
Pnkd	2.63719E-16	6.64	Syne1	2.47822E-16	-6.64
Lyn	2.63719E-16	-1.57	Tmub1	2.47822E-16	-2.77
Rap1gds1	2.63719E-16	6.64	Ubqln1	2.47822E-16	6.64
Fbln1	2.63719E-16	-6.64	Rap1gds1	2.47822E-16	-6.64
Katnb1	2.63719E-16	6.64	Usp15	2.47822E-16	0.96
Krt19	2.63719E-16	3.8	Gnao1	2.47822E-16	6.64
Krt84	2.63719E-16	-6.64	Fbln1	2.47822E-16	-6.64
Krt5	2.63719E-16	-6.64	Katnb1	2.47822E-16	6.64
Lgmn	2.63719E-16	6.64	Krt10	2.47822E-16	-6.64
Lrrc14	2.63719E-16	6.64	Krt4	2.47822E-16	6.64
Mtrr	2.63719E-16	-6.64	Krtap19-5	2.47822E-16	6.64
Mief1	2.63719E-16	6.64	Dcxr	2.47822E-16	6.64
Timm21	2.63719E-16	-6.64	Leprotl1	2.47822E-16	6.64
Immp1l	2.63719E-16	6.64	Clptm1l	2.47822E-16	-6.64
Map3k4	2.63719E-16	-6.64	Lmbrd1	2.47822E-16	6.64
Mad1l1	2.63719E-16	-6.64	Mtrr	2.47822E-16	6.64
Morf4l1	2.63719E-16	-6.64	Timm21	2.47822E-16	-6.64
Nelfb	2.63719E-16	-6.64	Mad1l1	2.47822E-16	-6.64
Nfyc	2.63719E-16	6.64	Rae1	2.47822E-16	-6.64
Nop9	2.63719E-16	-6.64	Myl7	2.47822E-16	6.64
Nup37	2.63719E-16	-6.64	Naa38	2.47822E-16	6.64
Otc	2.63719E-16	6.64	Sirt4	2.47822E-16	-6.64
Osbpl2	2.63719E-16	-6.64	Nup107	2.47822E-16	-6.64
Pi16	2.63719E-16	-6.64	Nop9	2.47822E-16	-6.64
Mtrf1	2.63719E-16	-6.64	Nup37	2.47822E-16	6.64
Ppig	2.63719E-16	6.64	Nrm	2.47822E-16	-6.64
Pik3cb	2.63719E-16	-6.64	Otc	2.47822E-16	-6.64
Gp1bb	2.63719E-16	-6.64	Ppig	2.47822E-16	6.64
Bcas2	2.63719E-16	6.64	Pik3cb	2.47822E-16	-2.01
Egf	2.63719E-16	-6.64	Pik3r4	2.47822E-16	6.64
Ddx20	2.63719E-16	6.64	Pla2g15	2.47822E-16	6.64
Grn	2.63719E-16	-6.64	Pfas	2.47822E-16	-6.64
Ptgis	2.63719E-16	6.64	Piezo1	2.47822E-16	6.64
Efr3a	2.63719E-16	-6.64	Gp1bb	2.47822E-16	6.64
Fam3c	2.63719E-16	6.64	Gp5	2.47822E-16	6.64
Ltv1	2.63719E-16	6.64	Il16	2.47822E-16	6.64
Mtss2	2.63719E-16	6.64	Protein C18orf25 homolog	2.47822E-16	6.64

Ntan1	2.63719E-16	-6.64	Dr1	2.47822E-16	-6.64
S100a14	2.63719E-16	-6.64	Efr3a	2.47822E-16	6.64
S100a16	2.63719E-16	6.64	Fam241b	2.47822E-16	-6.64
Son	2.63719E-16	-6.64	Mtss2	2.47822E-16	-6.64
Tgm1	2.63719E-16	-6.64	Ntan1	2.47822E-16	6.64
Dhx57	2.63719E-16	-6.64	Ppp1r14a	2.47822E-16	6.64
Pyroxd1	2.63719E-16	-6.64	Pof1b	2.47822E-16	6.64
Reps1	2.63719E-16	6.64	Icmt	2.47822E-16	6.64
Rab3d	2.63719E-16	-6.64	Pyroxd1	2.47822E-16	6.64
Rcc1l	2.63719E-16	6.64	Lamtor4	2.47822E-16	-6.64
Retn	2.63719E-16	6.64	Reps1	2.47822E-16	6.64
Arhgap18	2.63719E-16	-6.64	Retn	2.47822E-16	6.64
Wdr12	2.63719E-16	6.64	Arhgap18	2.47822E-16	-6.64
Rrn3	2.63719E-16	-6.64	Rrm2b	2.47822E-16	-6.64
Rpap3	2.63719E-16	6.64	Ctr9	2.47822E-16	6.64
Ctr9	2.63719E-16	6.64	Rbpms	2.47822E-16	6.64
Rbpms	2.63719E-16	-6.64	Slc25a26	2.47822E-16	-6.64
Slc25a26	2.63719E-16	-6.64	Htra4	2.47822E-16	6.64
Sltm	2.63719E-16	-6.64	Ccser2	2.47822E-16	6.64
Serinc1	2.63719E-16	6.64	Stk25	2.47822E-16	6.64
Ccser2	2.63719E-16	-6.64	Ulk3	2.47822E-16	6.64
Cdc42bpb	2.63719E-16	-6.64	Sfxn1	2.47822E-16	6.64
Nek3	2.63719E-16	6.64	Slc25a36	2.47822E-16	6.64
Ulk3	2.63719E-16	6.64	Sort1	2.47822E-16	6.64
Sfxn1	2.63719E-16	6.64	Snx21	2.47822E-16	6.64
Snx21	2.63719E-16	-6.64	Ston2	2.47822E-16	-6.64
Ston2	2.63719E-16	-6.64	Smap1	2.47822E-16	6.64
Stx18	2.63719E-16	6.64	Smchd1	2.47822E-16	6.64
Stxbp5	2.63719E-16	6.64	TCAIM	2.47822E-16	-6.64
Tbc1d7	2.63719E-16	6.64	Tpk1	2.47822E-16	6.64
Tbc1d9	2.63719E-16	-6.64	Serpina7	2.47822E-16	6.64
Traf6	2.63719E-16	-6.64	Traf6	2.47822E-16	6.64
Rela	2.63719E-16	-6.64	Tead1	2.47822E-16	6.64
Tmem245	2.63719E-16	6.64	Tra2a	2.47822E-16	6.64
TremL1	2.63719E-16	-6.64	Tspo	2.47822E-16	-6.64
Tnnt1	2.63719E-16	-6.64	TremL1	2.47822E-16	6.64
Tradd	2.63719E-16	-6.64	Ptpn23	2.47822E-16	6.64
Sart1	2.63719E-16	6.64	Atg12	2.47822E-16	6.64
Atg12	2.63719E-16	-6.64	Uncharacterized protein C15orf61 homolog	2.47822E-16	-6.64
Myo1e	2.63719E-16	6.64	Uncharacterized protein CXorf38 homolog	2.47822E-16	-6.64
Vps53	2.63719E-16	6.64	Myo1e	2.47822E-16	6.64
Proz	2.63719E-16	-6.64	Xpnpep2	2.47822E-16	6.64
Wipi1	2.63719E-16	6.64	Zbtb20	2.47822E-16	6.64
Xpnpep2	2.63719E-16	6.64	Comp	2.57778E-12	-0.61
Zbtb20	2.63719E-16	6.64	Adam17	2.84804E-11	1.32
Hck	2.68622E-13	-1.97	S100a8	4.30421E-11	1.63
Gemin5	3.70231E-13	-1.91	Saysd1	3.15077E-10	-1.24
Fbxl4	7.4362E-13	-1.2	Ighm	4.10893E-10	-0.57
Col6a6	1.77072E-12	-0.68	Bdh1	8.37845E-10	-0.68
Tmem230	3.15735E-12	-1.11	Myoc	3.85504E-09	-0.58
Adam17	4.20582E-12	-1.11	Ube2d3	1.1152E-08	0.72
N6amt1	4.6606E-12	-0.99	Cdc26	1.92089E-08	2.21
Gabpa	4.59718E-11	1.02	Rps6ka5	2.49664E-08	-1.44
Pdk4	7.89647E-11	0.71	Igfn1	3.93759E-08	-1.05
Fasn	2.37264E-10	-0.71	Ig kappa chain V-III region CBPC 101	5.32981E-08	1.38

Nmrk2	4.82184E-10	-0.72	Tbc1d4	6.26627E-08	-1.29
Krt81	1.20989E-09	-0.59	Ig gamma-2A chain C region	1.71586E-07	-0.52
Gbp6	3.19053E-09	1.53	Zfand1	1.90965E-07	0.51
Tspan9	4.38011E-09	-1.18	S100a14	2.01732E-07	2.01
Glul	1.70136E-08	-0.64	Zw10	9.3924E-07	-0.78
Serpina1e	1.73187E-08	-0.55	Chkb	2.0088E-06	0.99
Ranbp9	2.37653E-08	1.68	Hbb-b2	3.3687E-06	-0.48
Smox	4.24329E-08	-0.62	Proz	1.27546E-05	1.01
Stbd1	1.73051E-07	-0.51	H1-2	1.60144E-05	-0.5
Fabp1	1.7621E-07	1.53	Ptrhd1	1.60229E-05	-0.69
Jchain	2.11426E-07	-0.89	Ldhb	2.66237E-05	-0.48
Hsd17b11	2.62093E-07	-0.73	Washc4	3.06361E-05	0.88
Antkmt	2.95645E-07	-1.4	Fam98a	4.72431E-05	0.75
Fgb	3.02973E-07	-0.48	Kyat3	4.86802E-05	-0.39
Pof1b	3.43444E-07	-1.43	Ig gamma-3 chain C region	5.23739E-05	0.36
Cnn2	3.62187E-07	-0.91	Rela	5.45927E-05	-1.17
Cbr2	3.81962E-07	-0.53	Oxct1	6.39342E-05	-0.46
Usp8	5.90805E-07	-1.37	Smad2	6.42443E-05	-0.94
Smad2	6.52999E-07	-1.22	Nisch	0.000105406	1.22
Tbc1d4	1.69533E-06	-0.9	Thg1l	0.000117995	-1.6
Helb	1.84666E-06	1.85	Kera	0.000129075	-0.38
Ech1	2.0541E-06	0.55	Fga	0.000139229	0.37
Cfd	2.09275E-06	-0.6	Gabpa	0.000147142	0.57
Krt2	2.20415E-06	-1.57	Rpap3	0.000173239	-1.49
Ces1d	2.43277E-06	-0.44	Cntn4	0.000222274	-1.44
Aldoc	2.50435E-06	-0.63	Angptl7	0.000249091	-0.79
Dsp	3.49827E-06	-0.47	Ppp1r12c	0.000279378	-0.63
Amd2	6.14094E-06	-0.45	C1ra	0.000283886	1.29
Rsc1a1	6.63968E-06	1.23	Ndufab1	0.000470477	0.31
Nudt13	8.74224E-06	1.09	Vps37a	0.000488345	-1.02
Acaca	9.29749E-06	1.07	Tnc	0.000527025	-0.39
Pex10	9.39421E-06	-0.96	Abcd4	0.000528851	1.14
Krt31	1.51406E-05	-0.5	Stk11	0.000619536	1.45
H2-Ab1	1.71789E-05	1.34	Map2k5	0.000619962	1.47
Tubal3	2.39384E-05	-0.59	Ubap1	0.000654395	-0.91
Mocs2	2.50346E-05	-0.39	Ddt	0.000672608	-0.33
Hbb-y	3.4927E-05	-0.66	Spcs2	0.000698452	0.31
Thbs1	4.4225E-05	-0.47	Chchd4	0.000707062	-0.7
Jup	4.8829E-05	-0.48	Ivd	0.000756709	-0.44
Myl7	5.34437E-05	1.3	Tbc1d7	0.001069273	-1.07
Serac1	5.61984E-05	-0.52	Rrn3	0.00119248	1.39
Scyl2	5.74829E-05	-1.16	Slc25a19	0.001572944	0.73
Myo1d	8.11853E-05	0.79	Scaf8	0.001600494	-1.29
Fabp3	8.6521E-05	0.48	Serpina1e	0.001840316	-0.41
Plin3	9.67756E-05	-0.46	Tnni1	0.002077449	-0.35
Acot2	9.7282E-05	0.48	Kat6b	0.002153035	-0.72
Krt42	0.000149167	1.21	Cpne2	0.002179771	-0.74
Txnip	0.000149499	0.77	Tcof1	0.002179771	0.85
Zfand1	0.000166669	-0.44	Igkv12-41	0.002262598	-1.15
Ikbkb	0.000182236	0.55	Psmb4	0.002276143	0.28
Arg1	0.000201821	-1.09	Chchd6	0.002567924	-0.44
Slc27a1	0.00023361	0.47	Prkar2b	0.002852752	1.23
Igkv12-41	0.000267635	-1.06	Rilp	0.003939925	-0.45
Mri1	0.000280225	-0.41	Necap2	0.00395824	1.31
Fga	0.000365581	-0.35	Gcat	0.004037483	-0.75
Fkbp9	0.000376569	-0.91	Tmem41a	0.004987615	0.39
Tm9sf4	0.000427326	-0.52	Thbs4	0.005142103	-0.34
Mettl22	0.000448024	0.45	Sugp2	0.005431911	0.3

mgll	0.000448024	0.53	Fmo1	0.006326128	-0.29
Tpcn1	0.000481343	-1.3	Dnase1l1	0.006545327	0.35
Cygb	0.000481656	0.64	Tmem230	0.006620253	0.61
Dglucy	0.000488644	-0.44	Tpm3	0.00753138	-0.33
Mvk	0.000492293	-0.51	Cyb5d2	0.008236096	0.51
Pcna	0.000492293	-0.59	Col15a1	0.008368722	0.27
Hspb1	0.000548161	-0.33	Ormdl1	0.00839033	-0.77
Pip4p2	0.000608666	-0.74	Gbp6	0.00855757	-0.77
Mrps18c	0.000629453	-1	Ccar1	0.008762717	-0.28
Pus7	0.000629453	0.85	Myl2	0.008762717	-0.36
Rrm2b	0.000672465	-0.88	Akt1s1	0.008812477	-0.32
Ankfy1	0.000802793	0.8	Mblac2	0.008815744	0.33
Col4a2	0.00081901	0.52	Bcas1	0.009308638	1.24
Nqo1	0.000839393	-0.32	Ig heavy chain V region 93G7	0.009468498	1.24
Pc	0.000851545	-0.32	Trappc13	0.009945392	0.7
Enpp3	0.000903957	1.08	Suclg2	0.010160034	0.28
Sh3glb2	0.000953647	0.69	Cdc42ep1	0.010242695	-1.17
Maco1	0.001050404	-0.96	Wipi1	0.010673071	0.87
Col4a1	0.001065735	0.57	Kbtbd13	0.011008838	-1.2
Smox	0.001119789	-0.48	Coq10b	0.011074403	-0.29
Tnnc1	0.001196627	0.42	Fgb	0.011548211	0.27
Usp13	0.001296536	-0.4	Agpat5	0.012160156	-0.8
Acadl	0.001538847	0.42	Bcas2	0.012547193	-1.15
Decr1	0.001549205	0.42	Bst2	0.013308525	-0.79
Tnni1	0.001578749	0.42	Apoa2	0.013387726	0.67
Pik3c3	0.00167854	0.76	Ig heavy chain V-III region J606	0.013387726	0.89
Mtx2	0.00184611	0.49	Enah	0.013387726	-0.36
Fhl1	0.001938677	0.42	Slc25a15	0.013387726	0.61
Npr2	0.001995008	-1.25	Zswim8	0.013387726	0.8
Mapkapk3	0.002073105	-0.45	Iqgap2	0.013391167	-0.46
Pwp1	0.002206922	0.75	Uqcrh	0.013785848	-0.34
Abcd3	0.002221239	0.58	Tnnc1	0.013883358	-0.28
Plin5	0.002235041	0.71	Mrpl51	0.01391113	0.69
S100a10	0.002611804	0.46	Tbcel	0.014239101	0.38
Krt33b	0.002848835	-0.69	Tubgcp3	0.014358282	1.15
Apoa1	0.002851486	-0.29	Aldoc	0.014636679	0.41
Mocs1	0.004068612	-0.35	Sh2b1	0.015220222	0.37
Tpmt	0.004192065	1.03	Fgg	0.015278866	0.26
Serpina3k	0.004223926	-0.28	Aplp2	0.01564688	0.75
Nudt2	0.004614686	0.45	Acot13	0.016284968	-0.29
Nudt7	0.005446589	0.53	Maob	0.01663537	0.24
Arf6	0.005492588	-0.42	Gstk1	0.016636318	-0.27
Acox1	0.00550781	0.49	Timm23	0.017776147	0.42
Procr	0.005570221	-1.17	Nos1	0.017840024	-0.31
S100a9	0.005809123	-0.58	Ptms	0.017840024	0.42
Krt85	0.006057283	-1.17	Ighg2b	0.017994031	-0.28
Pts	0.006356755	-1.15	Krt81	0.018539353	0.24
Bckdhb	0.006754546	-0.34	Mrps17	0.019557448	-0.64
Ndufb1	0.007029449	0.39	Ftl1	0.0195821	-0.28
Myom3	0.007113024	0.38	Tspan15	0.019587296	1.05
Slc25a20	0.007223437	0.38	Ndufv3	0.02090465	0.23
Coasy	0.007430959	0.53	Apoe	0.021166365	0.26
Sh3kbp1	0.007430959	0.63	Apoc1	0.021490659	0.26
Dhrs4	0.008087104	0.39	Pus7	0.022023665	-0.69
Gsdma	0.008150571	-0.83	Ndrg1	0.022050105	0.39
	0.008150571	0.78	Csnk2a2	0.022505291	-0.72
Ivd	0.008150571	-0.27	Vps33a	0.022974231	-0.34
Plekhb1	0.008443573	-0.73	Ybx3	0.023137342	0.8

Ier3ip1	0.00854196	-0.86
Ces1c	0.008549016	-0.27
Ces2c	0.009264579	1.21
Col3a1	0.009381562	0.93
Lipe	0.00973257	0.44
Hspa1a	0.009823846	-0.3
Kng1	0.010604791	-0.27
Mrpl10	0.010673532	0.5
Klhl31	0.010673532	-0.25
Serpina6	0.011430677	-0.38
Plec	0.011430677	-0.39
Hk2	0.012206155	-0.25
Myl6b	0.012206155	0.37
Eci2	0.012445516	0.36
Pym1	0.013006845	-0.8
Atp2a2	0.013182119	0.36
Cat	0.013360766	0.37
Selenow	0.013835399	-0.34
Sfxn3	0.013885952	0.43
Mtatp6	0.013917066	0.36
Acaa2	0.014242964	0.36
Tnnt1	0.015027038	0.36
Tfeb	0.015903131	-0.56
Ly6a	0.016168384	-0.84
Rab22a	0.016273741	0.42
Mrpl22	0.016609183	0.68
Iqgap2	0.017262191	-0.37
Tomm20	0.018158721	0.42
Rps29	0.018256624	0.57
Suclg2	0.018995347	0.37
Dnajc11	0.019353448	0.38
Trappc2l	0.019578143	0.63
Oxct1	0.019895847	-0.24
Sdhd	0.020464642	-0.25
Vps18	0.020732001	0.56
Fxn	0.021581818	-0.3
Nme1	0.021581818	0.35
Tspo	0.021581818	-0.79
Atp6v1e1	0.022249101	-0.33
Bltp2	0.022255588	-0.6
Adgre5	0.022431299	0.73
Cntn4	0.022431299	1.12
Psme2	0.022431299	0.42
Srsf10	0.022431299	-0.75
Smdt1	0.022450817	0.57
Srrm2	0.022450817	-0.29
Aplp2	0.022560928	-0.64
Nccrp1	0.022590427	-1.05
Tbc1d10b	0.023043999	0.49
Fgg	0.023274388	-0.23
Gm10881	0.023274388	-0.29
Atp5mpl	0.023566999	0.35
Krt87	0.023566999	-0.77
Grb14	0.023912642	0.86
Snap47	0.025584563	1.1
Akt2	0.025822798	-0.28
Pfkfb1	0.028567125	-0.25
Antxr2	0.028779788	-0.56
Prkag2	0.029082992	-0.76
Camk2a	0.029912242	-0.29
Atad1	0.023213737	-0.27
Ly6a	0.025739539	-0.72
Rpl35	0.026815861	0.23
Usp8	0.026983036	0.71
Mrps27	0.027744333	-0.39
Fundc1	0.027744333	0.58
Protein Njmu-R1	0.027744333	1.04
Prg4	0.027744333	-0.88
Ap2s1	0.02861796	0.34
Acadsb	0.02861796	-0.28
Birc6	0.029820533	-0.49
Ncoa5	0.030850106	-1.03
Ncln	0.032147422	0.23
Synm	0.032384047	-0.43
Cltb	0.034415397	-0.29
Laptm4a	0.034471562	-0.9
Serpinh1	0.035533072	0.22
Krt33a	0.035608633	0.74
Nudt12	0.036298421	-0.67
Eif2b5	0.036602545	0.32
H2az1	0.036888202	0.22
Dynlt3	0.037452265	0.55
Dbt	0.037812785	-0.28
Arhgef1	0.03814374	-0.78
Serac1	0.03814374	-0.4
Lyn	0.038570651	-0.65
Basp1	0.038623481	-0.65
Myh7	0.039494302	-0.31
Gatd3	0.040424157	-0.31
Gtpbp8	0.040742298	-0.51
H2-Ab1	0.041550945	-0.95
Pdxdc1	0.042107484	0.68
G6pc3	0.042908665	-0.48
Scp2	0.043266574	-0.27
Mocs2	0.044622366	0.22

Myh7	0.03003865	0.34
Sqor	0.03003865	-0.26
Pdk3	0.031378347	-0.4
Pef1	0.032239614	-0.32
Afm	0.032548997	-0.35
Fastkd2	0.033140731	0.82
Oat	0.033714733	-0.24
Mtfmt	0.034019966	-0.73
Dsg1b	0.034155678	-0.5
Hscb	0.036167591	-0.28
Uchl5	0.036506024	-0.72
Rpl32	0.036590692	0.43
Dip2b	0.036600898	-0.83
Hadha	0.037110468	0.33
Naprt	0.037691897	0.84
Pacs1	0.037691897	-0.87
Plin1	0.038211253	0.4
Tango6	0.039425074	1.09
Spg21	0.039569451	-0.7
Csrp3	0.042725677	0.35
Tmem41a	0.042725677	-0.28
Tuba3a; Tuba3b	0.042725677	0.41
Plpp7	0.044016429	-0.4
Fetub	0.044335066	-0.31
Nt5c3a	0.044373232	0.55
Plcd4	0.044373232	-0.27
Eny2	0.044373232	1.11
Tmem65	0.044671048	0.38

Supplemental table 2: Differentially regulated proteins in Gastrocnemius muscle of WT and D4KO mice on a LCHP vs. a HCLP diet

Gene symbol	Adjusted p-value	log2 fold change	Gene symbol	Adjusted p-value	log2 fold change
WT LCHP vs. HCLP			*D4KO LCHP vs. HCLP*		
Ythdc2	2.5671E-16	6.64	Sfn	2.4921E-16	-6.64
Prkag2	2.5671E-16	-6.64	Dph2	2.4921E-16	-6.64
Nt5c3b	2.5671E-16	-6.64	Prkag2	2.4921E-16	-6.64
Mical3	2.5671E-16	-6.64	Mical3	2.4921E-16	-6.64
Acbd5	2.5671E-16	-6.64	Ces2c	2.4921E-16	-6.64
Them4	2.5671E-16	2.67	Retsat	2.4921E-16	6.64
Orm1	2.5671E-16	2.05	Adh7	2.4921E-16	6.64
Aqp4	2.5671E-16	-6.64	Orm1	2.4921E-16	2.04
Nat1	2.5671E-16	6.64	Serpina1d	2.4921E-16	1.09
Becn1	2.5671E-16	-6.64	Serpina1e	2.4921E-16	1.02
C4bpa	2.5671E-16	-6.64	Alpk2	2.4921E-16	-6.64
Calhm5	2.5671E-16	6.64	Txlna	2.4921E-16	6.64
Ceacam1	2.5671E-16	6.64	Zfand1	2.4921E-16	1.2
Slc7a2	2.5671E-16	-6.64	Ankrd40	2.4921E-16	6.64
Cnot10	2.5671E-16	6.64	Apoa4	2.4921E-16	-1.04
Cnot11	2.5671E-16	-6.64	Aqp4	2.4921E-16	-6.64
Cd2bp2	2.5671E-16	-6.64	Becn1	2.4921E-16	-6.64
Cd59a	2.5671E-16	6.64	Bet1	2.4921E-16	6.64
Cd99l2	2.5671E-16	-6.64	Actbl2	2.4921E-16	-1.03
Cemip2	2.5671E-16	-6.64	Abcb11	2.4921E-16	6.64
Cntf	2.5671E-16	6.64	Borcs6	2.4921E-16	6.64

Ccdc12	2.5671E-16	6.64	Clec10a	2.4921E-16	6.64
C9	2.5671E-16	1.93	C4bpa	2.4921E-16	-6.64
Cox6a1	2.5671E-16	-6.64	Micu2	2.4921E-16	6.64
Cyp20a1	2.5671E-16	6.64	Calm4	2.4921E-16	6.64
Nubp1	2.5671E-16	6.64	Pde4d	2.4921E-16	-6.64
Dera	2.5671E-16	-6.64	Ctnna3	2.4921E-16	6.64
Dgke	2.5671E-16	-6.64	Cd59a	2.4921E-16	-6.64
Dnmt3b	2.5671E-16	3.12	Cemip2	2.4921E-16	6.64
Polb	2.5671E-16	6.64	Zw10	2.4921E-16	6.64
Dolk	2.5671E-16	6.64	Cers2	2.4921E-16	6.64
Dusp26	2.5671E-16	-6.64	Cntf	2.4921E-16	-6.64
Dctn5	2.5671E-16	6.64	Cpsf1	2.4921E-16	6.64
Ltn1	2.5671E-16	-6.64	F13b	2.4921E-16	6.64
Entpd4	2.5671E-16	-6.64	Col4a2	2.4921E-16	-1.11
Efhd1	2.5671E-16	6.64	C9	2.4921E-16	1.48
Emcn	2.5671E-16	-6.64	Cpne2	2.4921E-16	6.64
Eif4e2	2.5671E-16	-6.64	Crtc2	2.4921E-16	6.64
Eif4ebp2	2.5671E-16	-6.64	Tmem63b	2.4921E-16	6.64
Exosc4	2.5671E-16	-6.64	Cuedc1	2.4921E-16	1.64
Ecm1	2.5671E-16	-6.64	Cox6a1	2.4921E-16	-6.64
Ezr	2.5671E-16	-6.64	Agbl1	2.4921E-16	-6.64
Fcho2	2.5671E-16	-6.64	Nubp1	2.4921E-16	-6.64
Far1	2.5671E-16	6.64	Bdh2	2.4921E-16	6.64
Fhip1a	2.5671E-16	-6.64	Dera	2.4921E-16	6.64
Fah	2.5671E-16	-6.64	Dgke	2.4921E-16	-6.64
Gnpda2	2.5671E-16	-6.64	Polr2a	2.4921E-16	-6.64
Glipr2	2.5671E-16	-6.64	Polr2d	2.4921E-16	-6.64
H2-K1	2.5671E-16	6.64	Dnajc24	2.4921E-16	6.64
Hbb-b2	2.5671E-16	1.29	Dnajc30	2.4921E-16	-6.64
H mgn5	2.5671E-16	-6.64	Itch	2.4921E-16	6.64
H mgb3	2.5671E-16	-6.64	Znf598	2.4921E-16	6.64
H mga1	2.5671E-16	-6.64	Enpp3	2.4921E-16	-6.64
H2ac7	2.5671E-16	6.64	Ece1	2.4921E-16	-6.64
H2bc21	2.5671E-16	-6.64	Akr1c6	2.4921E-16	-6.64
Ig alpha chain C region	2.5671E-16	-3.03	Exosc4	2.4921E-16	-6.64
Ighv3-6	2.5671E-16	6.64	Ezr	2.4921E-16	-6.64
Ig heavy chain V regions TEPC 15/S107/HPCM1/ HPCM2/HPCM3	2.5671E-16	-6.64	Supt16h	2.4921E-16	-6.64
Ig kappa chain V-III region CBPC 101	2.5671E-16	6.64	Flg2	2.4921E-16	6.64
Igkv9-120	2.5671E-16	6.64	Fbp1	2.4921E-16	-6.64
Kpna2	2.5671E-16	-6.64	Fah	2.4921E-16	-6.64
Gpr180	2.5671E-16	-6.64	Gprc5c	2.4921E-16	-6.64
Itgb6	2.5671E-16	6.64	Ghdc	2.4921E-16	6.64
Inf2	2.5671E-16	-1.79	Gnpnat1	2.4921E-16	6.64
Kcnj2	2.5671E-16	6.64	H2-K1	2.4921E-16	-6.64
Mff	2.5671E-16	6.64	Tsc1	2.4921E-16	6.64
Syne1	2.5671E-16	6.64	Hbb-b2	2.4921E-16	1
Nrip2	2.5671E-16	-6.64	Hbb-y	2.4921E-16	1.68
Acox1	2.5671E-16	1.34	Ig alpha chain C region	2.4921E-16	-1.68

Pnkd	2.5671E-16	6.64	Ig heavy chain V region 5-84	2.4921E-16	-6.64
Tmub1	2.5671E-16	2.76	Ig kappa chain V-II region 17S29.1	2.4921E-16	6.64
Rap1gds1	2.5671E-16	6.64	Ig kappa chain V-III region CBPC 101	2.4921E-16	6.64
Fbln1	2.5671E-16	2.13	Igkv9-120	2.4921E-16	-6.64
Krt10	2.5671E-16	6.64	Kpna2	2.4921E-16	-6.64
Krt19	2.5671E-16	-6.64	Itpr1	2.4921E-16	-6.64
Krt84	2.5671E-16	-6.64	Itgb6	2.4921E-16	6.64
Krt4	2.5671E-16	-6.64	Inf2	2.4921E-16	3.38
Krt75	2.5671E-16	-6.64	Syne1	2.4921E-16	-6.64
Krtap19-5	2.5671E-16	-6.64	Ubqln1	2.4921E-16	6.64
Lgmn	2.5671E-16	6.64	Rap1gds1	2.4921E-16	-6.64
Leprotl1	2.5671E-16	-6.64	Gnao1	2.4921E-16	6.64
Llgl1	2.5671E-16	-6.64	Krt19	2.4921E-16	-6.64
Lrrc14	2.5671E-16	6.64	Krt5	2.4921E-16	6.64
Lmbrd1	2.5671E-16	-6.64	Krt75	2.4921E-16	-6.64
Mrs2	2.5671E-16	6.64	Dcxr	2.4921E-16	6.64
Mtrr	2.5671E-16	-6.64	Llgl1	2.4921E-16	-6.64
Immp1l	2.5671E-16	6.64	Clptm1l	2.4921E-16	-6.64
Map3k4	2.5671E-16	-6.64	Mrs2	2.4921E-16	6.64
MLV-related proviral Env polyprotein	2.5671E-16	-6.64	Mtrr	2.4921E-16	6.64
Rae1	2.5671E-16	6.64	Mief1	2.4921E-16	-6.64
Myl7	2.5671E-16	-6.64	MLV-related proviral Env polyprotein	2.4921E-16	-6.64
Naa38	2.5671E-16	-6.64	Morf4l1	2.4921E-16	6.64
Nfyc	2.5671E-16	6.64	Sirt4	2.4921E-16	-6.64
Nup37	2.5671E-16	-6.64	Nelfb	2.4921E-16	6.64
Nrm	2.5671E-16	6.64	Nup107	2.4921E-16	-6.64
Otc	2.5671E-16	6.64	Nup37	2.4921E-16	6.64
Osbpl2	2.5671E-16	-6.64	Otc	2.4921E-16	-6.64
Abhd10	2.5671E-16	-6.64	Abhd10	2.4921E-16	-6.64
Pex10	2.5671E-16	-6.64	Pi16	2.4921E-16	6.64
Pik3cb	2.5671E-16	2.78	Mtrf1	2.4921E-16	6.64
Pik3r4	2.5671E-16	-6.64	Pxdn	2.4921E-16	-1.3
Pla2g15	2.5671E-16	-6.64	Pex10	2.4921E-16	-6.64
Pfas	2.5671E-16	6.64	Pik3cb	2.4921E-16	6.64
Gp1bb	2.5671E-16	-6.64	Piezo1	2.4921E-16	6.64
Plekha2	2.5671E-16	6.64	Gp1bb	2.4921E-16	6.64
Alox12	2.5671E-16	-6.64	Gp5	2.4921E-16	6.64
Bcas2	2.5671E-16	6.64	Plekha2	2.4921E-16	6.64
Egf	2.5671E-16	-6.64	Alox12	2.4921E-16	-6.64
Thg1l	2.5671E-16	6.64	Il16	2.4921E-16	6.64
Grn	2.5671E-16	-6.64	Ddx20	2.4921E-16	-6.64
Ptgis	2.5671E-16	6.64	Thg1l	2.4921E-16	6.64
Efr3a	2.5671E-16	-6.64	Protein C18orf25 homolog	2.4921E-16	6.64
Ltv1	2.5671E-16	6.64	Dr1	2.4921E-16	-6.64
Mtss2	2.5671E-16	6.64	Efr3a	2.4921E-16	6.64
Ntan1	2.5671E-16	-6.64	Fam241b	2.4921E-16	-6.64
Ppp1r14a	2.5671E-16	-6.64	Fam3c	2.4921E-16	-6.64
Pof1b	2.5671E-16	-6.64	Mtss2	2.4921E-16	-6.64

S100a16	2.5671E-16	6.64	Ntan1	2.4921E-16	6.64
Pyroxd1	2.5671E-16	-6.64	S100a14	2.4921E-16	6.64
Rbsn	2.5671E-16	6.64	Son	2.4921E-16	6.64
Rhbdd1	2.5671E-16	-6.64	Tgm1	2.4921E-16	6.64
Rps6ka5	2.5671E-16	6.64	Icmt	2.4921E-16	6.64
Wdr12	2.5671E-16	6.64	Dhx57	2.4921E-16	6.64
Rpap3	2.5671E-16	6.64	Pyroxd1	2.4921E-16	6.64
Rbpms	2.5671E-16	-6.64	Rbsn	2.4921E-16	6.64
Scarb1	2.5671E-16	6.64	Lamtor4	2.4921E-16	-6.64
Serinc1	2.5671E-16	6.64	Rab3d	2.4921E-16	6.64
Htra4	2.5671E-16	-6.64	Rcc1l	2.4921E-16	-6.64
Ccser2	2.5671E-16	-6.64	Rhbdd1	2.4921E-16	-6.64
Stk25	2.5671E-16	-6.64	Rrm2b	2.4921E-16	-6.64
Riok3	2.5671E-16	-6.64	Rps6ka5	2.4921E-16	6.64
Siae	2.5671E-16	-6.64	Rrn3	2.4921E-16	6.64
Slc25a36	2.5671E-16	-6.64	Rbpms	2.4921E-16	6.64
Sort1	2.5671E-16	-6.64	Sltm	2.4921E-16	6.64
Snx21	2.5671E-16	-6.64	Scarb1	2.4921E-16	6.64
Smap1	2.5671E-16	-6.64	Serpina3k	2.4921E-16	1.05
Smchd1	2.5671E-16	-6.64	Ccser2	2.4921E-16	6.64
TCAIM	2.5671E-16	6.64	Cdc42bpb	2.4921E-16	6.64
Tbc1d7	2.5671E-16	6.64	Nek3	2.4921E-16	-6.64
Serpina7	2.5671E-16	-6.64	Riok3	2.4921E-16	-6.64
Traf6	2.5671E-16	-6.64	Siae	2.4921E-16	-6.64
Tead1	2.5671E-16	-6.64	Snx21	2.4921E-16	6.64
Tra2a	2.5671E-16	-6.64	Stx18	2.4921E-16	-6.64
Tmem245	2.5671E-16	6.64	Stxbp5	2.4921E-16	-6.64
TremL1	2.5671E-16	-6.64	Tbc1d9	2.4921E-16	6.64
Gtpbp3	2.5671E-16	-6.64	Tpk1	2.4921E-16	6.64
Pip4p2	2.5671E-16	-6.64	Traf6	2.4921E-16	6.64
Baz1b	2.5671E-16	-6.64	Rela	2.4921E-16	6.64
Ptpn23	2.5671E-16	-6.64	Tspo	2.4921E-16	-6.64
Prpf31	2.5671E-16	-6.64	TremL1	2.4921E-16	6.64
Sart1	2.5671E-16	6.64	Gtpbp3	2.4921E-16	-6.64
Atg12	2.5671E-16	-6.64	Tnnt1	2.4921E-16	6.64
Uncharacterized protein CXorf38 homolog	2.5671E-16	6.64	Tradd	2.4921E-16	6.64
Vps53	2.5671E-16	6.64	Pip4p2	2.4921E-16	-6.64
Wipi1	2.5671E-16	6.64	Baz1b	2.4921E-16	-6.64
Adam17	2.6429E-13	-1.69	Prpf31	2.4921E-16	-6.64
Krt81	3.2395E-13	-1	Atg12	2.4921E-16	6.64
Elp2	4.2221E-12	-1.99	Uncharacterized protein C15orf61 homolog	2.4921E-16	-6.64
Ehbp1	1.4216E-11	-1.86	Proz	2.4921E-16	6.64
Fastkd2	1.2052E-09	1.78	Serpina1a	5.4971E-15	0.78
Jchain	2.8722E-09	-1.42	Ca1	5.4433E-14	0.76
Smox	7.0559E-09	-0.74	Myl7	1.4107E-13	-2.2
Apoa4	1.749E-08	-0.98	Saa4	1.4602E-13	1.67
Cfd	1.9057E-07	-1.03	H2bc21	1.6604E-13	1.55
Krt31	2.6875E-07	-0.97	N6amt1	8.2594E-12	1.23
Apoa2	2.7181E-07	1.51	Apoa2	2.0931E-11	1.72
Pxdn	9.3165E-07	-0.92	Creg1	2.8345E-11	-0.9
Ca1	1.1063E-06	0.79	Ptrhd1	1.1418E-10	-0.94
Serpina1d	1.115E-06	1	Ikbkb	1.5847E-10	-0.77

Deptor	1.8199E-06	-0.83	Hck	1.7135E-10	2.03
S100a14	1.9996E-06	-2.06	Pdk3	3.9666E-10	1.14
Rela	2.8043E-06	1.45	Ig kappa chain V-VI region NQ2-6.1	4.1728E-10	1.44
Scyl2	4.9993E-06	-1.42	Ca2	8.5841E-10	0.63
Selenow	5.6535E-06	-0.91	Igfn1	1.2295E-09	-1.18
Serpina3k	1.3909E-05	0.92	Apoc1	1.4685E-09	0.68
Kcnc1	2.7017E-05	-1.29	Enah	1.4818E-09	-0.62
Helb	2.9695E-05	1.78	Usp8	2.0073E-09	1.77
Jpt1	3.1895E-05	-0.96	Apoa1	2.1236E-09	0.61
Ig heavy chain V region 93G7	3.2439E-05	-1.86	Pf4	3.2737E-09	1.75
Pglyrp2	5.3994E-05	1.26	Mug1	5.3846E-09	0.6
Krt33b	8.3855E-05	-1.09	Hbb-b1	7.4854E-09	0.6
Mblac2	0.00010514	-0.61	Fgb	1.0044E-08	0.61
Serpina1e	0.0001167	0.88	Hba	1.4125E-08	0.59
Serpina1a	0.00012444	0.85	Col4a1	2.529E-08	-0.8
Ormdl1	0.00013891	1.18	Gpld1	6.2382E-08	0.99
Scp2	0.00022139	0.59	Sntb1	6.4342E-08	-0.61
Stbd1	0.00024872	-0.53	Tubal3	7.0263E-08	0.82
Tomm20	0.00025191	0.73	Akt1s1	7.9274E-08	-0.68
Mocs1	0.00028324	-0.49	Fabp1	8.5589E-08	-1.63
Bcas1	0.00029007	-1.65	Cacnb1	9.2911E-08	-0.86
Smoc2	0.00030317	-0.78	Mbl2	1.3576E-07	1.84
Smox	0.00031068	-0.81	Krt42	2.3941E-07	-1.46
Ctnna3	0.00036996	-0.74	S100a9	2.5133E-07	1.1
Cntn4	0.00037272	1.33	Mrtfb	2.8908E-07	-0.73
Ppp1r12c	0.00038826	0.85	H1-2	3.1751E-07	0.65
Dip2b	0.00041656	-1.46	Ig kappa chain V-II region 26-10	6.2934E-07	-0.69
Tm9sf4	0.00065049	-0.77	Nmrk2	6.4345E-07	0.63
Tspo	0.00066756	-1.24	Cpn2	6.7864E-07	0.87
C8b	0.0007958	0.76	Atp1b2	9.9582E-07	-0.51
Ppp2r2d	0.00080946	-0.93	Serpina1b	1.0457E-06	0.51
Atp1b2	0.00117325	-0.61	Slc4a1	1.2601E-06	0.51
Hsdl2	0.00120096	0.54	Clu	1.4845E-06	0.55
Col4a2	0.00127086	-0.54	Usp15	3.4436E-06	0.57
Lonp2	0.00146077	1.49	Leprotl1	3.914E-06	-1.72
Mrpl12	0.00164352	0.65	Aldoc	5.7341E-06	0.67
Mettl22	0.00170561	0.57	Apom	5.8744E-06	-1.74
Grk2	0.0017589	-1.34	Fga	8.6855E-06	0.5
Ig gamma-2A chain C region secreted form	0.00188285	0.61	Fbxl4	1.0968E-05	1.03
Tgm1	0.00202675	-0.97	Acox1	1.1271E-05	0.55
Cat	0.00213254	0.63	Selenow	1.5384E-05	-0.73
Shmt1	0.00228014	-0.61	Gbp6	1.7052E-05	-1.23
Aldh16a1	0.00239906	-0.86	Thbs4	1.7926E-05	-0.45
As3mt	0.00239906	-0.46	Dglucy	3.1235E-05	0.53
Ndufa3	0.00267724	0.49	Jchain	3.7838E-05	-1.17
Nudt13	0.00276331	0.95	Shmt1	4.1375E-05	-0.61
Akt2	0.00280185	-0.42	Msrb1	4.2306E-05	-1.18
Hsd17b4	0.00305655	0.51	Vps51	4.4894E-05	1.06
Dsp	0.00323194	-0.46	Bckdha	4.5606E-05	0.49
Mrps11	0.00348437	0.77	Cdc42ep1	5.3766E-05	-1.54

Aplp2	0.00351617	-0.89	Ig gamma-2A chain C region secreted form	5.8654E-05	-0.43
Fasn	0.00395544	-0.52	Ppp1r1a	5.929E-05	-0.64
Saa4	0.00413955	0.89	Tmem41a	6.2549E-05	0.53
Ddah1	0.00453513	0.68	Osbpl1a	7.0008E-05	-0.62
Scaf8	0.00498912	1.26	As3mt	7.2407E-05	-0.52
Aldoc	0.00524839	-0.62	Smpdl3a	8.0518E-05	-0.74
Polr1c	0.00530937	0.98	Thbs1	8.3966E-05	0.53
Fundc1	0.00568627	-0.93	Vps18	0.00010975	-0.86
Krt2	0.00594191	-1.2	Col3a1	0.00015159	-1.37
Krtap6-5	0.0069258	-1.22	Egfr	0.00018153	0.54
Ca14	0.00723016	-0.75	Smdt1	0.00020063	-0.87
Ppil3	0.00733211	0.87	C8b	0.00020211	0.73
Ndufa1	0.00811947	0.56	Bckdhb	0.00024288	0.47
Pdk4	0.00856944	0.69	Mocs2	0.00032997	0.41
Gabpa	0.00968034	0.66	Pus7	0.00045494	-0.98
Plin3	0.01016734	-0.39	Fgg	0.00045808	0.39
Krt33a	0.01027046	-0.85	Ahsg	0.00048112	0.39
Basp1	0.01029479	0.82	Kbtbd13	0.00048438	-1.43
Mvp	0.01152041	0.47	Smoc2	0.00050622	-0.64
Tpcn1	0.01251867	-1.17	Pafah1b2	0.00051575	-0.48
Mast1	0.01255492	-0.65	Col6a6	0.00053768	0.42
Mtfp1	0.01270572	0.48	Deptor	0.00058062	-0.49
Ig heavy chain V region AC38 205.12	0.01306445	0.74	Kiaa1671	0.00064105	-0.39
Rnf181	0.01359873	-1.07	S100a8	0.00065918	1.03
Snap47	0.01390514	1.09	Cntn4	0.00068395	-1.35
Cdc16	0.01414264	-1.02	Neu2	0.00068395	-0.56
Krt85	0.01421559	-1.25	Tmem230	0.00076867	0.77
Krt87	0.01431897	-0.95	Aldh16a1	0.000805	-0.95
Sntb1	0.01547074	-0.38	Cps1	0.00081753	-0.93
Acad8	0.01621697	0.44	Fxyd1	0.0008714	-0.46
Cyb5d2	0.01642286	-0.6	Padi2	0.0008714	-0.38
Unc80	0.01780528	-1.22	Pdk2	0.00087206	0.38
Timm10	0.01907404	0.55	Pts	0.00093971	1.25
Nup58	0.01907404	-0.8	Xxylt1	0.00096742	0.38
Ttc19	0.01932691	0.61	Oat	0.0010239	0.37
Cilp	0.02099539	0.85	Glul	0.00102455	0.45
Mrps33	0.02102945	0.81	Sp100	0.00103116	1.05
Comp	0.02233787	0.43	Ighm	0.00104505	0.41
G6pc3	0.0224782	0.68	Cat	0.00107057	0.39
Serpind1	0.02263171	0.63	Mrps18c	0.00111329	1.09
Ppp1r1a	0.02287177	-0.55	Atp1a2	0.00111414	-0.37
Mrpl22	0.02320688	0.77	Dnmt3b	0.00116368	-1.04
Myct1	0.02448938	-0.97	Myom3	0.00136149	-0.37
Uqcc3	0.02473627	0.84	Kera	0.00146563	-0.4
Fabp3	0.0247584	0.61	Rad50	0.00162273	-1.18
Tnnt1	0.0247584	0.48	Hsd17b11	0.00190319	0.59
Atp4a	0.02518388	-0.85	Phlda3	0.00190319	0.75
Tpm3	0.02545525	0.5	Rsc1a1	0.00190607	-0.98
Thoc5	0.0255377	-0.64	Coq10b	0.00196353	-0.43
Arg1	0.02592842	-1.01	C8g	0.00208388	0.8
Dsg1b	0.0260482	-0.73	Dip2b	0.00210563	-1.32
Atad1	0.02629018	0.43	Dctn6	0.00210775	-0.73

Nudt7	0.02722439	0.58
Uprt	0.02722439	-1
Acot2	0.02863416	0.6
Csnk2a2	0.02912732	0.8
Spta1	0.03001329	0.43
Acot1	0.03016317	0.9
Sh3kbp1	0.03126016	0.74
Tppp3	0.03126016	0.43
Gls	0.03180299	0.5
Rab8a	0.03302706	-0.85
Mmut	0.03317818	0.42
Hsd11b1	0.03662731	-0.58
Rrn3	0.03775767	-1.18
Serpina3n	0.03815504	0.42
Pex16	0.03928239	1.06
Vwa8	0.04013289	0.5
Ca2	0.04045083	0.58
Tspan15	0.04045083	-1.11
Anapc2	0.04149724	0.73
mt-Co3	0.04149724	0.41
Ctbs	0.04203544	0.74
Hgfac	0.04206623	-0.73

Sbk2	0.00217939	0.39
Sfxn1	0.00224441	1.12
Serpinf2	0.00272003	0.39
Ces1	0.00297267	0.87
Tspan9	0.0030046	0.8
Ppid	0.00302697	-0.42
H2-Q10	0.00304447	0.42
Ftl1	0.0037696	-0.41
Myct1	0.0037881	-1.11
Cilp2	0.00381951	-0.49
Ctbp2	0.00393236	-0.91
Tspan7	0.00396888	-1.24
Ig kappa chain V-V region MOPC 149	0.00424893	-1.23
Ndufa1	0.00458973	0.39
Prelp	0.00479839	-0.34
Carhsp1	0.00511063	0.71
Ig heavy chain V region 102	0.00511063	-0.91
Klhl31	0.00526662	0.32
Rab5b	0.0058262	-0.43
Arhgef1	0.00597802	-1
Htra4	0.00609297	-1.09
Map2k3	0.00657378	-0.37
Aldh1a2	0.00708254	1.04
Comp	0.00741306	-0.4
Txnip	0.00741306	-0.68
Blvrb	0.00767302	0.33
St3gal6	0.00896389	-0.47
Myo1d	0.0091241	-0.6
Serpind1	0.00956721	0.41
Vamp5	0.01011491	-0.4
Tnnc1	0.01023104	-0.36
Procr	0.01029782	1.03
Slirp	0.01031948	0.37
Mybph	0.01055743	-0.32
Tor1aip2	0.010661	-0.48
Eif1	0.01086847	0.37
Mvp	0.01088264	0.35
Srm	0.01093125	-0.83
Tst	0.01122473	0.33
Micos10	0.01125348	0.38
Apoc3	0.01139177	0.79
Abhd5	0.01150733	-0.65
Eif4e2	0.01152582	-1.04
Pzp	0.01195353	0.32
Bnip2	0.01250143	-0.83
Usp13	0.01293799	0.37
Tf	0.01380249	0.31
Oxct1	0.01380249	0.31
Pigu	0.01535527	0.72
Myom1	0.01551331	0.31
Ahsa2	0.0155834	0.62
Aspn	0.01560727	-0.3
Prkag3	0.01573063	0.36

Cnih4	0.01617473	-0.38
Tubb3	0.01749826	-0.41
Bpgm	0.01792391	0.29
Ppie	0.01792391	0.38
Zyg11b	0.01911274	0.92
Stx16	0.02043253	0.52
Kdm1a	0.0218695	0.85
Trmt10c	0.02190196	0.75
Fn1	0.02218371	0.3
Tnc	0.02218371	-0.37
Ubtf	0.02267375	-0.9
Cox7c	0.02309166	0.31
Serpinc1	0.02325251	0.3
Surf4	0.02325251	-0.29
Ca14	0.02395141	-0.68
Nefm	0.02395141	-0.28
Atp9a	0.02419363	-1.11
Mag	0.02436835	-0.95
Rgn	0.02482445	-1.04
Mmut	0.02490735	0.31
Pik3c3	0.02490735	-0.67
Capn3	0.02526117	-0.29
Sel1l	0.02553932	0.9
Ksr1	0.02770898	-0.5
Rrp12	0.02777886	-0.95
Napa	0.02814859	-0.33
Aldh1a1	0.02887608	0.29
Myoc	0.02909736	-0.36
Acbd5	0.02911721	-0.96
Mcee	0.02982601	0.33
Sh3kbp1	0.03117856	-0.57
Myo1e	0.03117856	0.92
Zbtb20	0.03117856	-0.97
Ggt5	0.03166706	-0.42
Ap1s2	0.03240713	0.8
Tpbgl	0.03335394	-0.72
Mtln	0.03429316	0.92
Dipk1a	0.03439632	0.7
Sqor	0.03507947	0.3
Dpp4	0.03587184	-0.61
Tiprl	0.03752351	-0.35
Mkln1	0.03765556	0.7
Mbp	0.03779172	-0.28
Tsen34	0.03779172	0.8
F2	0.03830821	0.28
Hsd11b1	0.03905027	-0.48
Rpl39	0.04006634	-0.4
Kng1	0.04014731	0.28
Laptm4a	0.04058625	-0.93
Metap2	0.04058625	0.29
Cygb	0.04066662	-0.48
Myadm	0.04172487	0.35
S100a10	0.04172487	-0.32
Tnni1	0.04172964	-0.28
Adam17	0.04242754	0.55

Exosc6	0.04301974	-0.97
Snap47	0.04324537	-0.93
Mustn1	0.04356383	-0.42
Mrps31	0.04365997	0.36
Prkar1a	0.04377837	0.29
Washc4	0.04380258	0.53
Hpx	0.04414444	0.27

7.5 List of figures

7.6 List of tables

Danksagung

Nun möchte ich mich herzlichst bei all jenen bedanken, die mich während meiner Dissertation unterstützt haben.

Zunächst möchte ich Prof. Dr. Hadi Al-Hasani danken. Zum einen bedanke ich mich für die Möglichkeit, meine Doktorarbeit an dem Institut für Klinische Biochemie und Pathobiochemie am Deutschen Diabetes Zentrum anzufertigen. Zum anderen bedanke ich mich, dass ich im Rahmen des Graduiertenkollegs 2576 „vivid“ die Möglichkeit hatte meine Forschungsergebnisse auf internen Veranstaltungen, nationalen und internationalen Kongressen präsentieren zu dürfen.

Außerdem gilt mein Dank Prof. Dr. Eckhard Lammert für die Übernahme des Zweitgutachtens und die hilfreichen Diskussionen im Rahmen des Graduiertenkollegs.

Mein großer Dank gilt Dr. Alexandra Chadt, die jederzeit selbstverständlich ansprechbar war, mir bei jeglichen Fragen und Problemen zur Seite stand und maßgeblich zur Lösung dieser beigetragen hat. Vielen Dank für die stets geöffnete Tür, die spannende und lehrreiche Zeit sowie die Anregungen und Diskussionen, die zu dem erfolgreichen Vorankommen des Projekts maßgeblich beigetragen haben.

Außerdem möchte ich mich für die tatkräftige Unterstützung bei den zahlreichen Versuchen mit den Mäusen bei Birgit Knobloch, sowie bei Anette Kurowski und Heidrun Podini für die Durchführung der *ex vivo* Versuche im Isotopenlabor bedanken.

Ebenfalls gilt mein großer Dank meinen Kolleg:innen des Instituts für Klinische Biochemie und Pathobiochemie. Insbesondere danke ich Dr. Lena Espelage, Pia Marlene Förster und Aleksandra Nikolić, die mir sowohl in intensiven Zeiten zur Seite standen als auch über die Arbeit hinaus eine großartige Unterstützung waren. Ohne eure alltägliche Unterstützung und das offene Ohr durch die Höhen und Tiefen, wären die letzten Jahre nur halb so schön und einprägsam gewesen.

Von Herzen möchte ich mich bei meinen Freunden, meinen Eltern, meinen Geschwistern und meiner Oma bedanken, die mir jederzeit mit Rat und Tat zur Seite standen und mich unaufhörlich ermutigt und unterstützt haben. Vielen Dank, dass ihr immer für mich da seid und mich bei jeder meiner Entscheidungen unterstützt.

Zu guter Letzt, jedoch eigentlich vorerst gilt mein Dank meinem Freund Bastian. Vielen Dank für deine Geduld und die Unterstützung in guten sowie in schlechten Tagen, an denen ich mich stets auf dich verlassen und zur Ruhe kommen konnte. Danke für deine täglichen Aufmunterungen und Ermutigungen während dieser intensiven Zeit.

Eidesstattliche Erklärung

Ich versichere an Eides Statt, dass die vorliegende Dissertation von mir selbstständig und ohne unzulässige fremde Hilfe unter Beachtung der „Grundsätze zur Sicherung guter wissenschaftlicher Praxis an der Heinrich-Heine-Universität Düsseldorf“ erstellt worden ist.

Ferner versichere ich, dass die Dissertation in der vorliegenden Form noch bei keiner anderen Institution eingereicht wurde.

Düsseldorf, 27.03.2024

_____

Anna Katharina Scheel